# REPORT DOCUMENTATION PAGE

Form Approved OMB No. 0704-0188



| 1. AGENCY USE ONLY (Leave blank) | 2. REPORT DATE | 3. REPORT TYPE AND DATES COVERED |
|---|---|---|
| | 1995 | Final Report |

4. TITLE AND SUBTITLE

Theoretical Investigations of Peculiarities of the Upper Stages Breakup Caused by Explosions of Mixing Hypergolic Propellants

5. FUNDING NUMBERS

F6170894W0929

6. AUTHOR(S)

Prof. Nickolay Smirnov

7. PERFORMING ORGANIZATION NAME(S) AND ADDRESS(ES)

Moscow State University
Faculty of Mechanics and Mathematics
Moscow 119899
Russia

8. PERFORMING ORGANIZATION REPORT NUMBER

N/A

9. SPONSORING/MONITORING AGENCY NAME(S) AND ADDRESS(ES)

EOARD
PSC 802 BOX 14
FPO 09499-0200

10. SPONSORING/MONITORING AGENCY REPORT NUMBER

SPC 94-4107

11. SUPPLEMENTARY NOTES

12a. DISTRIBUTION/AVAILABILITY STATEMENT

Approved for public release; distribution is unlimited.

12b. DISTRIBUTION CODE

A

13. ABSTRACT (Maximum 200 words)

This report results from a contract tasking Moscow State University as follows: Investigate the processes of energy release involved in the mixing of hypergolic propellants in weightlessness.



14. SUBJECT TERMS

Nil

15. NUMBER OF PAGES

158

16. PRICE CODE

N/A

| 17. SECURITY CLASSIFICATION OF REPORT | 18. SECURITY CLASSIFICATION OF THIS PAGE | 19. SECURITY CLASSIFICATION OF ABSTRACT | 20. LIMITATION OF ABSTRACT |
|---|---|---|---|
| UNCLASSIFIED | UNCLASSIFIED | UNCLASSIFIED | UL |

# Theoretical Investigations of Peculiarities of the Upper Stages Breakup Caused by Explosions of Mixing Hypergolic Ptopellants

**SPC 94-4107**

**Third (Final) Report:**

## Nonuniform Loading, Dynamical Deforming and Breakup of a Shell; Mass and Velocity Distributions of Fragments.


Investigators: Prof. Dr.Sc.-hab. N.N.Smirnov
Dr.Sc.-hab. A.B.Kiselev
M.Sc. V.F.Nikitin
Dr. I.D.Dimitrienko
Dr. V.R.Dushin



**Moscow - 1995**

# CONTENTS

# INTRODUCTION

By now the explosions of the upper stages were supposed to give the most essential contribution to the space debris production. Thus, investigation of the breakup of the upper stages is of great importance for further development of space contamination models.

It was only in 1981 when Don Kessler, NASA-JSC was able to correlate space debris from satellite breakups recorded by NORAD/ADCOM to upper stages of rocket carriers left on orbit after completion of their mission [1].

Since 1969 up to 1981, ten cases of breakup of Delta second stages left in orbit after mission took place [2]. The duration of stay of the vehicles in orbit before the explosion varied from 1 day up to 5 years.

One of the most probable potential causes of orbital breakups is fuel and oxidizer tanks overpressurization. Due to gradual heating of components oxidizer tank pressure would be higher than fuel tank pressure and would therefore be more critical. After oxidizer tank pressure reached the predicted burst pressure for the common bulkhead the fracture of the common bulkhead would allow mixing of the residual propellants that would most probably result in an explosion.

Theoretical investigations of breakup of fuel tanks as a result of an explosion of the combustible mixture of components showed that the results of breakup: number, mass distribution and velocities of fragments strongly depend on the peculiarities of the process of energy release inside the tank [3]. The investigations [2] were carried out for $H_2 - O_2$ premixed systems and applied for Arian fuel tanks explosions. But most of explosions in space are not that of $H_2 - O_2$ perfectly mixed gases awaiting an ignition source. They are caused by the mixing of hypergolic fuel components: $N_2O_4$ - MMH/UDMH (Aerozine 50), that have been in orbit for significant periods of time: weeks to years [4, 5]. As a consequence the propellants are in both vapour and liquid state and an unknown pattern of dispersal within the tank.

The conditions arise because first stage systems shut down on fuel or oxidizer depletion. Performance reserves are all in the second stage to deal with engine performance variance, winds, temperature and other performance variations.

To minimize inert mass such second stages usually use a common bulkhead and put the higher pressure on the Con Cave side. Structural materials for the walls chemically milled isogrid aluminium or stainless steel. The common bulkhead is Al or stainless free sheets over Al or composite honeycomb. No systematic failure mode is established but failure of bulkhead permeability is highly suspected. The energy release in breakup is not consistently related to residual propellant mass but to the mass of mixture of self-igniting components formed after the breakup of a bulkhead. A suspect case is: an initial ignition event propagating to multiple aggregated events.

Since "breakup models" are a major source of uncertainty in overall debris environmental models, a better model of a less idealized event, taking into account the process of mixing of hypergolic components and nonuniformities of concentrations, could make a significant contribution. In the best of circumstances such a model might help to answer the question why some events with less residual propellant mass are more energetic

than other events with greater propellant mass.

The destruction of the common bulkhead was adopted to be the most probable reason for explosion and breakup of the upper stages.

After the destruction of the common bulkhead the existing pressure gradient causes the formation of a jet of one component into the tank filled with the other component.

Hypergolic propellants need no ignition source since the reaction starts at first contact at any temperature. The large rate of chemical reaction as compared with the rate of diffusive mixing leads to establishing the conditions under which the reactants are unable to penetrate deep through a flame not entering into reaction. The main limiting factor in determining the rate of energy release, thus, is not the kinetics of chemical reaction but rather the rate of diffusive mixing of the propellants.

The rate of diffusive combustion determines the rate of pressure increase inside the vessel. The pressure increase up to a certain value leads to a breakup and expansion of reaction products and unburnt fuel and oxidizer.

Thus, the main peculiarity of the breakup caused by the explosion of mixing hypergolic propellants is that the total amount of energy released by the time of breakup depends on dynamics of mixing and the rate of diffusive combustion and can be practically independent of the total amount of the residual fuel and oxidant.

The rate of energy release responsible for wall loading and breakup is determined by turbulent mixing and diffusive combustion of the components after destruction of common bulkhead. The velocity of a jet, intensity of turbulence rate of combustion depend on the diameter of a hole in the bulkhead and the initial pressure gap. The results of theoretical investigation of the diffusive combustion inside a fuel tank, the rate of wall loading and the breakup of a thin-walled fuel tank are described in the present report.

The physical and mathematical model of unsteady turbulent mixing and combustion of multiphase propellants in weightlessness is described in the First Preliminary Report on the SPC 94-4107 [6].

The results of numerical modelling of combustion of purely gaseous components (fuel and oxidant) in a turbulent jet forming after a breakup of the common bulkhead is described in the Second (Interim) Report [7].

The present report contains the results of theoretical investigation of the influence of diameter of a hole in the bulkhead and the initial pressure gap on the rate of internal wall loading of the fuel tank.

The dynamical deforming and breakup of a shell under the influence of internal loading is investigated.

The number and mass distribution of fragments and its acceleration in the expanding flow of gas after the breakup is determined.

The third part of the present report contains a description of the software created to simulate the energy release involved in mixing hypergolic propellants and breakup phenomena.

# Part 1.

## Theoretical investigation of energy release in combustion of mixing hypergolic propellants inside a fuel tank, overpressurisation and breakup of the tank

The present part describes a theoretical background of the investigation of peculiarities of the energy release in the process of mixing of hypergolic propellants after a destruction of the common bulkhead separating components.

The §1.1 contains a mathematical model of the process providing the possibility to simulate the turbulent jet of one component penetrating the tank filled with the other component through a hole in the bulkhead taking into account the energy release in a turbulent diffusion flame established in the flow.

§1.2 describes mathematical model applied to simulate dynamical deforming and failure of the walls of the tank.

§1.3 is devoted to calculations of breakups of shells.

The fragments' velocity distribution is discussed in §1.4 and §1.5.

### §1.1. Mathematical modelling of unsteady combustion of nonpremixed propellants.

We regard the unsteady motion, turbulent mixing and combustion of gaseous components in a cylindrical vessel. At the initial instant the reactants are separated by a common bulkhead. The main parameters: pressures, temperatures, densities - are uniform in both containments, but pressures are essentially different. A hole of a definite area is opened in the bulkhead in the axis of symmetry instantaneously at time $t = 0$, that causes formation of compression and rarefaction waves in both containments. A turbulent jet of components penetrates the low pressure chamber and rarefaction wave propagates in the high pressure chamber.

Mixing of components initiates combustion in a low pressure chamber that leads to a rapid pressure increase and wall loading. Thus, main governing parameters of the process are the initial pressure ratio in both tanks and the size of the hole. These parameters are supposed to be varied within the numerical modelling to investigate different probable scenario of the development of the process.

The modified $k - \varepsilon$ model of turbulence will be used to describe the gas flow, mixing and combustion of components. Among all the chemical components involved in the process we will distinguish three groups: fuel, oxidant, reaction products. We assume that only these components play decisive role and that there is no necessity to distinguish all the intermediate and final products of thermal destruction of fuel and oxidant. We define $Y_k$ the mass concentration of the $k$-th component where $k = 0$ relates to oxidant, $k = f$ relates to fuel and $k = p$ relates to reaction products.

The mass balance equations for the $k$-th component has the following form:

$$\frac{\partial \rho_k}{\partial t} + \nabla \cdot (\rho_k \vec{u}_k) = \dot{\mathcal{M}}_k, \tag{1}$$

where $\rho_k$ is the density of a component, $\vec{u}_k$ is the velocity vector for this component, $\dot{\mathcal{M}}_k$ is the rate of mass increase per volume unit due to chemical reaction.

We involve the following notations and definitions: $\rho = \sum \rho_k$ - average density of the gas, $\vec{u} = \frac{1}{\rho} \sum_k \rho_k \vec{u}_k$ - mean velocity; $\vec{w}_k = \vec{u}_k - \vec{u}$ - the rate of diffusion of the $k$-th component, $I_k = \rho_k \vec{w}_k$ - the diffusive flux, $Y_k = \rho_k / \rho$ - mass concentration of the $k$-th component.

It follows from the definitions that

$$\sum_k Y_k = 1; \quad \sum_k I_k = 0.$$

The mass balance equation (1) can be transformed into:

$$\frac{\partial}{\partial t} \rho Y_k + \nabla \cdot (\rho \vec{u} Y_k) = \dot{\mathcal{M}}_k - \nabla \cdot I_k. \tag{2}$$

Summing up the equations (2) by all the components gives us the mass balance equation:

$$\frac{\partial \rho}{\partial t} + \nabla \cdot (\rho \vec{u}) = 0. \tag{3}$$

Averaging by Favre with the $\rho$ weight we obtain from (3) the averaged mass balance equation

$$\frac{\partial \bar{\rho}}{\partial t} + \nabla \cdot (\bar{\rho} \tilde{u}) = 0. \tag{4}$$

Averaging (2) in the same way and involving a notation $I_k^t = \bar{\rho} \widetilde{u'' Y_k''}$ for turbulent diffusion flux we obtain the averaged mass balance equation for the $k$-th component:

$$\frac{\partial \bar{\rho} \widetilde{Y}_k}{\partial t} + \nabla \cdot (\bar{\rho} \vec{\tilde{u}} \widetilde{Y}_k) = \overline{\dot{\mathcal{M}}_k} - \nabla \cdot (\bar{I}_k + I_k^t). \tag{5}$$

The momentum equation has the form:

$$\frac{\partial}{\partial t} \rho \vec{u} + \nabla \cdot (\rho \vec{u} \otimes \vec{u}) = -\nabla p + \rho \vec{g} + \nabla \cdot \tau, \tag{6}$$

where $p = \sum_k p_k$ is a total pressure in gas according to Dalton's law;

$$\tau = \sum_k \left( \tau_k - \frac{1}{\rho_k} I_k \otimes I_k \right)$$

is a viscous stress tensor for multicomponent flow; $-\frac{1}{\rho_k} I_k \otimes I_k$ - components of the tensor of diffusion stresses. Averaging (6) by Favre we obtain:

$$\frac{\partial}{\partial t} \bar{\rho} \vec{\tilde{u}} + \nabla \cdot (\bar{\rho} \vec{\tilde{u}} \otimes \vec{\tilde{u}}) = \bar{\rho} \vec{g} - \nabla \bar{p} - \nabla \cdot (\bar{\tau} + \tau^t), \tag{7}$$

where $\tau^t = -\bar{\rho}\vec{u}'' \otimes \vec{u}''$ is the Reynolds stress tensor.

To derive the energy balance we assume the gas being a mixture of perfect gases:

$$e_k = c_{vk}T + h_{0k}, \qquad p_k = \frac{R_g}{W_k}\rho_k T,$$

where $T$ is temperature, $c_{vk}$ - heat capacity of the $k$-th component at constant volume, $W_k$ is molar mass, $R_g$ - universal gas constant, $h_{0k}$ - chemical energy of the $k$-th component.

The total mixture energy $E$ and generalized heat flux $I_q$ for multicomponent gas mixture are determined in the following way:

$$E = \sum_k Y_k E_k = \sum_k \left(Y_k e_k + \frac{I_k \cdot I_k}{2\rho_k^2}\right) + \frac{u^2}{2},$$

$$I_q = \sum_k \left[I_{qk} + h_k I_k - \left(\tau_k - p_k I - \frac{I_k \otimes I_k}{2\rho_k}\right) \cdot \frac{I_k}{\rho_k}\right] = J_q + \sum_k h_k I_k,$$

where $h_k = e_k + \frac{p_k}{\rho_k}$ is the enthalpy of $k$-th component, $I$ is a unit tensor.

The energy balance equation for the mixture has the following form

$$\frac{\partial}{\partial t}\rho E + \nabla \cdot (\rho \vec{u} E) = \rho \vec{u} \cdot \vec{g} - \nabla \cdot p\vec{u} - \nabla \cdot I_q + \nabla \cdot (\tau \cdot \vec{u}). \tag{8}$$

The terms of second and higher orders of diffusion fluxes will be neglected in the expression for mixture energy. The equations of state will have the form:

$$p = R_g \rho T \sum_k \frac{Y_k}{W_k}; \qquad e = \sum_k Y_k (c_{vk}T + h_{0k}).$$

Averaging by Favre one can obtain from (8) the following equation:

$$\frac{\partial}{\partial t}\bar{\rho}\tilde{E} + \nabla \cdot (\bar{\rho}\vec{\tilde{u}}\tilde{E}) = \bar{\rho}\vec{\tilde{u}} \cdot \vec{g} - \nabla \cdot (\bar{p}\tilde{u}) - \nabla \cdot (\bar{I}_q + I_q^t) + \nabla \cdot (\overline{\tau \cdot u} + \tau^t \cdot \tilde{u}), \tag{9}$$

where

$$I_q^t = \bar{\rho} \sum_k c_{pk} \bar{Y}_k \widetilde{u''T''} + \sum_k \left(c_{pk}\widetilde{T} + h_{0k}\right) I_k^t = J_q^t + \sum_k (c_{pk}T + h_{0k}) I_k^t$$

is the generalized turbulent heat flux; $\widetilde{E} = \sum_k \bar{Y}_k (c_{vk}\widetilde{T} + h_{0k}) + \frac{\tilde{u}^2}{2} + k$ - the total mixture energy; $k$ is the average kinematic energy of turbulent pulsations.

To close the system of equations the standard $k$-epsilon model of turbulence for compressible flows is made use of.

The turbulent fluxes are modelled in the following way

$$\bar{\tau} + \tau^t = \bar{\rho}(\nu + \nu^t)\left(\nabla\vec{\tilde{u}} + \nabla\vec{\tilde{u}}^T - \frac{2}{3}\nabla \cdot \vec{\tilde{u}} I\right) - \frac{2}{3}\bar{\rho}kI,$$

$$\bar{I}_k + I_k^t = \bar{\rho}\left(D + \frac{\nu^t}{\sigma_i}\right)\nabla \cdot \bar{Y}_k, \tag{10}$$

$$\bar{J}_q + J_q^t = -\left(\bar{\lambda} + \bar{\rho} c_{pk} \frac{\nu^t}{\sigma_t}\right)\nabla \cdot T,$$

where $I$ is a unit tensor of the second order, $\nabla \vec{\tilde{u}}^T$ is the transposed matrix $\nabla \vec{\tilde{u}}$; $\nu$ - molecular kinematic viscosity; $\nu^t$ - turbulent kinematic viscosity; $D$ - mean molecular diffusion coefficient; $\bar{\lambda}$ - mean heat conductivity coefficient for mixture.

The energy dissipation term in the equation (9) is assumed to be transformed in the following way:

$$\nabla \cdot \left(\overline{\tau \cdot \vec{u}} + \tau^t \cdot \vec{\tilde{u}}\right) = \nabla \cdot \left((\bar{\tau} + \tau^t) \cdot \vec{\tilde{u}}\right).$$

The turbulent kinematic viscosity is modelled according to the $k$-epsilon model:

$$\nu^t = C_\mu^0 f_\mu \frac{k^2}{\varepsilon}, \tag{11}$$

where $\varepsilon$ is the dissipation of turbulent pulsations.

The model is closed by the two equations for the kinetic energy of turbulent pulsations $k$ and its decay due to dissipation $\varepsilon$:

$$\frac{\partial}{\partial t}(\bar{\rho}k) + \nabla \cdot (\bar{\rho}\vec{\tilde{u}}k) = \nabla \cdot \left(\bar{\rho}(\nu + \frac{\nu^t}{\sigma_k})\nabla k\right) + \tau^t : \nabla \tilde{u} - \bar{\rho}\varepsilon, \tag{12}$$

$$\frac{\partial}{\partial t}(\bar{\rho}\varepsilon) + \nabla \cdot (\bar{\rho}\vec{\tilde{u}}\varepsilon) = \nabla \cdot \left(\bar{\rho}(\nu + \frac{\nu^t}{\sigma_\varepsilon})\nabla \varepsilon\right) + \frac{\varepsilon}{k}\left(C_{1\varepsilon}\tau^t : \nabla \tilde{u} - C_{2\varepsilon}\bar{\rho}\varepsilon\right). \tag{13}$$

To take into account the near-wall damping effect the coefficients $C_\mu$, $C_{1\varepsilon}$, $C_{2\varepsilon}$ of the original $k$-epsilon model are modified in accordance with the so-called "Low Reynolds" models [8]. Those coefficients are

$$C_\mu = C_\mu^0 f_\mu; \qquad C_{1\varepsilon} = C_{1\varepsilon}^0 \frac{f_1}{f_\mu}; \qquad C_{2\varepsilon} = C_{2\varepsilon}^0 f_2, \tag{14}$$

where $f_\mu$, $f_1$, $f_2$ are positive functions such that $0 < f_\mu \leq 1$; $1 \leq f_1$; $0 < f_2 \leq 1$, and which depend on two local Reynolds numbers

$$R_t = \frac{k^2}{\nu\varepsilon}; \qquad R_y = \sqrt{k}\frac{y}{\nu}, \tag{15}$$

where $y$ is a distance from the nearest wall. For the Lam-Bremhorst low Reynolds $k$-$\varepsilon$ model the functions are determined in the following way:

$$f_\mu = \left[1 - \exp(-0.0165 R_y)\right]^2 (1 + 20.5/R_t),$$

$$f_1 = 1 + \left(\frac{0.05}{f_\mu}\right)^3, \tag{16}$$

$$f_2 = 1 - \exp(-R_t^2).$$

The values of the constants of the $k$ - $\varepsilon$ model are the following:

$$C_\mu^0 = 0.09; \qquad \sigma_k = 1; \qquad \sigma_\varepsilon = 1.3; \tag{17}$$

$$C_{1\varepsilon}^0 = 1.45; \qquad C_{2\varepsilon}^0 = 1.92; \qquad \sigma_i = \sigma_t = \sigma_y = 1.$$

The wall boundary conditions for $k$ and $\varepsilon$ are:

$$k = 0; \qquad \frac{\partial \varepsilon}{\partial \vec{n}} = 0, \tag{18}$$

$\vec{n}$ - normal vector to the wall.

The boundary conditions on the walls for the other components are the following:

$$\vec{u}_n|_\Gamma = 0; \qquad \vec{u}_\tau|_\Gamma = 0; \tag{19}$$

$$\frac{\partial Y_k}{\partial \vec{n}}|_\Gamma = 0; \qquad \frac{\partial T}{\partial \vec{n}}|_\Gamma = 0.$$

Thus, it is assumed that the walls of the tank are noncathalitic and adiabatically isolated and there is no slip condition on the wall.

The initial conditions are the following: uniform pressure, temperature and concentrations distributions in both sections of the tank, -

$$x > 0: \quad p = p_{f0}; \quad T = T_{f0}; \quad Y_f = 1; \quad Y_0 = 0; \quad Y_p = 0;$$

$$x < 0: \quad p = p_{00}; \quad T = T_{00}; \quad Y_f = 0; \quad Y_0 = 1; \quad Y_p = 0; \tag{20}$$

$$p_{00} > p_{f0}.$$

Hypergolic propellants have a very low temperature of ignition and chemical reaction practically starts at any temperature as soon as the reactants come in contact. The kinetic rate of chemical reaction is also very high and in combustion of hypergolic propellants the process is more limited by diffusive transport of the reactants to the reaction zone than by kinetics. To describe this process a concept of diffusion flame can be rather fruitful. Diffusive flame represents a rather thin zone of chemical reactions (it can be wrinkled, of course), where the concentrations of reaction products are very high and the concentrations of the reactants are low due to the fact that reactants are unable to penetrate deep through the flame not entering into the reaction. The rate of chemical transformation is determined by the fluxes of fuel and oxidant to the flame zone due to molecular and turbulent diffusion. One of the difficulties of the problem we are going to solve is that the location of a diffusive flame is not known in advance and the flame evolves in the zone of turbulent mixing of the components.

To model mathematically a chemical reaction we shall use the following approach: consider the rate of reaction depending on the product of mass concentration of species both present simultaneously in one and the same macroscopically small volume. This product is a limiting factor because on consuming of one of the reagents (fuel or oxidant) the reaction terminates. A coefficient of large value in the formula replaces for hypergols the usual Arrhoeneous dependence of temperature applied for conventional fuels. To

garantee the stability of the calculations we need to use the two-step scheme with correction of the reaction rate. The reaction rate is given by a formula

$$\tilde{\omega} = A(\frac{\rho Y_0}{W_0})^{\nu_0}(\frac{\rho Y_f}{W_f})^{\nu_f}, \tag{21}$$

where $A$ is a dimensional coefficient of a large value; $W$ - molar mass of the reagents; subscripts 0, $f$ relate to oxidant and fuel respectively, $\nu_0$, $\nu_f$ - stoichiometric coefficients of the reactants.

The mass rates of production of components in chemical reaction are given by the following formulae:

$$\begin{aligned} \dot{m}_0 &= -\nu_0 W_0 \tilde{\omega}; \\ \dot{m}_f &= -\nu_f W_f \tilde{\omega}; \\ \dot{m}_p &= \nu_p W_p \tilde{\omega}; \end{aligned} \tag{22}$$

where subscript "p" relates to the reaction products.

On the second step we choose the stabilizing parameters $q_0$, $q_f$, $q_p$ to stabilize the calculations of component consumption equations (5)

$$\begin{aligned} q_0 &= \min\left\{1,\ 0.3\frac{\max\{\rho Y_0, 0.01\}}{|\dot{m}_0| h_t}\right\}; \\ q_f &= \min\left\{1,\ 0.3\frac{\max\{\rho Y_f, 0.01\}}{|\dot{m}_f| h_t}\right\}; \\ q_p &= \min\left\{1,\ 0.3\frac{\max\{\rho Y_p, 0.01\}}{|\dot{m}_p| h_t}\right\}, \end{aligned} \tag{23}$$

then choose a unique stabilizing parameter for all components:

$$q = \min\{q_0, q_f, q_p\},$$

and determine the corrected value of the chemical reaction rate

$$\omega = \tilde{\omega} \cdot q. \tag{24}$$

Then the final rates of chemical reactions in the equations (5) are determined by formulae:

$$\begin{aligned} \dot{\mathcal{M}}_0 &= -\nu_0 W_0 \omega; \\ \dot{\mathcal{M}}_f &= -\nu_f W_f \omega; \\ \dot{\mathcal{M}}_p &= \nu_p W_p \omega. \end{aligned} \tag{25}$$

To determine the reaction rate $\omega$ we shall use the notation

$$\dot{\mathcal{Y}} = (\frac{\rho Y_0}{W_0})^{\nu_0}(\frac{\rho Y_f}{W_f})^{\nu_f}, \tag{26}$$

that will be named the intensity of the reaction. Thus, the final formula for the rate of chemical reaction will take the form

$$\omega = A\dot{\mathcal{Y}}q. \tag{27}$$

Maximal values of $\dot{\mathcal{Y}}$ show the location of flame zone in the turbulent flow.

The numerical procedure to solve the above system of equations for turbulent flow of viscous heat conductive chemically reacting mixture of gases in a bounded volume was described in [7]. We regard an axisymmetrical two-dimensional unsteady-state problem. To solve the system we involve splitting by coordinates: it simplifies the procedure and increases the possible time step. The splitting is done according to MacCormack [9 - 12].

## §1.2. Internal loading of the walls of the tank

Generally internal loading of the walls of the tank in diffusive combustion of propellants is not uniform due to nonuniformities of combustion process and energy release caused by initial nonuniformities of concentrations of species. Results of numerical modelling for pressure isolines (see Ref.[7] and Part 3 of the present paper) show the nonuniformity of pressure distribution near the wall. Theoretical models of dynamical internal loading of the shell [3] show that the internal stressses in the shell depend upon loading of the shell by internal pressure $p(t)$. Nonuniformities of initial pressure distribution will cause the initial nonuniformities in shell stresses that will lead to dilatant wave propagation in the shell itself. The velocity of those waves will be

$$c_s = \sqrt{\frac{E}{(1-\nu^2)\rho_{s0}}}, \tag{28}$$

where $E$, $\nu$ are the Young modulus and Poisson coefficient of the material of the shell, $\rho_{s0}$ - density of the material in the initial undisturbed condition.

Stress wave propagation in the shell lead to creating a uniform stress field in the shell in a way similar to how compression and rarefaction waves in gas contribute to establishing a uniform pressure distribution inside the tank. The main difference is that characteristic wave propagation velocities in the shell $c_s$ are of the order of magnitude higher than that in gas. Thus, the field of stresses in the shell will be uniform much earlier than that in the gas phase.

To perform some simple estimates one must examine the characteristic duration of the process of energy release inside a tank in diffusive conbustion. Results of numerical modelling show that for a tank of characteristic size $r = 1$ m (see [7]) the characteristic time of combustion is: $\tau_c = 10^{-3} \div 10^{-2}$ s.

The wave propagation velocity in alluminium alloy (28) is approximately 4.5 km/s.

Thus, the characteristic length of wave propagation during the combustion process for the model tank will be

$$L_s = 4.5 \div 45 \text{ m}$$

that is much larger than the characteristic size of the tank itself.

The estimates show that under these conditions the assumption of the uniform stress field established inside the shell by the end of combustion process is quite reasonable, while some nonuniformities in a pressure field inside the tank can be still present.

The characteristic times for wall loading and dynamical deforming of the walls are much less than that for combustion process: $\tau_e \approx 10^{-4}$ s. Thus dynamical deforming of the shell and breakup at early stages could be determined locally, while at later stages it should be regarded with account of averaged stresses.

To solve the problem we shall make use of the approach developed in [3] for a thin-walled shell. The following basic assumptions will be made:

1. The shell is thin $h/r_* \ll 1$ ($h$ - thickness, $r_*$ - effective radius).
2. The material is considered to be elastoviscoplastic.
3. The field of tensile stresses is supposed to be uniform.

4. Momentum equation for a shell is solved locally with account of local internal loading, tensile stresses and spherical curvature with effective radius $r_*$.
5. The breakup conditions are considered to be determined on the basis of the entropic criterion of a limit specific dissipation [3].
6. The breakup process is supposed to take place as a result of the action of tensile ring stresses, consuming the elastic energy accumulated in the shell by the time of breakup.
7. The work of external forces in the breakup time, transformation of some part of elastic energy into the kinetic energy of fragments and spallation effects are not taken into consideration.

Then the momentum equation has the form:

$$\rho_s \dot{v} = \frac{p(t)}{h} - 2\frac{\sigma_\theta}{r}, \tag{29}$$

where $\rho_s$ - density, $v$ - radial velocity, $r$ - current value of the shell radius of curvature, $\sigma_\theta$ - ring stress (the averaged stress over the shell thickness), a dot over a symbol means a material derivative with respect to time.

The rate of ring deformation is determined by:

$$\dot{\varepsilon}_\theta = \frac{v}{r}, \tag{30}$$

other deformations are absent due to the shell thinness.

The equation of mass conservation has the form $\dot{\rho}_s/\rho_s = -2\dot{\varepsilon}_\theta$ from where we have:

$$\rho_s = \rho_{s0}\exp(-2\varepsilon_\theta), \tag{31}$$

where $\rho_0$ is the initial density.

State equations of elastoviscoplastic material for a spherical case have the following form:

$$\dot{S}_\theta = \frac{2}{3}\mu\dot{\varepsilon}_\theta - \frac{\mu}{\eta}S_\theta\left(1 - \frac{J_0}{3|S_\theta|}\right)H\left(1 - \frac{J_0}{3|S_\theta|}\right), \tag{32}$$

where $\| S \|$ is a deviator of a stress tensor:

$$\sigma_\theta = \sigma + S_\theta, \quad \sigma_\varphi = \sigma_\theta, \quad \sigma_r = \sigma + S_r = 0, \quad 2S_\theta + S_r = 0;$$

$$\sigma_\theta = 3S_\theta. \tag{33}$$

Here $\mu$ - shear modulus, $\eta$ - dynamic viscosity of material, $J_0$ - static limit of elasticity in simple tension, $H(x)$ - the unit Heavyside function. Herewith the stress tensor $\sigma_{ij}$ is divided into spherical $\sigma\delta_{ij}$ and deviator $S_{ij}$ partials and it is assumed that rates of deformations can be divided into the rates of elastic and plastic ones and a plastic flow is incompressible:

$$\dot{\varepsilon}_\theta = \dot{\varepsilon}^e_\theta + \dot{\varepsilon}^p_\theta, \quad \dot{\varepsilon}_\varphi = \dot{\varepsilon}_\theta, \quad \dot{\varepsilon}_r = \dot{\varepsilon}^e_r + \dot{\varepsilon}^p_r = 0, \quad 2\dot{\varepsilon}^p_\theta + \dot{\varepsilon}^p_r = 0. \tag{34}$$

Specific (per mass unit) elastic energy $E$ and mechanical dissipation $D$ can be determined by integration of the formulae:

$$\dot{E} = 2\frac{\sigma_\theta}{\rho}\dot{\varepsilon}^e_\theta, \quad \dot{D} = 2\frac{\sigma_\theta}{\rho}\dot{\varepsilon}^p_\theta. \tag{35}$$

Rates of elastic and plastic deformations are determined by the formulae:

$$\dot{\varepsilon}_\theta^e = \frac{\dot{S}_\theta}{2\mu} + \frac{2}{3}\dot{\varepsilon}_\theta, \qquad \dot{\varepsilon}_\theta^p = \dot{\varepsilon}_\theta - \dot{\varepsilon}_\theta^e. \tag{36}$$

Calculation of the shell temperature in deforming for adiabatic approximation can be performed by the following procedure:

$$\rho c_\sigma \dot{T} + 2\alpha_v \dot{S}_\theta T = 6 S_\theta \dot{\varepsilon}_\theta^p. \tag{37}$$

Herein $c_\sigma$ is the heat capacity at constant stresses, $\alpha_v$ is the coefficient of volumetric expansion.

Criterion of the shell breakup is the entropic criterion of a limit specific dissipation that for the model considered is reduced to mechanical dissipation:

$$D|_{t=t_*} = D_*, \tag{38}$$

where $D_*$ is the constant of limit specific dissipation determined with using the experiments on spalation fracture in a plane collision of plates [13]. A detailed description of the method of determining the critical dissipation $D_*$ was given in [3].

The equation of state of material (32) contains static elasticity modulus in simple tension $J_0$ and shear modulus as parameters. It is known that in dynamical deforming of materials with essential changes of temperature, density, pressure and with growth of plastic deformations these parameters undergo changes. The elasticity limit $J_0$ and shear modulus $\mu$ are assumed to change in accordance with Steinberg-Guinan model [14]:

$$J_0 = J_0^0(1+\beta\varepsilon_u^p)^n\big(1 - \beta\sigma\big(\frac{\rho_{s0}}{\rho_s}\big)^{1/3} - \chi(T_s - T_0)\big), \tag{39}$$

$$J_0^0(1+\beta\varepsilon_u^p)^n \le J_{max},$$

$$\mu = \mu_0\big(1 - b\sigma\big(\frac{\rho_{s0}}{\rho_s}\big)^{1/3} - \chi(T - T_0)\big). \tag{40}$$

Here $J_0^0$, $\mu_0$ are values of parameters under the normal conditions, $\varepsilon_u^p = 2|\varepsilon_\theta^p|$ is the intensity of plastic deformations; $\beta$, $n$, $b$, $\chi$, $J_{max}$ are constants of the material. These constants for many materials present in [14].

The last term in the equation (39) shows that there is a dependence of elasticity limit on the mean wall temperature $T_s$. This temperature changes due to adiabatic heating of material in deformations and due to conductive heating of the wall contacting hot reaction products in combustion process.

The increase of temperature in dynamical deforming of the shell can be described by the equation (37).

The conductive heating of the wall depends upon the internal temperature of gases and the average expected time of heating. Results of numerical modelling of diffusive combustion inside tanks ([7] and Part 3 of the present report) show that temperatures of gas near the walls can reach 3000 K in some places. That brings us to the necessity of estimating the wall heating in combustion process. The exact solution of the problem of heating of a wall being in contact with nonuniform varying with time gas flow is rather

complicated. Thus, to obtain simple estimates we'll use the following approach. The characteristic velocity of the thermal wave propagation in the material is

$$c_t = \frac{1}{2}\sqrt{\frac{\lambda_s}{\rho_s c_\sigma \tau}}, \tag{41}$$

where $\lambda_s$ is a heat conductivity coefficient, $\tau$ - characteristic time of the process. Assuming that the material of the wall is characterized by the following parameters:

$$\lambda_s = 10^2 \text{ w/m} \cdot \text{K}; \quad \rho_s = 2.7 \cdot 10^3 \text{ kg/m}^3;$$

$$c_\sigma = 934 \text{ J/kg} \cdot \text{K};$$

and characteristic time of the process $\tau_c = 10^{-3} \div 10^{-2}$ s, one obtains the values of velocities

$$c_t = 0.03 \div 0.09 \text{ m/s}.$$

The above estimates show that for the walls $2 \div 3$ mm thick the conductive heating during characteristic times $\tau_c \approx 10^{-3} \div 10^{-2}$ s will be negligibly small.

One can easily come to a conclusion that in case the destruction criterion is satisfied within the characteristic time of a rapid pressure increase in combustion, the conductive heating doesn't play any important role in the breakup process.

The situation can turn out to be different for the cases when the destruction criterion is not satisfied during the time of combustion. The shell is deformed and loaded by the end of combustion process and can stay in the position for a long time. Then the characteristic time of the whole process regarded can surpass the characteristic time of heat conductivity:

$$\tau_h = h^2/(\frac{\lambda_s}{\rho_s c_\sigma}). \tag{42}$$

By that time the increase of mean temperature of the wall can play an important role in the breakup process. The increase of temperature $T_s$ will lead to the decrease of elasticity limit $J_0$ (equation (39)) that leads in turn to the decrease of tensile stress $\sigma_\theta$, elastic strains $\varepsilon_\theta^e$ and causes increase of plastic strains $\varepsilon_\theta^p$ (equations (32), (33), (36)). Elastic energy accumulated by the shell will decrease and dissipation $D$ will increase (35).

Thus, the increase of temperature can lead to the situation when the increased dissipation $D$ surpasses the critical value $D_*$ and the criterion of breakup is satisfied (38). Under these conditions the breakup process can take place much later after combustion and energy release processes are terminated. By the time pressure turns out to be uniform inside the tank and temperature uniformity is achieved due to intensive turbulent mixing of gases inside the tank and heat conductivity processes. To get rough estimates of temperature growth inside the walls we'll use the following approach. Consider that the heated zone propagates with the velocity of a thermal wave. Then

$$\Delta T_s = \begin{cases} \frac{1}{2h}(T_{av} - T_0) \int_0^t c_t dt; & t \le \tau_h \\ \frac{1}{2}(T_{av} - T_0); & t > \tau_h; \end{cases} \tag{43}$$

and the dynamics of mean wall temperature $T$ in time can be determined from (37) and (43) by the following formula

$$T(t+\Delta t) = T(t) + \frac{1}{\rho_{s0} c_\sigma}\Big(6 S_\theta \dot{\varepsilon}^p_\theta - 2\alpha_v \dot{S}_\theta T(t)\Big)\Delta t + \\ + \sqrt{\frac{\lambda_s}{\rho_{0s} c_\sigma}} \frac{T_{av} - T_0}{2h}\big(\sqrt{t+\Delta t} - \sqrt{t}\big) H(\tau_h - t); \qquad (44)$$

where $H(x)$ is the unit Heavyside function; $T_{av}$ - average temperature inside the tank near the wall. This temperature depending on characteristic time of the process can be determined either locally or with account of mixing inside the tank

$$T_{av} = \int_V \rho T dv \Big/ \int_V \rho dv.$$

Summing up the assumptions of the model it should be mentioned that the process under consideration can have three characteristic times:
the characteristic time of wave propagation inside the shell itself $\tau_w = R^*/c_s$;
the characteristic time of gasdynamics processes inside the tank $\tau_c$;
the characteristic time of heat conductivity $\tau_h$.

The gasdynamics time is usually determined by a ratio

$$\tau_c = \frac{r^*}{a_c}, \qquad (45)$$

where $a_c$ is a sound velocity in gas. But within the frames of the problem regarded the gasdynamics processes are burdened with chemical processes and diffusive mixing. Thus, we determine the characteristic time $\tau_c$ not from the formula (45) but rather from the numerical solution of the problem of diffusive combustion of hypergolic propellants inside a fuel tank.

The following relationship between the characteristic times is valid:

$$\tau_w \ll \tau_c \ll \tau_h; \qquad (46)$$

$$\tau_w = \frac{r^*}{c_s} = \frac{r^*}{\sqrt{\dfrac{E}{(1-\nu^2)\rho_{s0}}}}; \qquad \tau_c = \frac{r^*}{a_c}; \qquad \tau_h = \frac{h^2 \rho_{s0} c_\sigma}{\lambda}.$$

Since we are examining the breakup process the characteristic time for our problem $\tau_p$ will be the time interval between the destruction of the common bulkhead and the breakup of the whole tank.

If $\tau_p \sim \tau_w$ then nonuniformity of parameters both in the shell and in the gas phase is essential, heat conductivity doesn't play any role.

If $\tau_p \sim \tau_c$, then only gas phase nonuniformities are essential, and nonuniformities in the shell and heat conductivity do not play any role.

If $\tau_p \sim \tau_h$ then nonuniformities of stresses in gas and shell are not important but heat conductivity can play an important role.

Analyzing the problem we found out that

$$\tau_p > \tau_c.$$

Thus, it is necessary to foresee several possibilities within the frames of numerical modelling: breakup conditions can be reached within the time of combustion ($\tau_p \sim \tau_c$), the criterion of destruction can be satisfied after considerable heating of the shell ($\tau_p \sim \tau_h$), or the breakup criterion can be never satisfied ($\tau_p \longrightarrow \infty$).

## §1.3. Calculations of Breakups of Shells Under the Influence of Internal Loading

As soon as the destruction criterion (38) is satisfied:

$$D \geq D_*, \tag{47}$$

a breakup of a shell takes place. The number of fragments obtained in a shell breakup can be found from the balance of the elastic energy accumulated by a shell by the time of breakup and the work necessary for breaking off the material. To describe the probability distribution function of fragments in terms of mass in explosive destruction of shells the Weibull distribution will be used [3]:

$$N(< m) = N_0\left[1 - \exp\left(-(\frac{m}{m_*})^{\Lambda}\right)\right]. \tag{48}$$

Here $N(< m)$ is the number of fragments with mass less than $m$; $N_0$ is the total number of fragments with mass more than 0 (a theoretical constant); $m_*$ - the characteristic mass of distribution; $\Lambda$ - the index of fragmentation quality.

In case $\Lambda$ and $m_*$ satisfy the conditions of unimodal distribution [3] the formula (48) describes satisfactory the mass distribution of fragments in breakup or rather thin shells subjected to uniform loading. In more complex cases of breakup a two-modal hyperweibull distribution was suggested.

In our case the scenario of fragmentation for small characteristic times of the process $\tau_p$ can differ from that described in [3] for the case of uniform loading. The breakup can start in the zones of maximal internal loading and then cracks will develop in the zones of lower internal loading but with the same level of tensile ring stresses. The first stage of the process within the zones of high internal loading is initiated by the increase of internal pressure and growth of dissipation $D$.

In the zones of lower internal loading the rate of loading is not enough to initiate the breakup process. Thus in the second stage the breakup process is initiated by the cracks coming from the damaged zone.

The common point of the both scenario is that in both cases the destruction is governed by the balance of the accumulated elastic energy and the work consumed to break the material (to form the cracks).

The difference of mechanisms leads to the different spectra of mass distribution of fragments. Thus generally it could be necessary to use two distributions of the type (48) with different parameters to describe these two zones of breakup.

For relatively high values of characteristic time ($\tau_p > \tau_c$) theory developed in [3] for one unimodal distribution (48) is appliable.

Here we shall describe the theoretical background of breakup investigation. Let an area of an initial external lagrangian surface of a fragment be equal to $s$, its internal surface to be also equal to $s$ (due to the shell thinness) and area of its lateral surface $2ph$ where $p$ is the semiperimeter of the contour $s$. The fragment's mass is $m = \rho_0 hs$, therefore distribution in terms of mass (48) can be presented in the form of distribution in terms of areas $s$ of fragments:

$$N(< s) = N_0 F(s), \tag{49}$$

where

$$F(s) = \begin{cases} 1 - \exp\left(-\left(\frac{s-s_{min}}{s_*}\right)^{\Lambda}\right), & s_{min} < s < s_{max} \\ 0, & s < s_{min} \\ 1, & s > s_{max} \end{cases} \tag{50}$$

Formula (50) involves the following notations:
$s_{min}$ - minimal possible area of fragment,
$s_{max}$ - maximal possible area of fragment.

Both values are to be determined in the process of solution.

Parameters $\Lambda$ and $s_*$ characterize the distribution function $F(s)$ and could be determined from an independent experiment.

We shall use the values of these parameters determined in [3] for breakup of thin shells on the basis of the experiment ESOC 2-3.

The fragmentation of the tank will be regarded locally with account of nonuniformity of internal loading resulting in nonuniformity of elastic energy distribution inside the shell.

The total lagrangian area of the tank is divided into several sections. Let the sections be numbered $\alpha = 1, ..., L$.

The mean value of elastic energy is calculated in each section

$$E_{*\alpha} = \frac{1}{S_\alpha} \iint_{S_\alpha} E_* ds. \tag{51}$$

The density of distribution of fragments versus area can be obtained from formulae (49), (50):

$$N(ds) = N_{0\alpha} f(s) ds = N_{0\alpha} F'(s) ds; \tag{52}$$

$$f(s) = \begin{cases} 0, & s < s_{min}; \\ \frac{\Lambda}{s-s_{min}} \left(\frac{s-s_{min}}{s_*}\right)^{\Lambda} \exp\left(-\left(\frac{s-s_{min}}{s_*}\right)^{\Lambda}\right), & s_{min} < s < s_{max}; \\ 0, & s > s_{max}. \end{cases}$$

The total area of fragments must be equal to the initial area of section $S_\alpha$

$$S_\alpha = \int_0^\infty sN(ds) = N_{0\alpha} \int_0^\infty sf(s)ds. \tag{53}$$

Taking into account the type of the function $f(s)$ (52) one can obtain the following formula

$$S_\alpha = N_{0\alpha} \int_{s_{min}}^{s_{max}} sf(s)ds. \tag{54}$$

The function $f(s)$ has singularity at $s = s_{min}$ for the values $\Lambda < 1$. But the integral is finite

$$\int_{s_{min}}^{s_{max}} sfds \approx s_* \Big[\delta_{max} \exp\left(-\left(\delta_{max} - \delta_{min}\right)^{\Lambda}\right) + \\ + \int_{\Delta}^{\delta_{max}-\delta_{min}} \Lambda(y + \delta_{min}) y^{\Lambda-1} \exp(-y^{\Lambda}) dy + \frac{\Lambda}{\Lambda+1} \Delta^{\Lambda+1} + \delta_{min} \Delta^{\Lambda} \Big],$$

where $\delta_{max} = s_{max}/s_*$; $\delta_{min} = s_{min}/s_*$; $\Delta \ll 1$ - small parameter, determining the precision of calculating the integral (54).

Thus to determine $N_{0\alpha}$ one obtains formula, that follows from (54):

$$N_{0\alpha} = S_\alpha \Big( \int_{s_{min}}^{s_{max}} s f(s) ds \Big)^{-1}. \tag{56}$$

To determine $s_{max}$ one must take into account that the maximal area of fragments can't exceed the total area of the section $S_\alpha$.

Formula (49) is valid under the assumption

$$N_0 > 1.$$

Thus following the assumption

$$N(< s) < N_0 : s_{min} < s < s_{max}$$

one can determine $s_{max}$ by formula

$$N(< s_{max}) = N_0 - 1,$$

that gives the following estimate

$$1 = N_{0\alpha} \exp\Big( -\big(\frac{s_{max} - s_{min}}{s_*}\big)^\Lambda \Big) \tag{57}$$

or

$$s_{max} = s_{min} + s_* \big(\ln\ N_0\big)^{1/\Lambda}. \tag{58}$$

Equations (56) and (58) give us the possibility to determine the values $N_{0\alpha}$ and $s_{max\alpha}$ for the section regarded.

The elastic energy $S_\alpha h \rho_0 E_*$, accumulated by the shell by the time of breakup $t = t_*$ is spent to form breakup surfaces around fragments

$$N_{0\alpha} \int_0^\infty \gamma h p(s) f(s) ds = S_\alpha h \rho_0 E_* k_E, \tag{59}$$

where $\gamma$ is the specific energy consumed for formation of the free surface unit, $p(s)$ is the semiperimeter of a fragment of the area $s$, $h$ - thickness of the shell, $k_E$ $(0 < k_E \leq 1)$ is the coefficient of elastic energy consumption for formation of breakup surfaces.

Equation (59) can be rewritten with account of (53) in the following form

$$N_{0\alpha} \int_0^\infty \big(p(s) - \frac{\rho_{0s} E_{*\alpha} k_E}{\gamma} s\big) f(s) ds = 0, \tag{60}$$

or with account of real density of distribution (52):

$$N_{0\alpha} \int_{s_{min}}^{s_{max}} \big(p - \frac{\rho_{0s} E_{*\alpha} k_E}{\gamma} s\big) f(s) ds = 0. \tag{61}$$

The relative arbitrariness of the limits of the integral (61) drives one to conclusion that the equation is satisfied when the function under integral equals to zero for all types of fragments:

$$p = \frac{\rho_{0s} E_{*\alpha} k_E}{\gamma} s. \tag{62}$$

Physically the equation (62) means that one half of the energy necessary to form a breakup surface around each fragment with area $s$ is extracted from the mass of fragment itself and the other half - from outside (from the neighbouring fragments).

On introducing a dimensionless coefficient of shape $k = s/p^2$ one obtains

$$k = \Big(\frac{\gamma}{\rho_{0s} E_{*\alpha} k_E}\Big)^2 / s. \tag{63}$$

For plane figures the shape coefficient changes within the limits:

$$0 < k \leq \frac{1}{\pi}. \tag{64}$$

The maximal value of $k$ corresponds to figure bounded by a circle. Thus the solution (62) gives us some restrictions for the smallest possible area of fragments within the section regarded:

$$s \geq \pi \Big(\frac{\gamma}{\rho_{0s} E_{*\alpha} k_E}\Big)^2, \tag{65}$$

thus determining $s_{min}$ for every section

$$s^{\alpha}_{min} = \pi \Big(\frac{\gamma}{\rho_{0s} E_{\alpha} k_E}\Big)^2, \quad \alpha = 1, ..., L. \tag{66}$$

Equations (56), (58) and (66) form a closed system to determine the number and distribution of fragments within each section.

In case the amount of elastic energy is too low and the restriction (65) prohibits formation of fragments

$$\pi \Big(\frac{\gamma}{\rho_{0s} E_{*\alpha 1} k_E}\Big)^2 > S_{\alpha 1}, \tag{67}$$

then two neighbouring sections can be reunified to form a section $S_{\alpha 12} = S_{\alpha 1} + S_{\alpha 2}$ and the restriction (65) is checked once more for the mean value of elastic energy $E_{*\alpha 12}$. The following possibilities are regarded:

1. The mean value of elastic energy is too low:

$$\pi \Big(\frac{\gamma}{\rho_{0s} E_{*\alpha 12} k_E}\Big)^2 > S_{\alpha 12}. \tag{68}$$

Then the reunification is done once more:

$$S_{\alpha 3} = S_{\alpha 1} + S_{\alpha 2} + S_{\alpha 3}.$$

2. The mean value of elastic energy is high:

$$\pi \Big(\frac{\gamma}{\rho_{0s} E_{*\alpha 12} k_E}\Big)^2 \leq S_{\alpha 12}. \tag{69}$$

Then the equations (61) - (64) are solved to determine the number and mass distribution function of fragments for the section $S_{\alpha 12}$.

To perform the calculations one should extract $K$ groups of fragments with definite areas $s_j$ $(j = 1, ..., K)$ from the total spectrum of the shell fragments. Then the number of fragments within each group can be determined by a formula:

$$N_{j\alpha} = \left[F_\alpha\left(\frac{s_j + s_{j+1}}{2}\right) - F_\alpha\left(\frac{s_{j-1} + s_j}{2}\right)\right] N_{0\alpha}. \qquad (70)$$

The total number of fragments of the $j$-th group obtained in a breakup of the whole vessel is determined by summing up all fragments of the size in all sections of the shell:

$$N_j = \sum_{\alpha=1}^{L} N_{j\alpha}. \qquad (71)$$

## §1.4. Velocity Distributions of Fragments

Theoretical models to determine final velocities of fragments in a breakup process for the case of uniform symmetrical loading were worked out in [3]. The formula to determine fragment's law of motion looks as follows:

$$m_j \frac{d\vec{v}_j}{dt} = -hs_j \frac{\partial p}{\partial r}|_{r=x} - \frac{c_d}{2} S\rho|\vec{v}_j - \vec{u}|(\vec{v}_j - \vec{u}), \tag{72}$$

$$\frac{dx_j}{dt} = \vec{v}_j,$$

where

$$S = s_j \cos\ \alpha + \left(h + \frac{l_j^2}{4r_0}\right) l_j \sin\ \alpha; c_d = c_d(\alpha, f_j), \qquad f_j = l_j^2/s_j,$$

$$m_j = \rho_s h s_j,$$

$m$ is the mass of a fragment, $\vec{v}$ - fragment's velocity, $\vec{u}$ - velocity of gas, $s_j$ - area of the surface (one side), $h$ - fragment's thickness, $c_d$ - the drag coefficient, $S$ - the effective area facing the flow, $\alpha$ is the angle of the orientation ($\alpha = 0$ if fragment is faced perpendicular to the flow), $l_j$ is the characteristic size of a fragment , $f$ is the shape coefficient, $r_0$ - the curvature radius of fragments.

The initial conditions for the equation (72) are the following:

$$t = 0: \qquad \vec{v}_j = \vec{v}_{j*}; \qquad x = r_{0j}, \tag{73}$$

where $\vec{v}_{j*}$ is the velocity of the shell just before the breakup.

Analyzing the equation (72) drives us to the conclusion that on the first stages of fragments acceleration the first term plays the most important role as velocities of gas and fragments are practically equal and the pressure gradient between the internal and external surfaces of fragments $\frac{\partial p}{\partial r}$ is rather large. In time the pressure gradient decreases and the relative velocity $|\vec{v} - \vec{u}|$ increases due to more rapid acceleration of gas.

Numerical investigation of fragments' acceleration showed [3] that the breakup velocity $\vec{v}_{j*}$ and initial acceleration under the influence of the pressure gradient give a major contribution to the final velocity of fragments. Drag force $c_d S\rho(\vec{v}_j - \vec{u})|\vec{v}_j - \vec{u}|$ doesn't play important role due to the fact that by the time relative velocity increases the density of the gas goes down.

Investigations of characteristic times of the process show that in case the breakup takes place within the time $\tau_p \sim \tau_c$ nonuniformities of the internal loading turn out to be essential in the problem of fragments' acceleration.

The breakup process is determined by the tensile stresses and deformations inside the shell. Their distribution is uniform by the time of breakup since $\tau_p \sim \tau_c \gg \tau_w$ and the assumption of an equivalent sphere with the radius $r_*$ is quite valid.

The velocities of the expansion of the shell are determined by local acceleration of fragments under the influence of internal loading $p(t)$ (equations (29) and (72)). Thus nonuniformities of internal pressure distributions will play an important role in determining fragments' final velocity.

In our model we determine initial fragments' velocities $\vec{v}_{s*}$ integrating the equations locally for all fragments of the shell:

$$\rho_s \frac{dv_s}{dt} = \frac{p_s(t)}{h} - 2\frac{\sigma_\theta}{r}, \tag{74}$$

$$\frac{dr}{dt} = v_s;$$

$$v_s|_{t=0} = 0; \qquad r|_{t=0} = r_s,$$

where $p_s(t)$ distribution along the shell is obtained from the solution of gasdynamics problem of internal diffusion combustion (§1.1 ); $r_s$ is the initial distance from the center of the tank to a fragment of the shell under consideration.

Integration of the equation (74) gives us the possibility to obtain estimates of radial velocity distribution in the shell by the time of breakup ($t = t_*$).

## §1.5. Correlation of Velocity and Mass Distributions of fragments

The model developed in §1.4 makes it possible to obtain in the fragments' velocity distributions along the walls of the tank. Then it is possible to determine the mean velocity of fragments in a definite section:

$$v_{s\alpha} = \frac{1}{S_\alpha} \iint_{S_\alpha} v_{s*} ds. \tag{75}$$

The number of fragments of each size (or mass) $N_{j\alpha}$ is determined within each section as described in §1.3, thus providing us with local fragments' distribution function versus mass. The total numbers of fragments of different masses $N_j$ can be obtained in the following way:

$$N_j = \sum_{\alpha=1}^{L} N_{j\alpha}; \qquad j = 1, ..., K. \tag{76}$$

The velocity distribution of fragments versus mass can be obtained by formula:

$$v_j = \frac{\sum_{\alpha=1}^{L} N_{j\alpha} v_{s\alpha}}{N_{0\alpha j}}; \qquad j = 1, ..., K. \tag{77}$$

Minimal and maximal velocities distributions versus mass are also important.

## Part 2.

# Results of numerical modelling of a breakup caused by combustion of mixing propellants

## §2.1. Investigation of the influence of initial pressure ratio and size of a damage in the bulkhead on combustion of mixing hypergolic propellants

Theoretical modelling of the process of turbulent jet formation and combustion in a cylindrical vessel with a coaxial opening was described in [7]. The mathematical model of the process is discussed in Part 1, §1.1. The present calculations deal with the case when fuel occupies the upper larger part of the tank and the oxidant occupies the lower part. Pressure in the oxidant is higher than that in the fuel section, at $t = 0$ fuel and oxidant come in contact in the section of culindrical coaxial opening, chemical reaction and a gas flow start simultaneously.

The list of values of parameters, the calculations were performed for, is given in the Table 1. The diameter of the tank was assumed 1m. The diameter of the opening was varied from 10 to 90 cm.

Figs. 1 - 3 show the isolines of pressure (a), temperature of gas (b) and turbulent kinematic energy (c) for the times $t_1 = 4.5 \cdot 10^{-4}$ s, $t_2 = 4.876 \cdot 10^{-3}$ s, $t_3 = 4.316 \cdot 10^{-4}$ s respectively for the case with the smallest opening $d = 10$ cm. The arrows on the figures correspond with velocity vectors in gas. Solid curves of different intensity are the lines of equal values of parameters. The intensity of the colour (from dark black to light grey) corresponds with the value of the parameter. The scale of colours and values of parameters is given in the upper right corner of each figure. The units and the parameter under consideration are named in the upper left corner. The time in seconds after opening the membrane is given in the lower right corner of each figure.

It is seen that diffusive combustion causes a pressure increase in the flame zone that gives birth to compression waves and expanding flow in both chambers (Figs. 1a, 2a). The compression waves reflect from the walls that causes the further increase of the wall pressure (Figs. 2a, 3a). Temperature is maximal in the opening at the very beginning (Fig.1b) but in the longrun the zone of maximal temperature and the diffusion flame itself are pushed inside the fuel tank by a convective gas flow (Figs. 2b, 3b). Being maximal in the opening at the very beginning (Fig.1c) turbulent energy generated by the gas flow increases in both chambers (Fig. 2c), but both maximums are removed by the gas flow towards the center of the fuel tank. Fig.2c shows the moment when maximum appearing in the oxidant tank is being pumped into the opening. In time the level of turbulence lowers down due to dissipation effects (Fig. 3c) and combustion extinguishes.

Figs. 4 - 7 show the results for the case of a coaxial opening of a larger diameter ($d = 24$ cm). The rate of energy release is higher for a larger opening. Maximal temperatures appear in the opening (Fig.4b). Pressures reach the highest value in the

Table 1.

| | |
|---|---|
| 65 | Grid points along OX |
| 33 | Grid points along OR |
| 1.0000 | Vessel dimension along X |
| 0.5000 | Vessel dimension along R |
| 0.25000 | Oxidizer compartment length |
| 0.5000 | Gap in the bulkhead radius |
| 5.00000e-002 | Molar weight of oxidizer |
| 5.00000e-002 | Molar weight of fuel |
| 5.00000e-002 | Molar weight of products |
| 1.00000e+000 | Stoicheometric coefficient for oxidizer |
| 1.00000e+000 | Stoicheometric coefficient for fuel |
| 2.00000e+000 | Stoicheometric coefficient for products |
| 4.15500e+002 | Heat capacity at V=const for oxidizer |
| 4.15500e+002 | Heat capacity at V=const for fuel |
| 4.15500e+002 | Heat capacity at V=const for products |
| 5.81700e+002 | Heat capacity at p=const for oxidizer |
| 5.81700e+002 | Heat capacity at p=const for fuel |
| 5.81700e+002 | Heat capacity at p=const for products |
| 2.00000e+006 | Initial pressure in fuel |
| 4.00000e+002 | Initial temperature in fuel |
| 1.70000e+006 | Initial pressure in oxid |
| 4.00000e+002 | Initial temperature in oxid |
| 1.00000e-005 | viscosity at norm cond in oxidizer |
| 1.00000e-005 | viscosity at norm cond in fuel |
| 1.00000e-005 | viscosity at norm cond in products |
| 9.00000e-001 | Prandtl number in oxidizer |
| 7.00000e-001 | Prandtl number in fuel |
| 7.20000e-001 | Prandtl number in products |
| 1.00000e+000 | Schmidt number in oxidizer |
| 1.00000e+000 | Schmidt number in fuel |
| 1.00000e+000 | Schmidt number in products |
| 9.00000e+006 | Reaction heat per fuel mass |

opening more close to its perimeter (Fig.4a) that can be explained by the higher rate of diffusive combustion due to the higher level of turbulence (Fig. 4c) originating in the gradient flow on interaction of gas flowing through the opening with the remains of the bulkhead. After the reflection of compression waves from the walls pressures in the oxidant tank increase to a higher values than in the fuel tank that gives birth to an intense gas flow from the lower to the upper chamber (Fig.5). The jet in the upper chamber collides the wall that causes slowing down of the flow (Fig. 5a). The level of turbulence is much higher (Fig. 5c) than in case of a smaller opening.

The interaction of the jet with diffusion flame (Fig. 6a) causes the formation of a torroidal vertex in the fuel tank that contributes to further mixing of the components and increase of turbulent energy (Fig. 6c). Up to the time the rate of production of turbulence surpasses the rate of its dissipation.

Combustion in the fuel tanks brings to an increase of pressure to a higher levels than in the lower tank and a reversive flow starts through the opening (Fig. 7a). The flow forms another torroidal vertex in the lower tank and increases the level of turbulence there (Fig. 7c).

Figs. 8 - 11 show the isolines of pressure, temperature and turbulent energy for a larger opening ($d$ = 50 cm). The rate of pressure increase is much higher (Figs. 8a, 9a, 10a) due to the higher rate of total energy release in a diffusion flame of a larger area. The level of turbulence is very high from the very beginning (Fig. 8c) and it increases both in the primary jet (Fig. 9c, the direction of flow is from the lower to the upper tank) and in the reverse flow from the upper tank (Fig. 10c). Both flows are very intensive. The zone of maximal temperature (Fig. 8b) is pushed out of the opening by the primary flow into the upper tank (Fig. 9b) and then pumped by the reverse flow into the lower chamber (Fig. 10b). Temperatures reach higher values inside the tanks for a wider opening and the wall temperatures are maintained considerably high in some zones (Figs. 10b, 11c) that can influence the properties of the material and the breakup process. Pressure distribution inside the tanks turns to be more uniform and only transverse waves travel inside the tank along the axis (Figs. 10a, 11a).

Figs. 12 - 15 show the results for the case of a very wide opening when the remains of the bulkhead just form a ring on the walls of the tank. The process of energy release and pressure increase is still more rapid (Figs. 12 a, b). Maximal level of turbulence appears to be in the vicinity of the remains of the bulkhead that serve as a turbulizing ring (Fig. 12c).

The increase of turbulence intensifies chemical reaction (due to diffusive mixing) that is reflected in the increase of temperature in these zones (Fig. 12b) and higher intensity of the expanding flow. Wall pressure reaches high values very rapidly (Fig. 13a) and then pressure distribution turns to be more uniform with regular compression waves reflecting from the top and bottom walls of the cylindrical tank (Figs. 14a, 15a). The level of turbulence is very high all over the tank (Figs. 13c, 14c, 15c). Wall temperature is maintained at high level (Figs. 14b, 15b) surpassing 3000 K in some zones.

Figs. 16 - 19 show the results for the case of the absence of the common bulkhead. Diffusive combustion starts in the crossection of the tank, but the flowfield is far from being one-dimensional at the very beginning (Fig. 16a). Reaction is more rapid near the walls (Fig. 16b) due to the higher level of turbulence (Fig. 16c). Later the flame induced turbulence (Figs. 17c, 18c, 19c) leads to a more uniform distribution of the

parameters (Figs. 17a, 18a, 19a). The levels of pressures and temperatures inside the tank (Figs. 17b, 18b, 19b) are nearly the same as in the previous case.

The combustion gives birth to a periodic transverse flow inside the tank with periodical reflections from the top and bottom of the cylinder.

The level of turbulence is maximal in the vicinity of the axis of the tank and evolves periodically from the upper to the lower tank and back (Figs. 18c, 19c).

The results of numerical investigations of diffusive combustion after opening a hole in a bulkhead of propellants' tanks show that the intensity of combustion and turbulent mixing increases with the increase of diameter of a hole and the increase of initial pressure.

Diffusive combustion takes place periodically in both tanks due to convective periodical flows appearing due to pressure difference in both tanks.

The characteristic time of gasdynamical processes inside the tanks involving energy release and pressure increase is: $\tau_c \cong 10^{-3} \div 10^{-2}$ s.

By the time $\tau = 10^{-1}$ s pressure turns to be nearly uniform in both tanks.

Gasdynamical processes at characteristic times $t < 10^{-3}$ s manifest essential pressure fluctuations and nonuniformities of internal loading of the walls of the tank. Periodical compression and rarefaction waves exist inside the tank up to times of the order $10^{-2}$ s.

Combustion produces zones of high temperature reaction products. These zones can be found near the walls of the tanks and exist there for a long time, thus heating the material of the walls and changing its properties. Temperatures of gas near the walls can exceed 3000 K in some places.

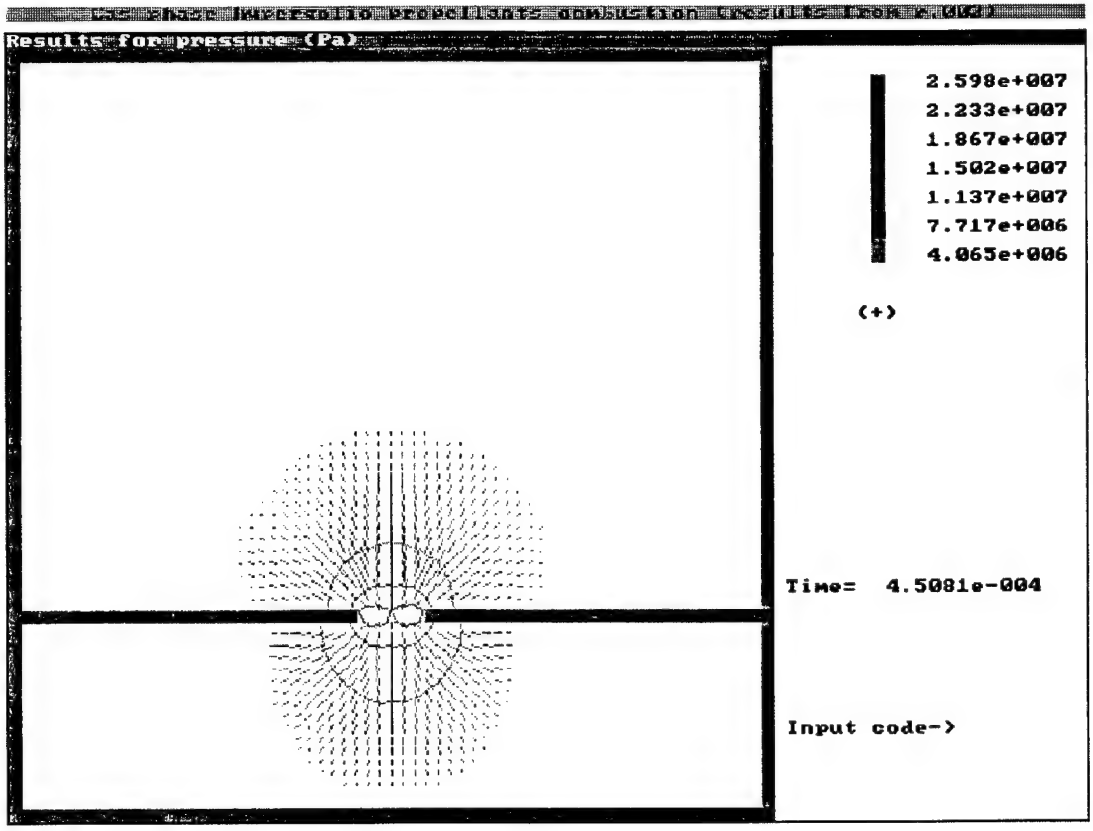
Results for pressure (Pa)
2.598e+007
2.233e+007
1.867e+007
1.502e+007
1.137e+007
7.717e+006
4.065e+006
(+)
Time= 4.5081e-004
Input code->

Fig. 1a.

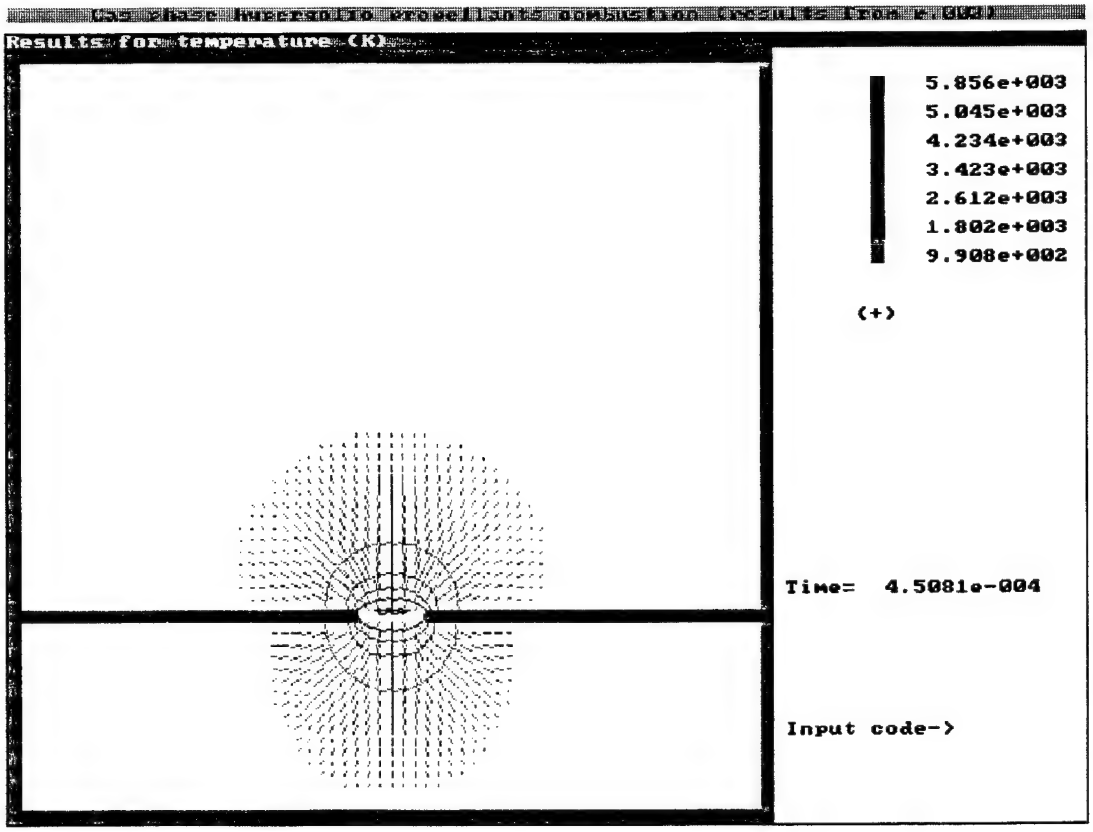
Results for temperature (K)
5.856e+003
5.045e+003
4.234e+003
3.423e+003
2.612e+003
1.802e+003
9.908e+002
(+)
Time= 4.5081e-004
Input code->

Fig. 1b.

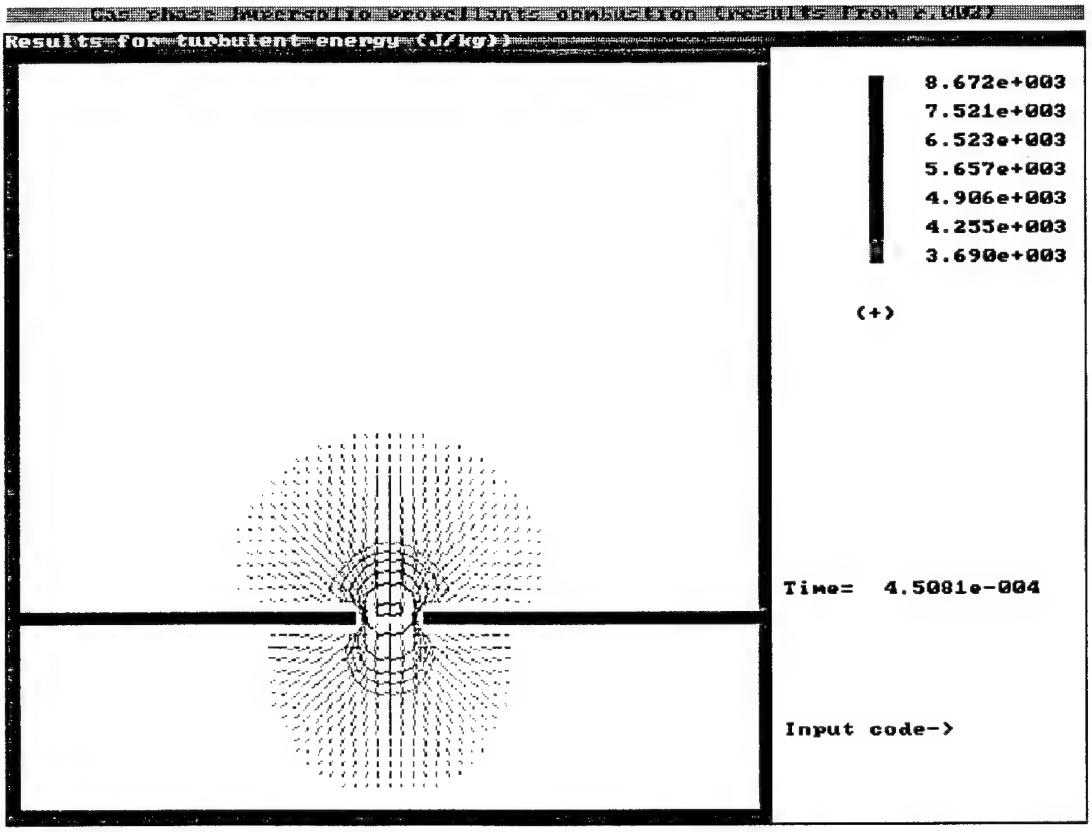
Results for turbulent energy (J/kg)
8.672e+003
7.521e+003
6.523e+003
5.657e+003
4.906e+003
4.255e+003
3.690e+003
(+)
Time= 4.5081e-004
Input code->

Fig. 1c.

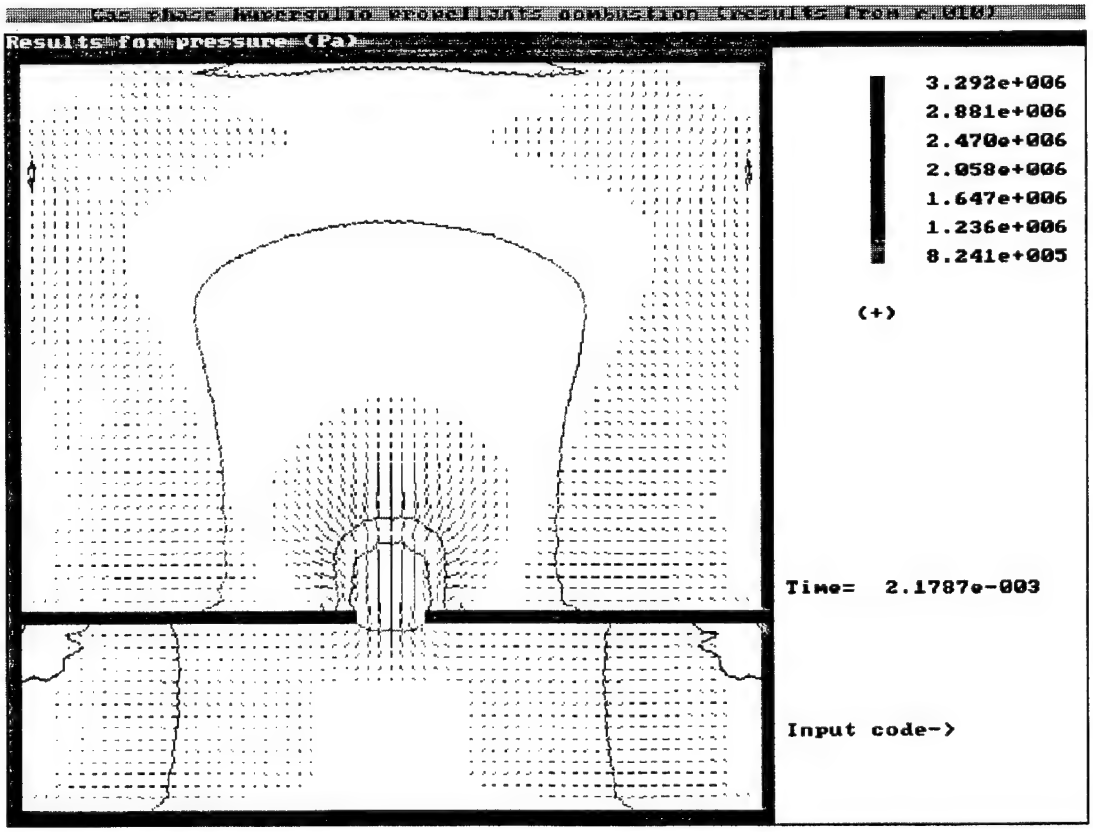
Results for pressure (Pa)
3.292e+006
2.881e+006
2.470e+006
2.058e+006
1.647e+006
1.236e+006
8.241e+005
(+)
Time= 2.1787e-003
Input code->

Fig. 2a.

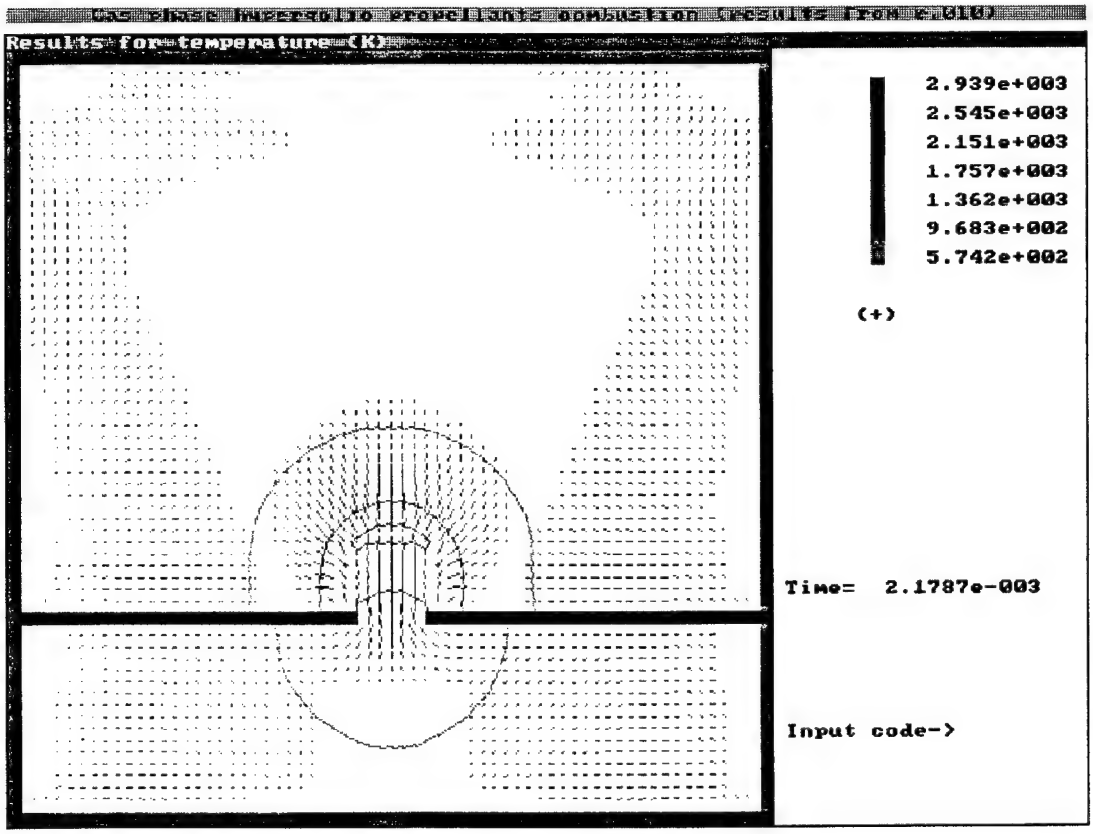
Results for temperature (K)
2.939e+003
2.545e+003
2.151e+003
1.757e+003
1.362e+003
9.683e+002
5.742e+002
(+)
Time= 2.1787e-003
Input code->

Fig. 2.B.

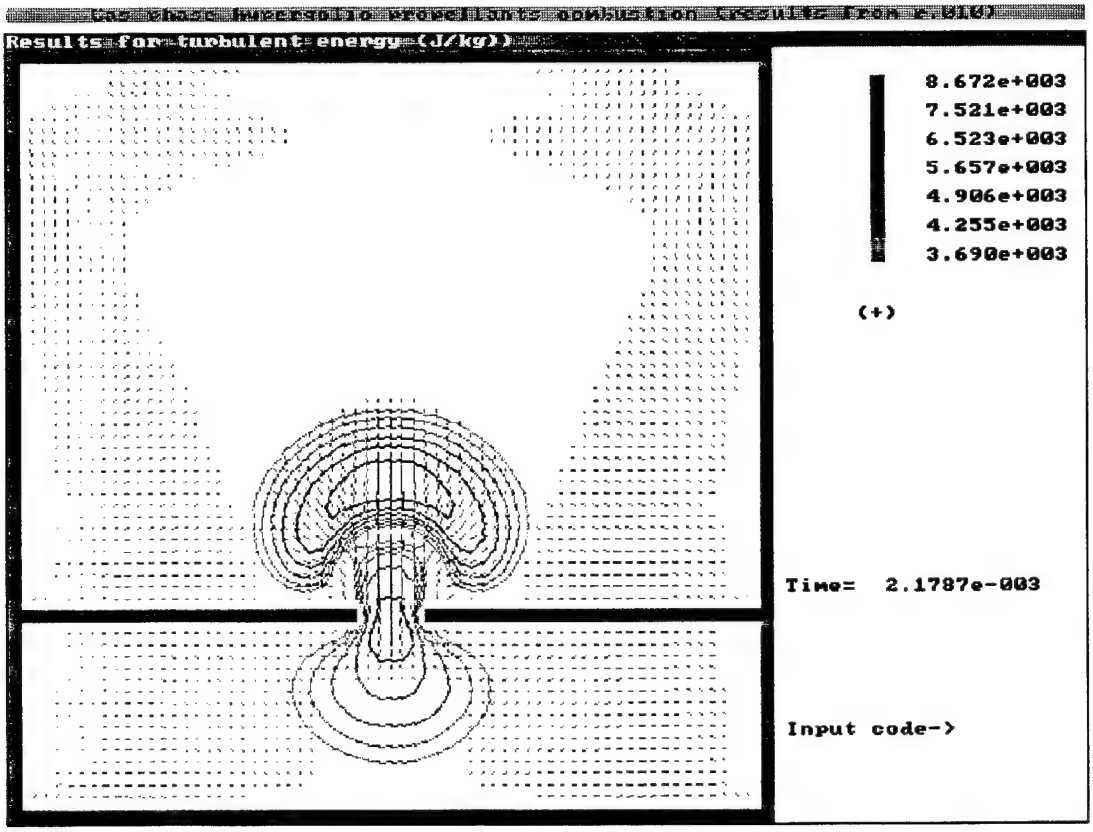
Results for turbulent energy (J/kg)
8.672e+003
7.521e+003
6.523e+003
5.657e+003
4.906e+003
4.255e+003
3.690e+003
(+)
Time= 2.1787e-003
Input code->

Fig. 2c.

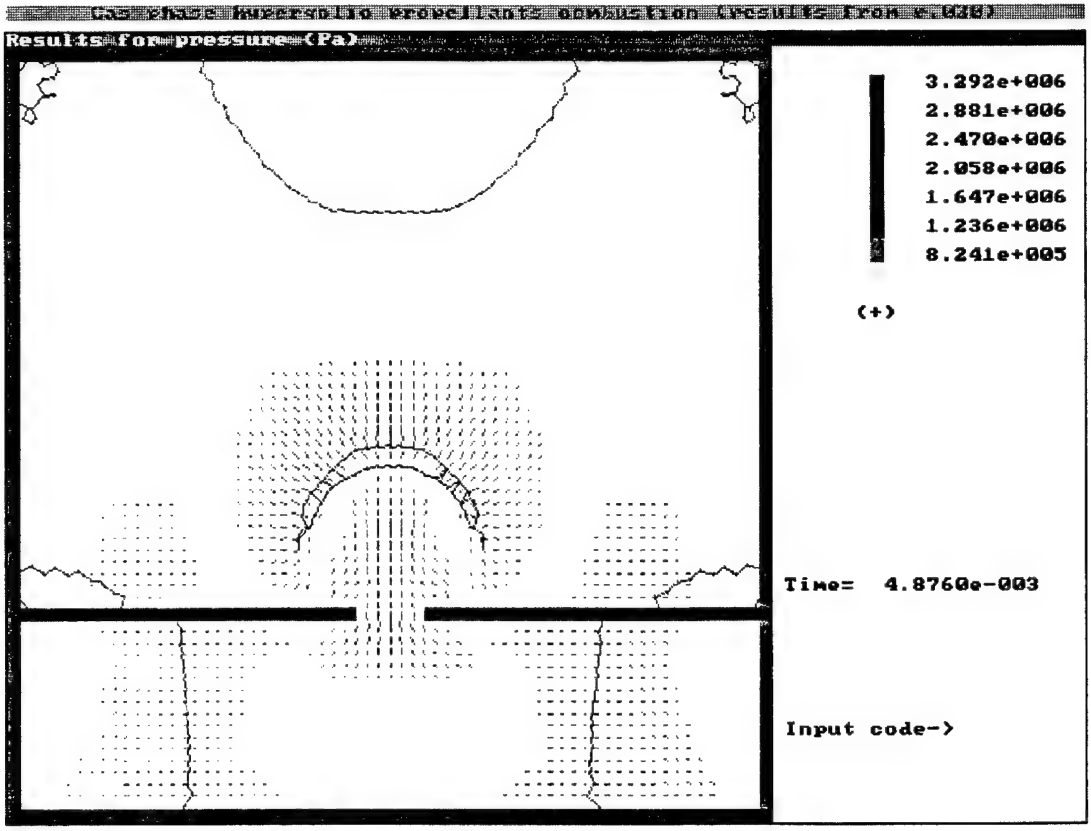
Results for pressure (Pa)
3.292e+006
2.881e+006
2.470e+006
2.058e+006
1.647e+006
1.236e+006
8.241e+005
(+)
Time= 4.8760e-003
Input code->

Fig. 3a.

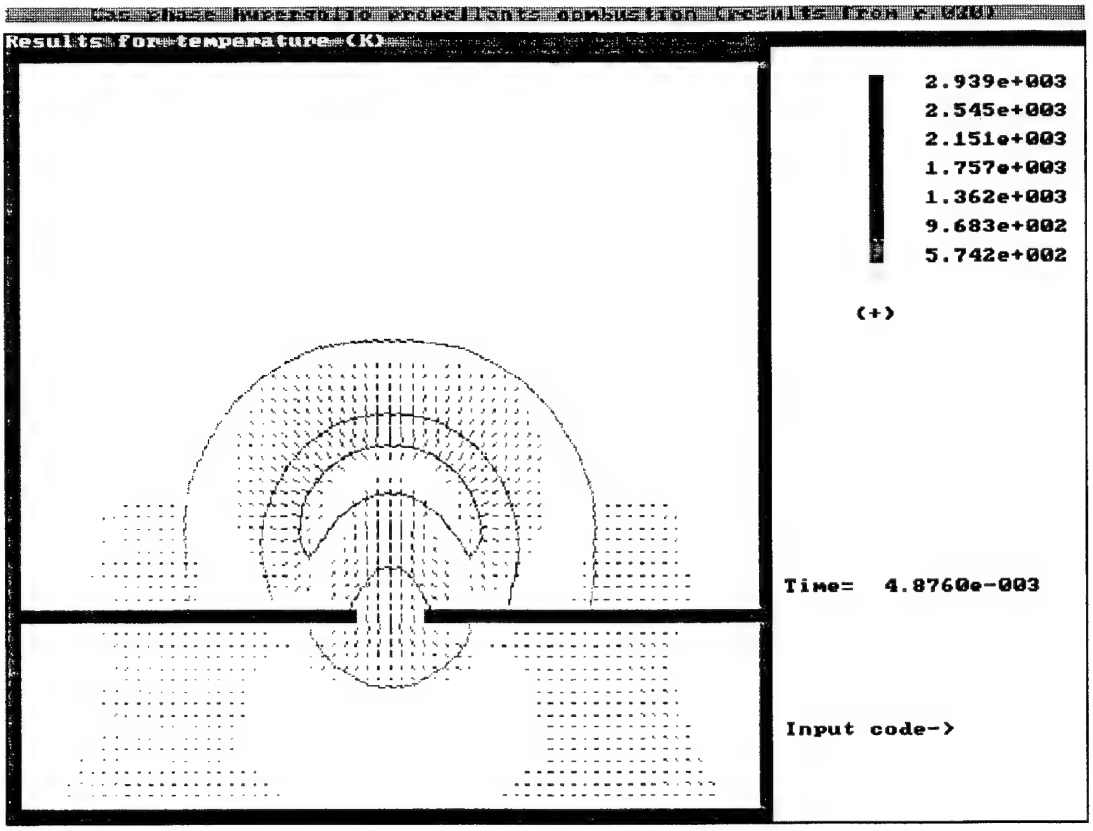
Results for temperature (K)
2.939e+003
2.545e+003
2.151e+003
1.757e+003
1.362e+003
9.683e+002
5.742e+002
(+)
Time= 4.8760e-003
Input code->

Fig. 3b.

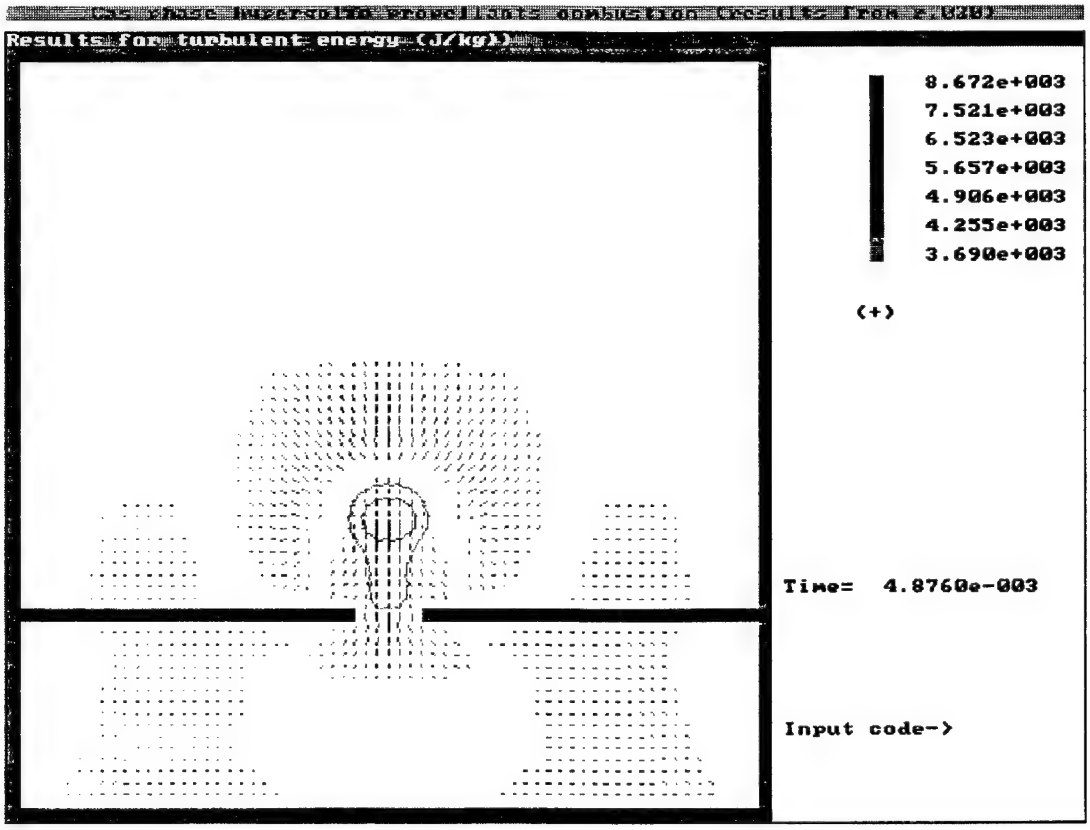
Results for turbulent energy (J/kg)
8.672e+003
7.521e+003
6.523e+003
5.657e+003
4.906e+003
4.255e+003
3.690e+003
(+)
Time= 4.8760e-003
Input code->

Fig. 3c.

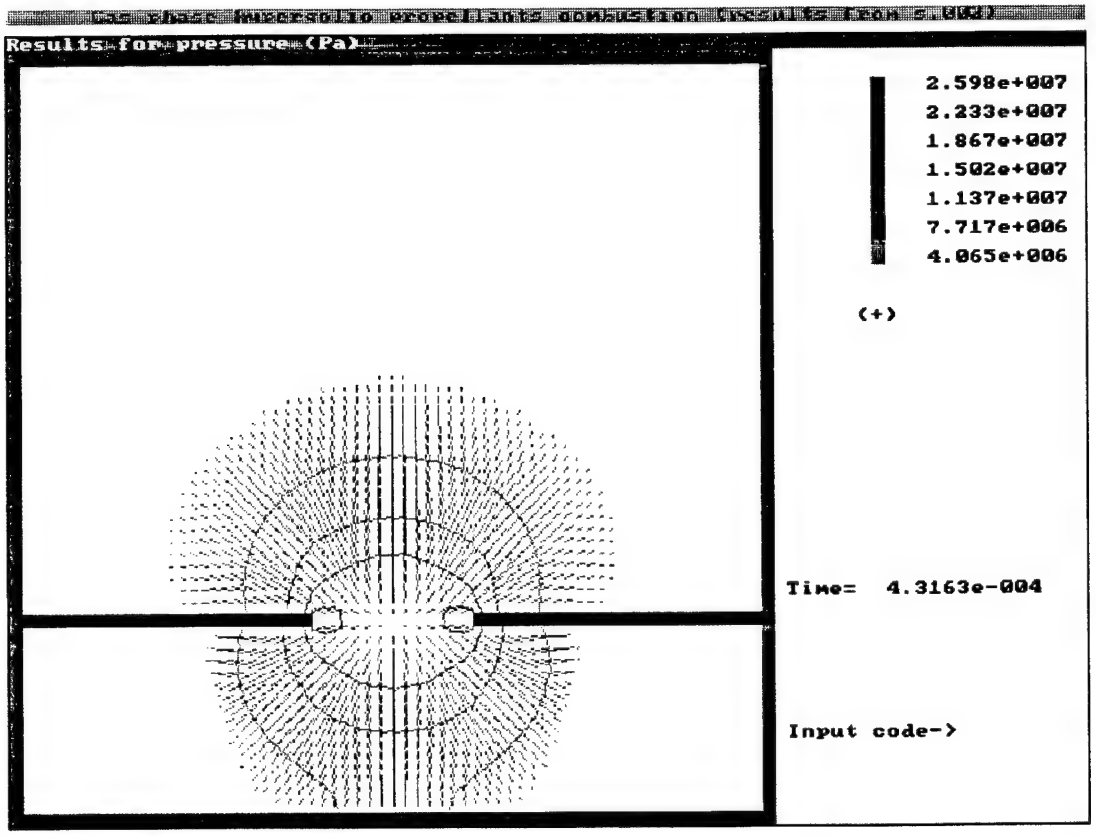
Results for pressure (Pa)
2.598e+007
2.233e+007
1.867e+007
1.502e+007
1.137e+007
7.717e+006
4.065e+006
(+)
Time= 4.3163e-004
Input code->

Fig. 4a.

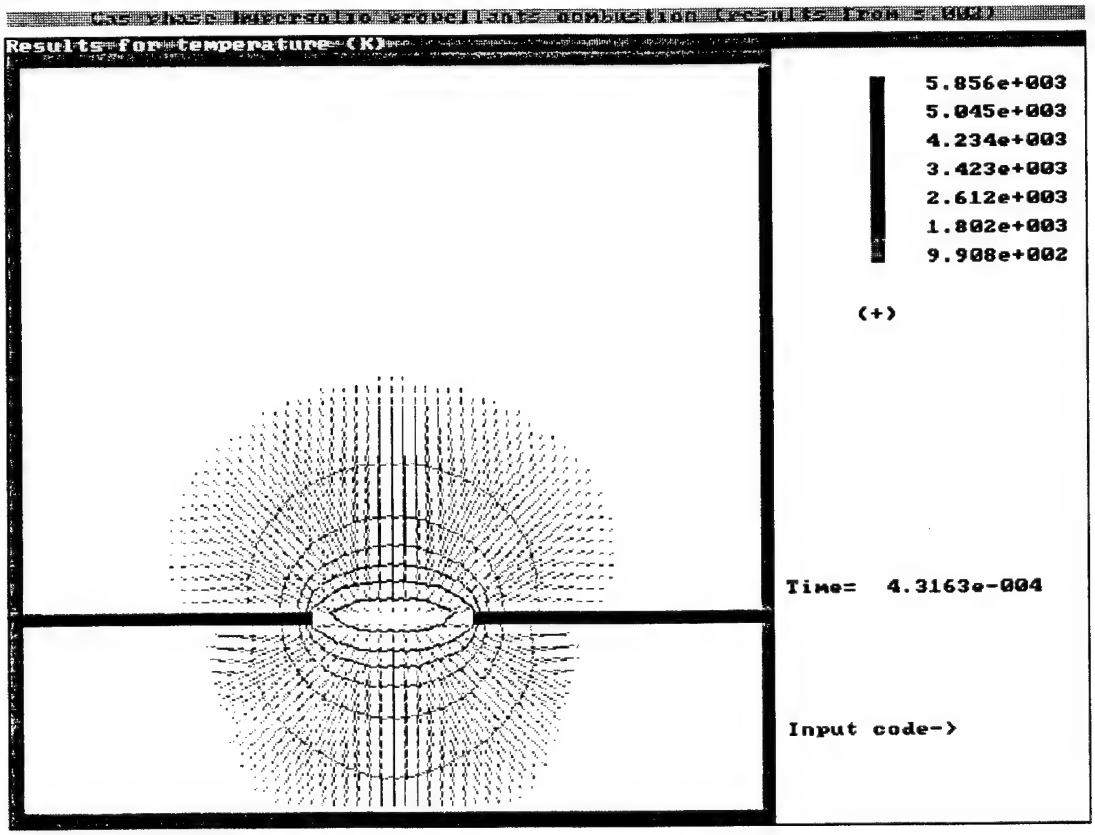
Results for temperature (K)
5.856e+003
5.045e+003
4.234e+003
3.423e+003
2.612e+003
1.802e+003
9.908e+002
(+)
Time= 4.3163e-004
Input code->

Fig. 4b.

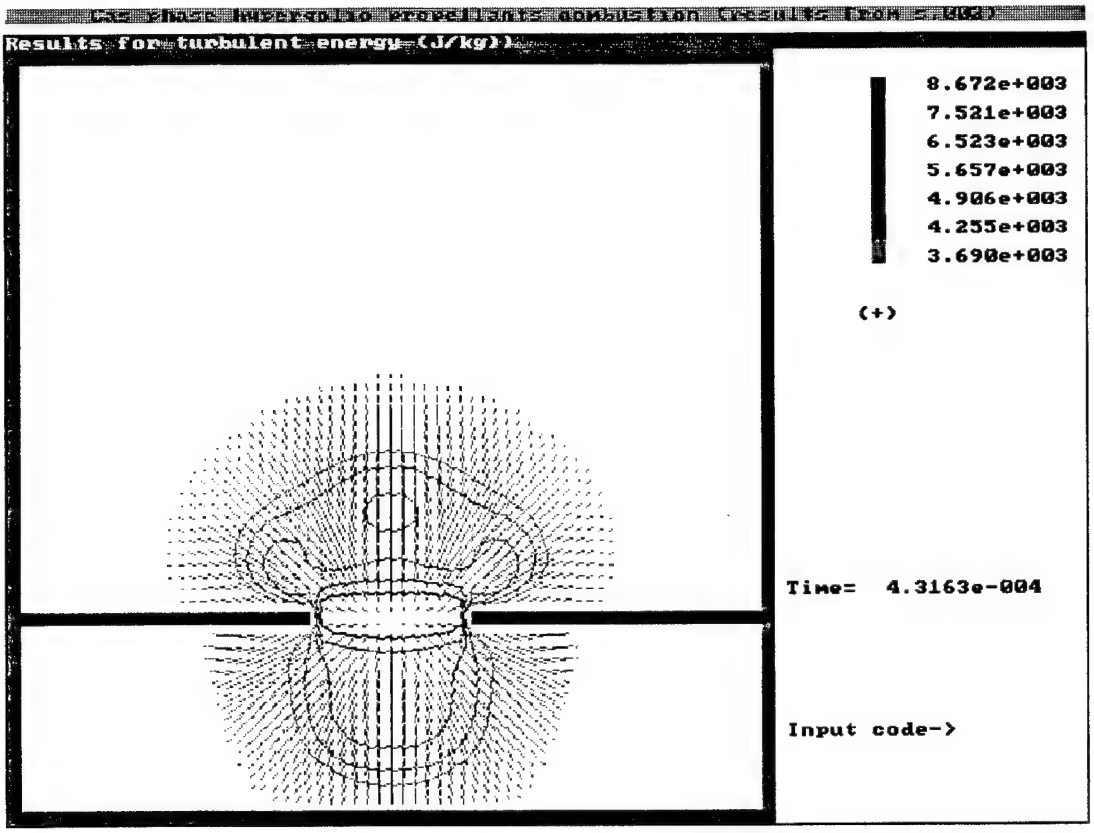
Results for turbulent energy (J/kg)
8.672e+003
7.521e+003
6.523e+003
5.657e+003
4.906e+003
4.255e+003
3.690e+003
(+)
Time= 4.3163e-004
Input code->

Fig. 4c.

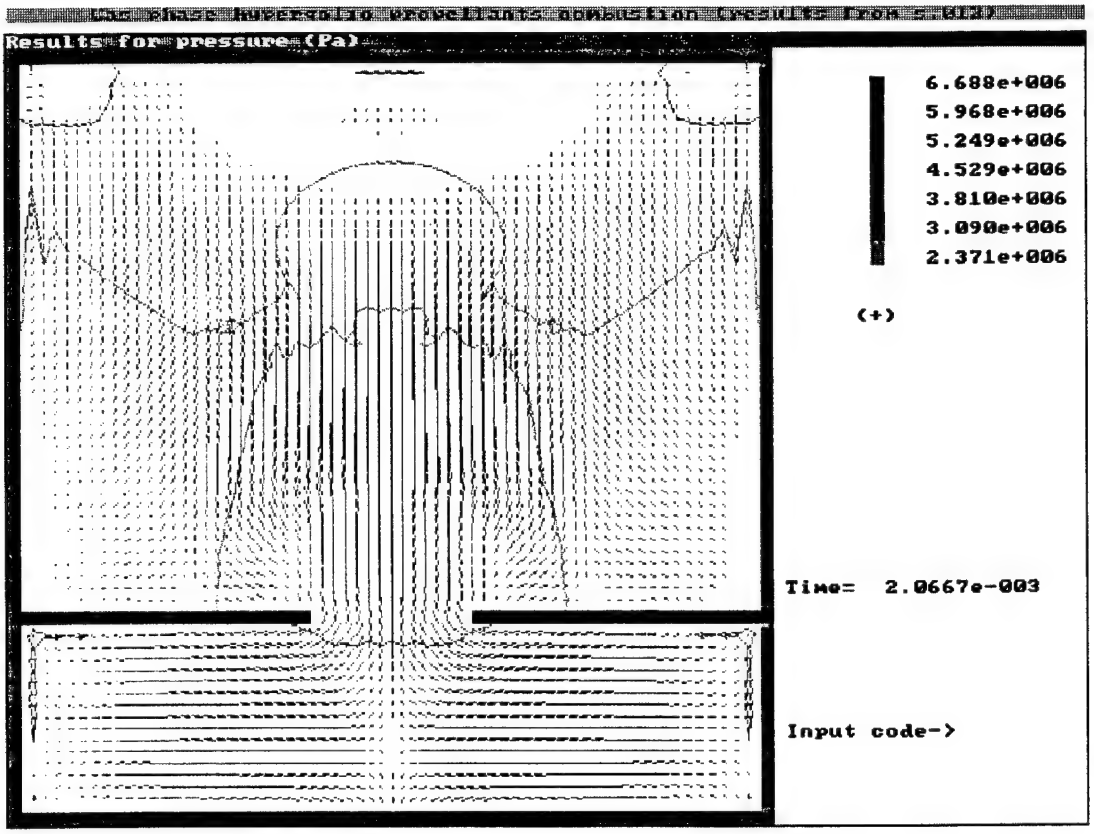
Results for pressure (Pa)
6.688e+006
5.968e+006
5.249e+006
4.529e+006
3.810e+006
3.090e+006
2.371e+006
(+)
Time= 2.0667e-003
Input code->

Fig. 5a.

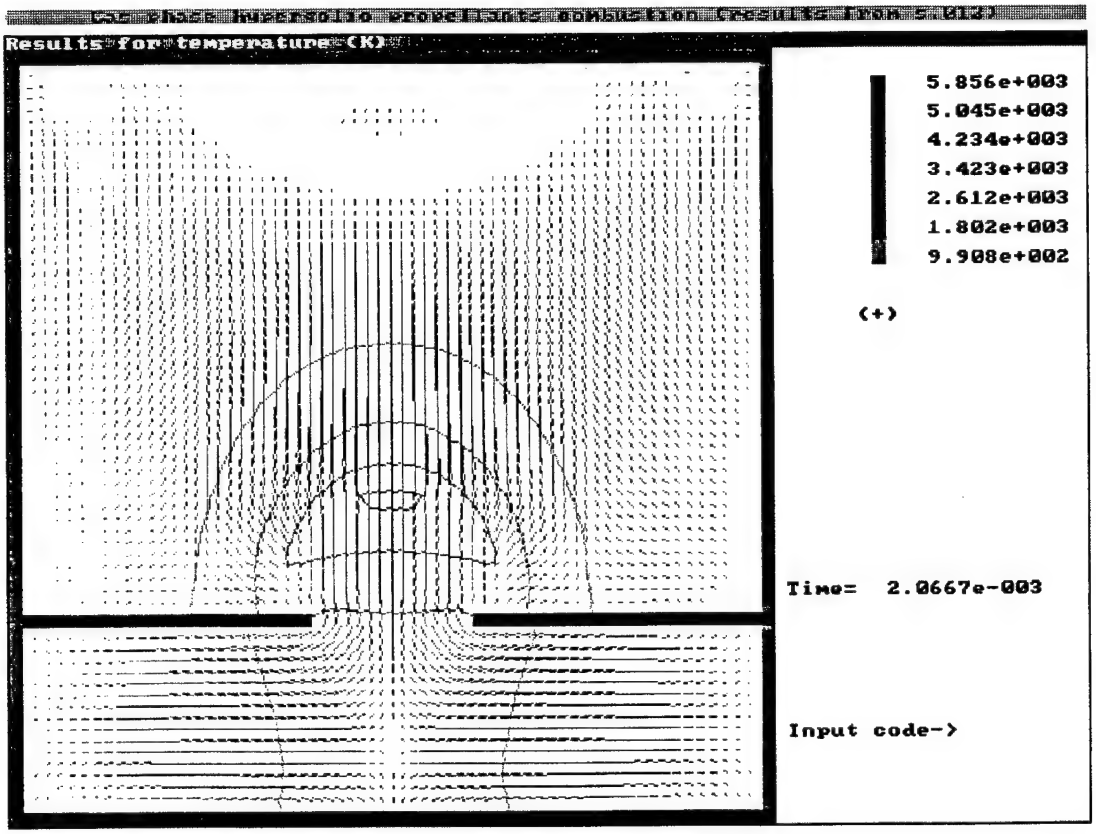
Results for temperature (K)
5.856e+003
5.045e+003
4.234e+003
3.423e+003
2.612e+003
1.802e+003
9.908e+002
(+)
Time= 2.0667e-003
Input code->

Fig. 5b.

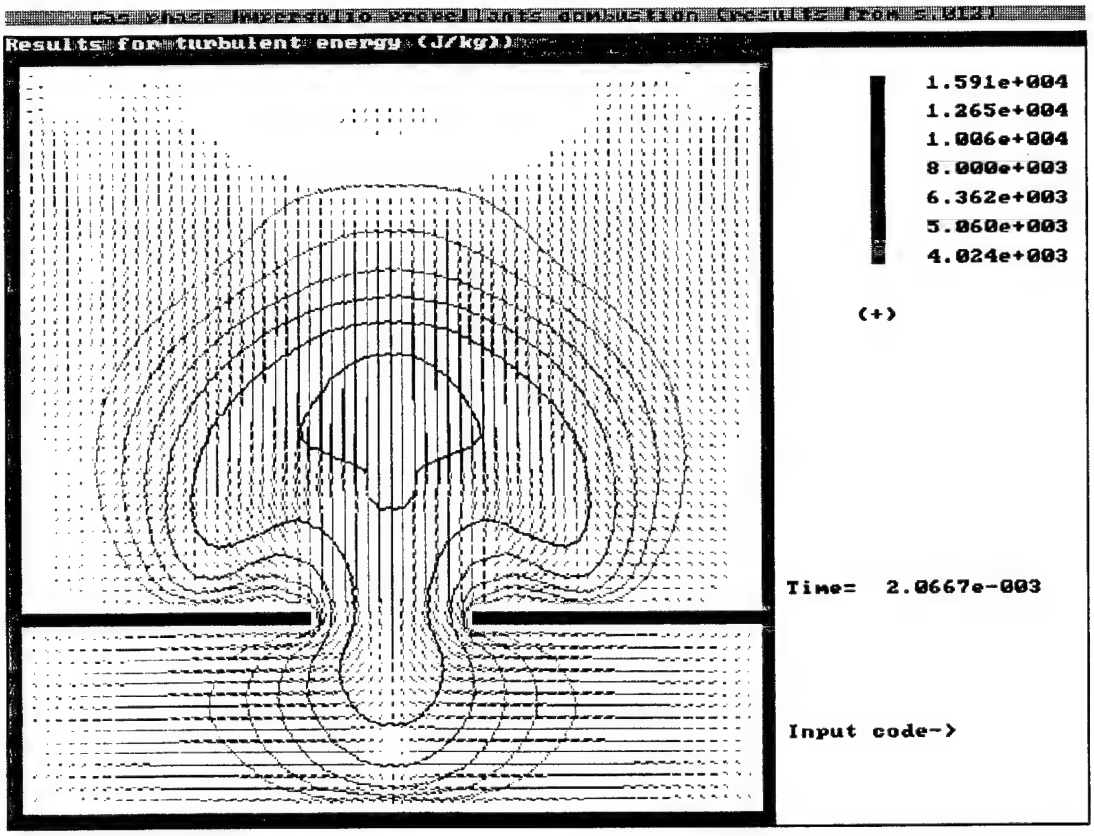
Results for turbulent energy (J/kg)
1.591e+004
1.265e+004
1.006e+004
8.000e+003
6.362e+003
5.060e+003
4.024e+003
(+)
Time= 2.0667e-003
Input code->

Fig. 5c.

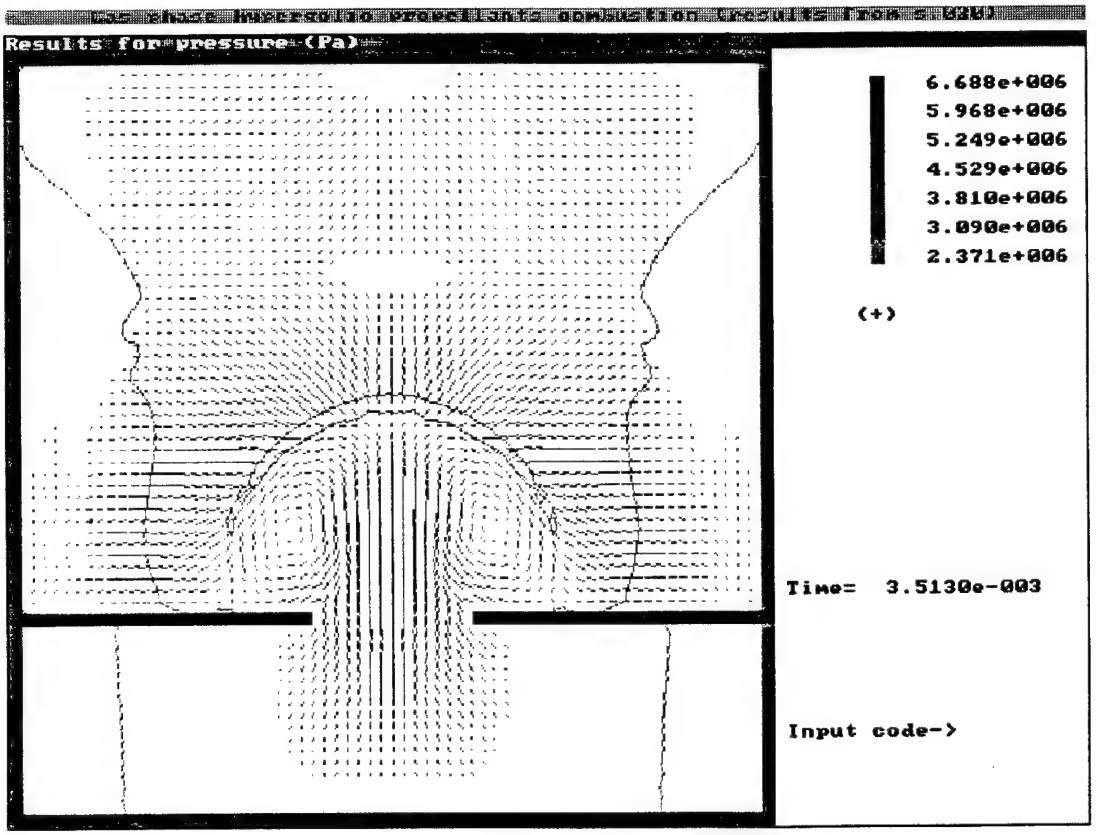
Results for pressure (Pa)
6.688e+006
5.968e+006
5.249e+006
4.529e+006
3.810e+006
3.090e+006
2.371e+006
(+)
Time= 3.5130e-003
Input code->

Fig. 6a.

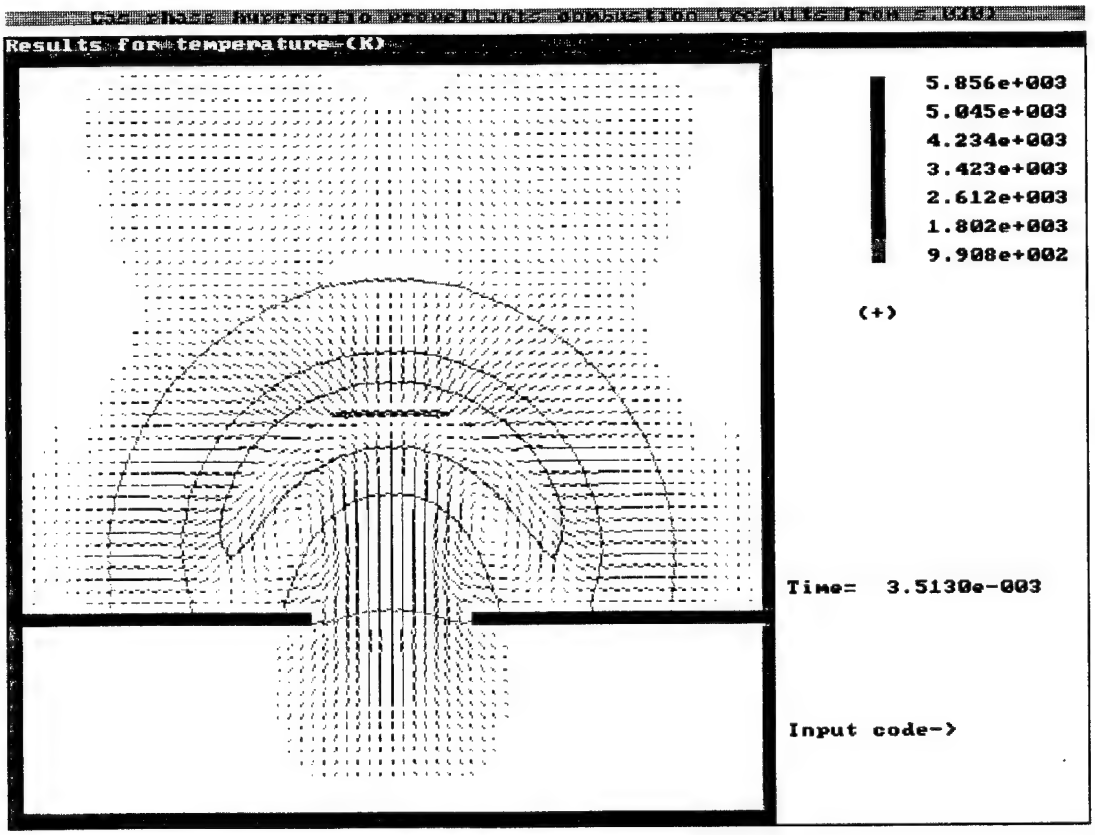
Results for temperature (K)
5.856e+003
5.045e+003
4.234e+003
3.423e+003
2.612e+003
1.802e+003
9.908e+002
(+)
Time= 3.5130e-003
Input code->

Fig. 6b.

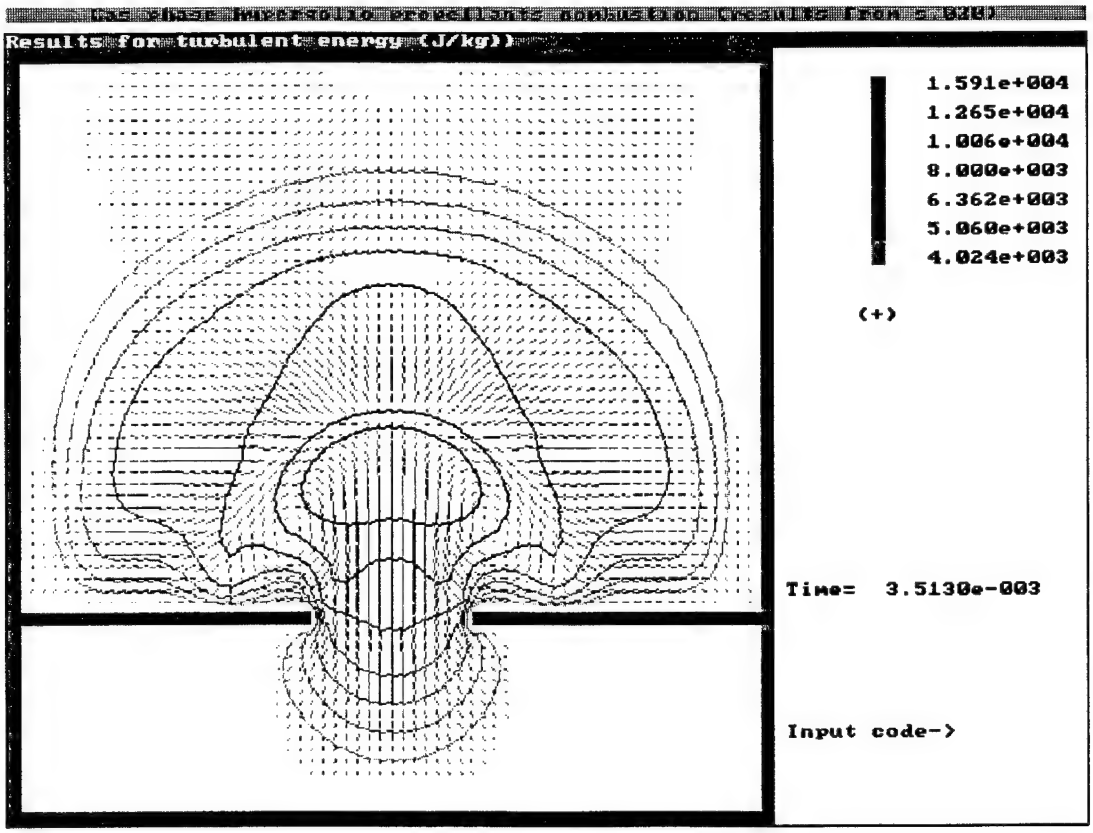
Results for turbulent energy (J/kg)
1.591e+004
1.265e+004
1.006e+004
8.000e+003
6.362e+003
5.060e+003
4.024e+003
(+)
Time= 3.5130e-003
Input code->

Fig. 6c.

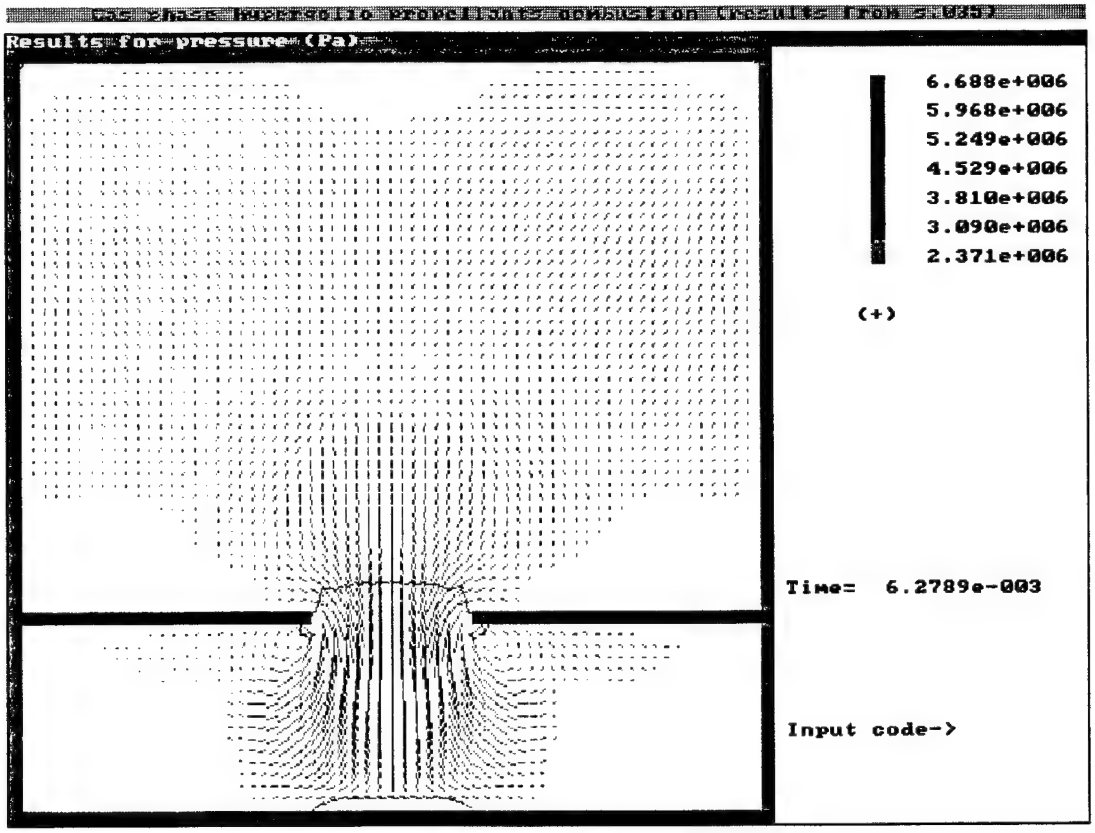
Results for pressure (Pa)
6.688e+006
5.968e+006
5.249e+006
4.529e+006
3.810e+006
3.090e+006
2.371e+006
(+)
Time= 6.2789e-003
Input code->

Fig. 7a.

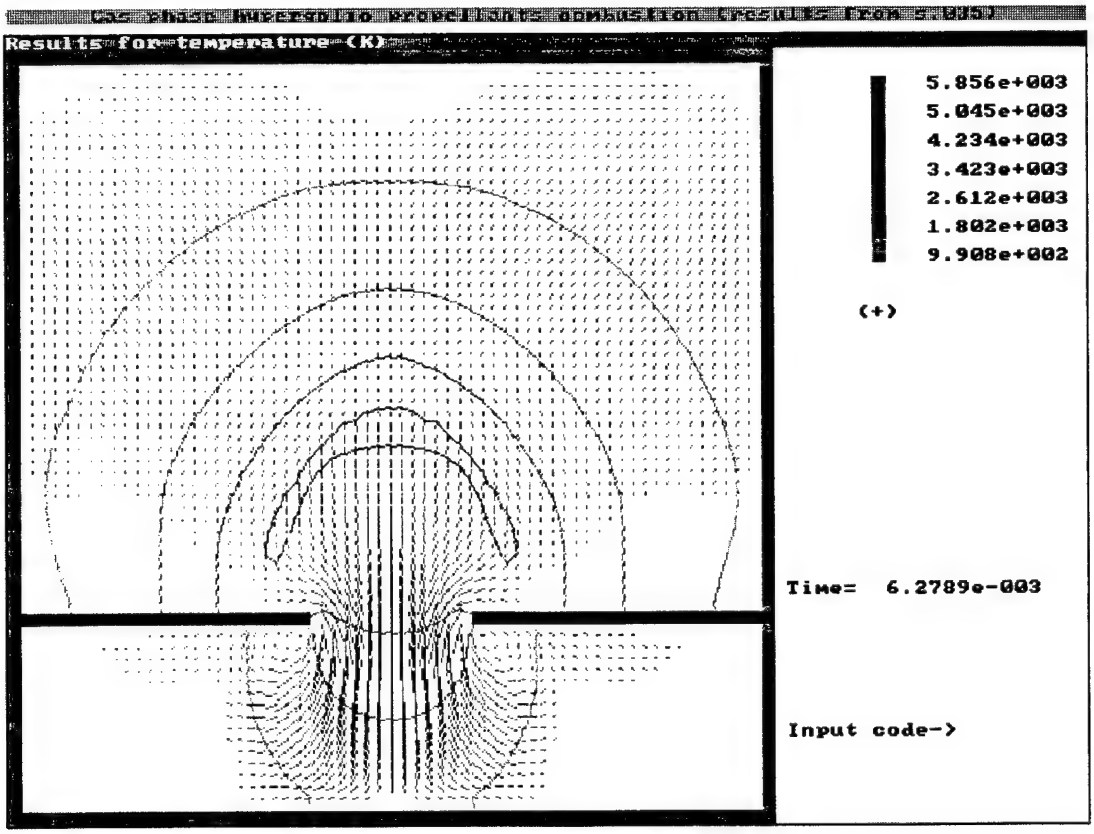
Results for temperature (K)
5.856e+003
5.045e+003
4.234e+003
3.423e+003
2.612e+003
1.802e+003
9.908e+002
(+)
Time= 6.2789e-003
Input code->

Fig. 7b.

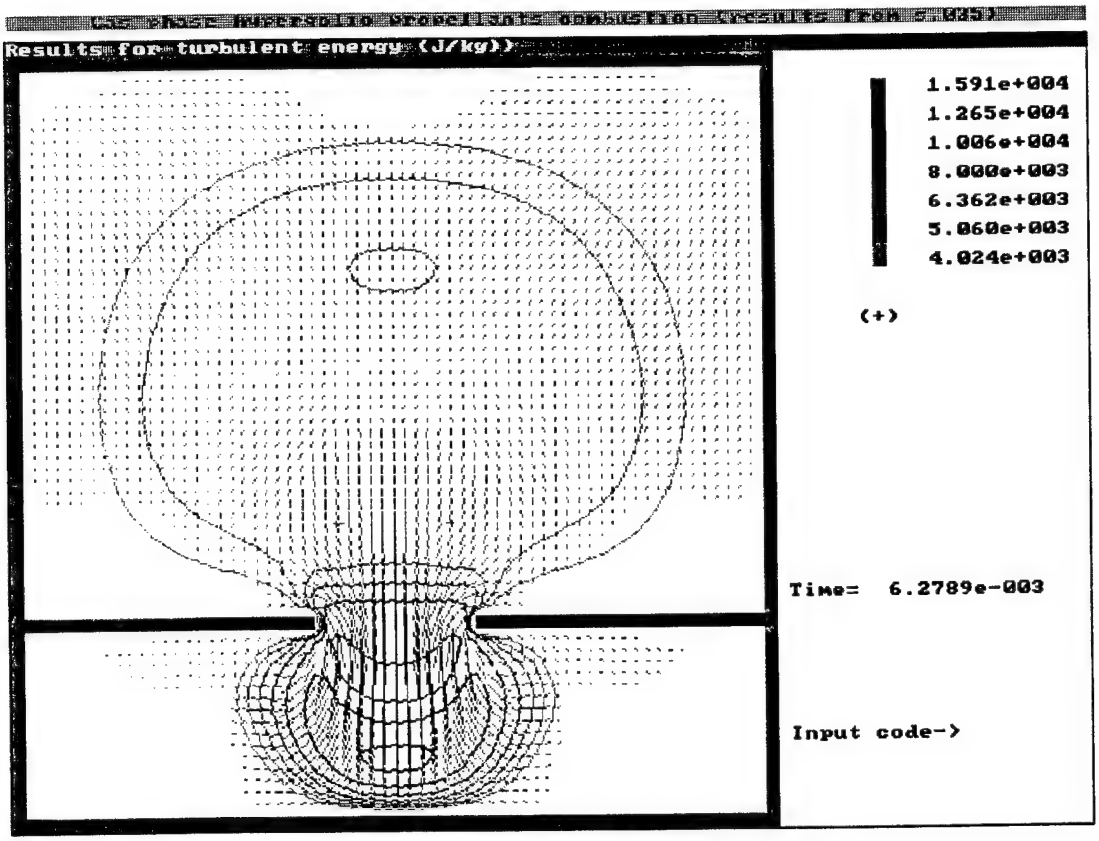
Results for turbulent energy (J/kg)
1.591e+004
1.265e+004
1.006e+004
8.000e+003
6.362e+003
5.060e+003
4.024e+003
(+)
Time= 6.2789e-003
Input code->

Fig. 7c.

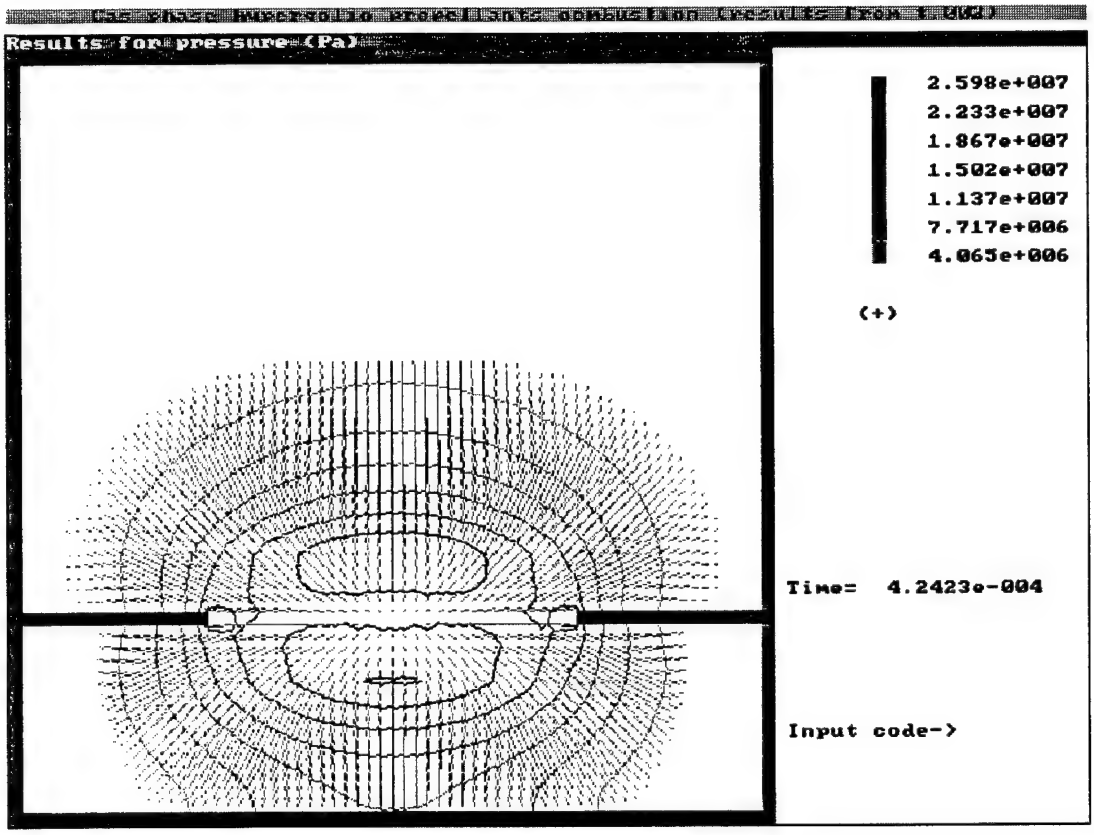
Results for pressure (Pa)
2.598e+007
2.233e+007
1.867e+007
1.502e+007
1.137e+007
7.717e+006
4.065e+006
(+)
Time= 4.2423e-004
Input code->

Fig. 8a.

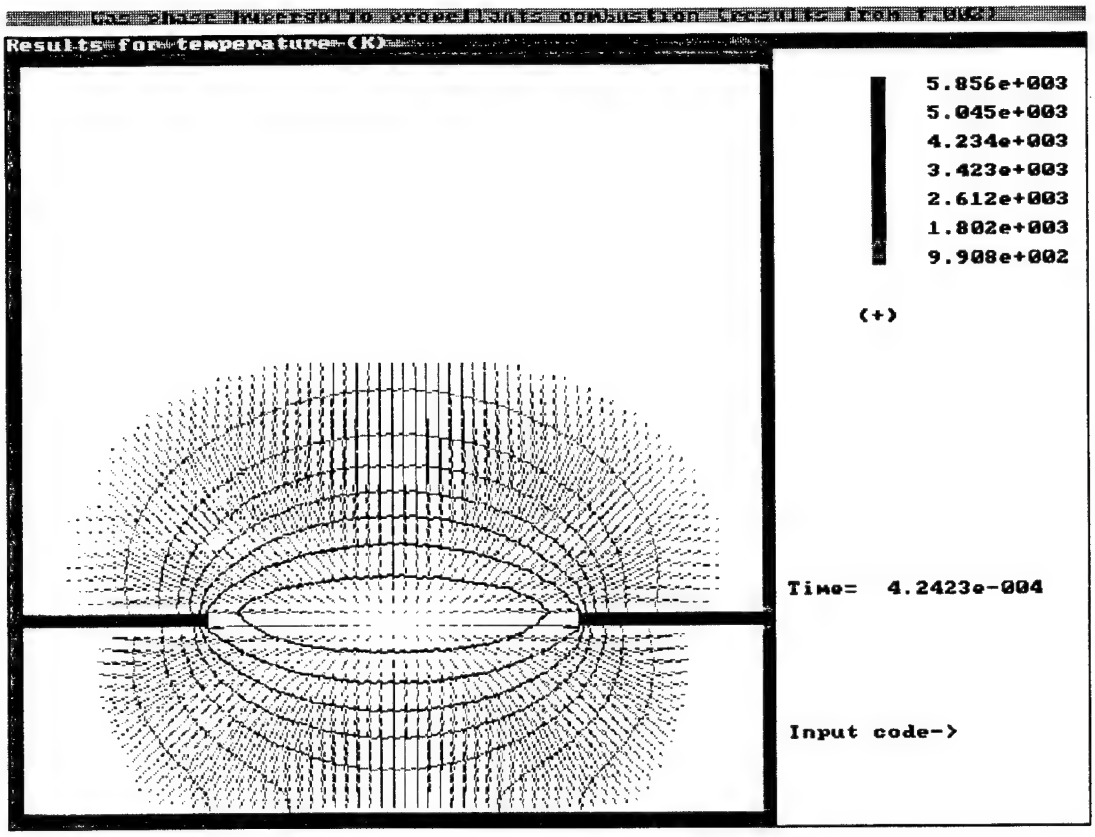
Results for temperature (K)
5.856e+003
5.045e+003
4.234e+003
3.423e+003
2.612e+003
1.802e+003
9.908e+002
(+)
Time= 4.2423e-004
Input code->

Fig. 8b.

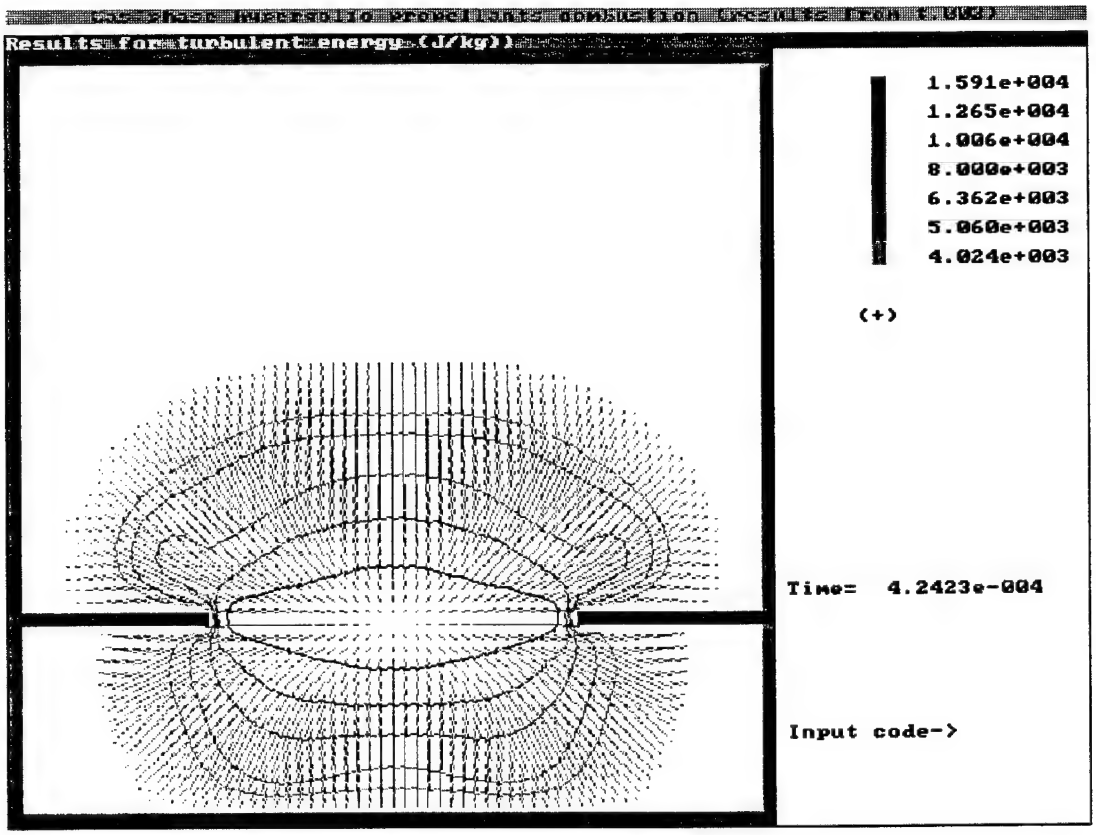
Results for turbulent energy (J/kg)
1.591e+004
1.265e+004
1.006e+004
8.000e+003
6.362e+003
5.060e+003
4.024e+003
(+)
Time= 4.2423e-004
Input code->

Fig. 8c.

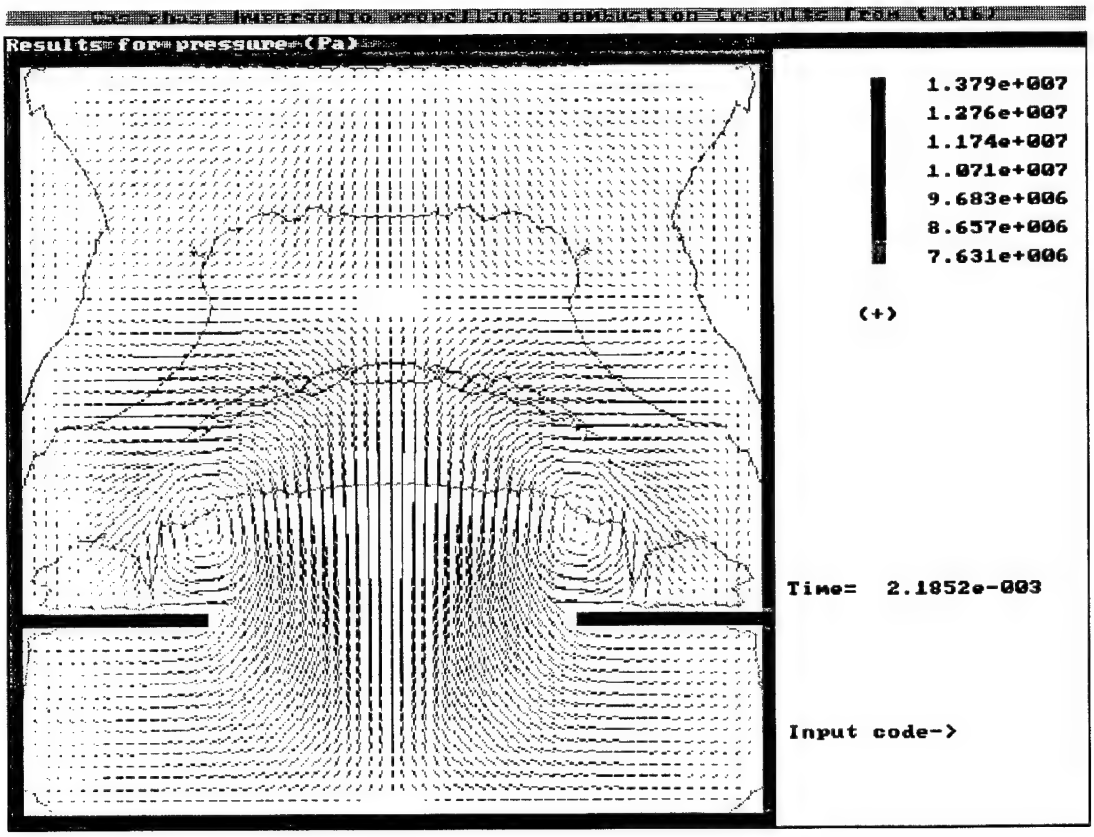
Results for pressure (Pa)
1.379e+007
1.276e+007
1.174e+007
1.071e+007
9.683e+006
8.657e+006
7.631e+006
(+)
Time= 2.1852e-003
Input code->

Fig. 9a.

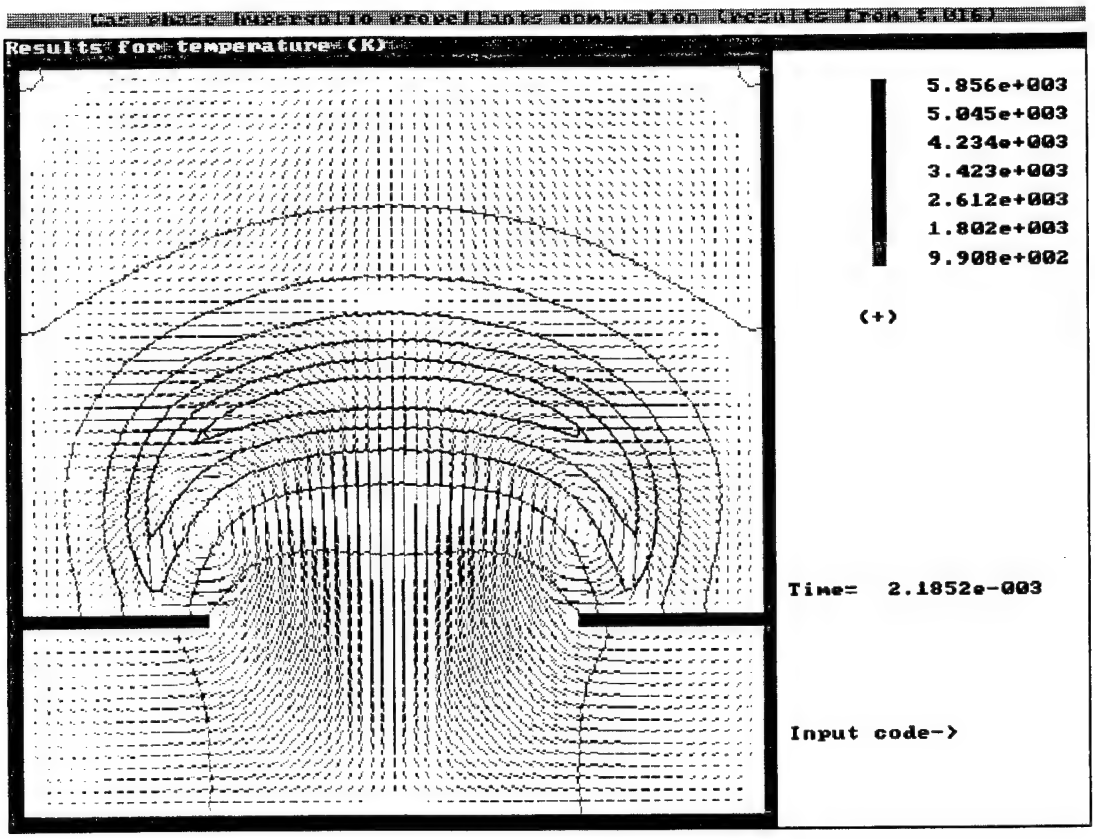
Results for temperature (K)
5.856e+003
5.045e+003
4.234e+003
3.423e+003
2.612e+003
1.802e+003
9.908e+002
(+)
Time= 2.1852e-003
Input code->

Fig. 9b.

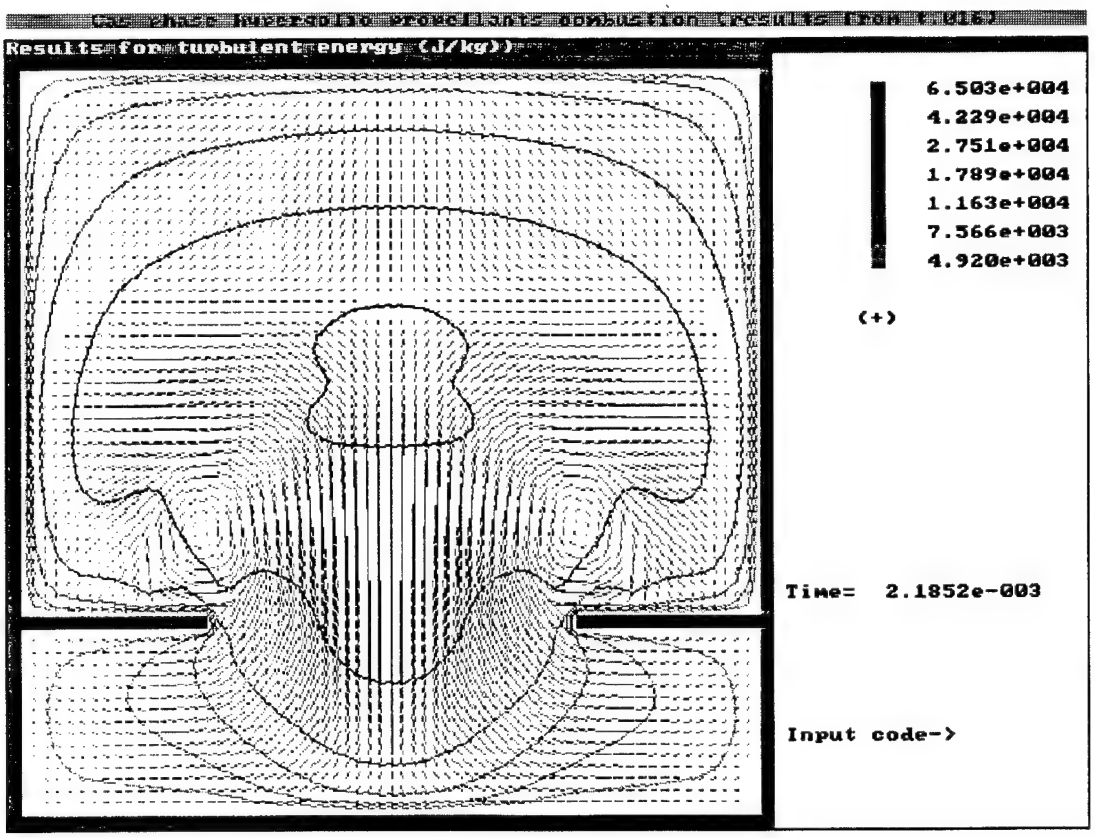
Results for turbulent energy (J/kg)
6.503e+004
4.229e+004
2.751e+004
1.789e+004
1.163e+004
7.566e+003
4.920e+003
(+)
Time= 2.1852e-003
Input code->

Fig. 9c.

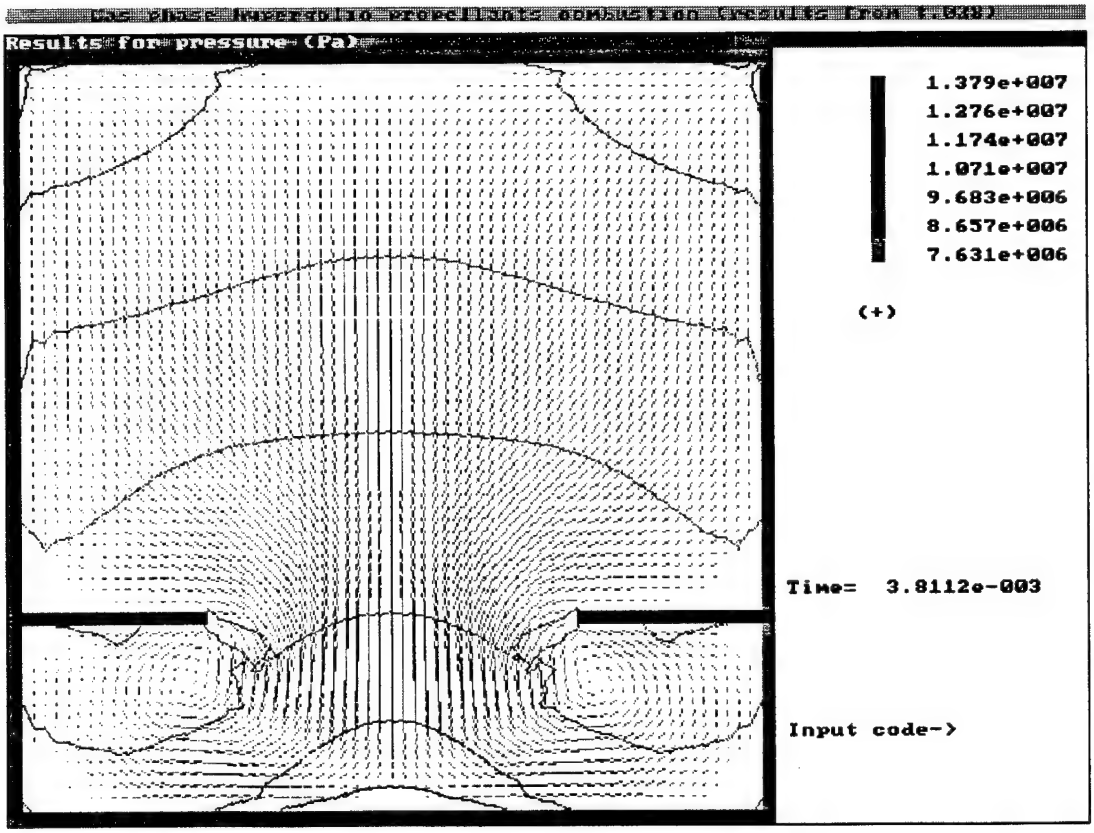
Results for pressure (Pa)
1.379e+007
1.276e+007
1.174e+007
1.071e+007
9.683e+006
8.657e+006
7.631e+006
(+)
Time= 3.8112e-003
Input code->

Fig. 10a.

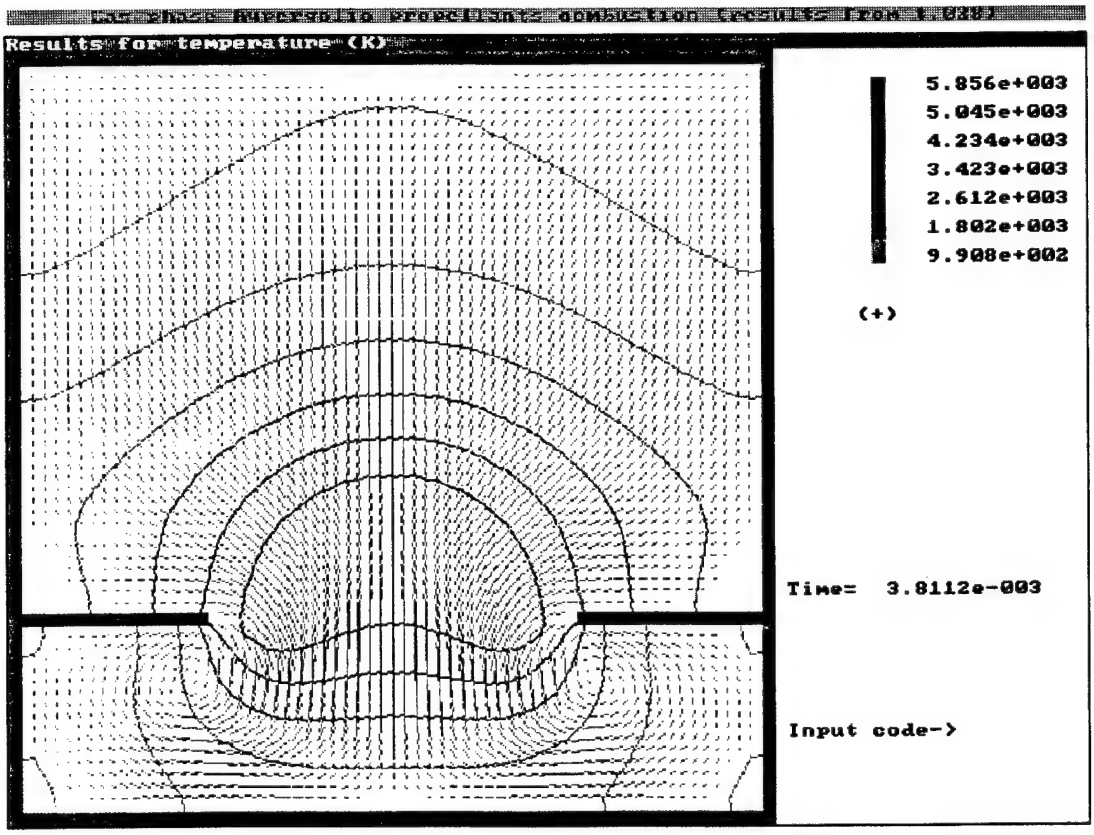
Results for temperature (K)
5.856e+003
5.045e+003
4.234e+003
3.423e+003
2.612e+003
1.802e+003
9.908e+002
(+)
Time= 3.8112e-003
Input code->

Fig. 10b

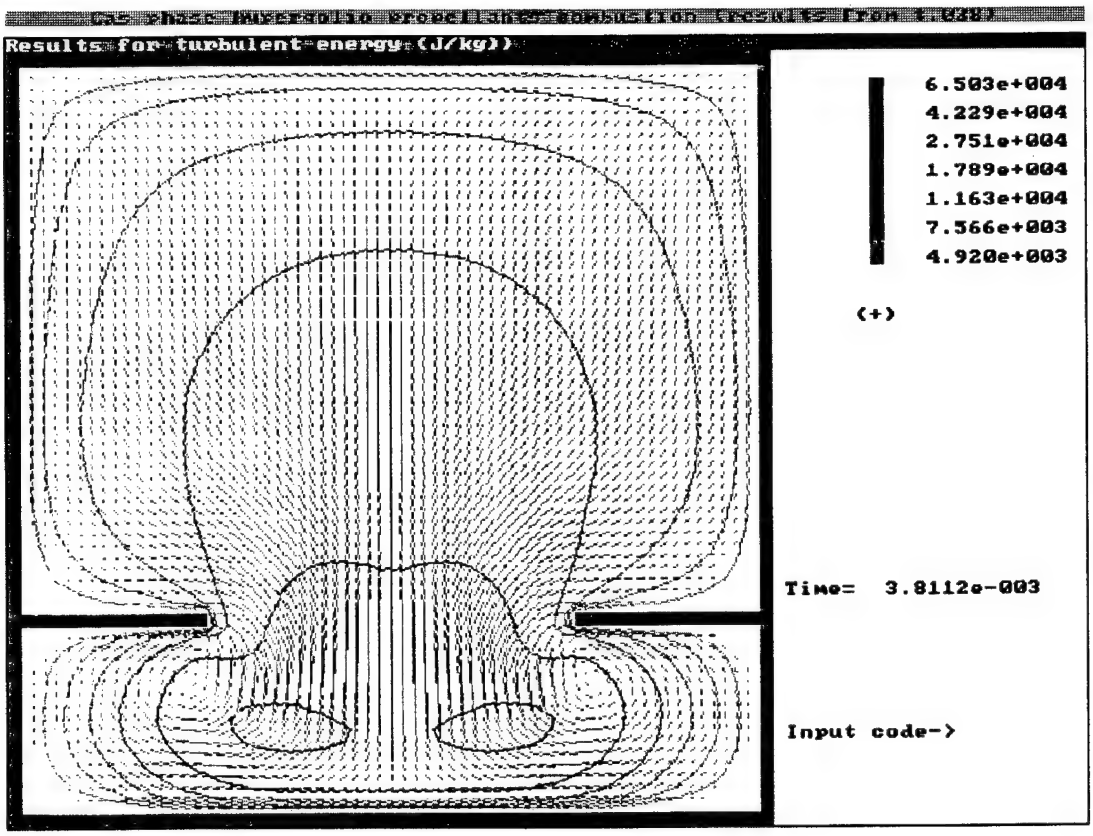
Results for turbulent energy (J/kg)
6.503e+004
4.229e+004
2.751e+004
1.789e+004
1.163e+004
7.566e+003
4.920e+003
(+)
Time= 3.8112e-003
Input code->

Fig. 10c.

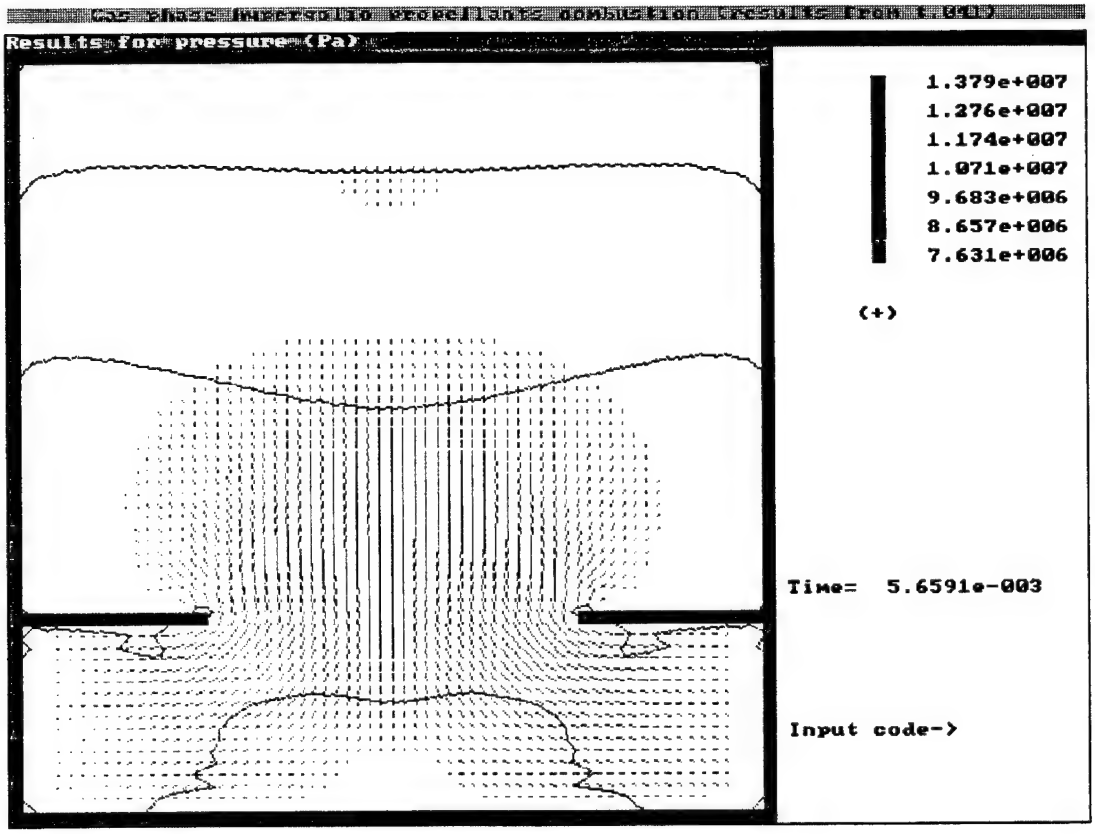
Results for pressure (Pa)
1.379e+007
1.276e+007
1.174e+007
1.071e+007
9.683e+006
8.657e+006
7.631e+006
(+)
Time= 5.6591e-003
Input code->

Fig. 11a.

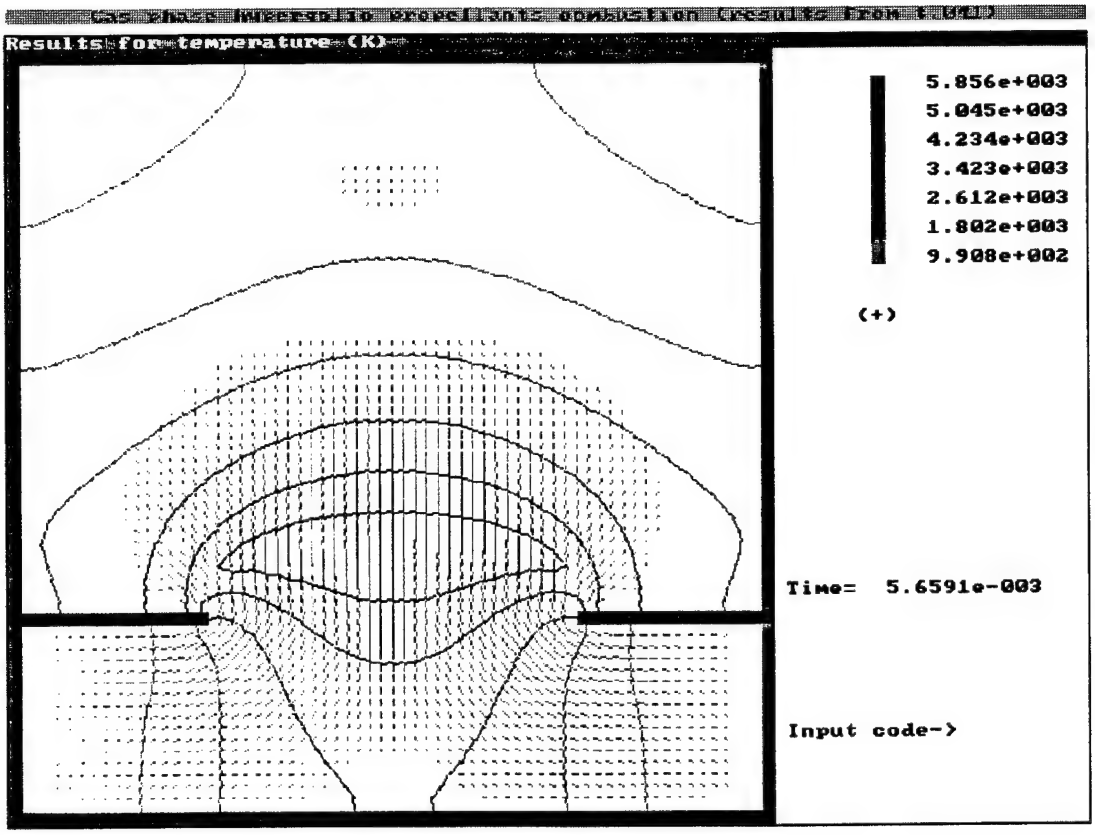
Results for temperature (K)
5.856e+003
5.045e+003
4.234e+003
3.423e+003
2.612e+003
1.802e+003
9.908e+002
(+)
Time= 5.6591e-003
Input code->

Fig. 11b.

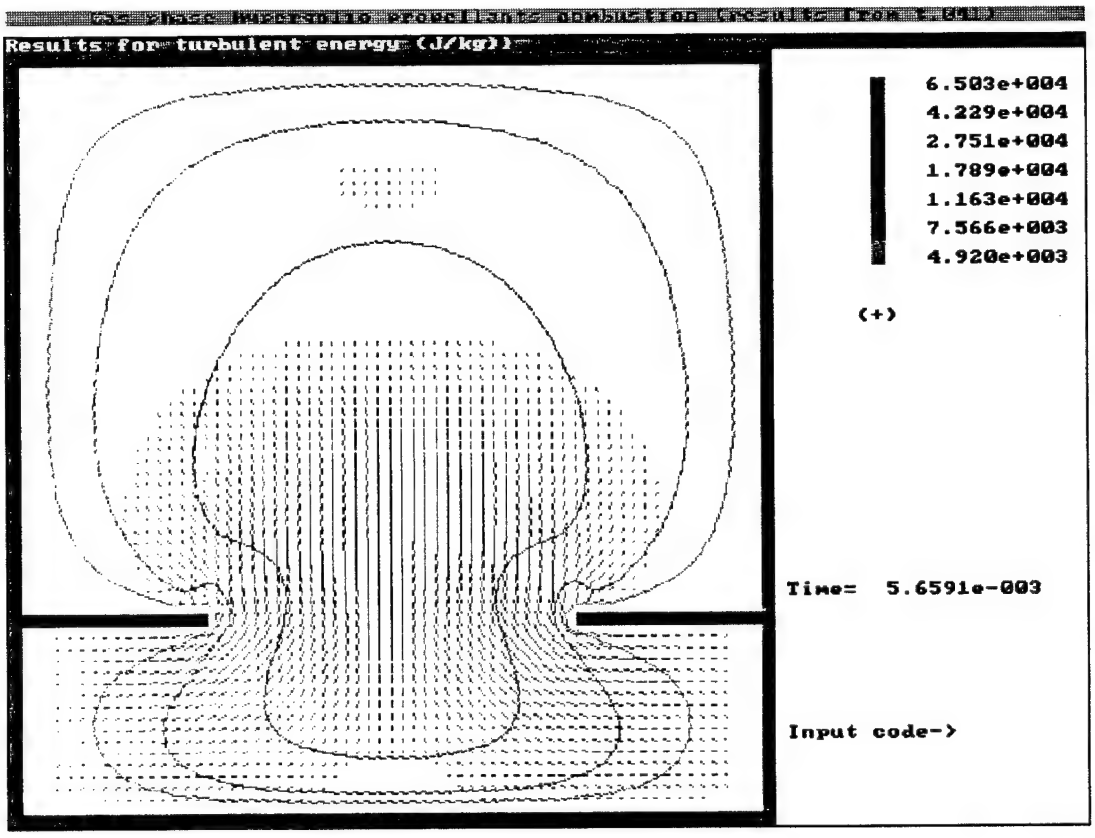
Results for turbulent energy (J/kg)
6.503e+004
4.229e+004
2.751e+004
1.789e+004
1.163e+004
7.566e+003
4.920e+003
(+)
Time= 5.6591e-003
Input code->

Fig. 11c.

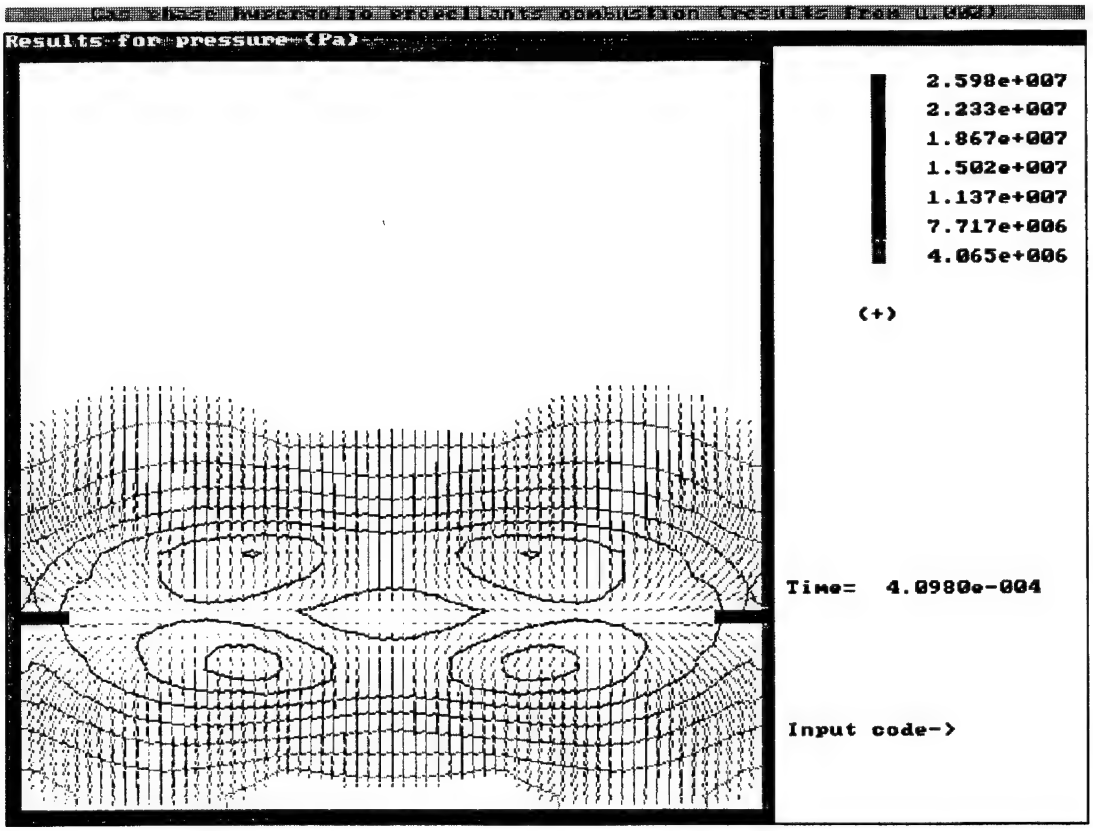
Results for pressure (Pa)
2.598e+007
2.233e+007
1.867e+007
1.502e+007
1.137e+007
7.717e+006
4.065e+006
(+)
Time= 4.0980e-004
Input code->

Fig. 12 a.

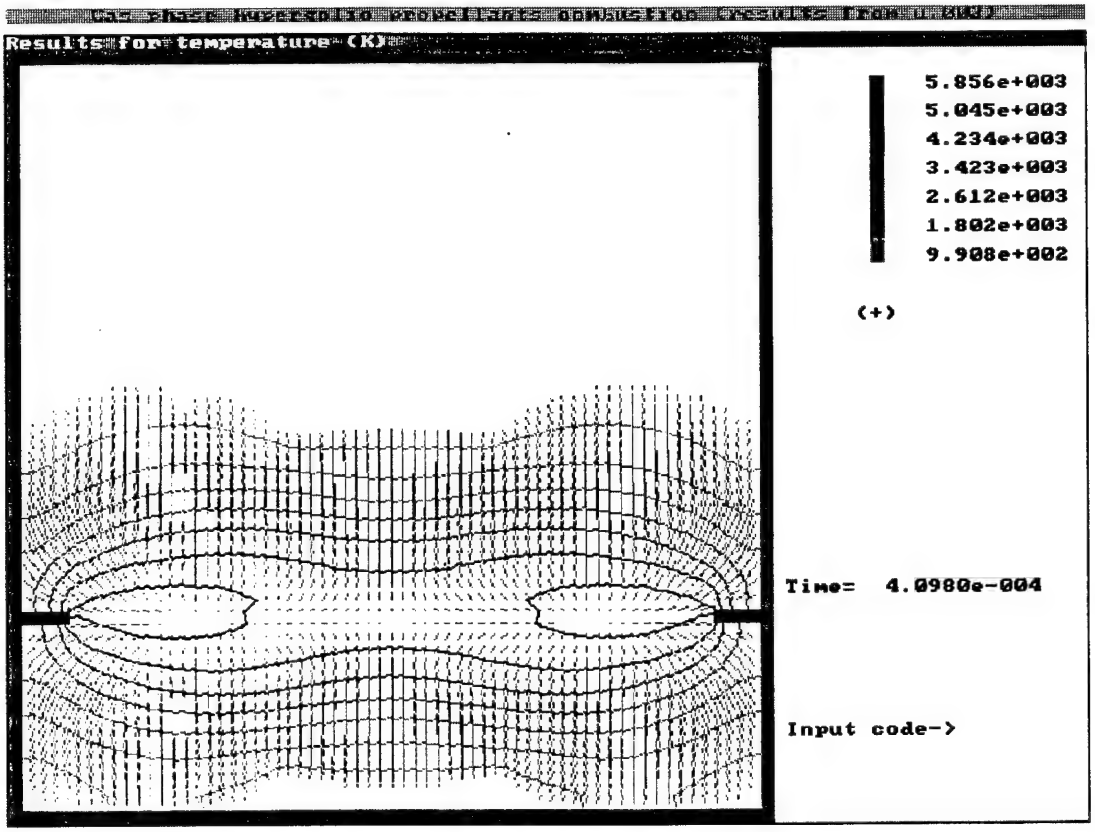
Results for temperature (K)
5.856e+003
5.045e+003
4.234e+003
3.423e+003
2.612e+003
1.802e+003
9.908e+002
(+)
Time= 4.0980e-004
Input code->

Fig. 12 b.

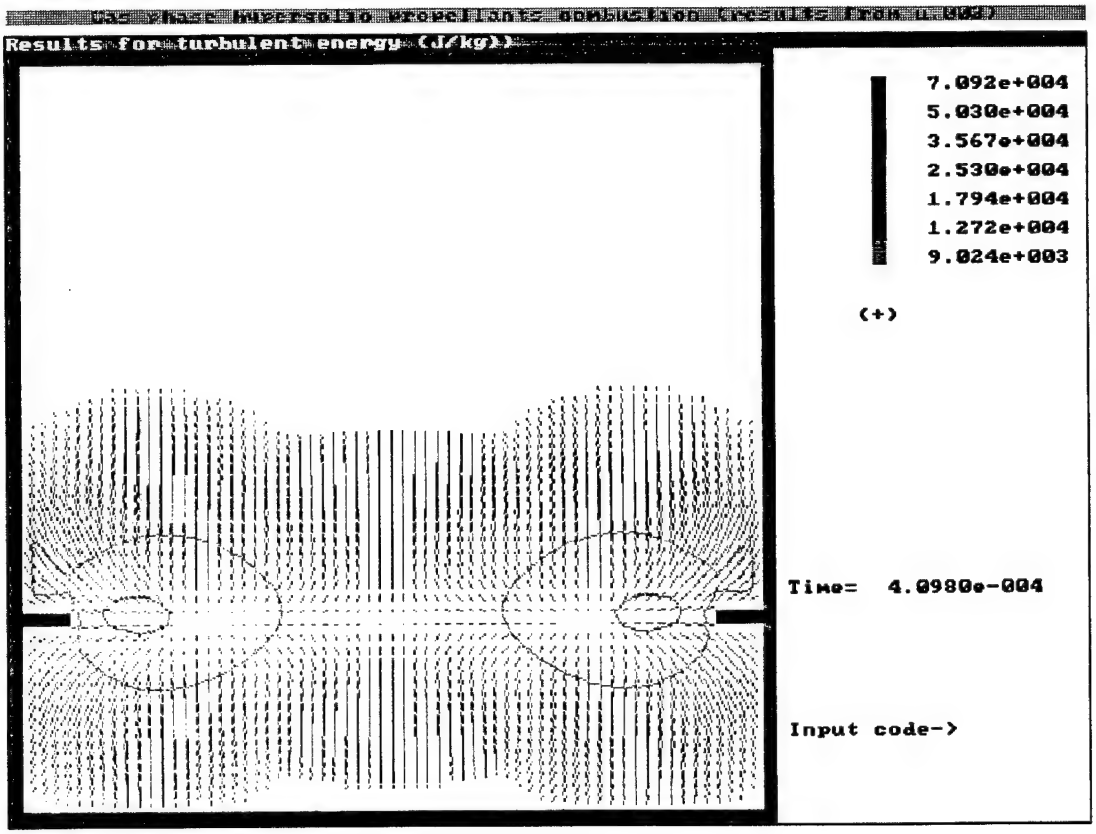
Results for turbulent energy (J/kg)
7.092e+004
5.030e+004
3.567e+004
2.530e+004
1.794e+004
1.272e+004
9.024e+003
(+)
Time= 4.0980e-004
Input code->

Fig. 12c.

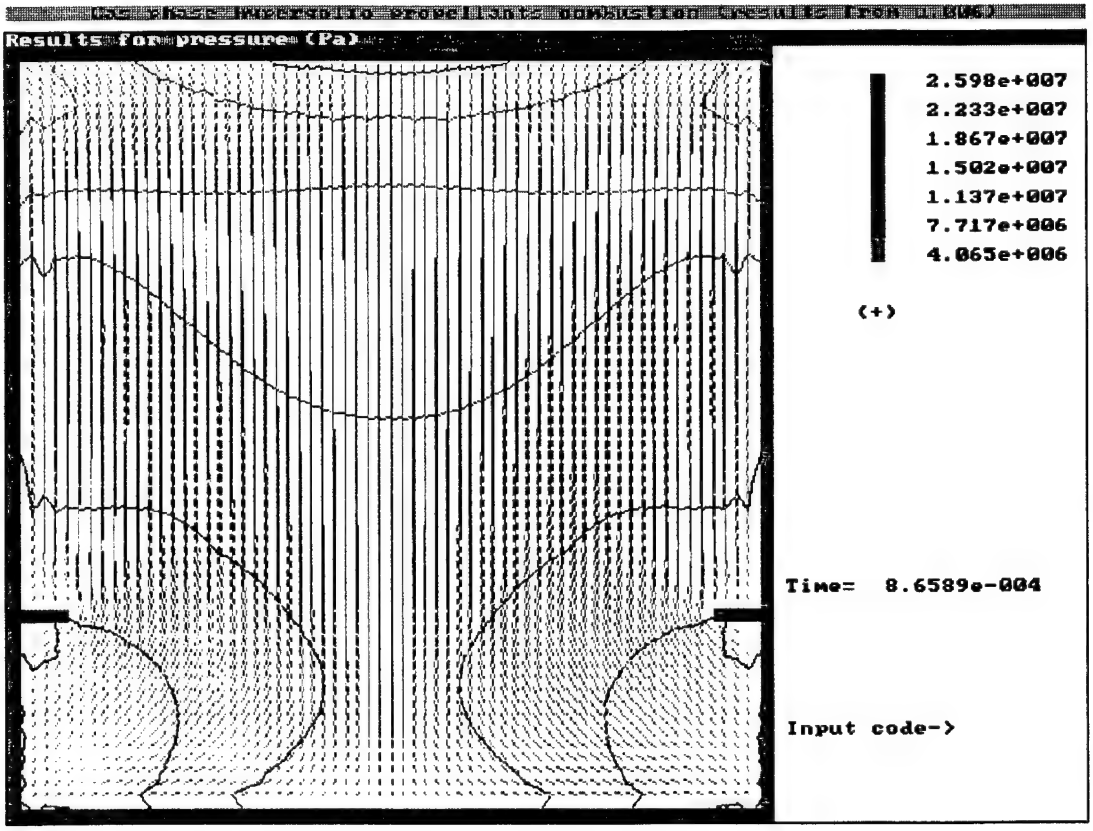
Results for pressure (Pa)
2.598e+007
2.233e+007
1.867e+007
1.502e+007
1.137e+007
7.717e+006
4.065e+006
(+)
Time= 8.6589e-004
Input code->

Fig. 13a

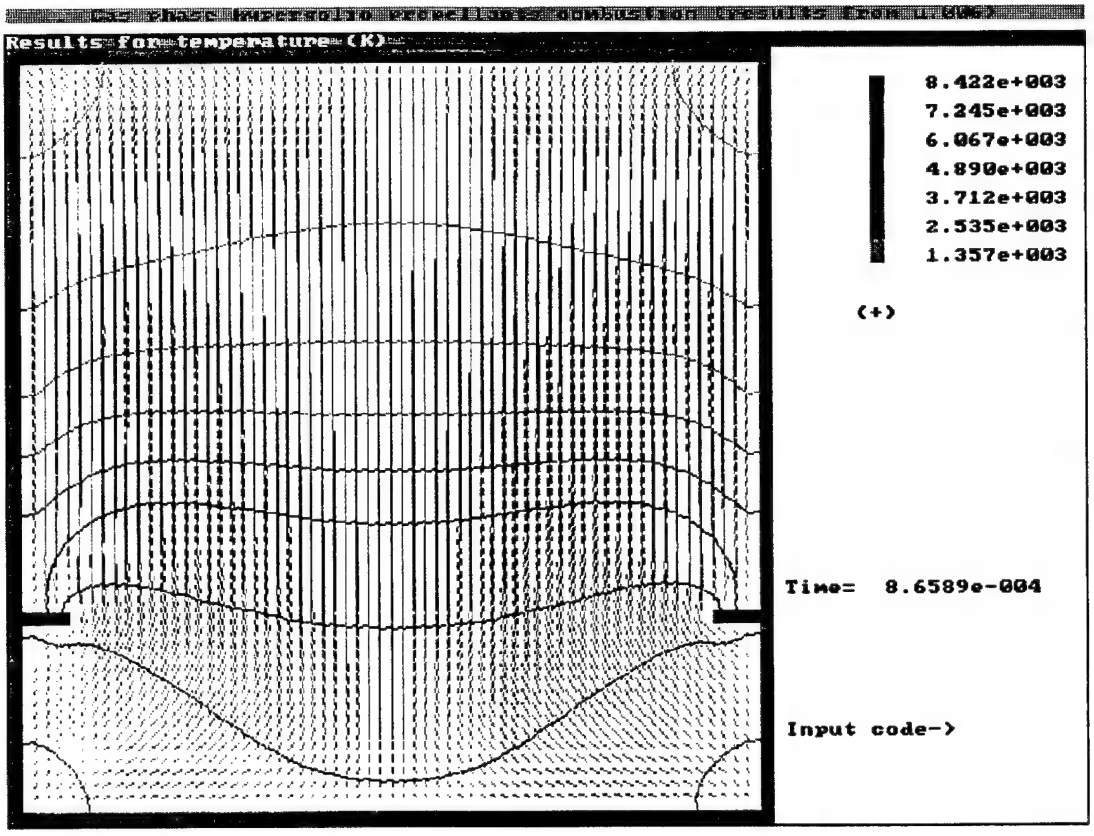
Results for temperature (K)
8.422e+003
7.245e+003
6.067e+003
4.890e+003
3.712e+003
2.535e+003
1.357e+003
(+)
Time= 8.6589e-004
Input code->

Fig. 13 b.

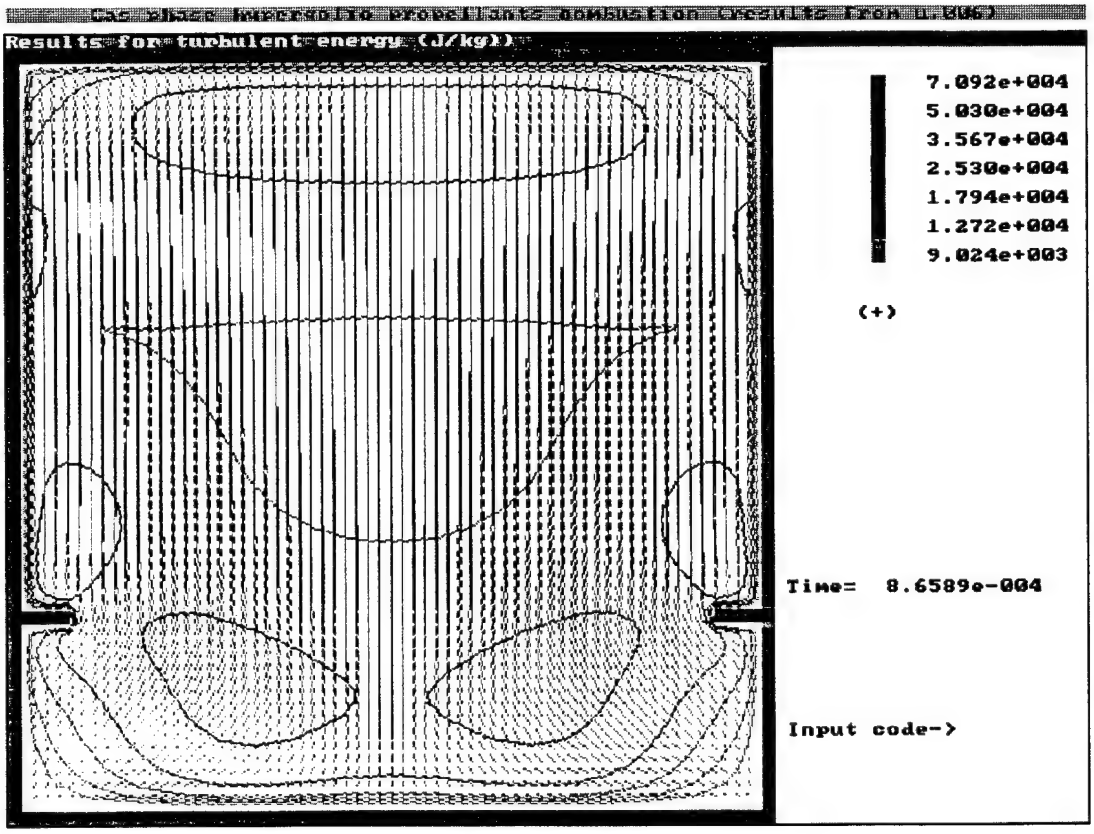
Results for turbulent energy (J/kg))
7.092e+004
5.030e+004
3.567e+004
2.530e+004
1.794e+004
1.272e+004
9.024e+003
(+)
Time= 8.6589e-004
Input code->

Fig. 13c.

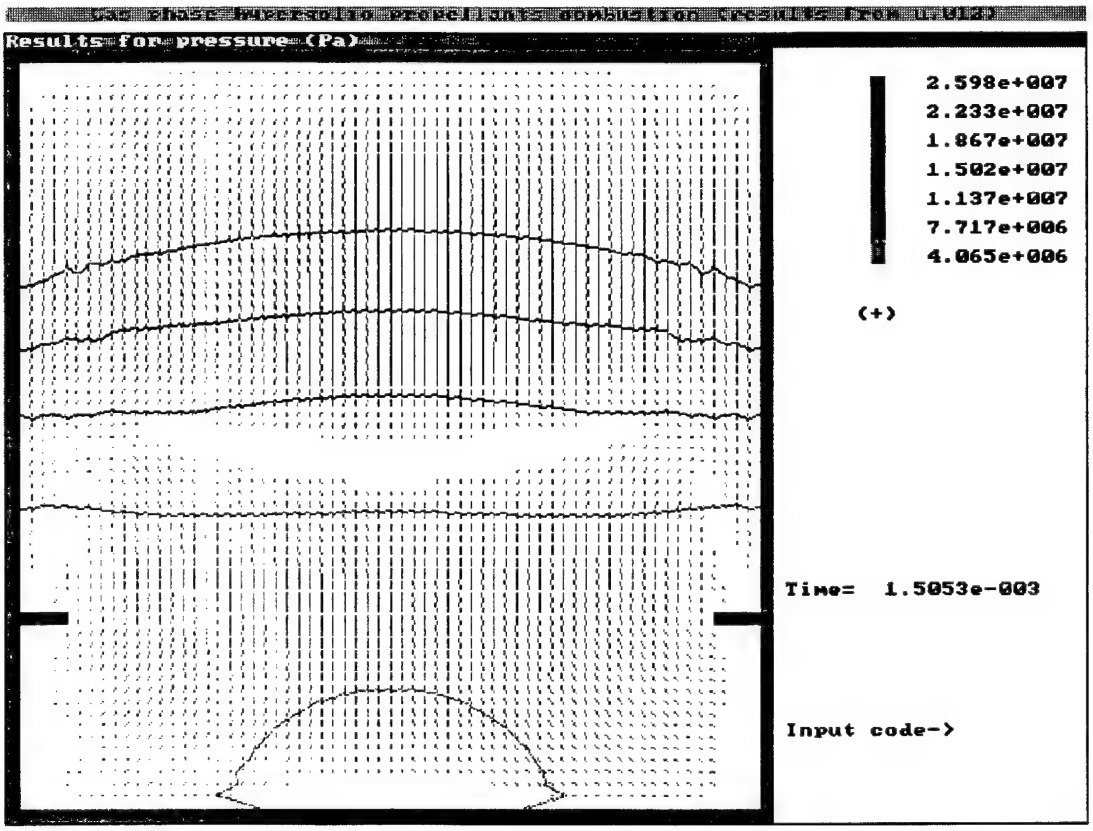
Results for pressure (Pa)
2.598e+007
2.233e+007
1.867e+007
1.502e+007
1.137e+007
7.717e+006
4.065e+006
(+)
Time= 1.5053e-003
Input code->

Fig. 14a.

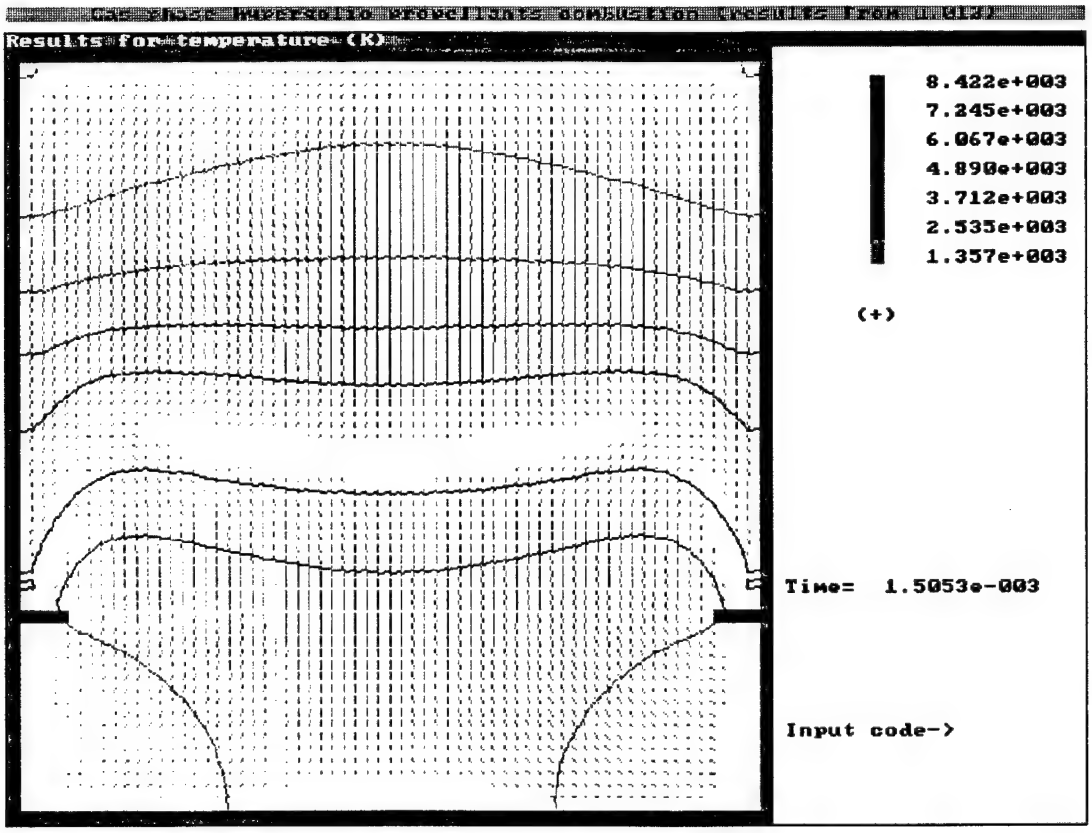
Results for temperature (K)
8.422e+003
7.245e+003
6.067e+003
4.890e+003
3.712e+003
2.535e+003
1.357e+003
(+)
Time= 1.5053e-003
Input code->

Fig. 14 B.

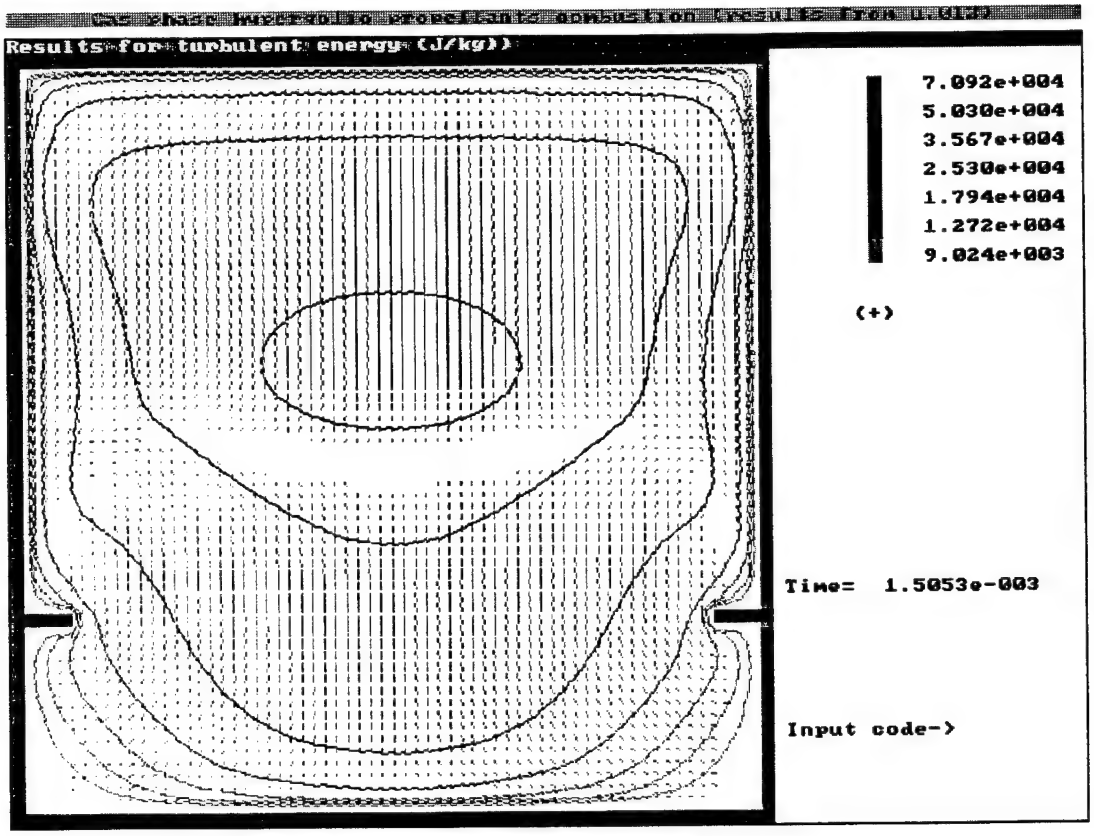
Results for turbulent energy (J/kg)
7.092e+004
5.030e+004
3.567e+004
2.530e+004
1.794e+004
1.272e+004
9.024e+003
(+)
Time= 1.5053e-003
Input code->

Fig. 14c.

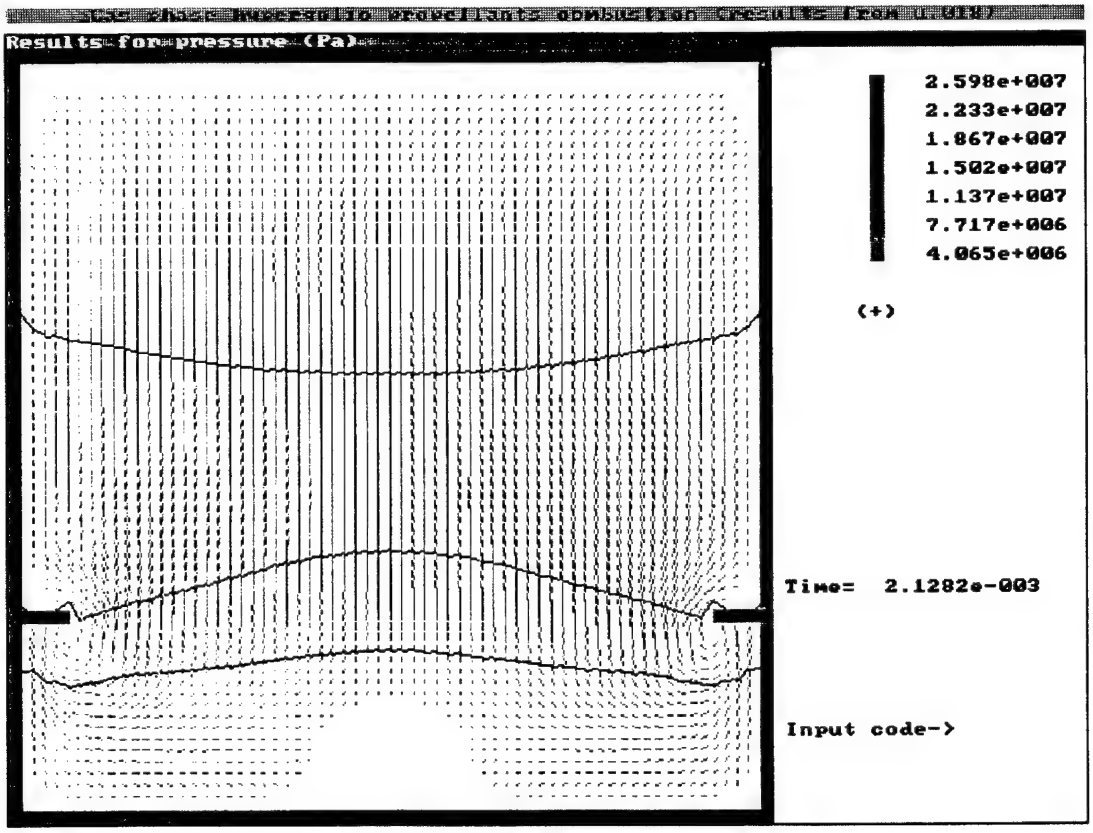
Results for pressure (Pa)
2.598e+007
2.233e+007
1.867e+007
1.502e+007
1.137e+007
7.717e+006
4.065e+006
(+)
Time= 2.1282e-003
Input code->

Fig. 15a.

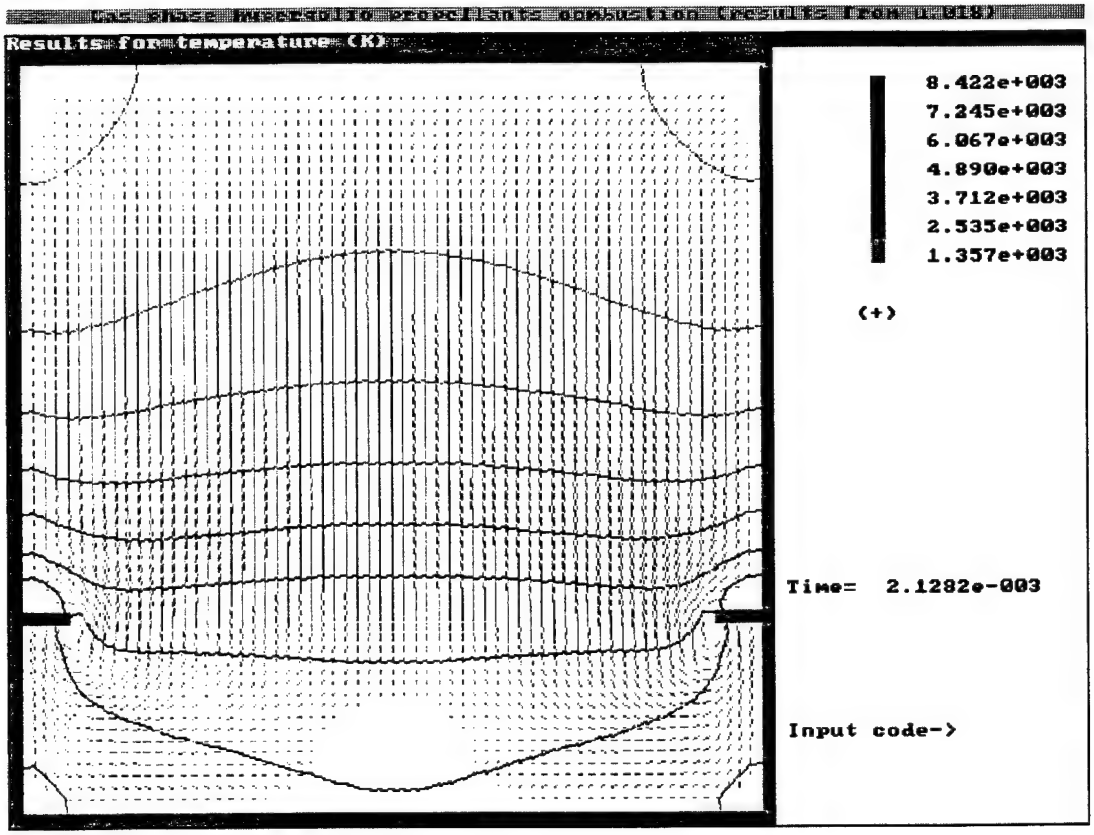
Results for temperature (K)
8.422e+003
7.245e+003
6.067e+003
4.890e+003
3.712e+003
2.535e+003
1.357e+003
(+)
Time= 2.1282e-003
Input code->

Fig. 15b.

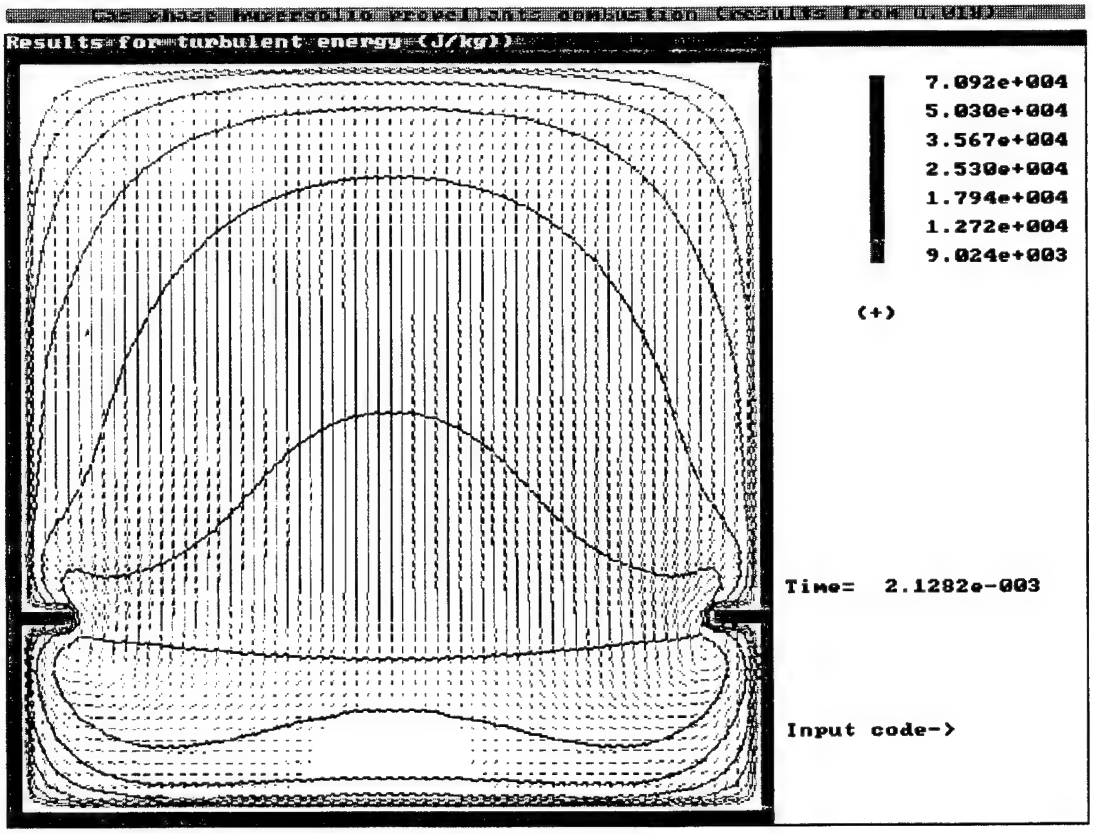
Results for turbulent energy (J/kg)
7.092e+004
5.030e+004
3.567e+004
2.530e+004
1.794e+004
1.272e+004
9.024e+003
(+)
Time= 2.1282e-003
Input code->

Fig. 15c.

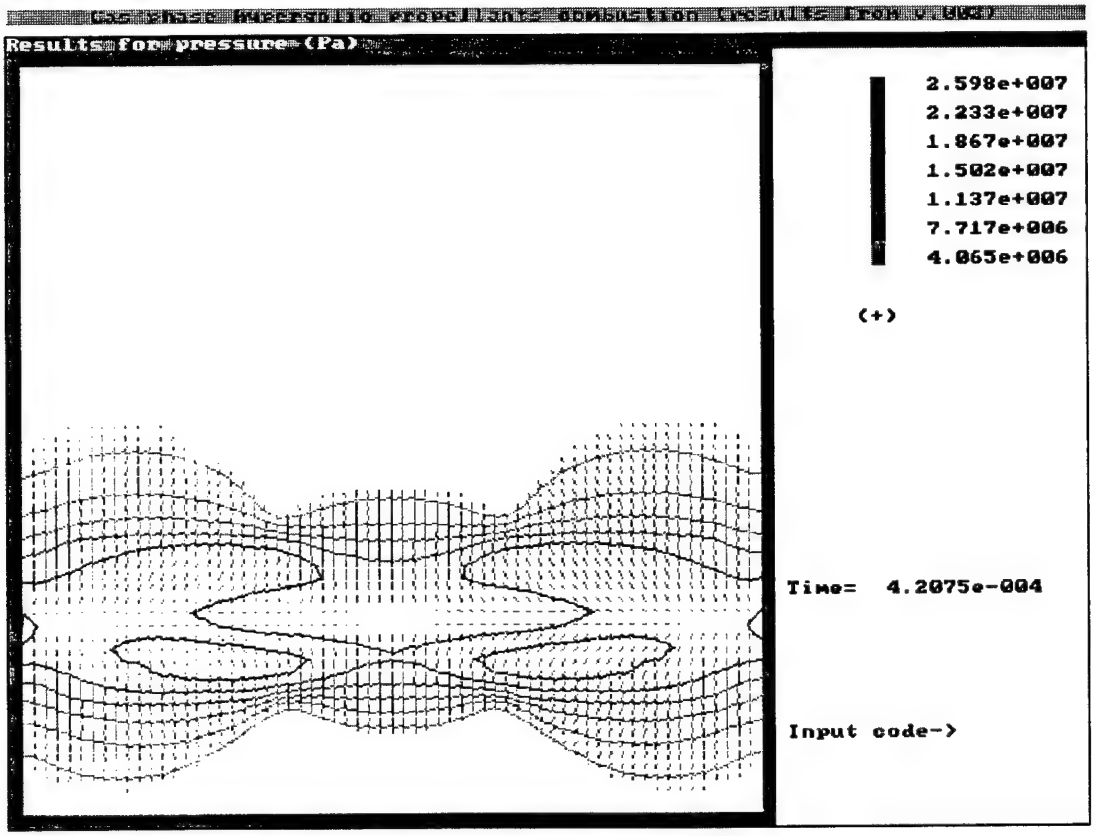
Results for pressure (Pa)
2.598e+007
2.233e+007
1.867e+007
1.502e+007
1.137e+007
7.717e+006
4.065e+006
(+)
Time= 4.2075e-004
Input code->

Fig. 16a.

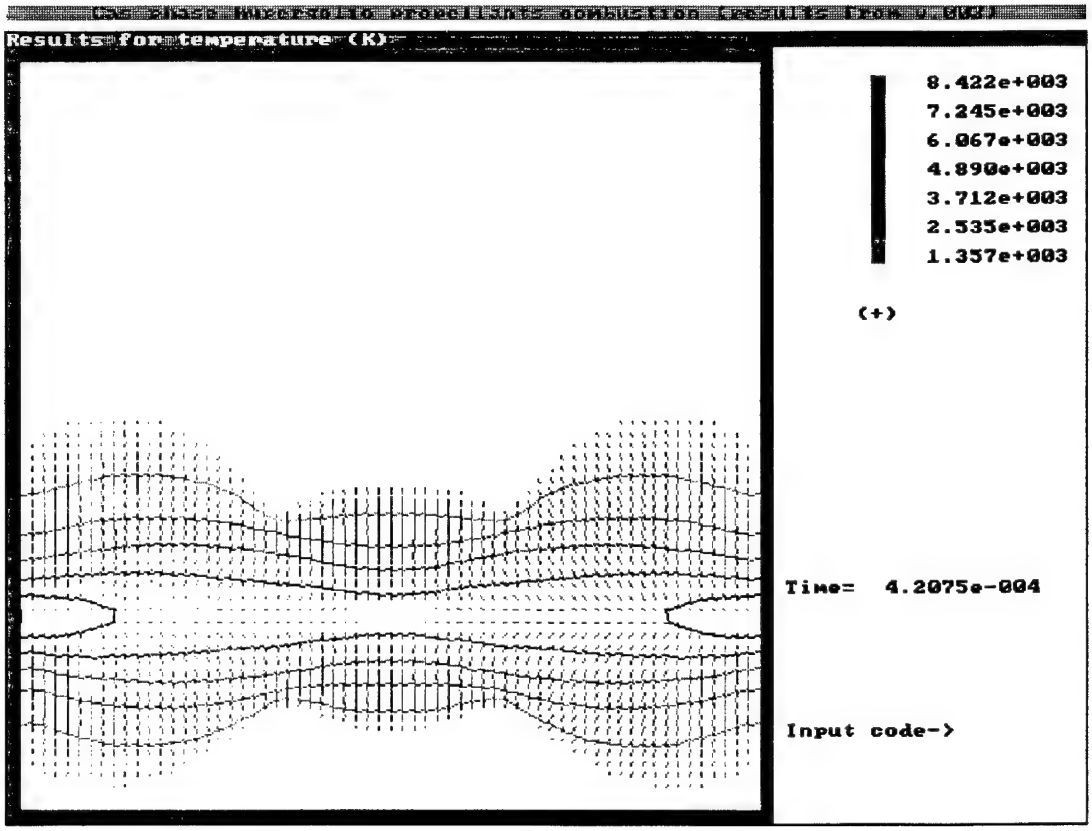
Results for temperature (K)
8.422e+003
7.245e+003
6.067e+003
4.890e+003
3.712e+003
2.535e+003
1.357e+003
(+)
Time= 4.2075e-004
Input code->

Fig. 16b.

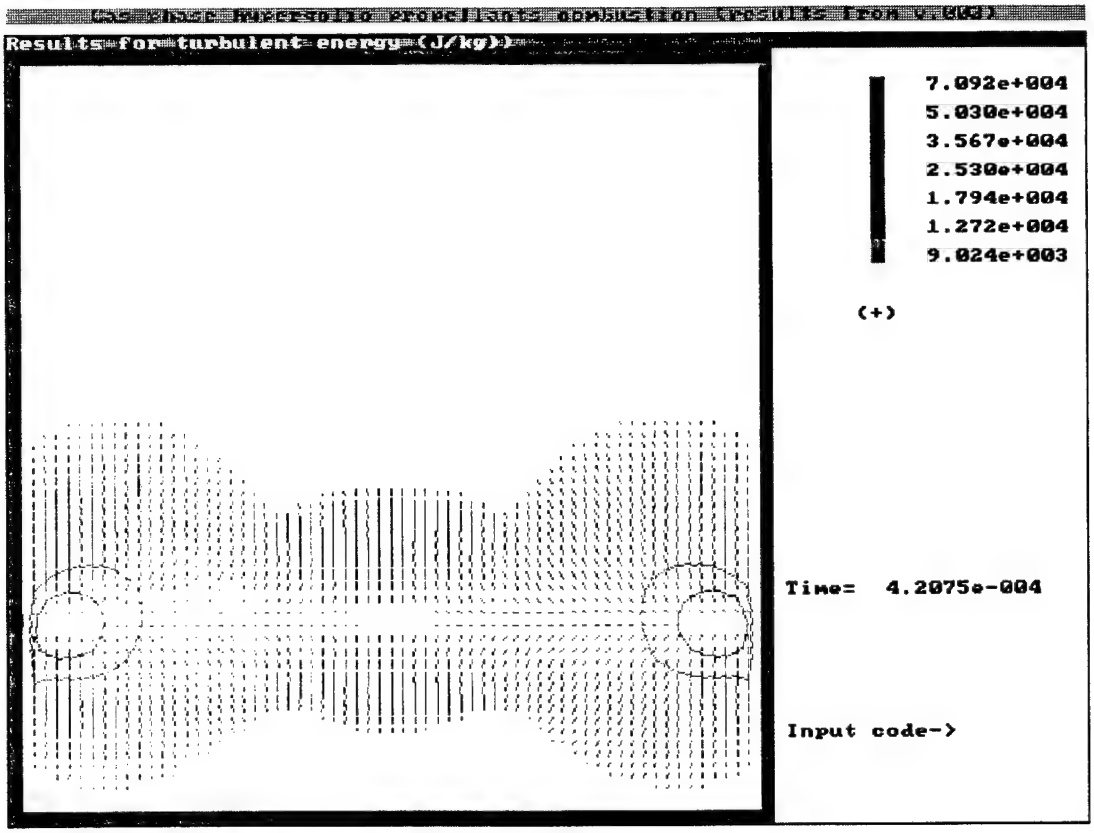
Results for turbulent energy (J/kg)
7.092e+004
5.030e+004
3.567e+004
2.530e+004
1.794e+004
1.272e+004
9.024e+003
(+)
Time= 4.2075e-004
Input code->

Fig. 16c.

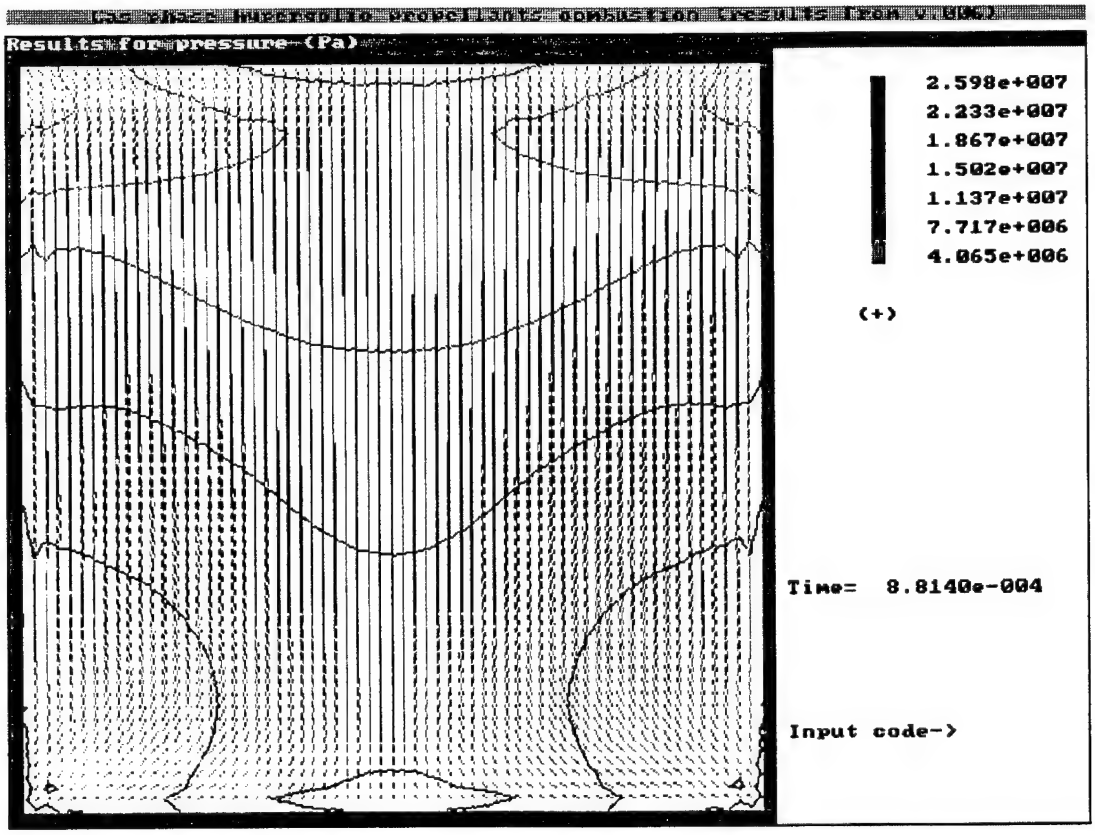
Results for pressure-(Pa)
2.598e+007
2.233e+007
1.867e+007
1.502e+007
1.137e+007
7.717e+006
4.065e+006
(+)
Time= 8.8140e-004
Input code->

Fig. 17a.

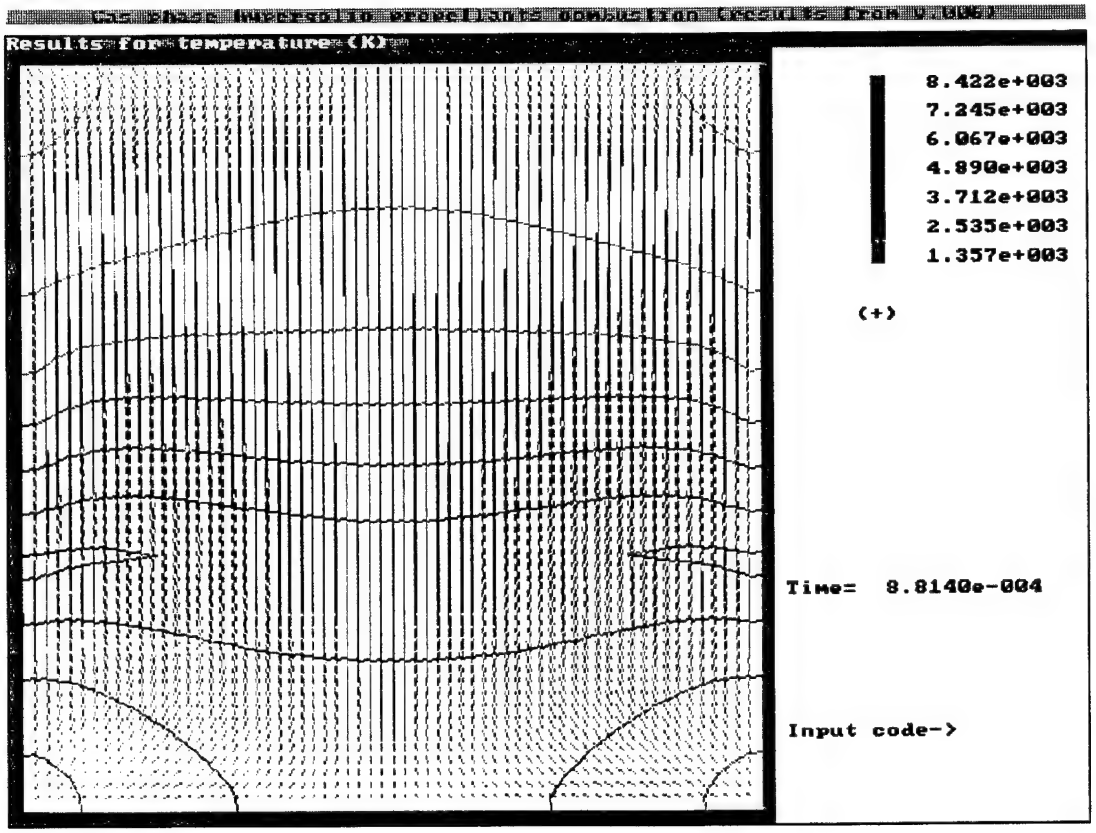
Results for temperature (K)
8.422e+003
7.245e+003
6.067e+003
4.890e+003
3.712e+003
2.535e+003
1.357e+003
(+)
Time= 8.8140e-004
Input code->

Fig. 17b.

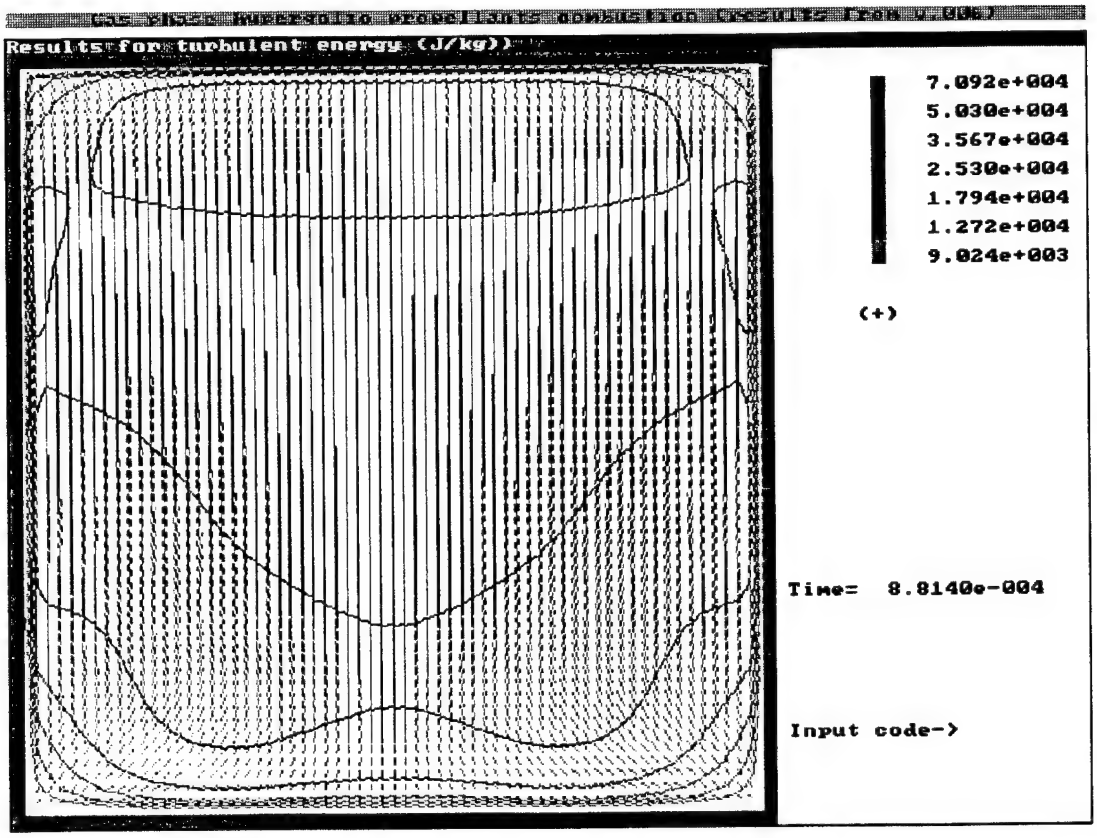
Results for turbulent energy (J/kg)
7.092e+004
5.030e+004
3.567e+004
2.530e+004
1.794e+004
1.272e+004
9.024e+003
(+)
Time= 8.8140e-004
Input code->

Fig. 17c.

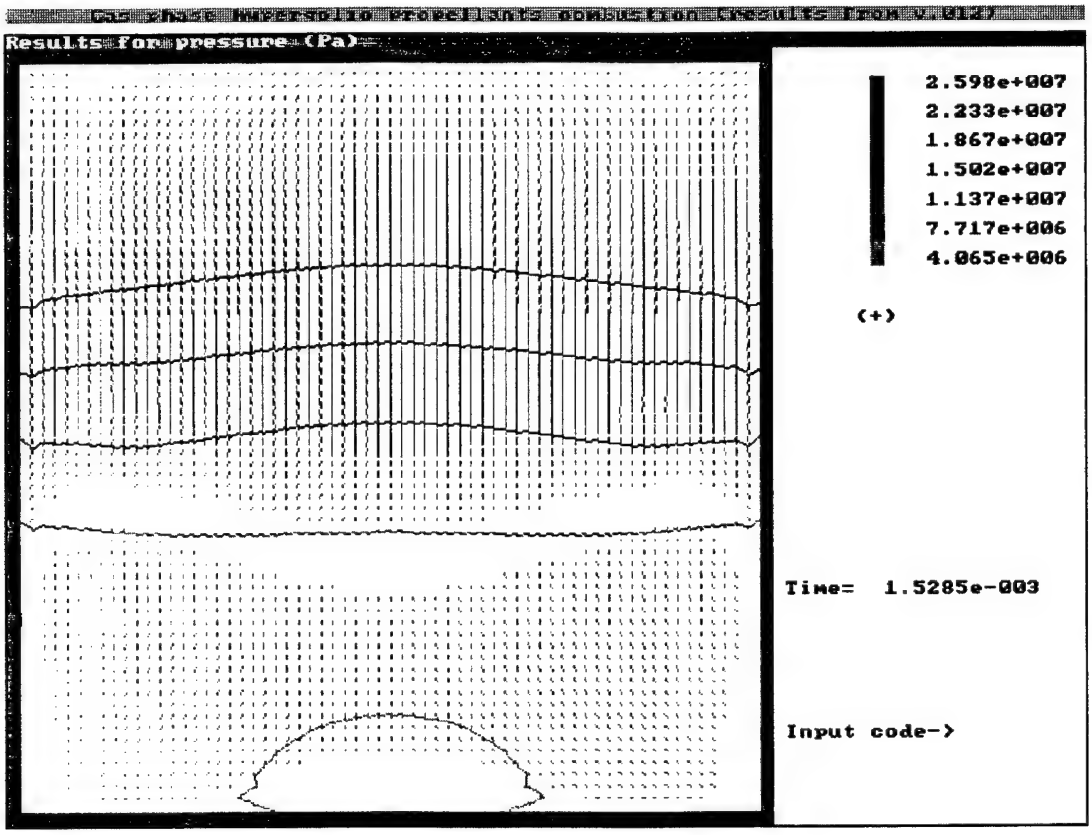
Results for pressure (Pa)
2.598e+007
2.233e+007
1.867e+007
1.502e+007
1.137e+007
7.717e+006
4.065e+006
(+)
Time= 1.5285e-003
Input code->

Fig. 18a.

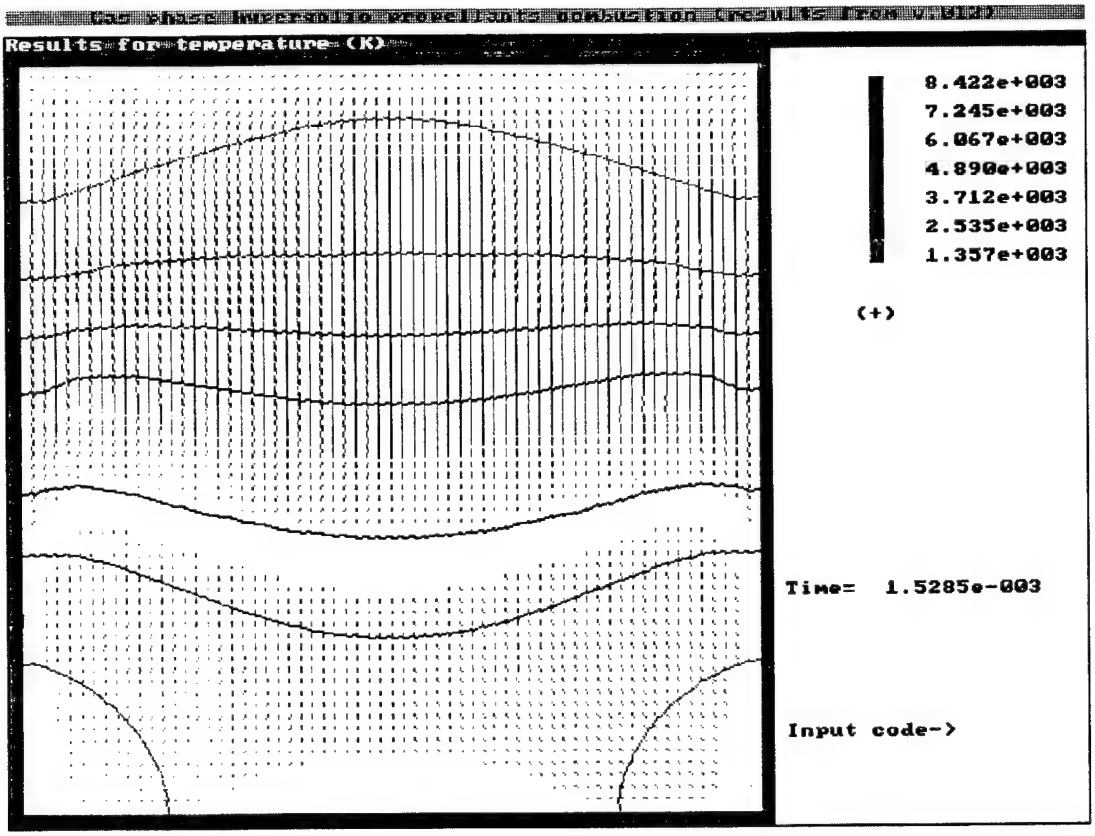
Results for temperature (K)
8.422e+003
7.245e+003
6.067e+003
4.890e+003
3.712e+003
2.535e+003
1.357e+003
(+)
Time= 1.5285e-003
Input code->

Fig. 18b.

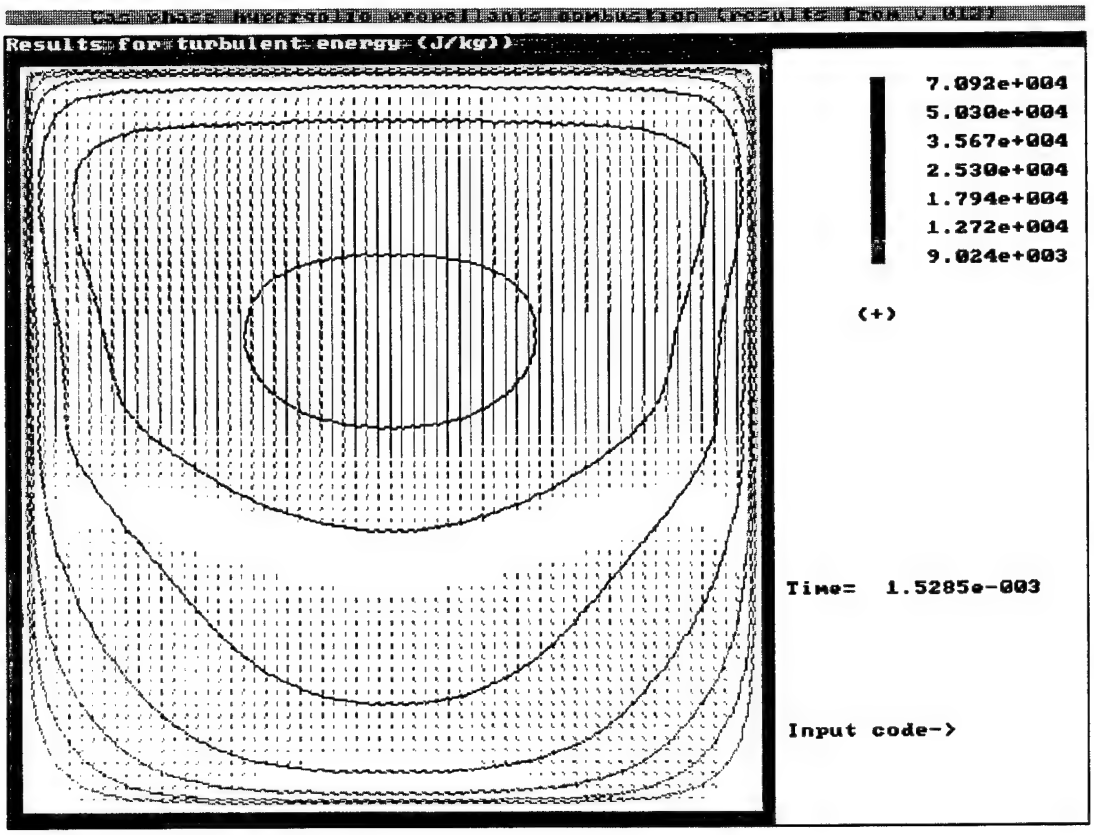
Results for turbulent energy (J/kg)
7.092e+004
5.030e+004
3.567e+004
2.530e+004
1.794e+004
1.272e+004
9.024e+003
(+)
Time= 1.5285e-003
Input code->

Fig. 18c.

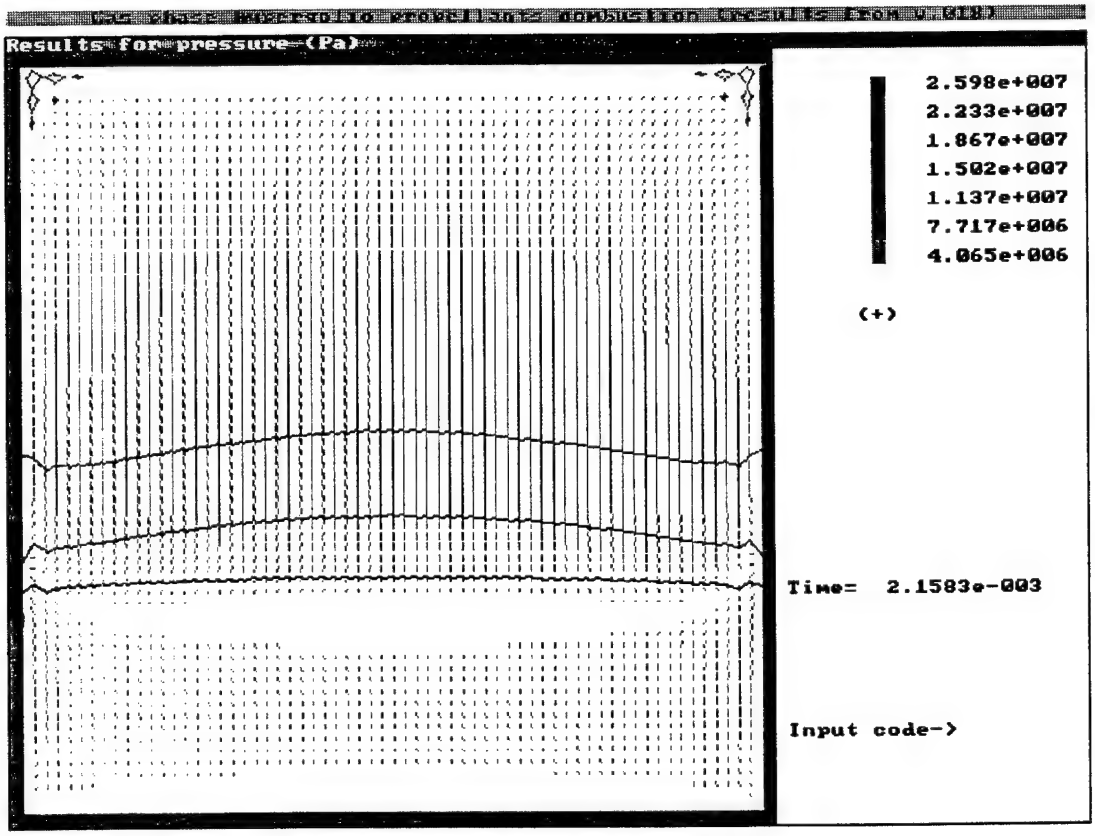
Results for pressure (Pa)
2.598e+007
2.233e+007
1.867e+007
1.502e+007
1.137e+007
7.717e+006
4.065e+006
(+)
Time= 2.1583e-003
Input code->

Fig. 19a.

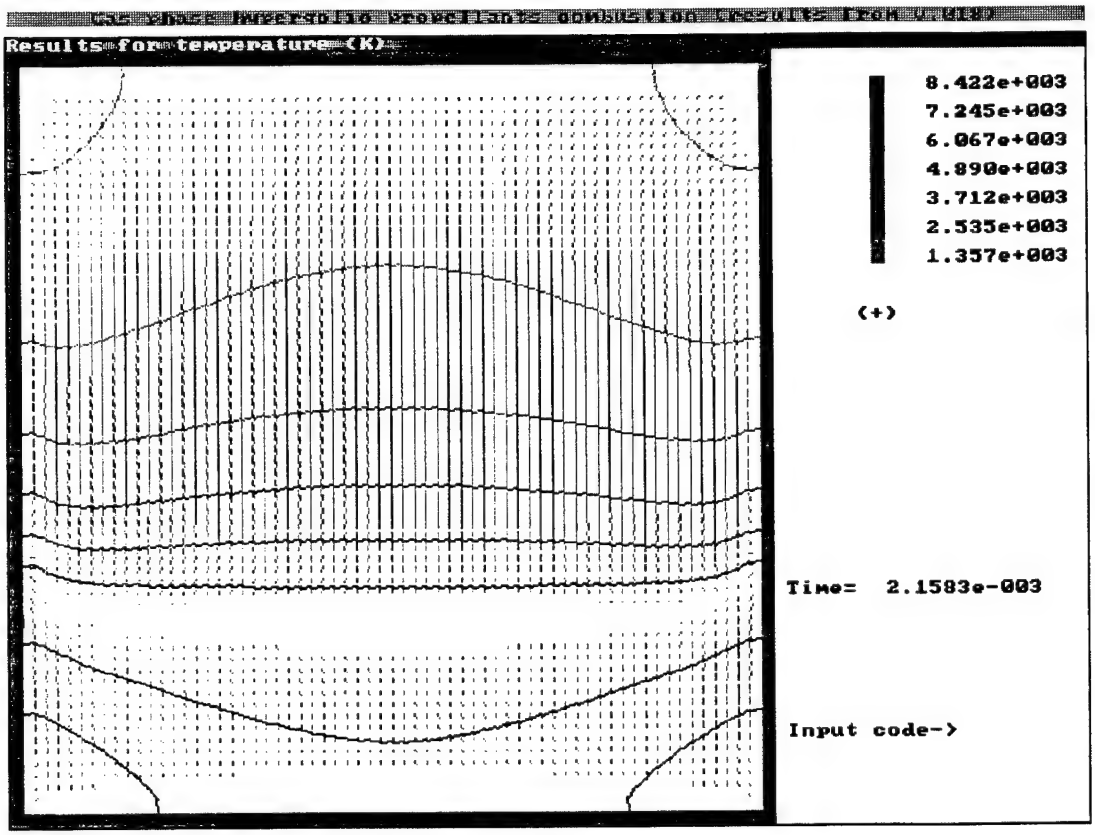
Results for temperature (K)
8.422e+003
7.245e+003
6.067e+003
4.890e+003
3.712e+003
2.535e+003
1.357e+003
(+)
Time= 2.1583e-003
Input code->

Fig. 19 b.

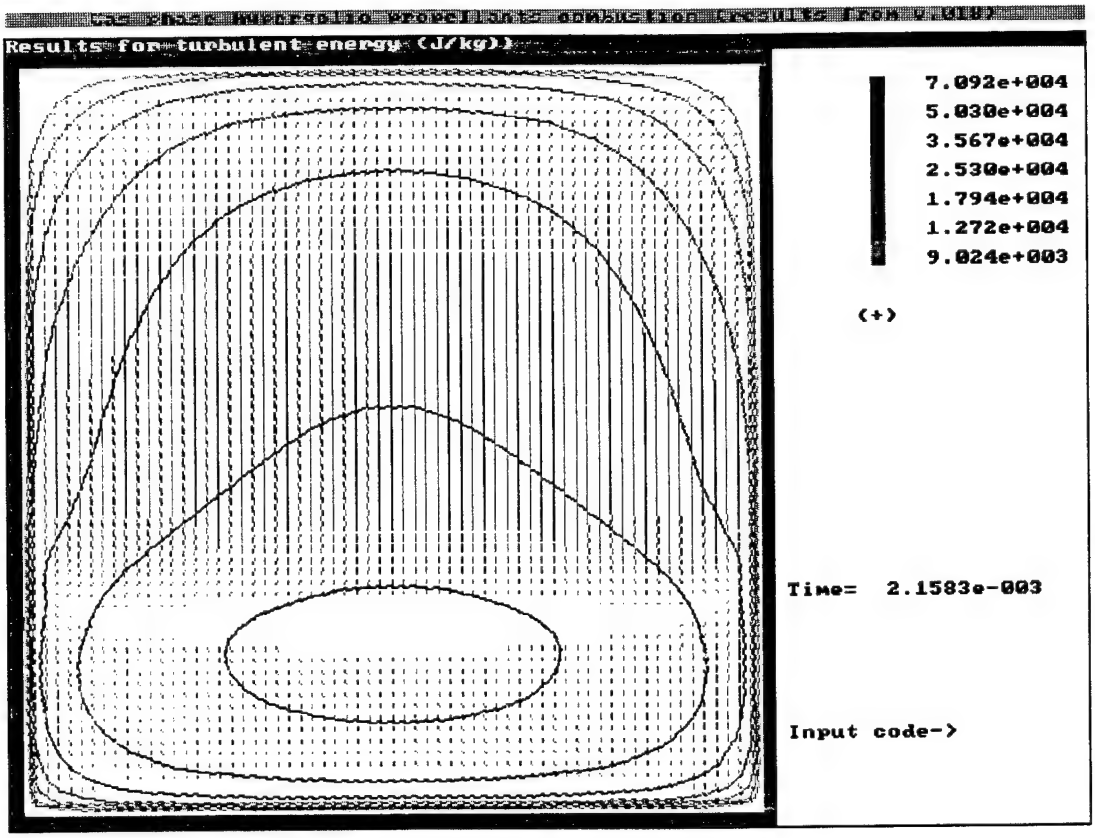
Results for turbulent energy (J/kg)
7.092e+004
5.030e+004
3.567e+004
2.530e+004
1.794e+004
1.272e+004
9.024e+003
(+)
Time= 2.1583e-003
Input code->

Fig. 19c

## §2.2. Results of numerical investigations of wall loading and breakup in diffusive combustion inside propellants' tank

To model the wall loading a test case was chosen wherein the diameter of a coaxial opening was one half of the total diameter of the tank $d_0$ ($d_0 = 1$ m). The thickness of the walls was considered to be $h_0 = 2 \cdot 10^{-3}$ m. Fig. 20 shows pressure evolution inside the tank for different times that reflects the wall loadings that happen to be nonuniform and variable in time.

Fig. 21a,b,c,d,e reflect the temperature evolution for different times. It is seen from the Figs.21 that temperature distribution near the walls is also essentially nonuniform. Different colours in Figs. 20, 21 correspond to different values of parameters. The scale is given in the upper right corner of each figure.

Mass concentrations of species: oxidant, fuel and reaction products - are shown in Figs.22-24 a, b, c for three different time moments. It is seen from the figures that growth of the amount of reaction products with time lowers the reaction rate of diffusion combustion as it turns to be more difficult for the components (fuel and oxidant) to penetrate through reaction products to enter the reaction zone.

Fig.25 shows the evolution of turbulent kinetic energy in time. The growth of turbulence starts in the ring zone near the boundaries of the opening in the bulkhead and then spreads in the flow. Fig. 26 show the distribution of turbulent dissipation $\varepsilon$ for the time corresponding to that in Fig.25e.

Figs. 27, 28 show the evolution of wall pressure and tensile ring stress. The coordinate axis starts in the center of the bottom of the cylinder and moving along the wall reaches the center of the top plate. Vertical lines on the figures reflect the connections of the side surface of the cylinder with the top and bottom surfaces.

Figs. 29, 30 show the plots of dissipation $D$ and elastic energy $E$ of the shell in a logarithmic scale for the times corresponding to that on Fig.28.

The breakup takes place when dissipation in one of the sections overcomes the critical value. Then the number and masses of fragments in each section are determined. Final velocities of fragments in each section of the shell are determined. Profiles of final velocities of fragments along the walls are shown in Fig.31a,b. The nonuniformity of velocities' distribution is caused by the nonuniformities of wall loading in diffusive combustion contrary to wall loading in explosion caused by detonation process [3]. Fig. 31a shows velocity of the shell for $t = t_*$ when destruction starts. Fig.31b shows final velocities of fragments after acceleration in the expanding gas flow.

Profiles of numbers of fragments per square unit $N_s$ are shown in Fig. 32. It is seen that in some zones of the shell very few fragments is produced due to low values of accumulated elastic energy.

The total number of fragments versus mass distribution function is shown in Fig. 33. The corresponding velocities distributions calculated on the base of (75) are shown in Fig. 34. Mean velocity is shown on the diagram (Fig.34) in blue colour. The upper and lower bounds of velocities are shown in brown and green colours respectively. The distribution obtained shows that the mean velocity of large fragments is less than that of smaller fragments. For very small fragments final velocity doesn't depend on mass

and is practically constant for a particular case of a breakup. This result is in a good agreement with the well-known velocity distributions [15].

The result showing the decrease of the velocity for larger fragments is reasonable for compact elements due to different rate of the acceleration. But for flat plates of constant thickness with orientation normal to the flow final velocity usually is independent of mass (area) that can be easily seen from the equations (70), (72). In our case velocity distribution versus masses of fragments appeared due to nonuniformity of loading: the less loaded zones accumulated less elastic energy and obtained smaller final velocity. Those zones can produce only large fragments in a breakup process. While the smaller fragments are produced mostly in the highly loaded zones and posess higher velocity and the smallest objects have nearly the same velocity as their formation is provided by nearly the same level of internal loading.

Fig.35 shows the fragments' distribution functions versus mass for different sections $S_\alpha$ of the walls of the cylinder. The corresponding section is indicated on the axis below that starts in the center of the bottom of the cylinder and finishes in the center of the top plate.

Another numerical experiment was carried out for the same values of governing parameters as the previous one but for a thicker wall of the tank $h = 4 \cdot 10^{-3}$ m.

By the time of breakup in the previous case ($h = 2 \cdot 10^{-3}$ m) the dissipation accumulated in the shell has nowhere reached the critical value. The increase of dissipation was terminated for some time, but later due to gradual heating of the shell and decrease of the elasticity limit of material $J_0$ (39) plastical deformations increase rapidly and cause the increase of dissipation $D$. The breakup takes place when dissipation overcomes the critical value $D_*$. The characteristic of this scenario of breakup is the greater fraction of large fragments due to a smaller amount of accumulated elastic energy performing the work of breakup.

Thus, in combustion of mixing hypergolic propellants after a destruction of the common bulkhead two possible scenario of breakup can take place.

Breakup can take place within the characteristic time of energy release in combustion. Then the nonuniformities of loading cause the origin of a rather wide spectrum of fragments mass and velocity distribution.

Breakup can take place in a much longer time after the destruction of the bulkhead when combustion and gasdynamic processes inside the tank are terminated. Such a breakup is a result of gradual heating of the shell and lowering its elasticity limit. This type of breakup is characteristized by a narrow spectrum of velocity distribution due to the fact that in this case internal loading turns to be practically uniform.

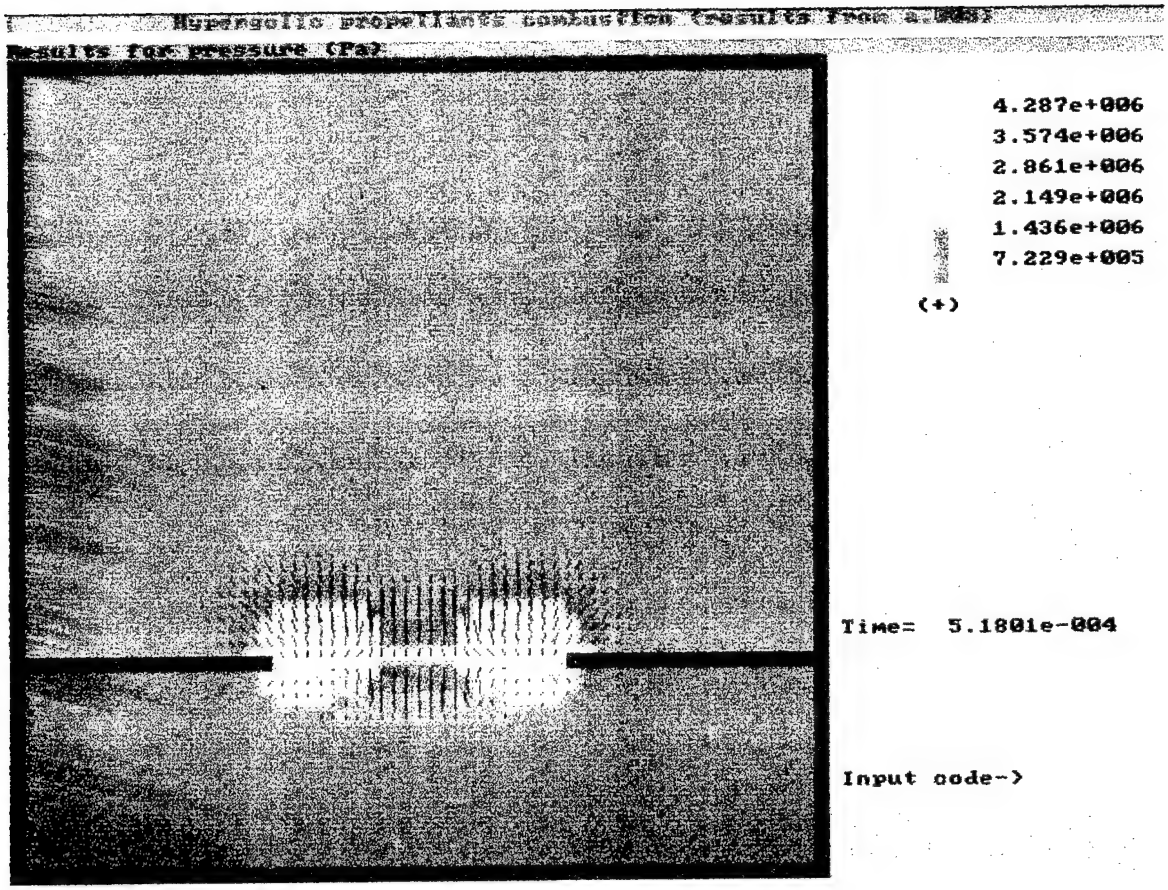
Hypergolic propellants combustion (results from a.
Results for pressure (Pa)
4.287e+006
3.574e+006
2.861e+006
2.149e+006
1.436e+006
7.229e+005
(+)
Time= 5.1801e-004
Input code->

Fig. 20a.

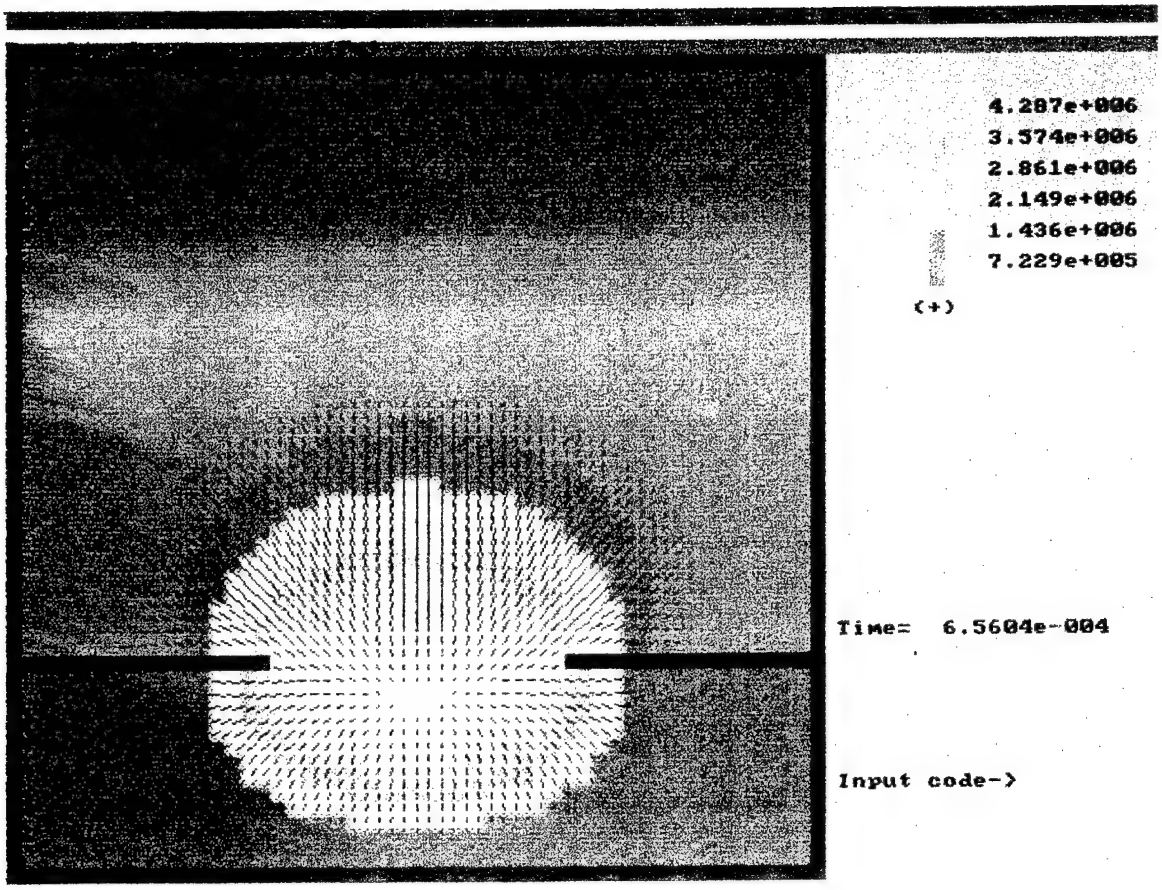
4.287e+006
3.574e+006
2.861e+006
2.149e+006
1.436e+006
7.229e+005
(+)
Time= 6.5604e-004
Input code->

Fig. 20 b.

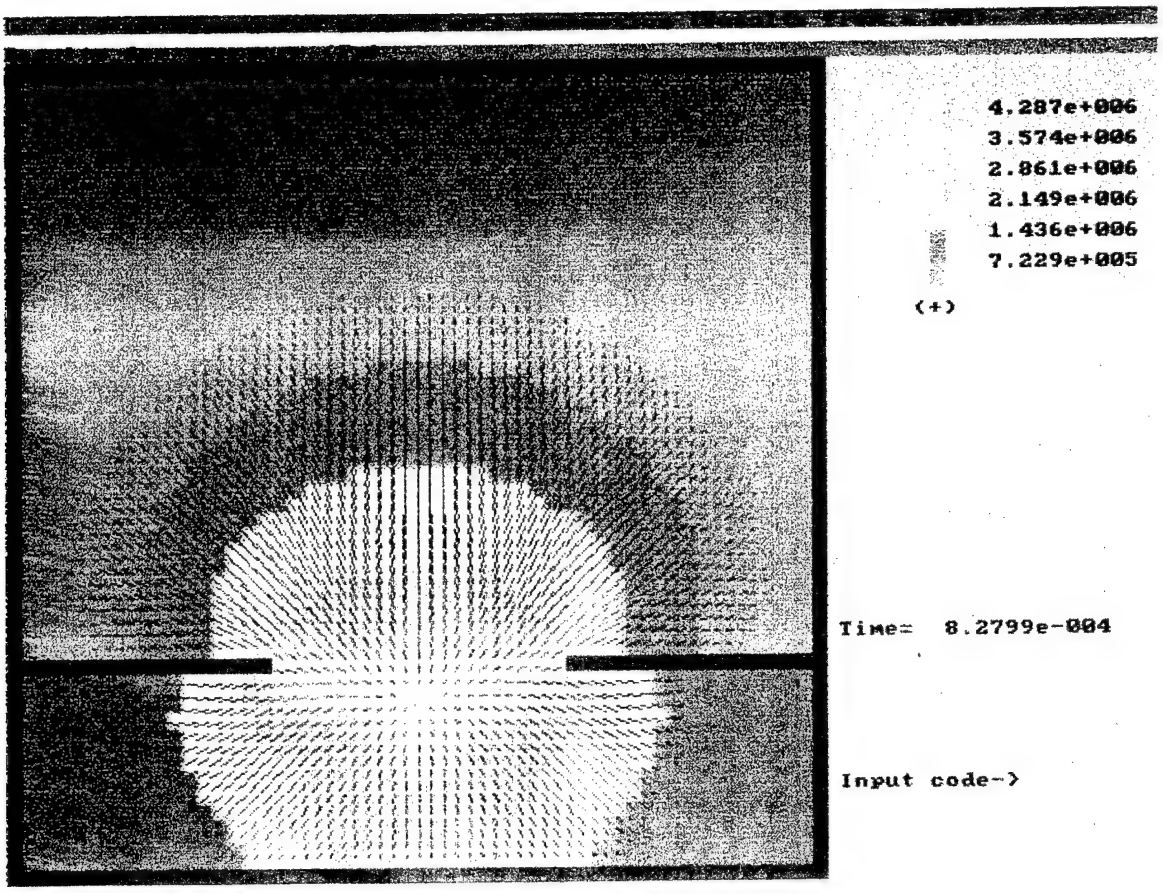
4.287e+006
3.574e+006
2.861e+006
2.149e+006
1.436e+006
7.229e+005
(+)
Time= 8.2799e-004
Input code->

Fig. 20c.

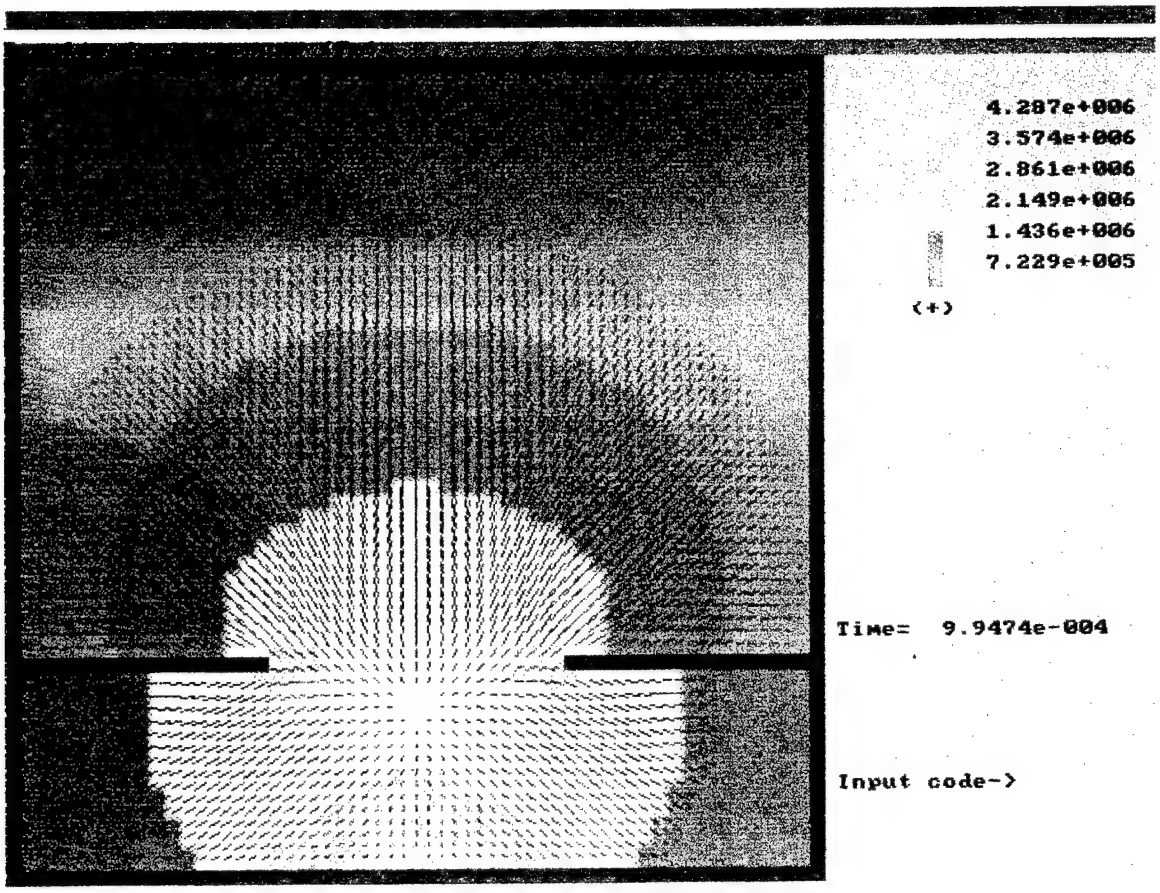
4.287e+006
3.574e+006
2.861e+006
2.149e+006
1.436e+006
7.229e+005
(+)
Time= 9.9474e-004
Input code->>

Fig. 20 d.

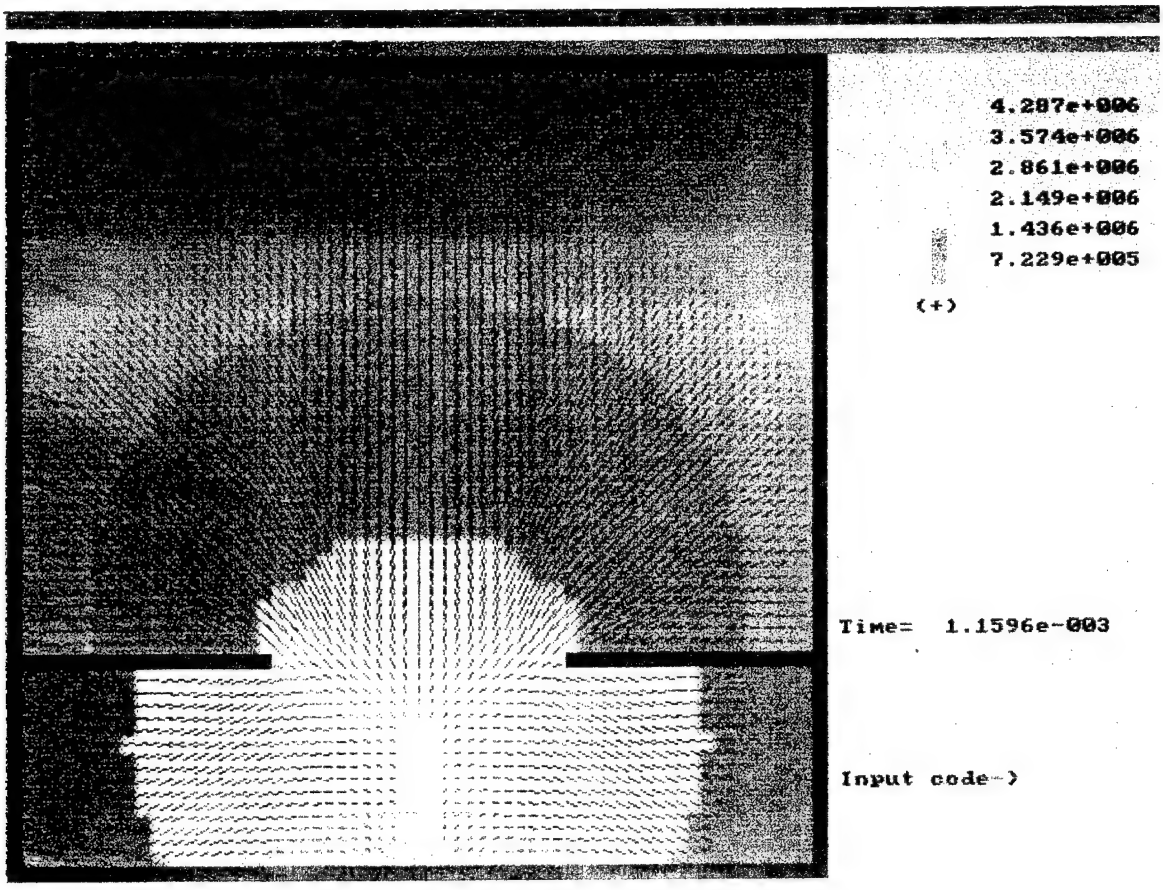
4.287e+006
3.574e+006
2.861e+006
2.149e+006
1.436e+006
7.229e+005
(+)
Time= 1.1596e-003
Input code->

Fig. 20e.

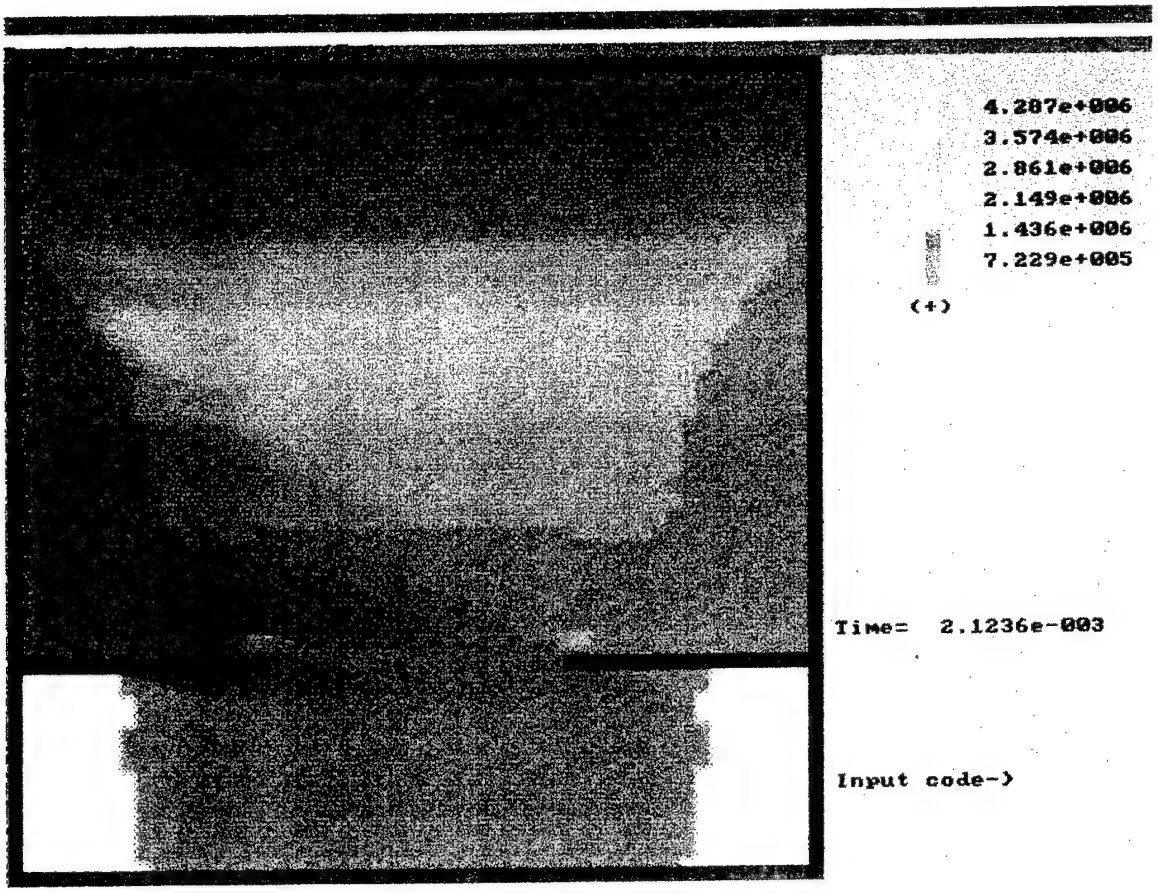
4.287e+006
3.574e+006
2.861e+006
2.149e+006
1.436e+006
7.229e+005
(+)
Time= 2.1236e-003
Input code->

Fig. 20f.

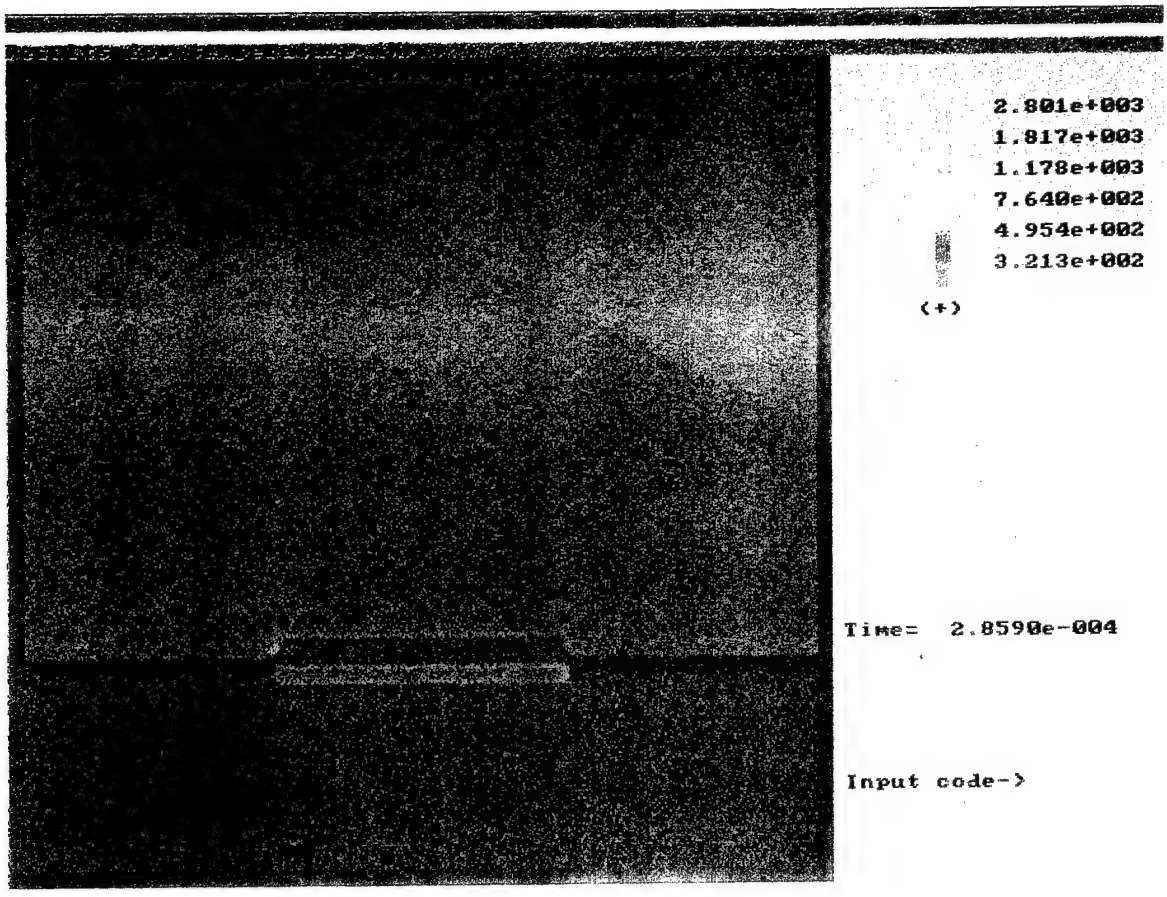
2.801e+003
1.817e+003
1.178e+003
7.640e+002
4.954e+002
3.213e+002
(+)
Time= 2.8590e-004
Input code->

Fig. 21a.

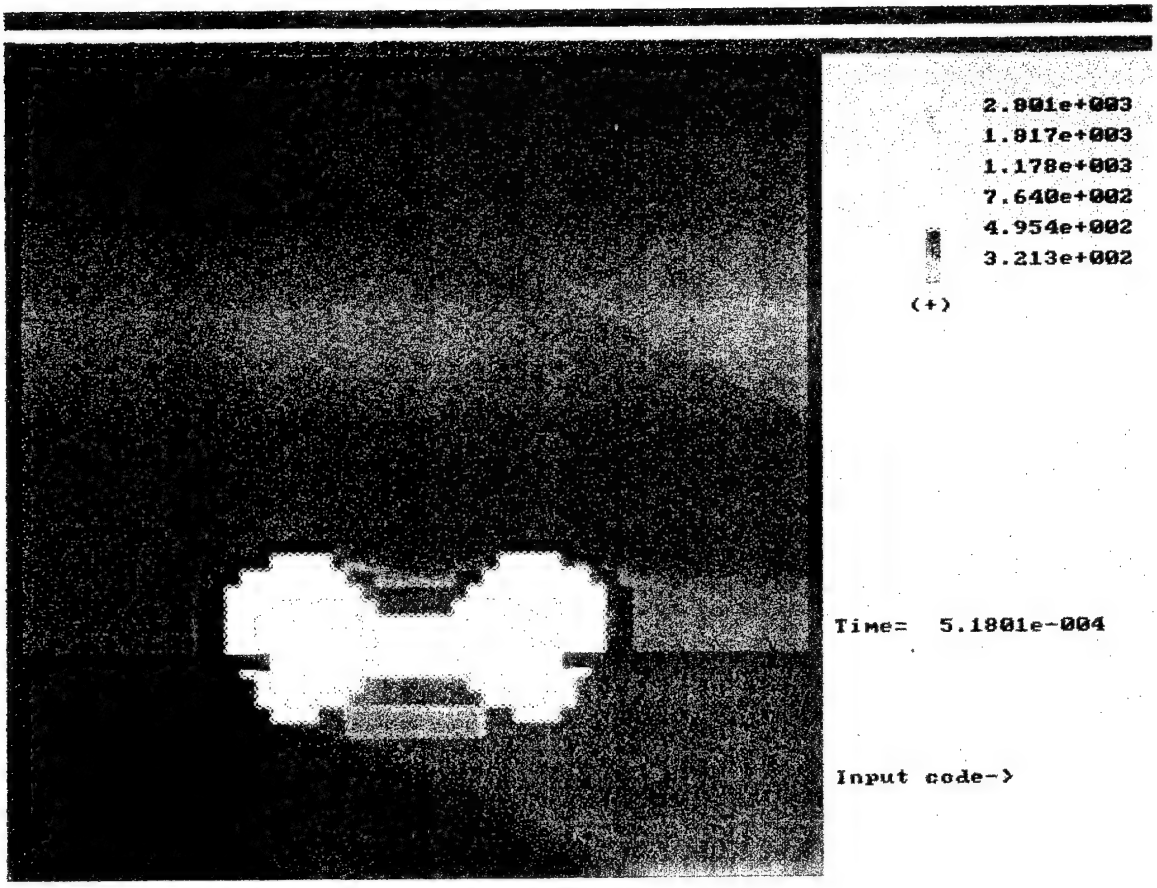
2.801e+003
1.817e+003
1.178e+003
7.640e+002
4.954e+002
3.213e+002
(+)
Time= 5.1801e-004
Input code->>

Fig. 21 b.

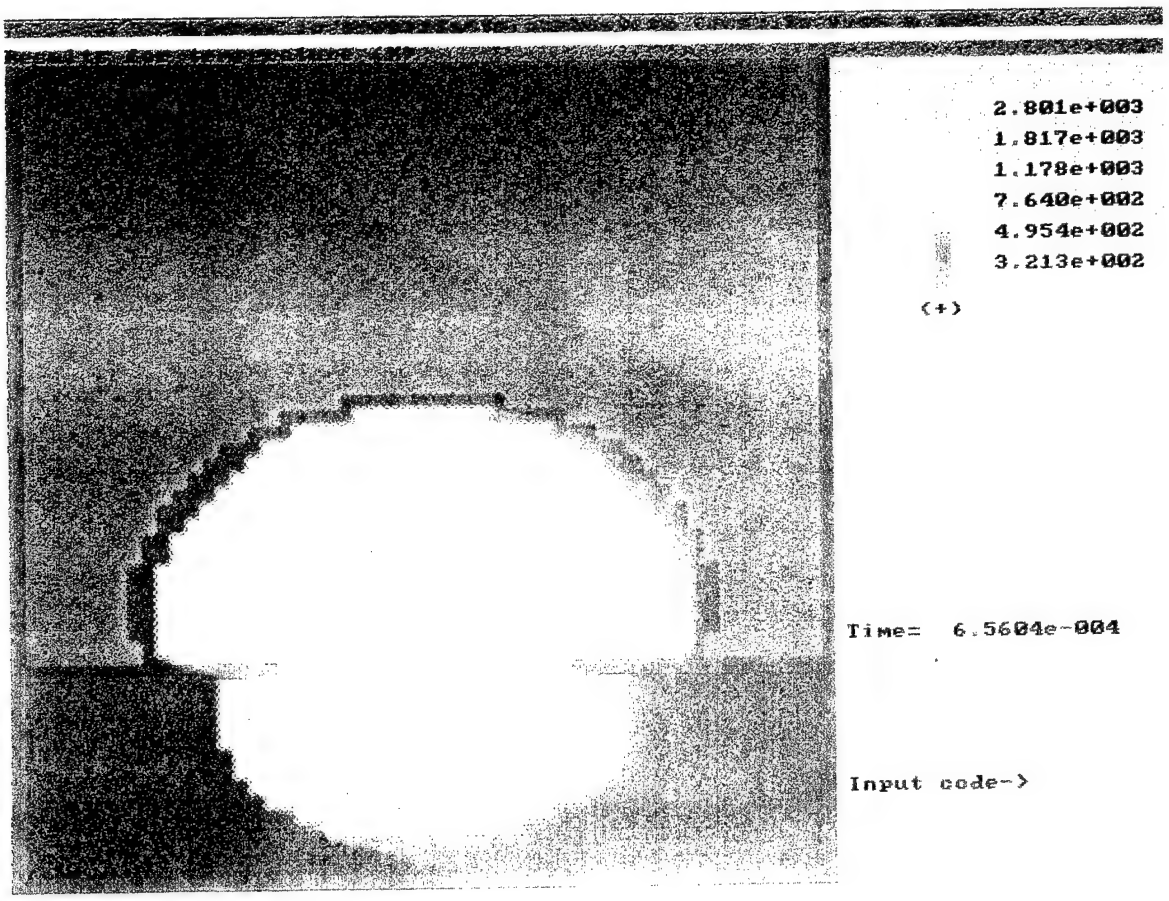
2.801e+003
1.817e+003
1.178e+003
7.640e+002
4.954e+002
3.213e+002
(+)
Time= 6.5604e-004
Input code->

Fig. 21c.

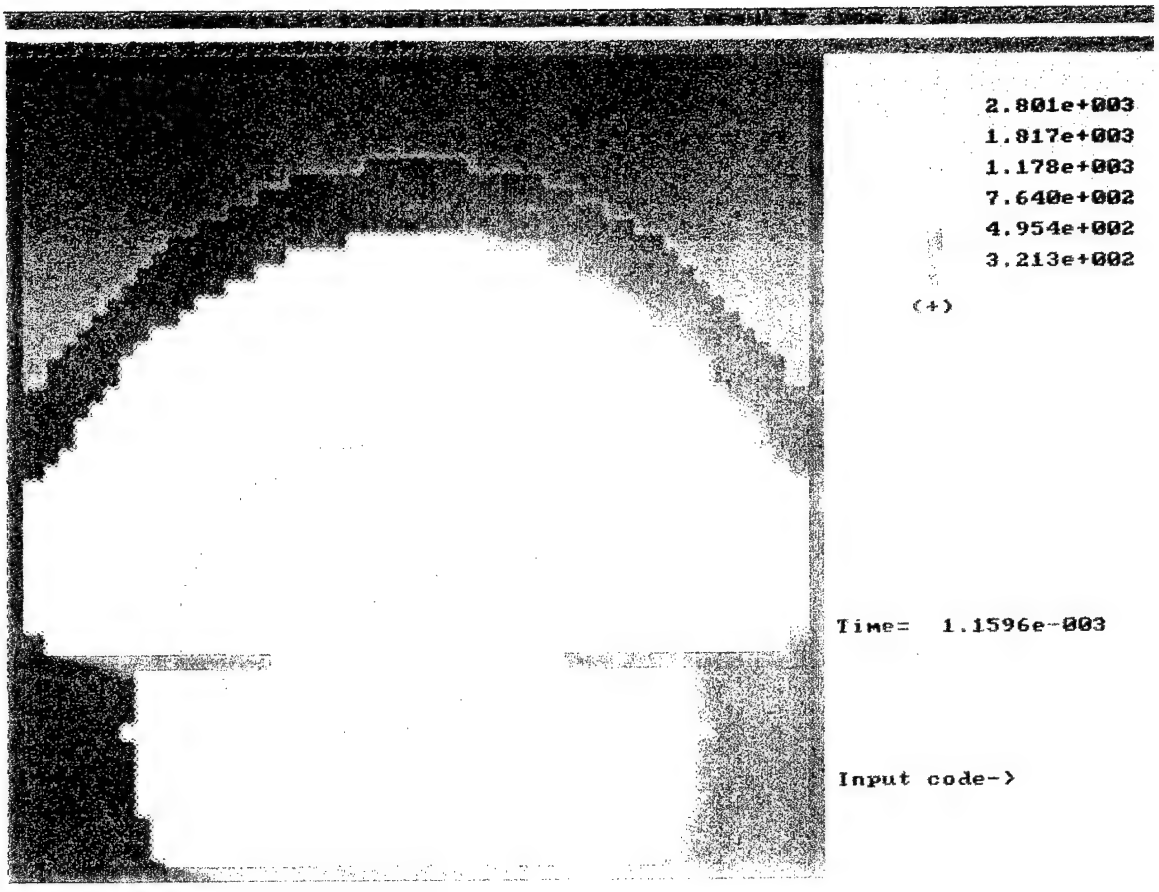
2.801e+003
1.817e+003
1.178e+003
7.640e+002
4.954e+002
3.213e+002
(+)
Time= 1.1596e-003
Input code->>

Fig. 21d.

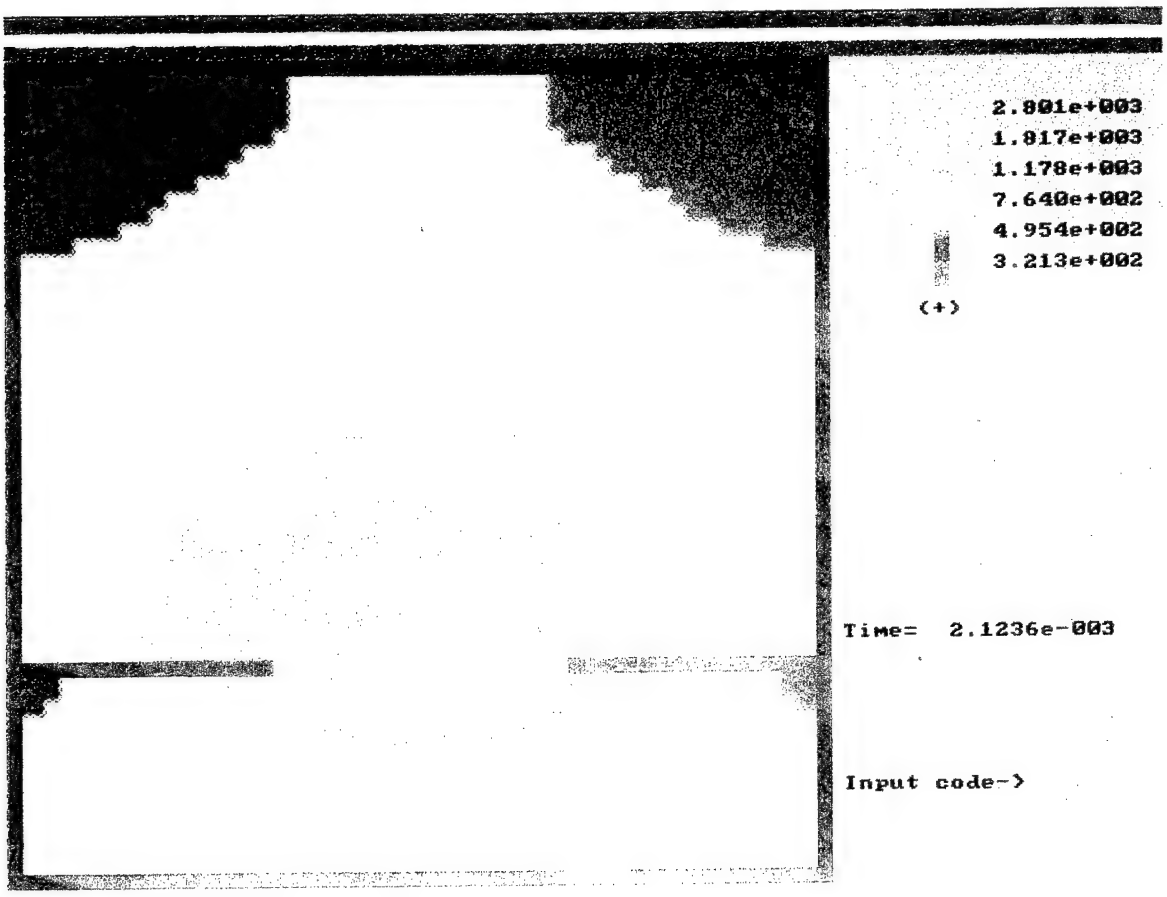
2.801e+003
1.817e+003
1.178e+003
7.640e+002
4.954e+002
3.213e+002
(+)
Time= 2.1236e-003
Input code->

Fig. 21e.

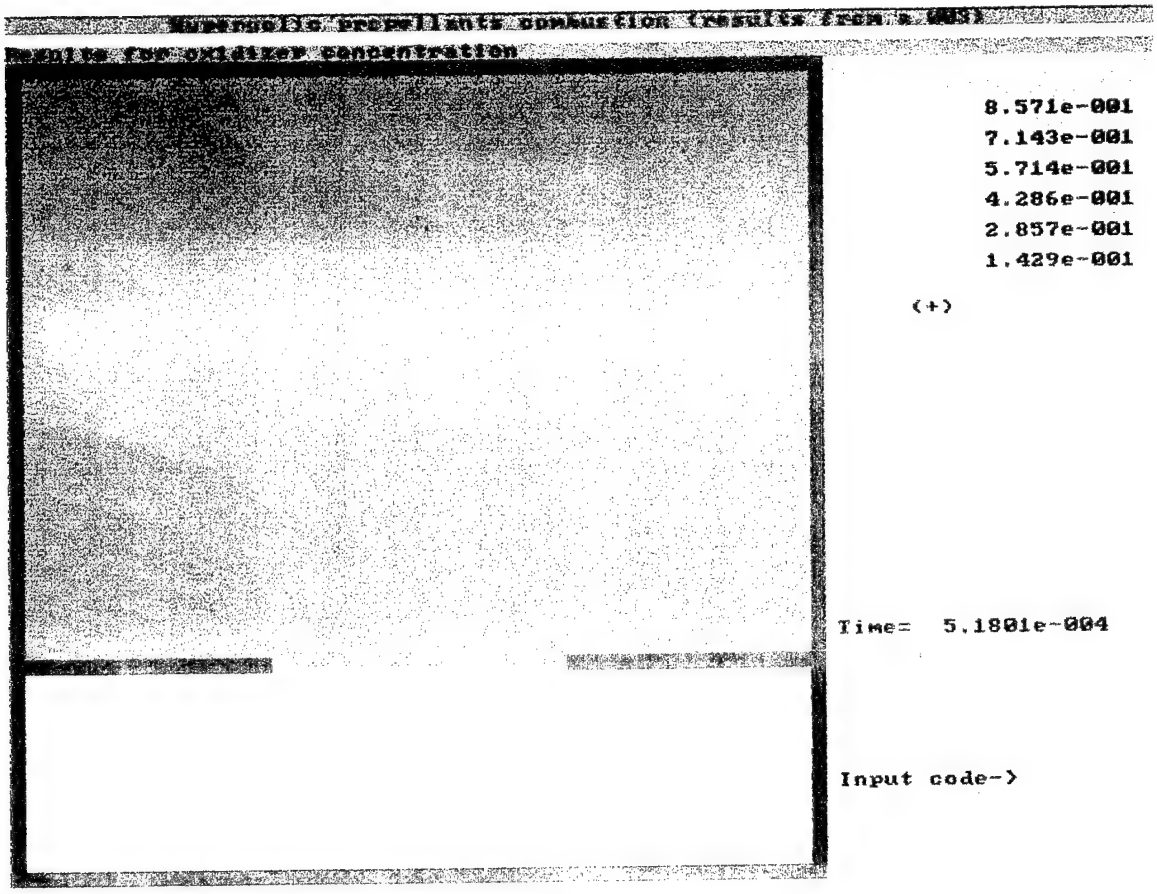
8.571e-001
7.143e-001
5.714e-001
4.286e-001
2.857e-001
1.429e-001
(+)
Time= 5.1801e-004
Input code->

Fig. 22a.

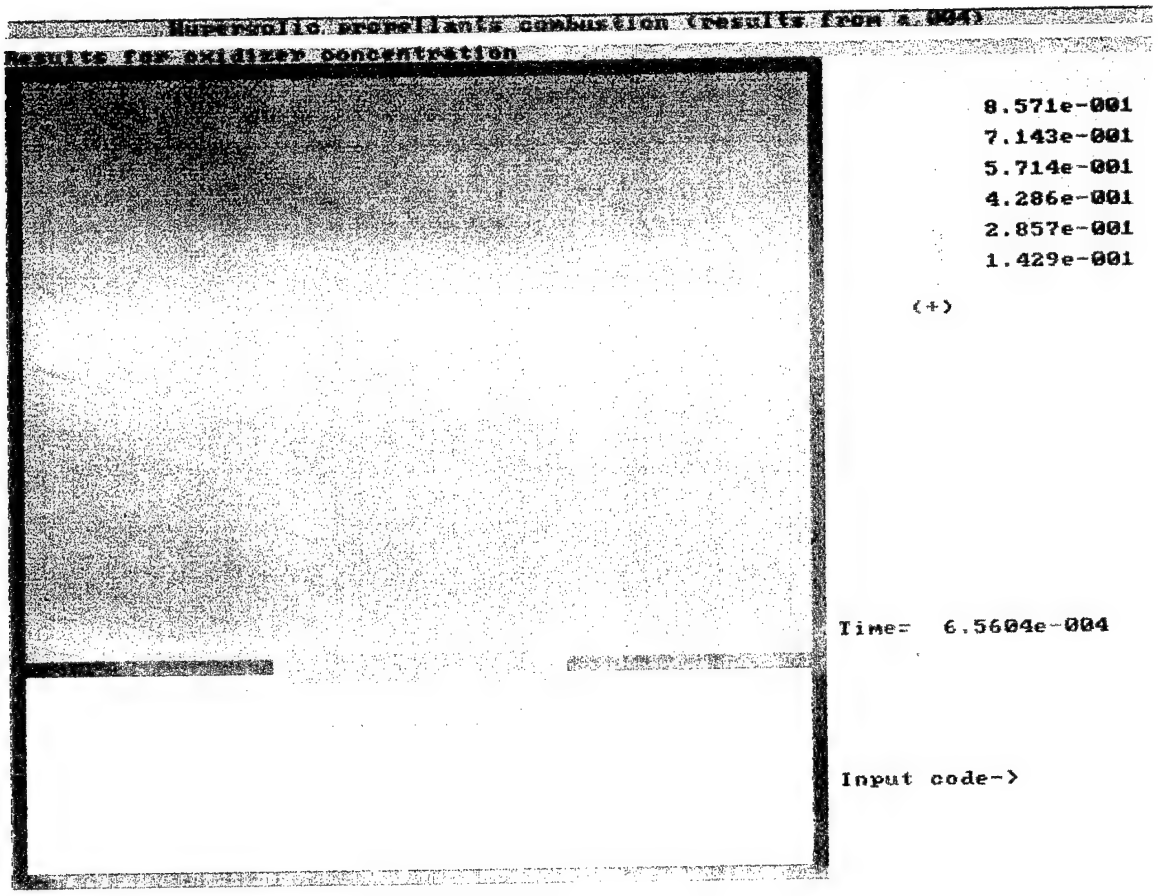
Hypergolic propellants combustion (results from 4.004)
Results for oxidizer concentration
8.571e-001
7.143e-001
5.714e-001
4.286e-001
2.857e-001
1.429e-001
(+)
Time= 6.5604e-004
Input code->

Fig. 22 b.

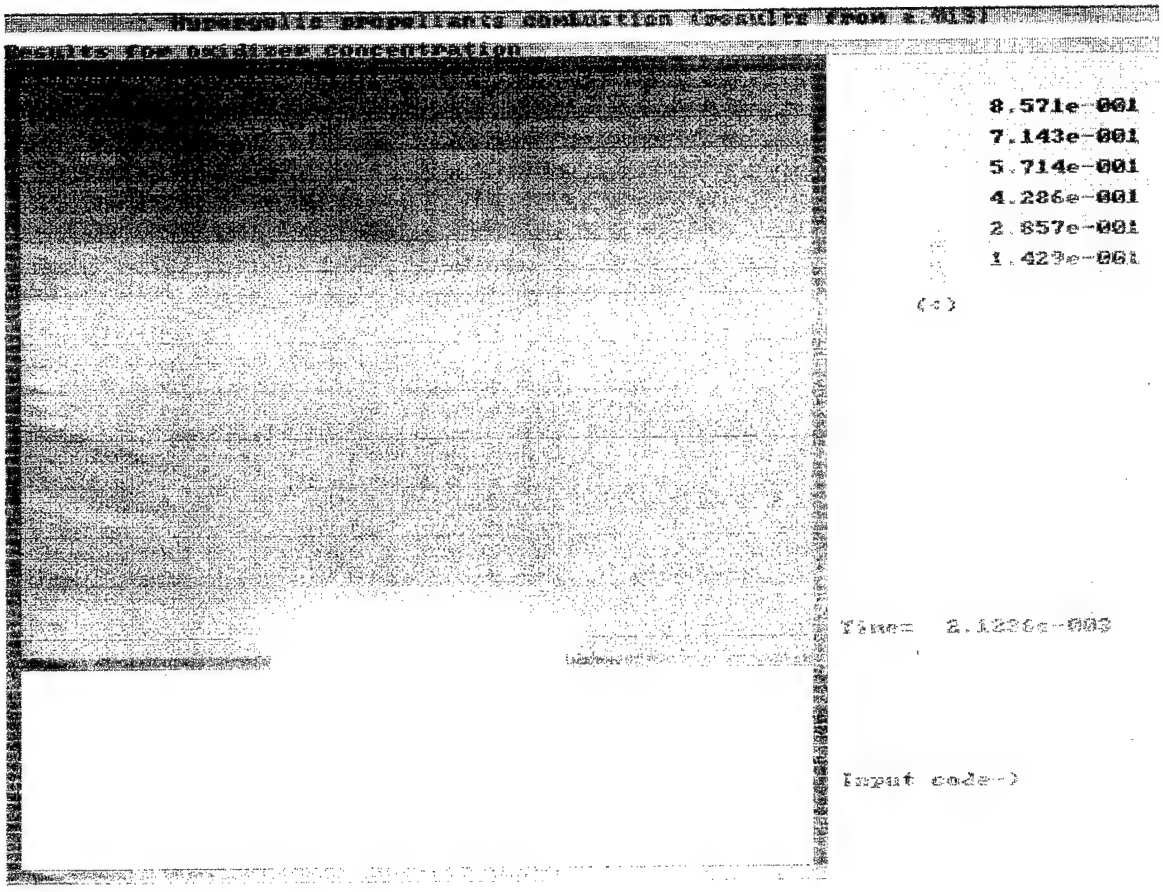
8.571e-001
7.143e-001
5.714e-001
4.286e-001
2.857e-001
1.429e-001
Time=
Input code=

Fig. 22c.

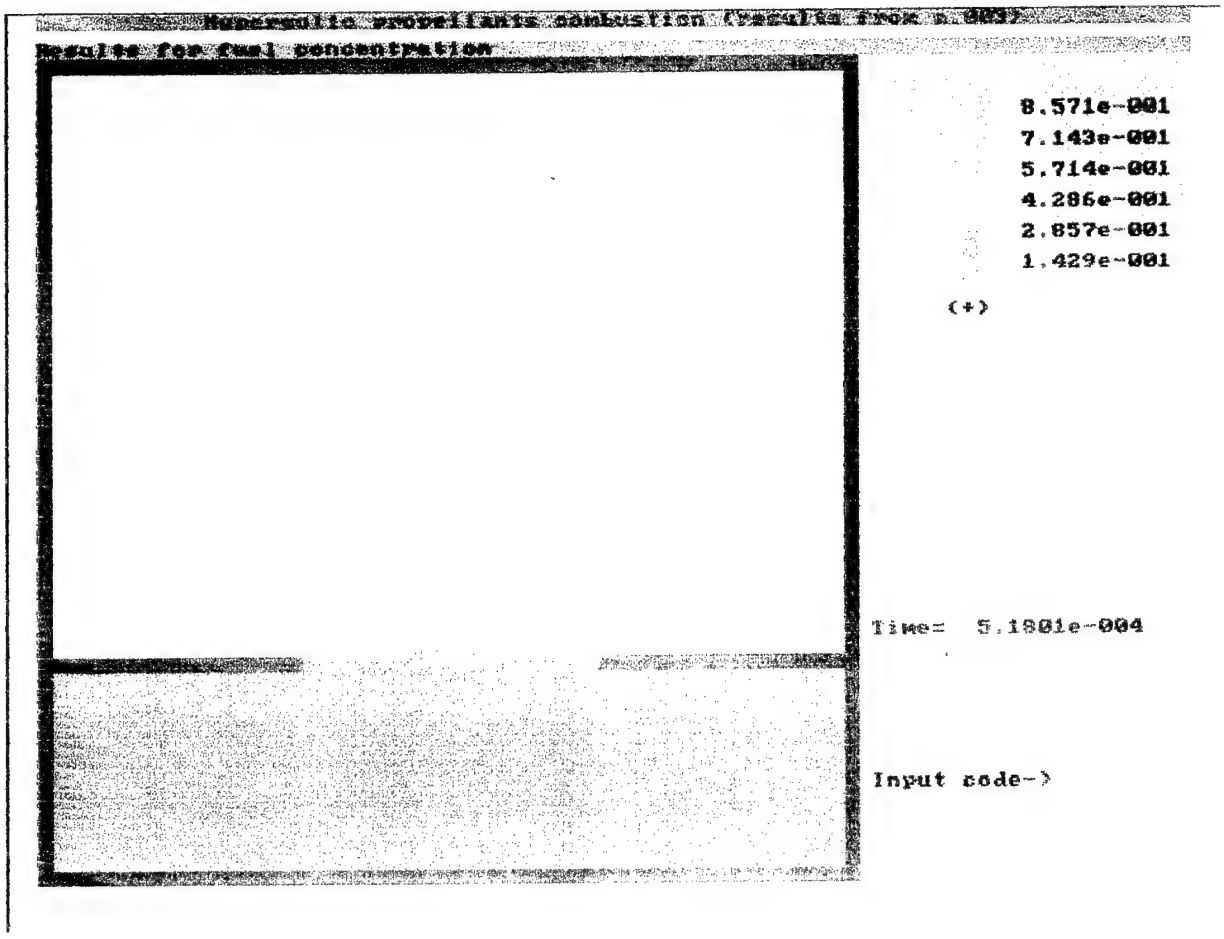
Hypergolic propellants combustion (results from n.003)
Results for fuel concentration
8.571e-001
7.143e-001
5.714e-001
4.286e-001
2.857e-001
1.429e-001
(+)
Time= 5.1981e-004
Input code->

Fig. 23a.

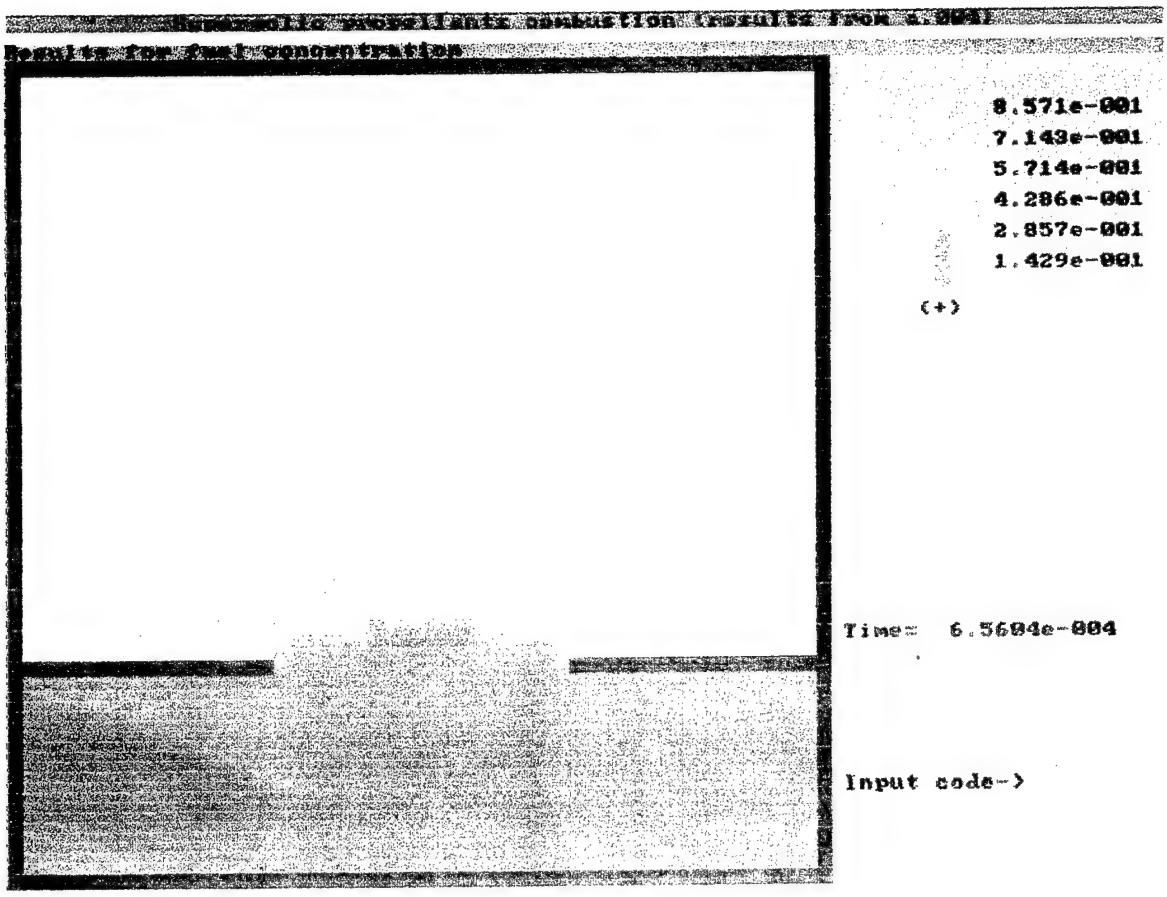
8.571e-001
7.143e-001
5.714e-001
4.286e-001
2.857e-001
1.429e-001
(+)
Time= 6.5604e-004
Input code->

Fig. 23 b.

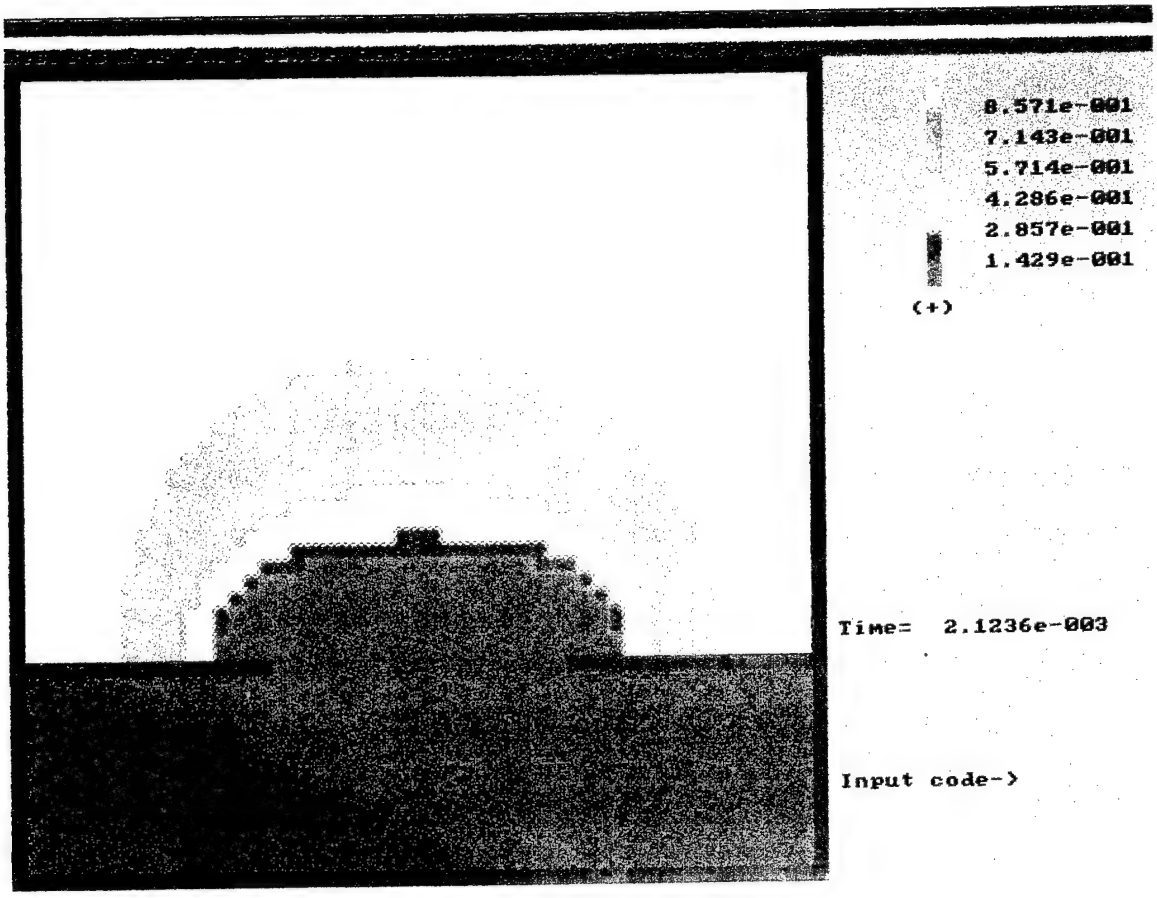
8.571e-001
7.143e-001
5.714e-001
4.286e-001
2.857e-001
1.429e-001
(+)
Time= 2.1236e-003
Input code->

Fig. 23c.

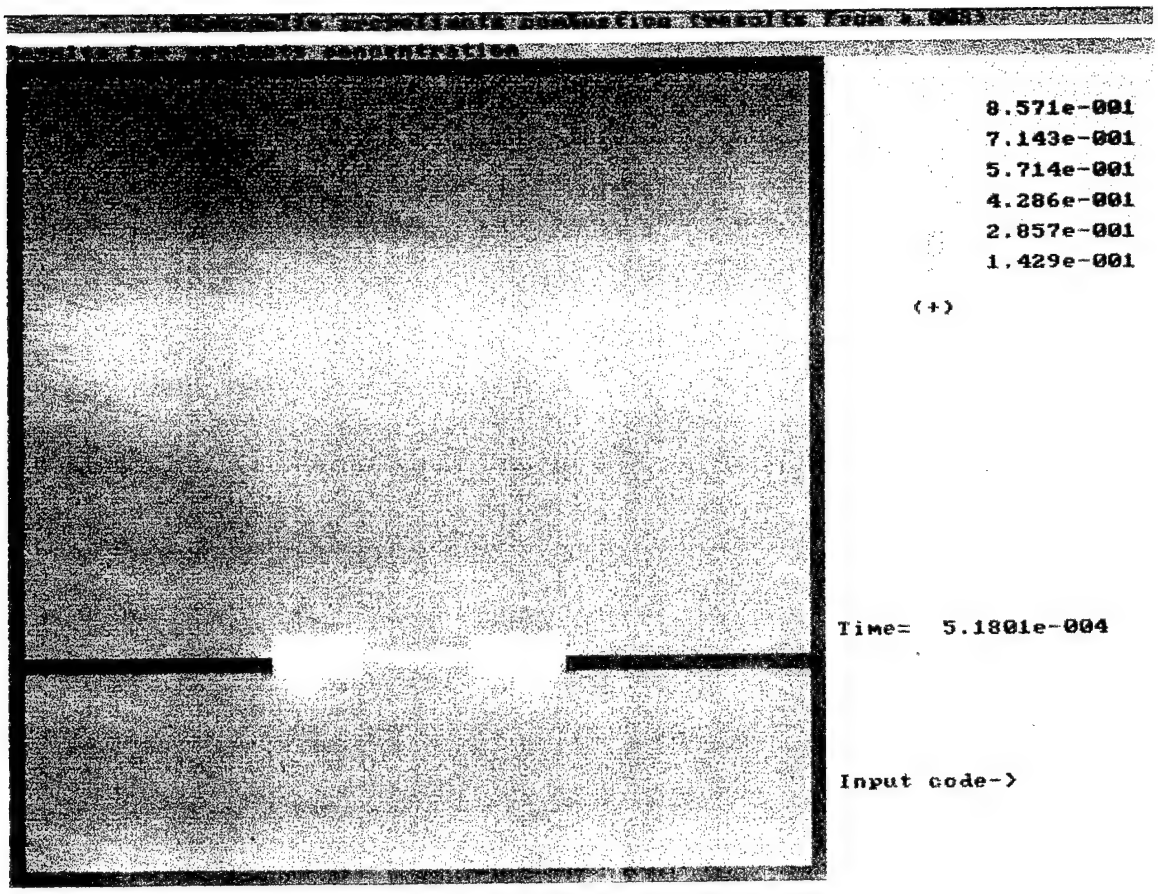
8.571e-001
7.143e-001
5.714e-001
4.286e-001
2.857e-001
1.429e-001
(+)
Time= 5.1801e-004
Input code->

Fig. 24a.

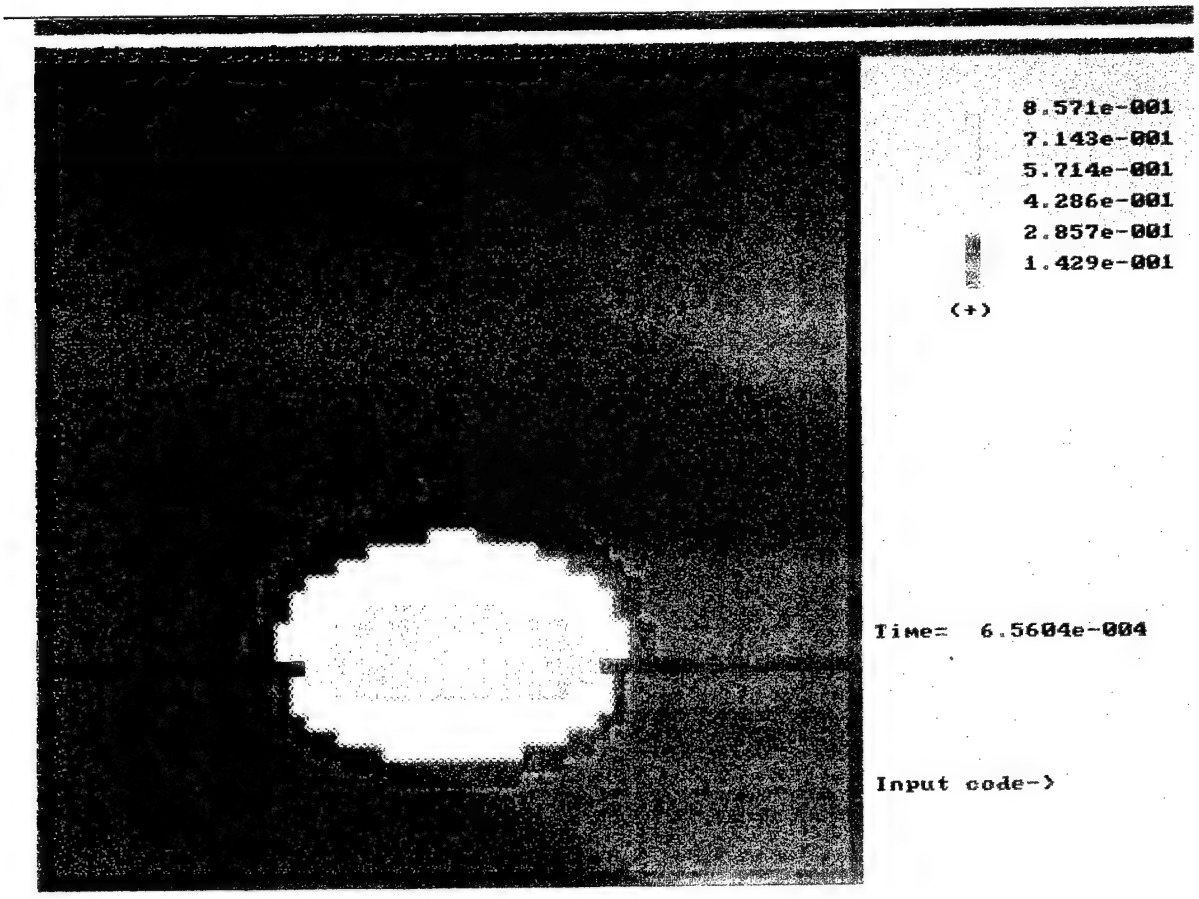
8.571e-001
7.143e-001
5.714e-001
4.286e-001
2.857e-001
1.429e-001
(+)
Time= 6.5604e-004
Input code->

Fig. 24 B.

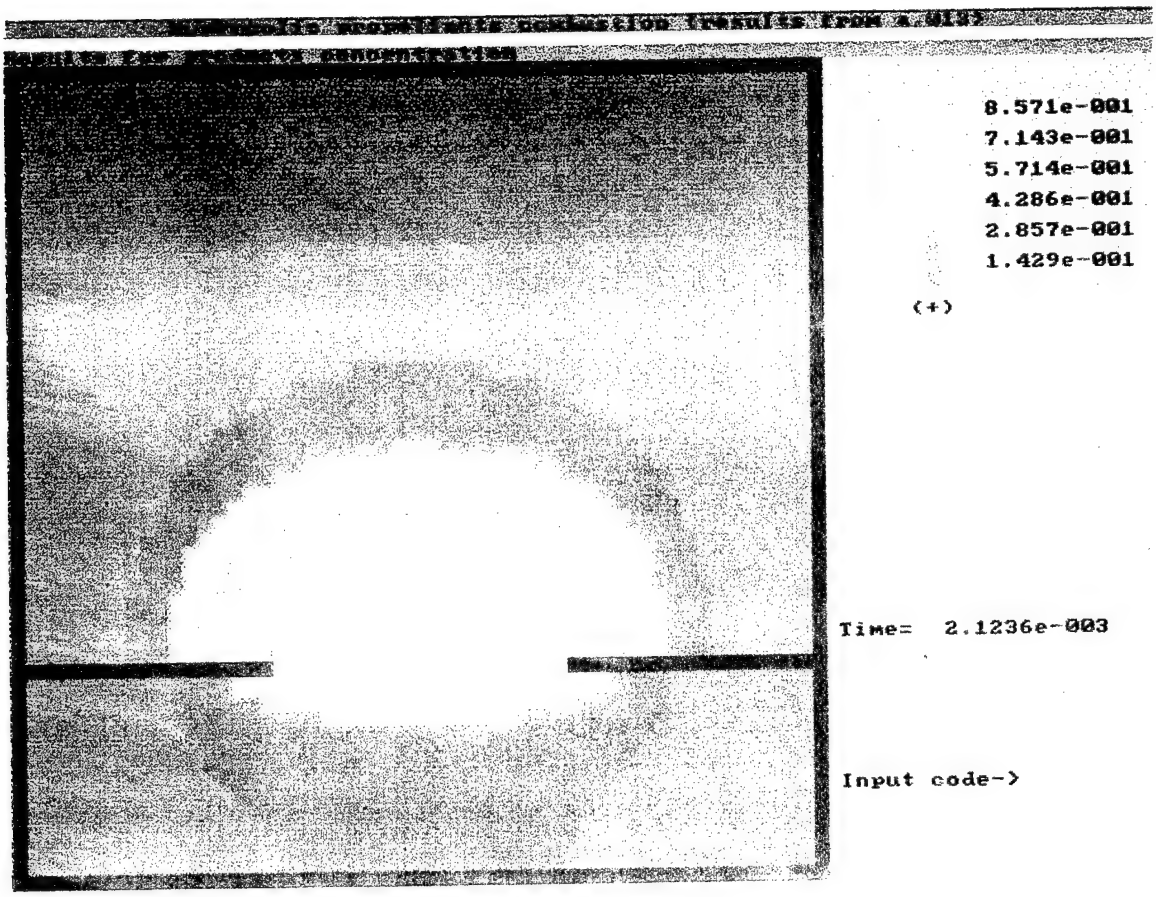
8.571e-001
7.143e-001
5.714e-001
4.286e-001
2.857e-001
1.429e-001
(+)
Time= 2.1236e-003
Input code->

Fig. 24c.

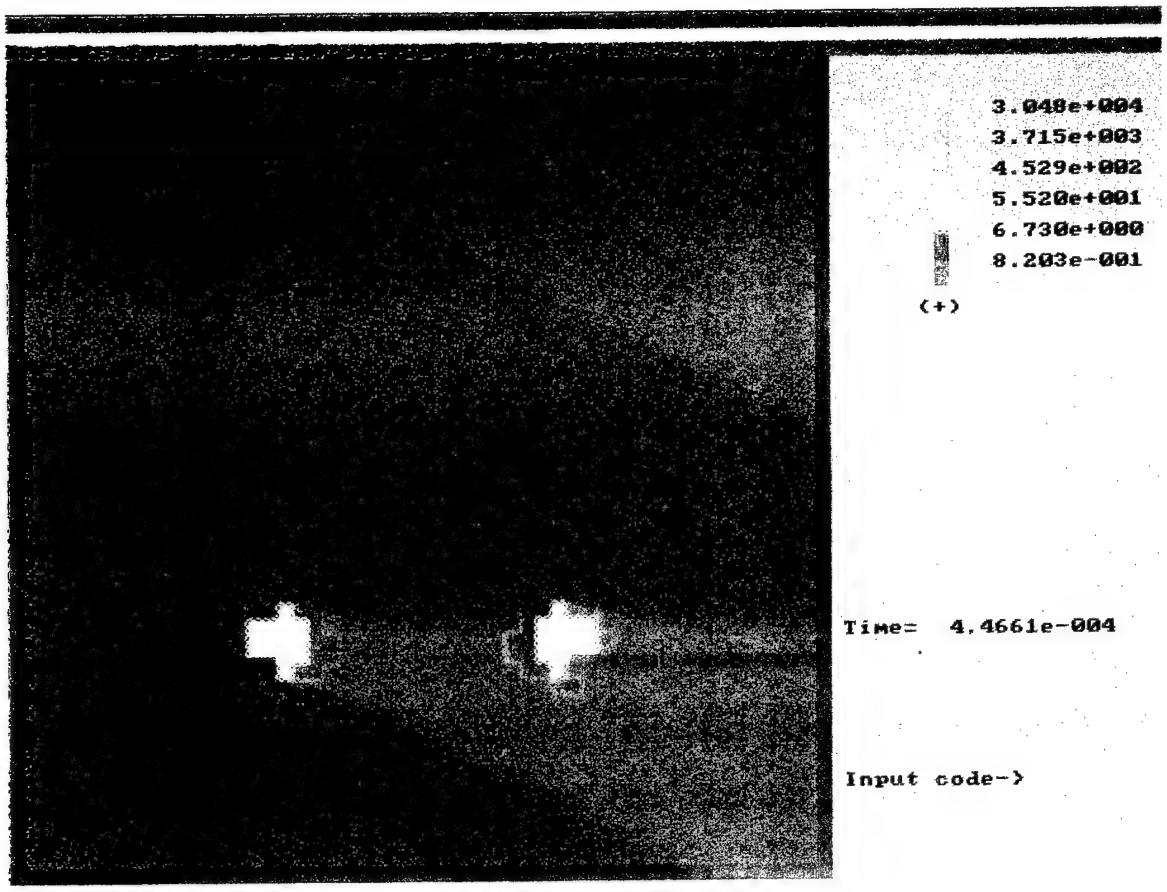
3.048e+004
3.715e+003
4.529e+002
5.520e+001
6.730e+000
8.203e-001
(+)
Time= 4.4661e-004
Input code->

Fig. 25 a.

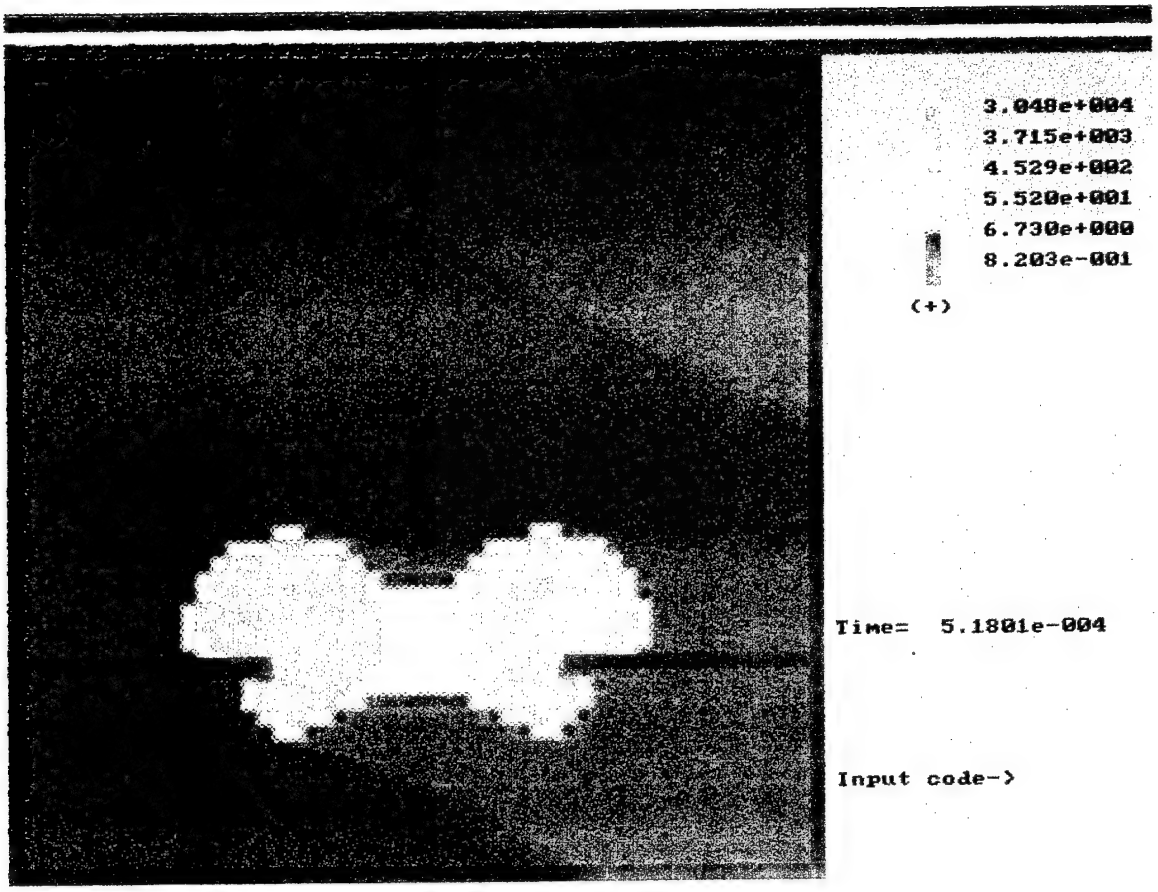
3.048e+004
3.715e+003
4.529e+002
5.520e+001
6.730e+000
8.203e-001
(+)
Time= 5.1801e-004
Input code->

Fig. 25b.

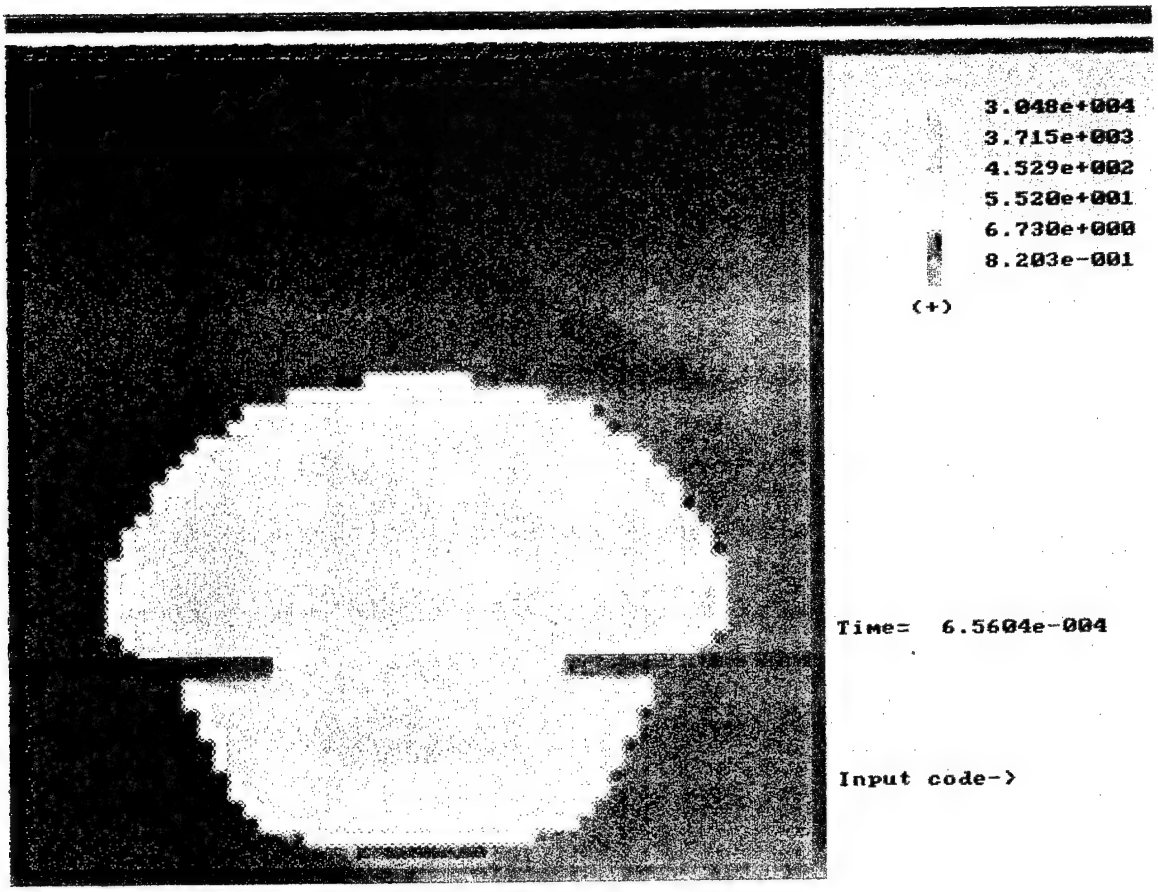
3.048e+004
3.715e+003
4.529e+002
5.520e+001
6.730e+000
8.203e-001
(+)
Time= 6.5604e-004
Input code->

Fig. 25c.

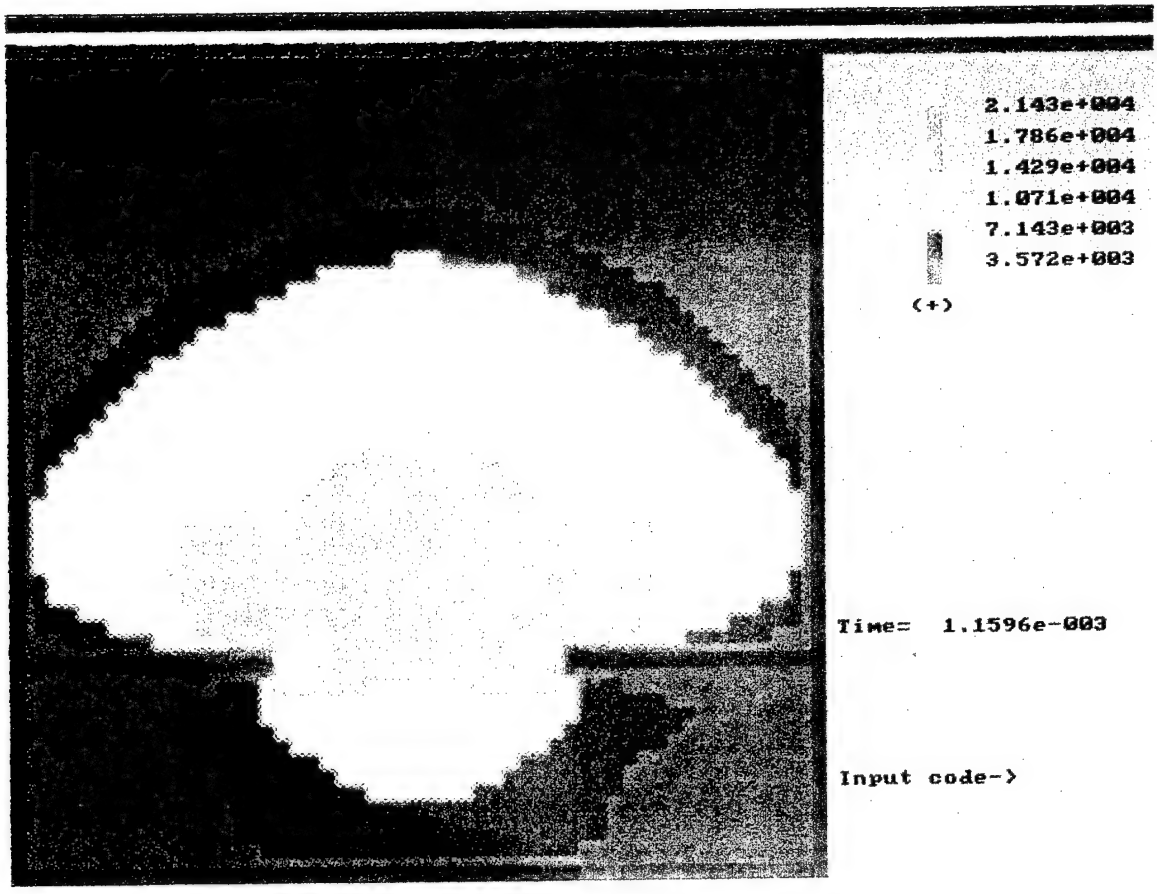
2.143e+004
1.786e+004
1.429e+004
1.071e+004
7.143e+003
3.572e+003
(+)
Time= 1.1596e-003
Input code->

Fig. 25 d.

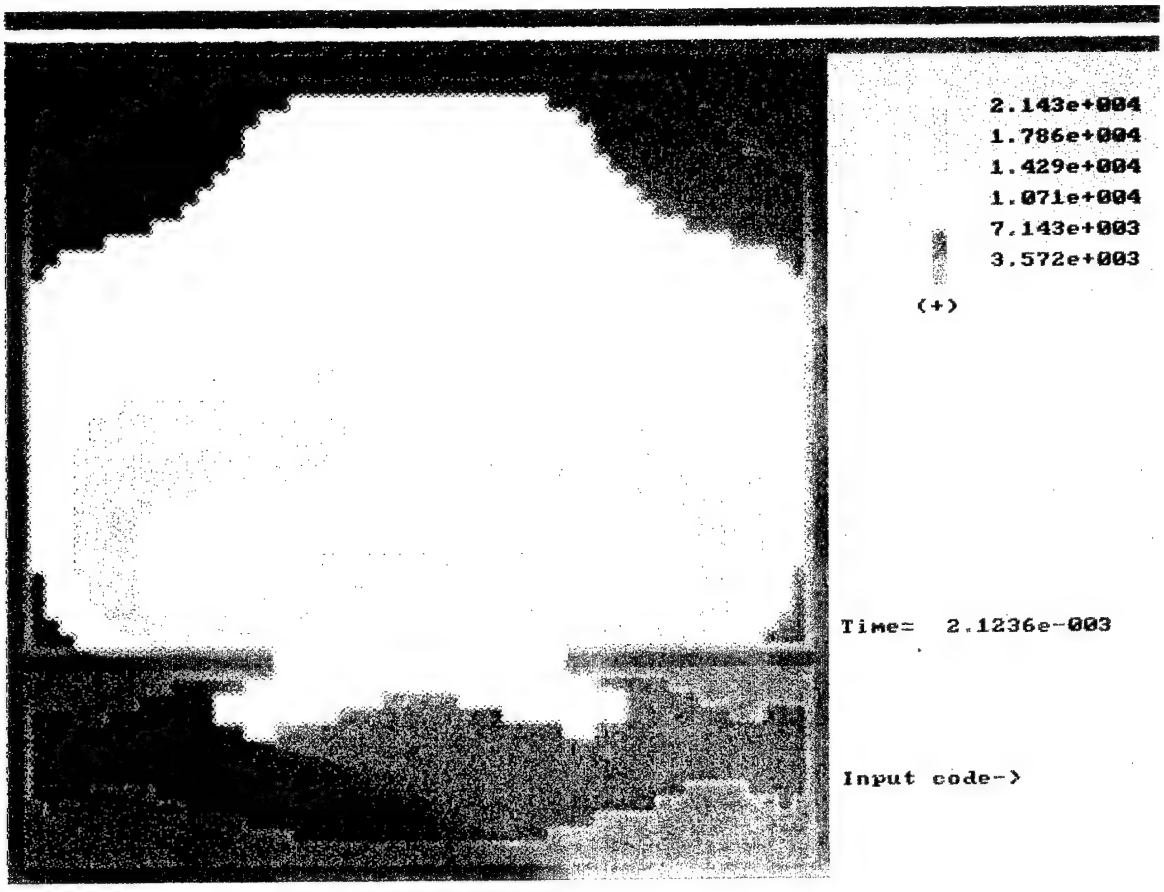
2.143e+004
1.786e+004
1.429e+004
1.071e+004
7.143e+003
3.572e+003
(+)
Time= 2.1236e-003
Input code->>

Fig.25e.

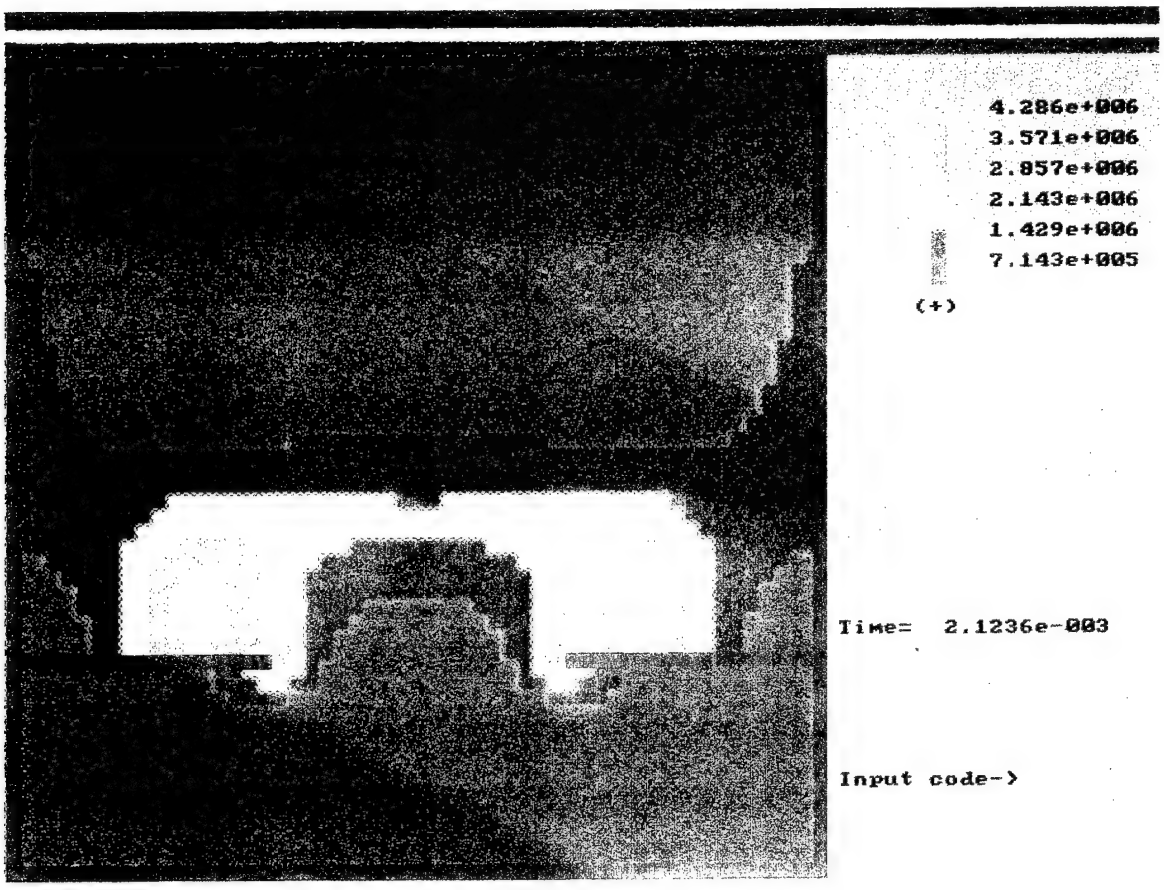
4.286e+006
3.571e+006
2.857e+006
2.143e+006
1.429e+006
7.143e+005
(+)
Time= 2.1236e-003
Input code->

Fig. 26.

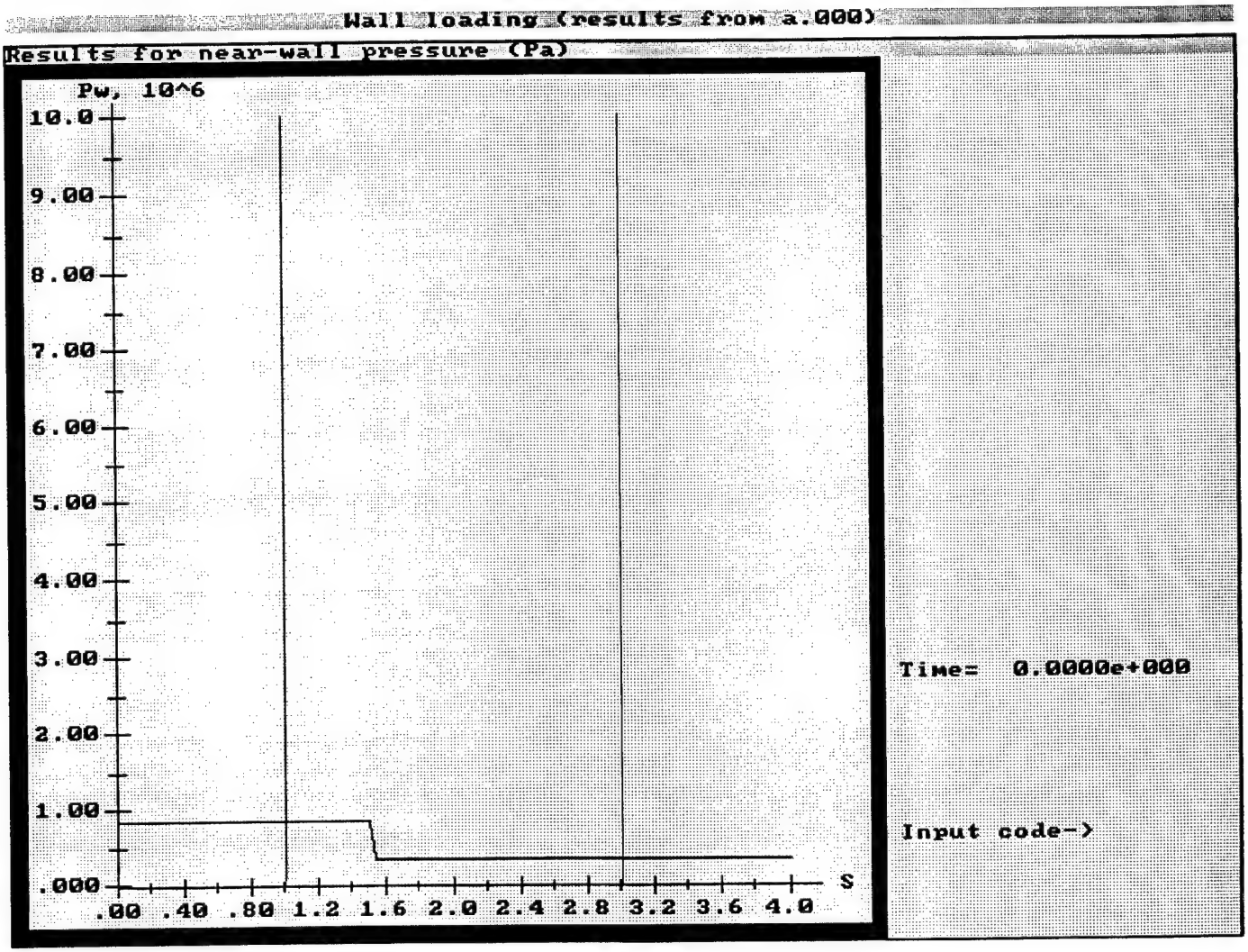
Wall loading (results from a.000)
Results for near-wall pressure (Pa)
Pw, 10^6
10.0
9.00
8.00
7.00
6.00
5.00
4.00
3.00
2.00
1.00
.000
.00 .40 .80 1.2 1.6 2.0 2.4 2.8 3.2 3.6 4.0
S
Time= 0.0000e+000
Input code->

Fig. 27a.

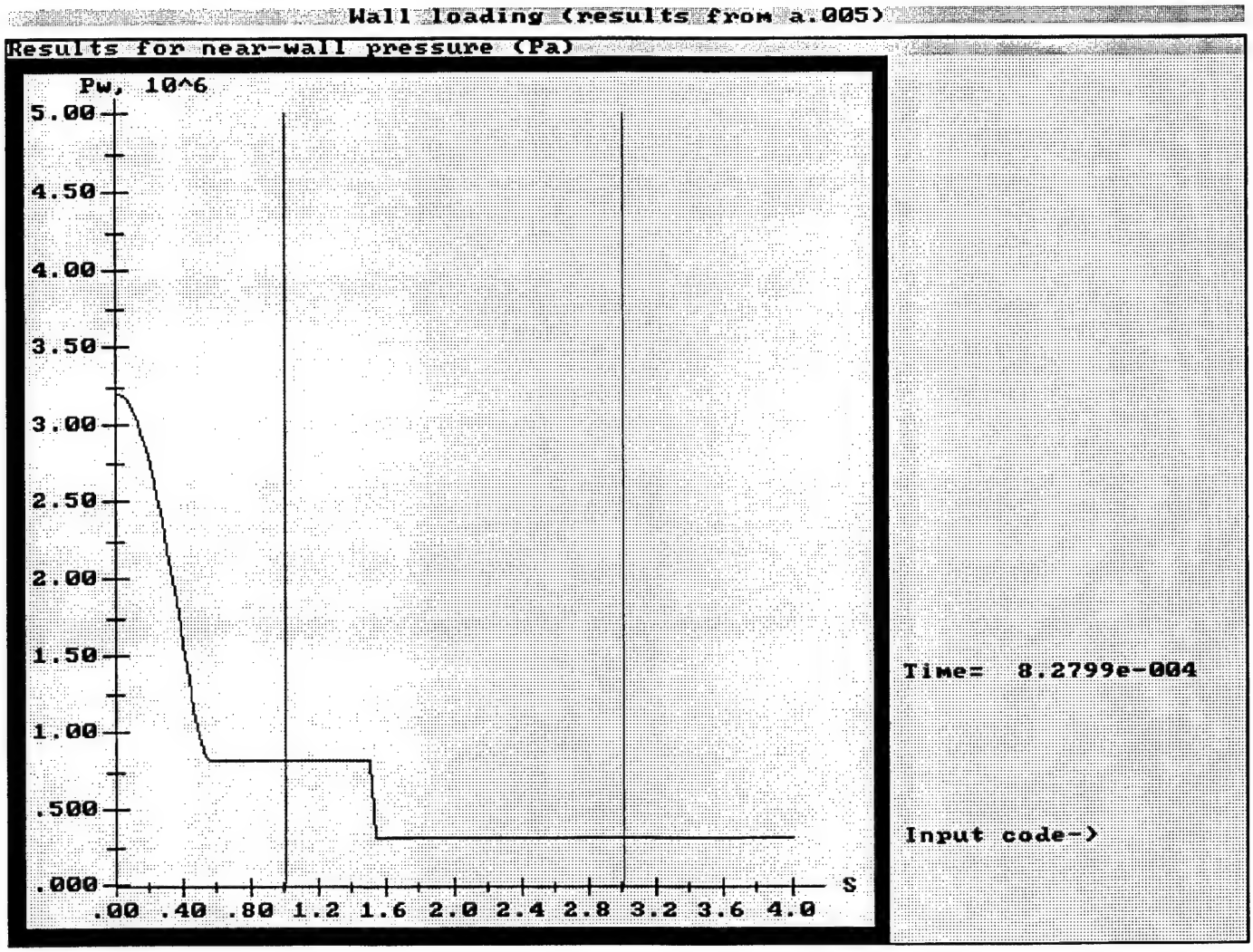
Wall loading (results from a.005)
Results for near-wall pressure (Pa)
Pw, 10^6
5.00
4.50
4.00
3.50
3.00
2.50
2.00
1.50
1.00
.500
.000
.00 .40 .80 1.2 1.6 2.0 2.4 2.8 3.2 3.6 4.0
S
Time= 8.2799e-004
Input code->

Fig. 27b.

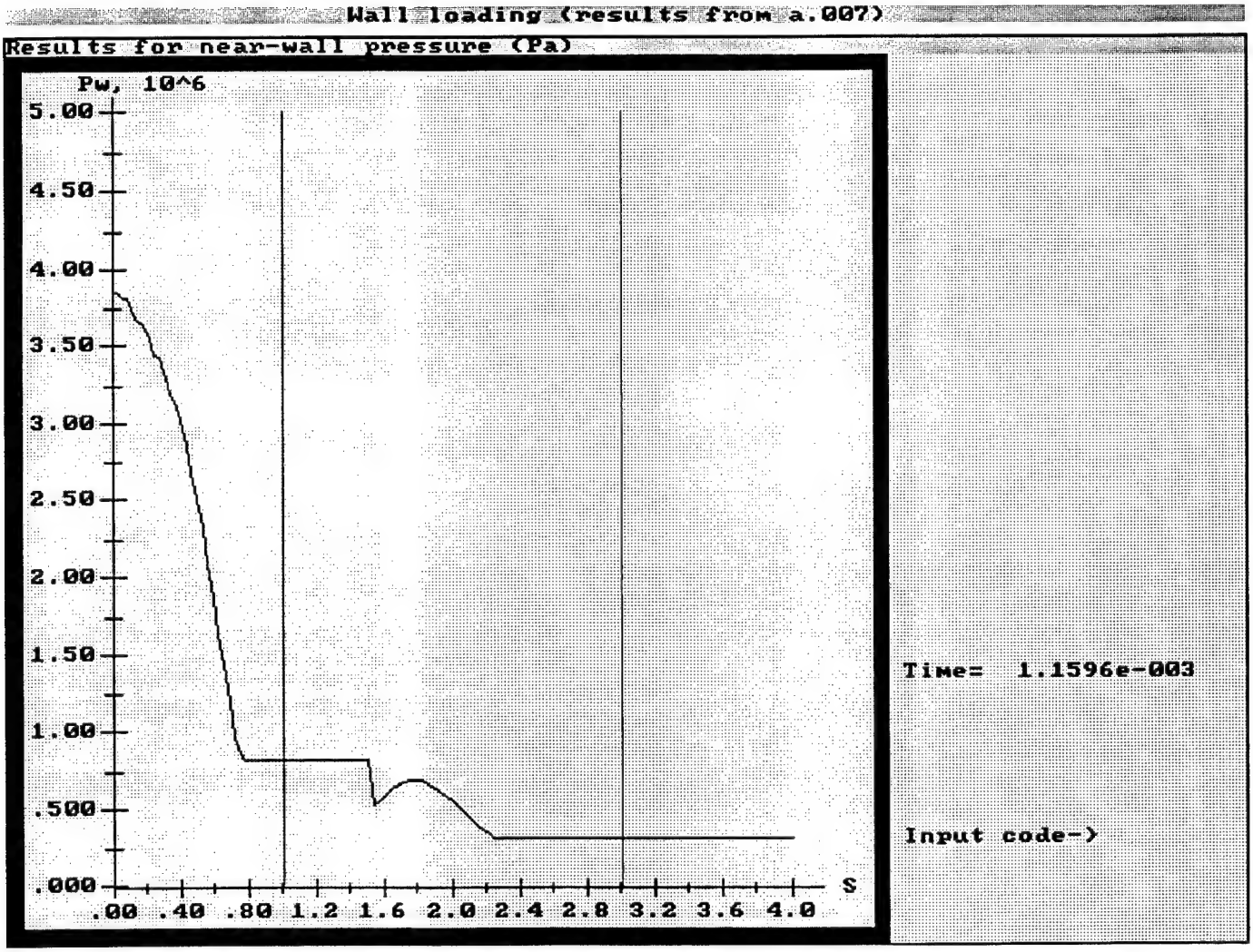
Wall loading (results from a.007)
Results for near-wall pressure (Pa)
Pw, 10^6
5.00
4.50
4.00
3.50
3.00
2.50
2.00
1.50
1.00
.500
.000
.00 .40 .80 1.2 1.6 2.0 2.4 2.8 3.2 3.6 4.0
S
Time= 1.1596e-003
Input code->

Fig. 27c.

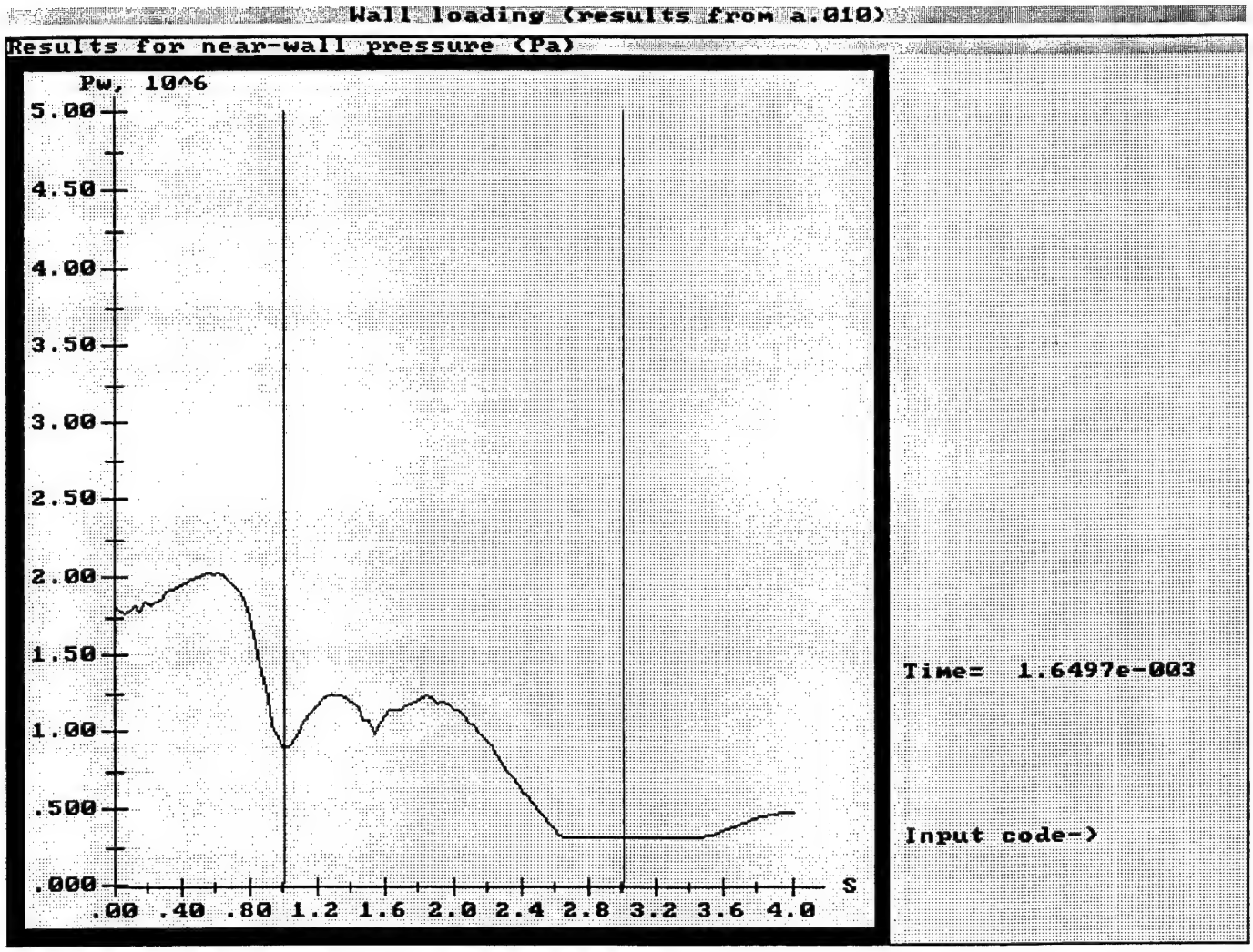
Wall loading (results from a.010)
Results for near-wall pressure (Pa)
Pw, 10^6
5.00
4.50
4.00
3.50
3.00
2.50
2.00
1.50
1.00
.500
.000
.00 .40 .80 1.2 1.6 2.0 2.4 2.8 3.2 3.6 4.0
S
Time= 1.6497e-003
Input code->

Fig. 27d.

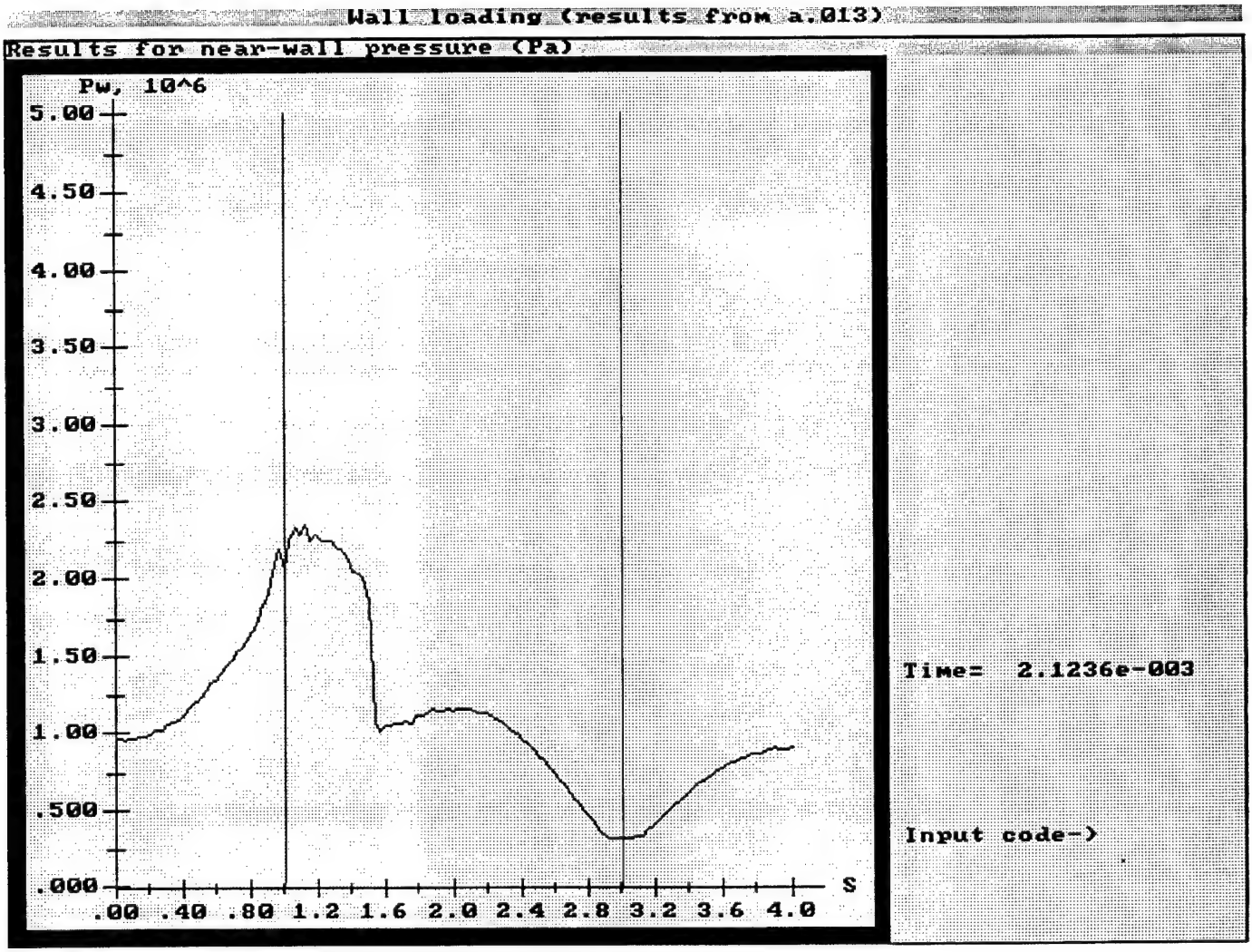
Wall loading (results from a.013)
Results for near-wall pressure (Pa)
Pw, 10^6
5.00
4.50
4.00
3.50
3.00
2.50
2.00
1.50
1.00
.500
.000
.00 .40 .80 1.2 1.6 2.0 2.4 2.8 3.2 3.6 4.0
S
Time= 2.1236e-003
Input code->

Fig. 27e.

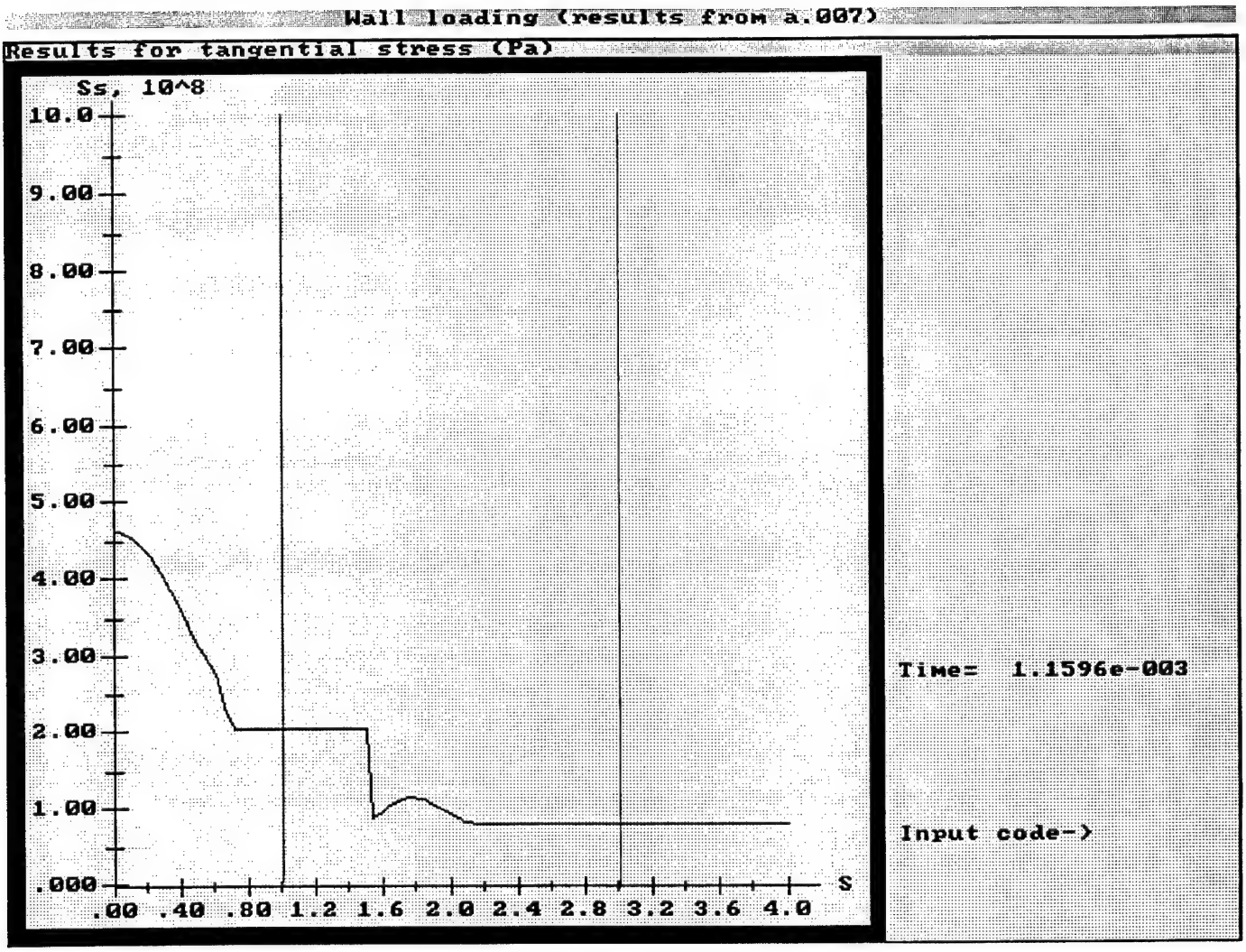
Wall loading (results from a.007)
Results for tangential stress (Pa)
Ss, 10^8
10.0
9.00
8.00
7.00
6.00
5.00
4.00
3.00
2.00
1.00
.000
.00 .40 .80 1.2 1.6 2.0 2.4 2.8 3.2 3.6 4.0
S
Time= 1.1596e-003
Input code->

Fig. 28a.

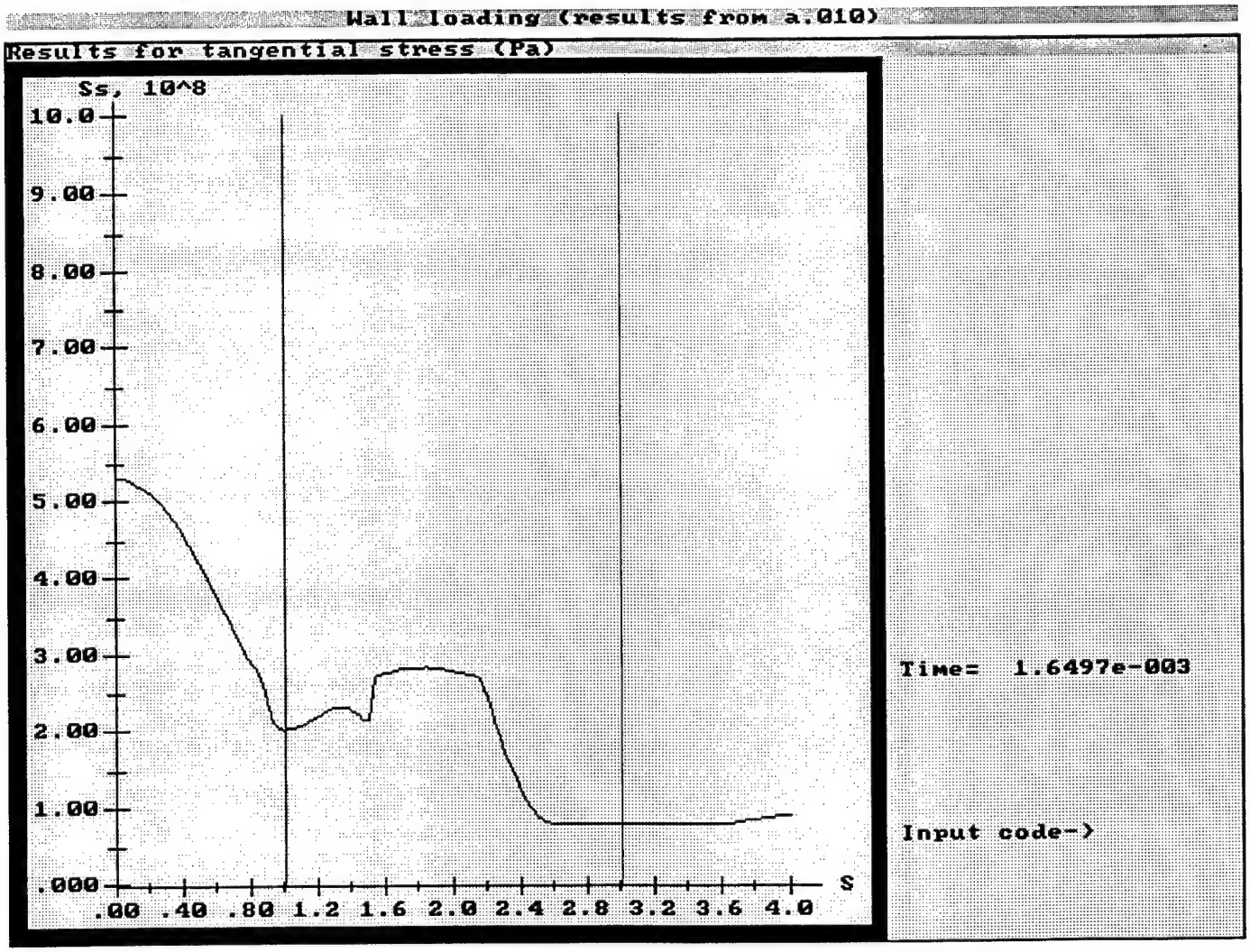
Wall loading (results from a.010)
Results for tangential stress (Pa)
Ss, 10^8
10.0
9.00
8.00
7.00
6.00
5.00
4.00
3.00
2.00
1.00
.000
.00 .40 .80 1.2 1.6 2.0 2.4 2.8 3.2 3.6 4.0
S
Time= 1.6497e-003
Input code->

Fig. 28 b.

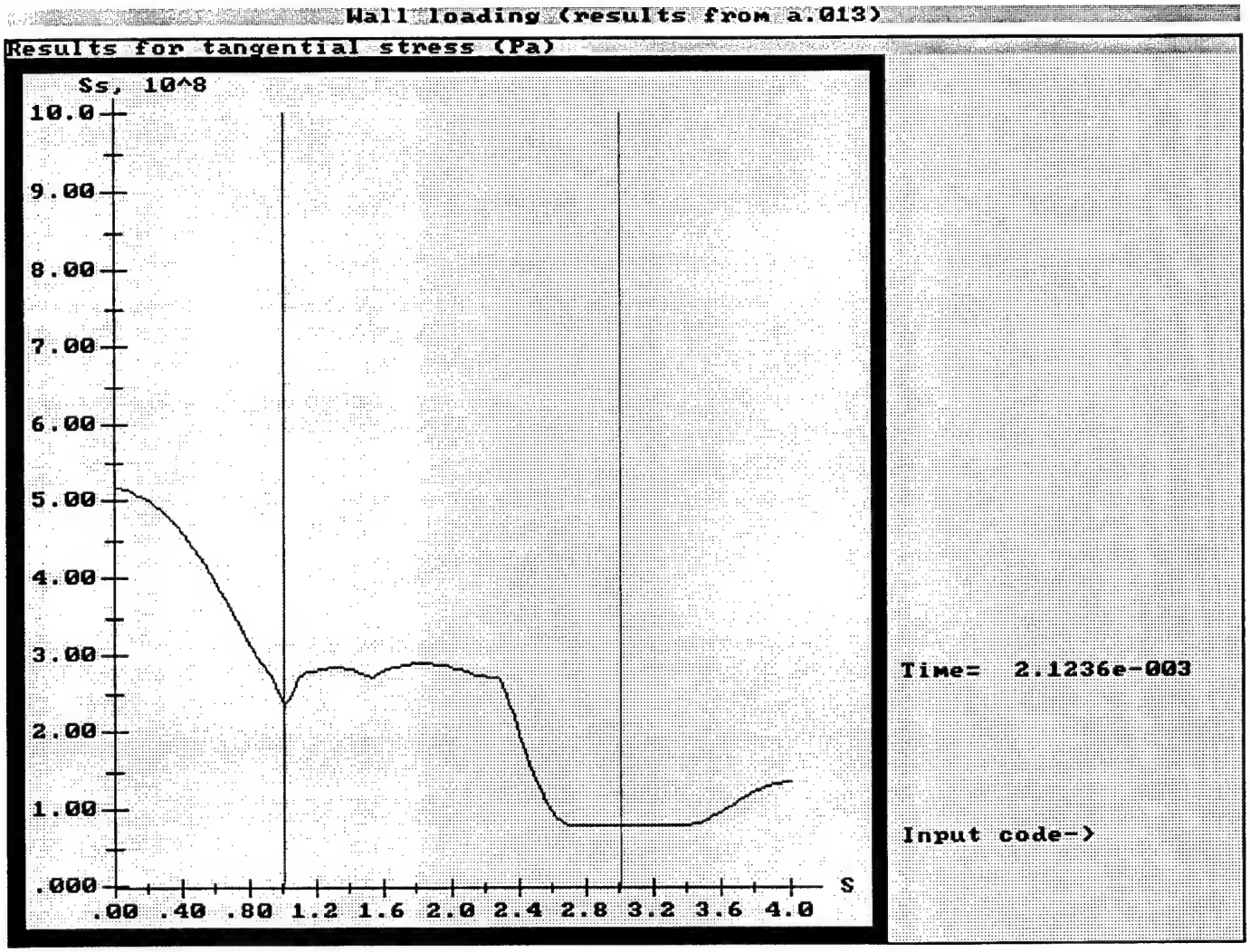
Wall loading (results from a.013)
Results for tangential stress (Pa)
$s, 10^8
10.0
9.00
8.00
7.00
6.00
5.00
4.00
3.00
2.00
1.00
.000
.00 .40 .80 1.2 1.6 2.0 2.4 2.8 3.2 3.6 4.0
S
Time= 2.1236e-003
Input code->

Fig. 28c.

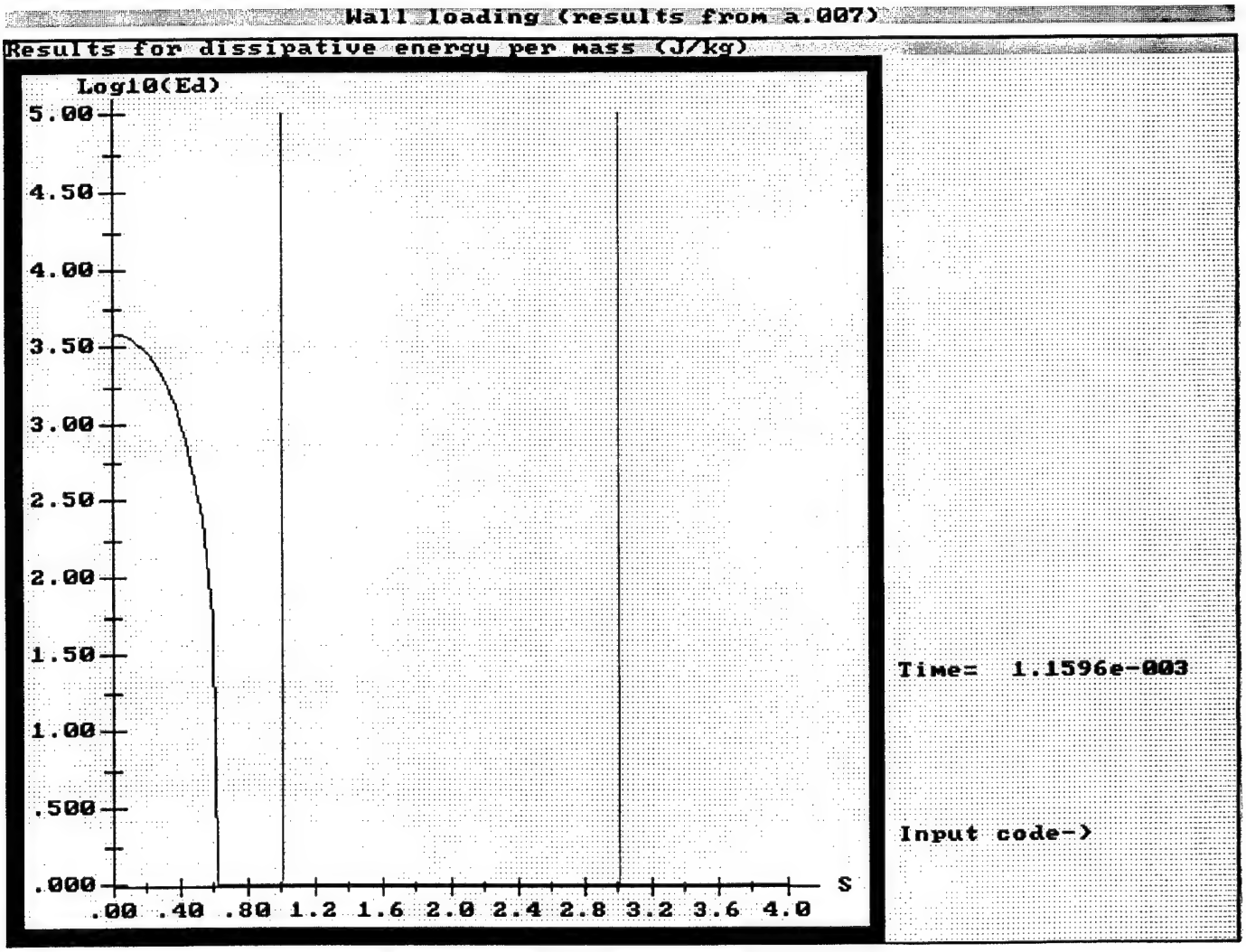
Wall loading (results from a.007)
Results for dissipative energy per mass (J/kg)
Log10(Ed)
5.00
4.50
4.00
3.50
3.00
2.50
2.00
1.50
1.00
.500
.000
.00 .40 .80 1.2 1.6 2.0 2.4 2.8 3.2 3.6 4.0
S
Time= 1.1596e-003
Input code->

Fig. 29a.

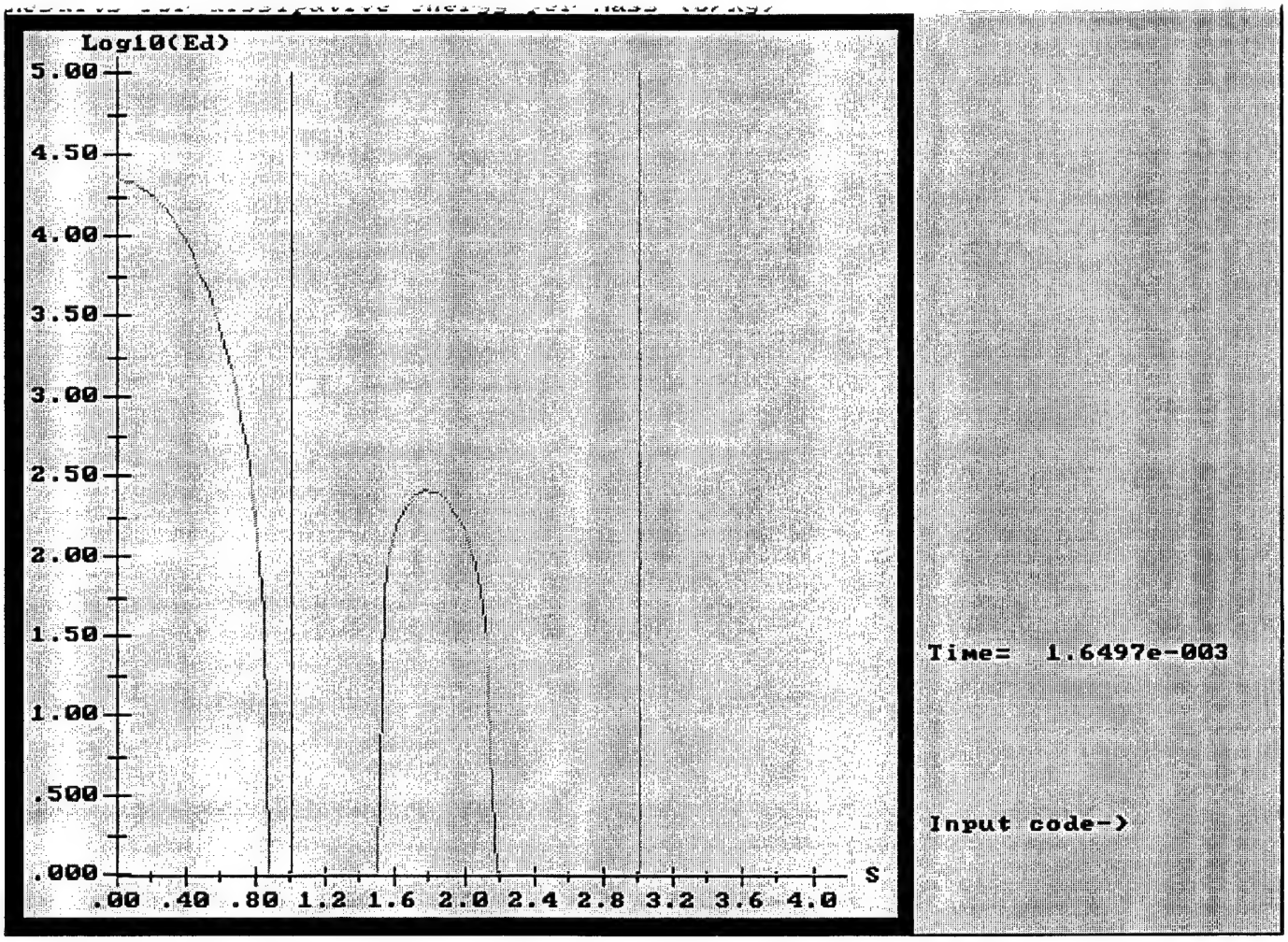
Log10(Ed)
5.00
4.50
4.00
3.50
3.00
2.50
2.00
1.50
1.00
.500
.000
.00 .40 .80 1.2 1.6 2.0 2.4 2.8 3.2 3.6 4.0
S
Time= 1.6497e-003
Input code->

Fig. 29B.

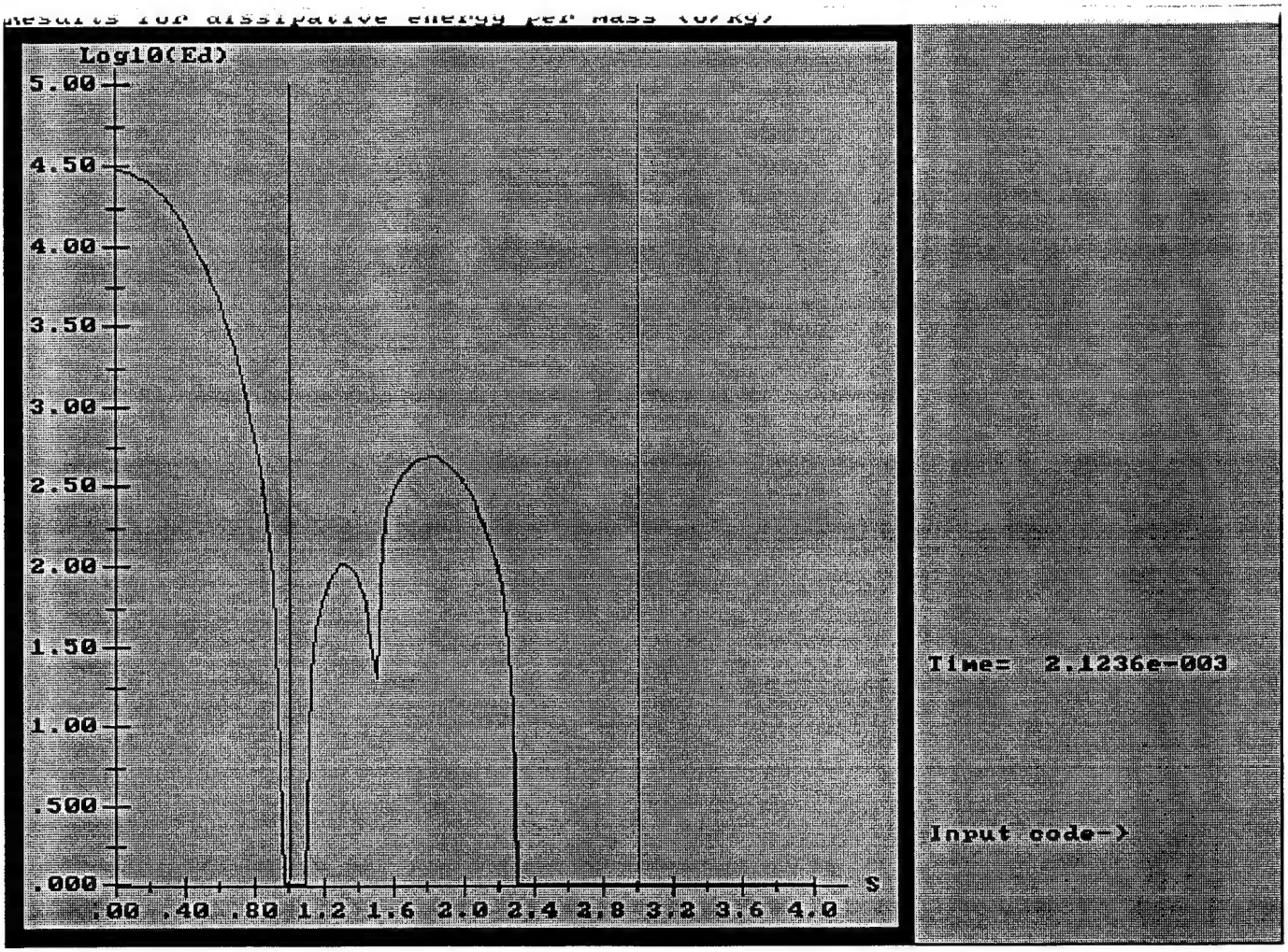
Results for dissipative energy per mass (J/kg)
Log10(Ed)
5.00
4.50
4.00
3.50
3.00
2.50
2.00
1.50
1.00
.500
.000
.00 .40 .80 1.2 1.6 2.0 2.4 2.8 3.2 3.6 4.0
S
Time= 2.1236e-003
Input code->

Fig. 29c.

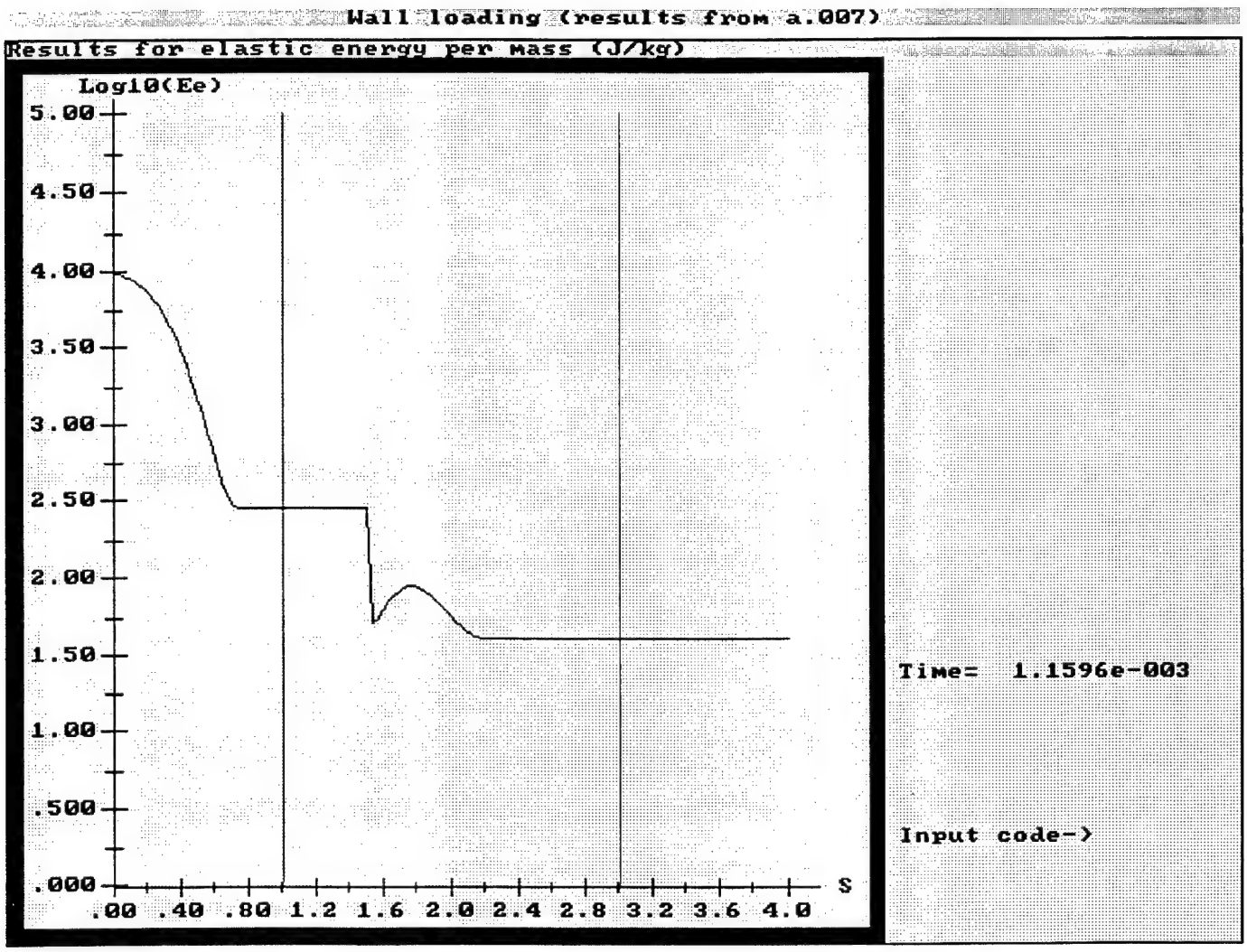
Wall loading (results from a.007)
Results for elastic energy per mass (J/kg)
Log10(Ee)
5.00
4.50
4.00
3.50
3.00
2.50
2.00
1.50
1.00
.500
.000
.00 .40 .80 1.2 1.6 2.0 2.4 2.8 3.2 3.6 4.0
S
Time= 1.1596e-003
Input code->

Fig. 30a.

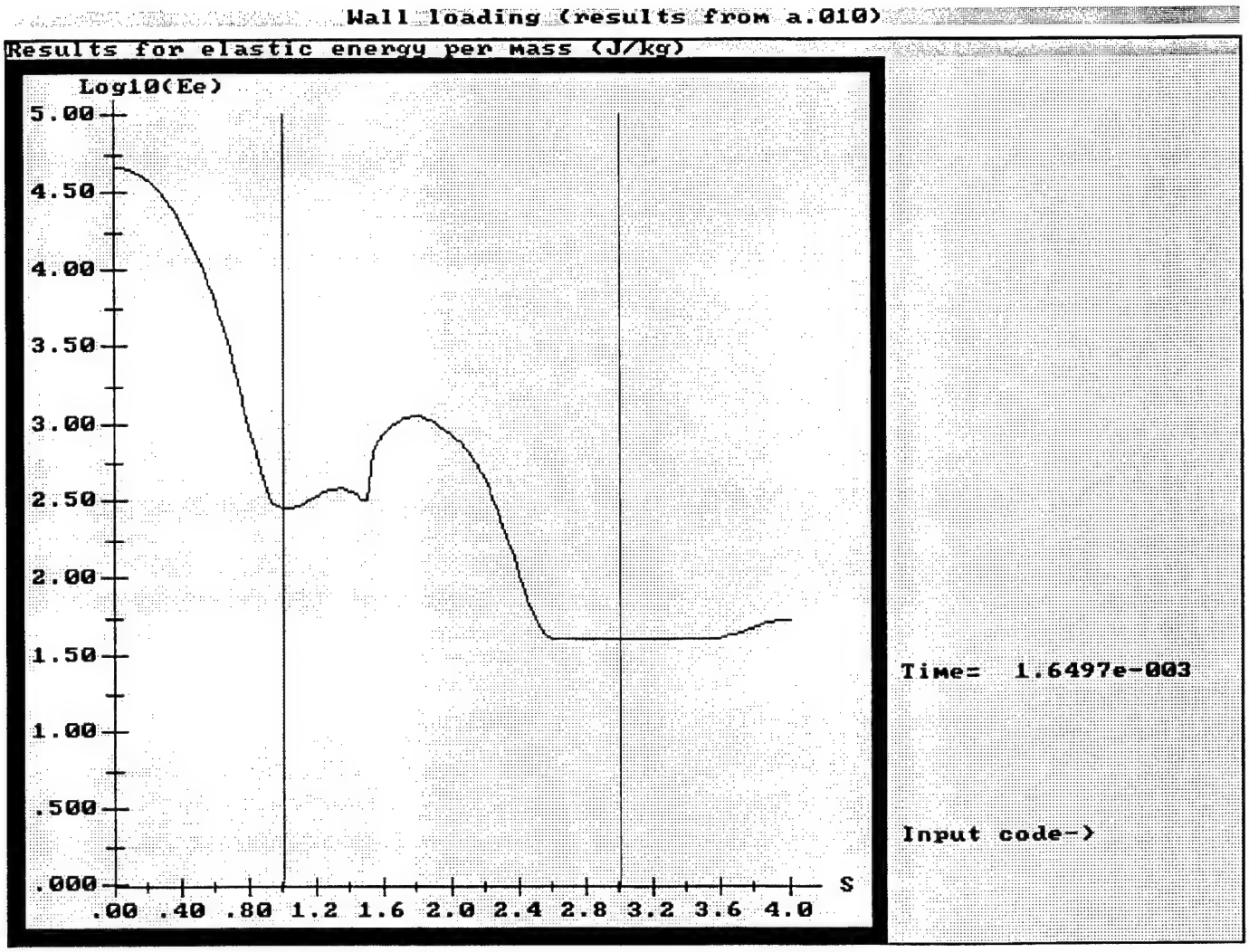
Wall loading (results from a.010)
Results for elastic energy per mass (J/kg)
Log10(Ee)
5.00
4.50
4.00
3.50
3.00
2.50
2.00
1.50
1.00
.500
.000
.00 .40 .80 1.2 1.6 2.0 2.4 2.8 3.2 3.6 4.0
S
Time= 1.6497e-003
Input code->

Fig. 30b.

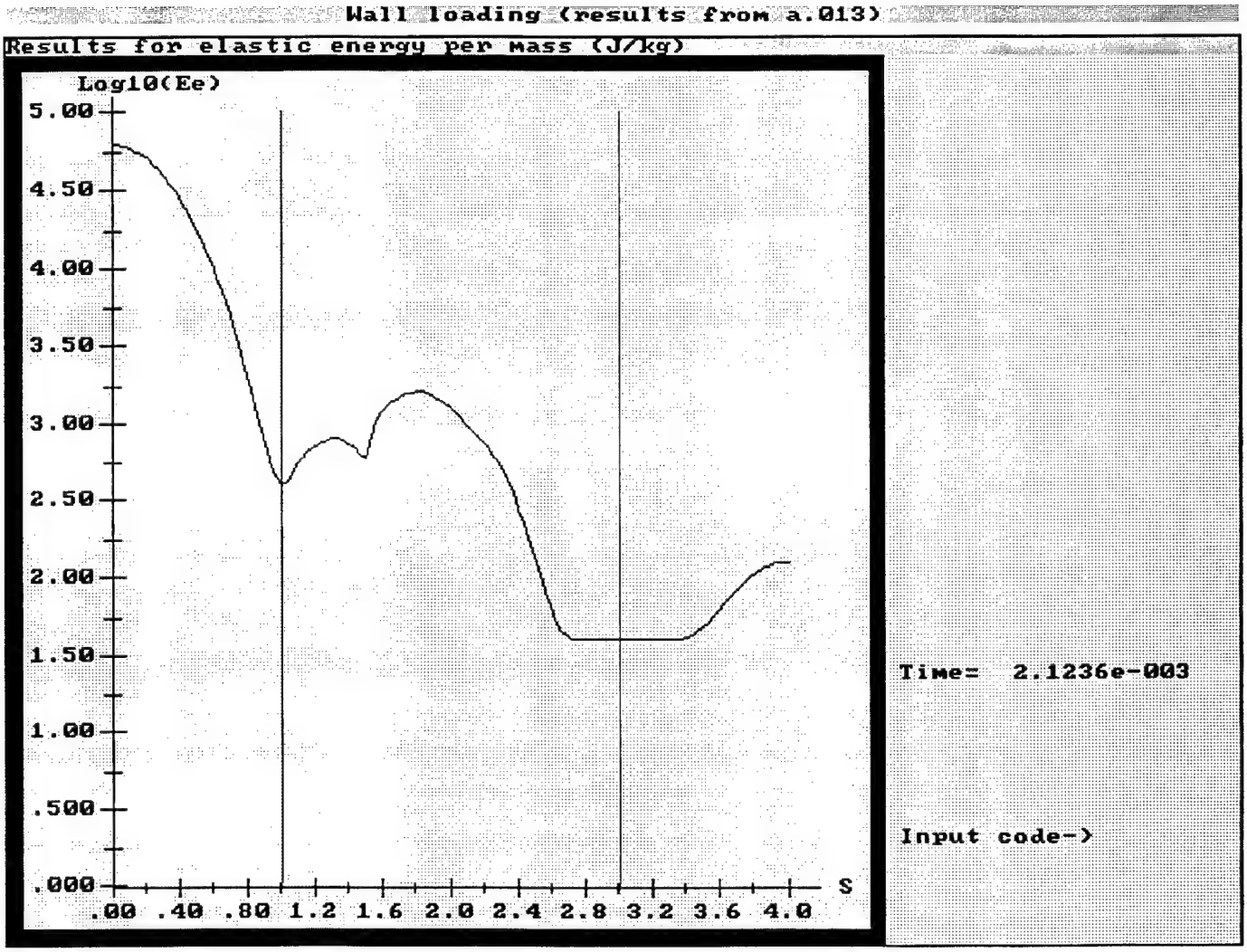
Wall loading (results from a.013)
Results for elastic energy per mass (J/kg)
Log10(Ee)
5.00
4.50
4.00
3.50
3.00
2.50
2.00
1.50
1.00
.500
.000
.00 .40 .80 1.2 1.6 2.0 2.4 2.8 3.2 3.6 4.0
S
Time= 2.1236e-003
Input code->

Fig. 30c.

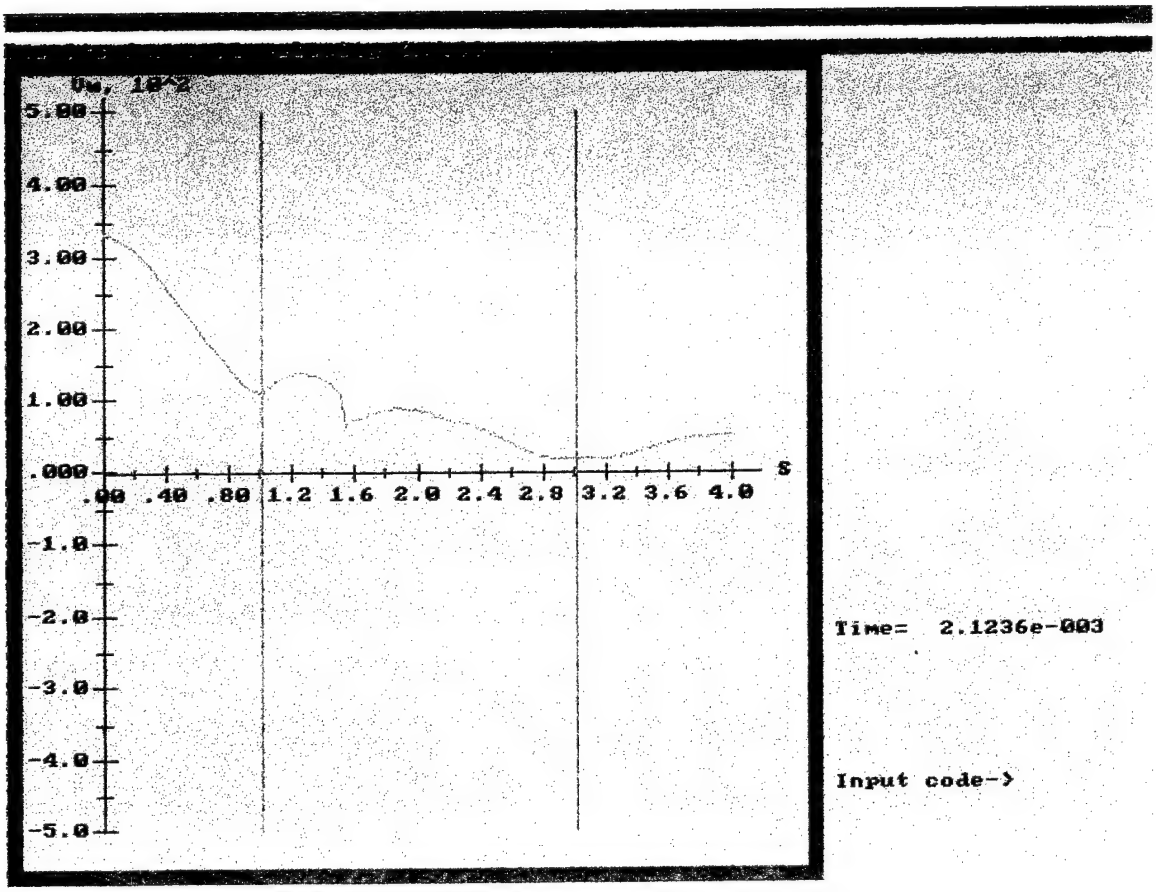
Ow, 10^2
5.00
4.00
3.00
2.00
1.00
.000
-1.0
-2.0
-3.0
-4.0
-5.0
.00 .40 .80 1.2 1.6 2.0 2.4 2.8 3.2 3.6 4.0
S
Time= 2.1236e-003
Input code->

Fig. 31a.

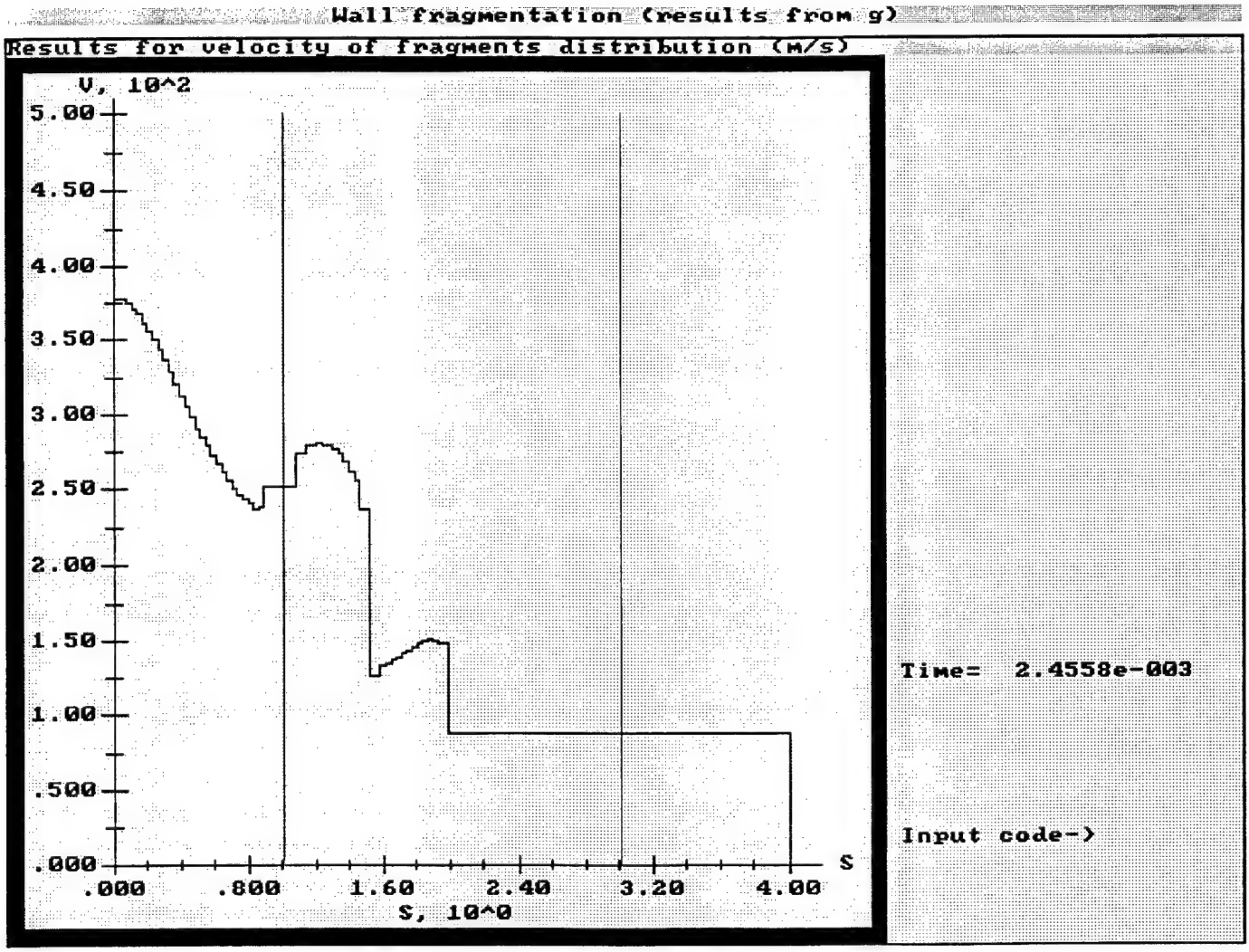
Wall fragmentation (results from g)
Results for velocity of fragments distribution (m/s)
V, 10^2
5.00
4.50
4.00
3.50
3.00
2.50
2.00
1.50
1.00
.500
.000
.000
.800
1.60
2.40
3.20
4.00
S
S, 10^0
Time= 2.4558e-003
Input code->

Fig. 31 b.

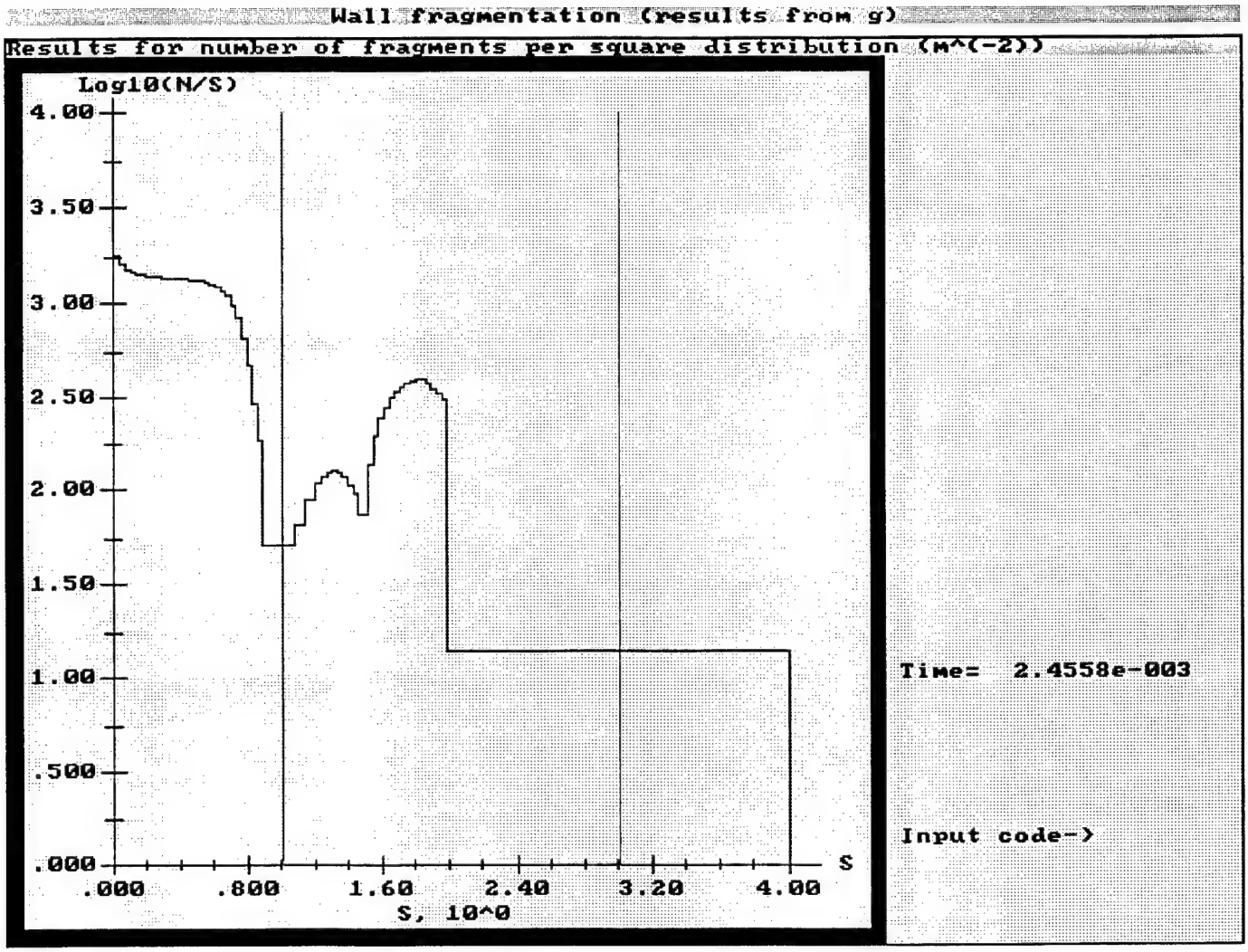
Wall fragmentation (results from g)
Results for number of fragments per square distribution (m^(-2))
Log10(N/S)
4.00
3.50
3.00
2.50
2.00
1.50
1.00
.500
.000
.000
.800
1.60
2.40
3.20
4.00
S
S, 10^0
Time= 2.4558e-003
Input code->

Fig. 32.

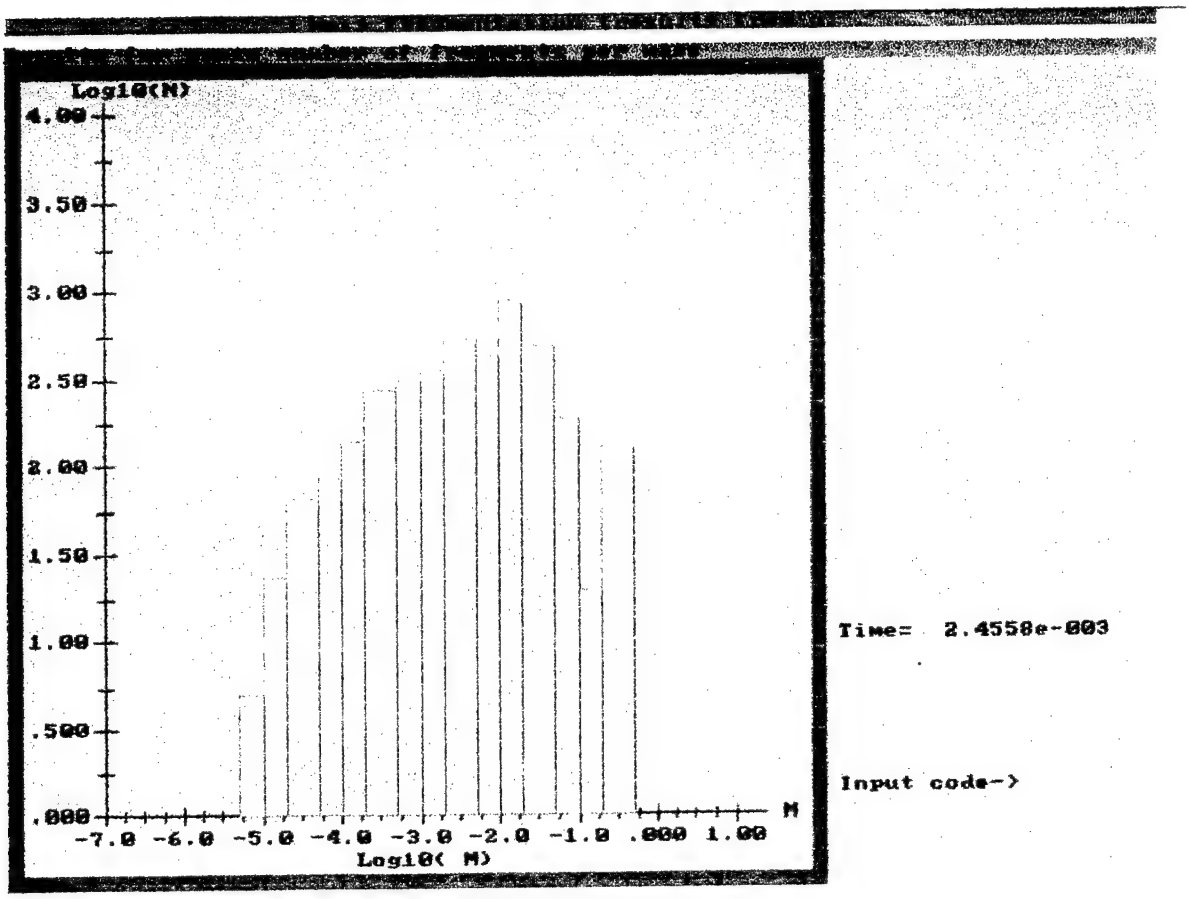
Log10(N)
4.00
3.50
3.00
2.50
2.00
1.50
1.00
.500
.000
-7.0 -6.0 -5.0 -4.0 -3.0 -2.0 -1.0 .000 1.00
Log10( M)
M
Time= 2.4558e-003
Input code->

Fig. 33.

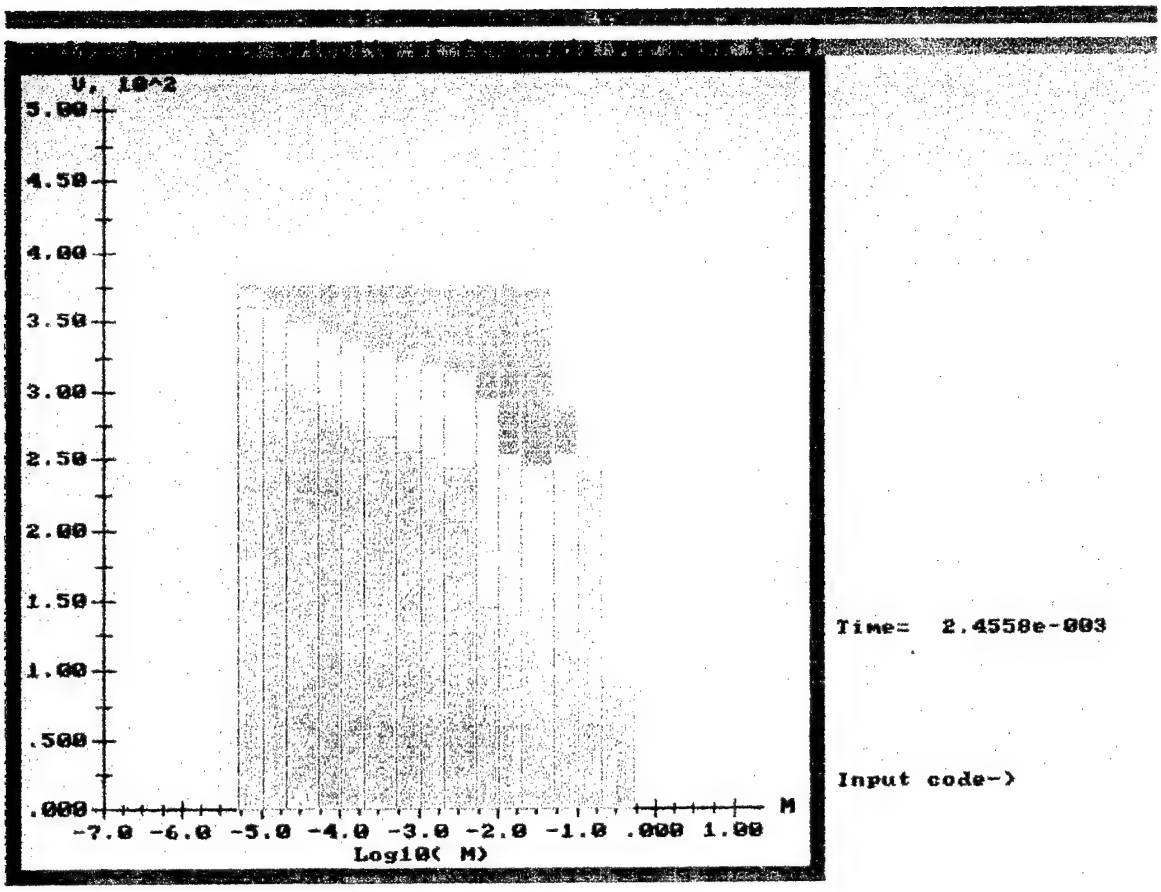
V, 10^2
5.00
4.50
4.00
3.50
3.00
2.50
2.00
1.50
1.00
.500
.000
-7.0 -6.0 -5.0 -4.0 -3.0 -2.0 -1.0 .000 1.00
M
Log10( M)
Time= 2.4558e-003
Input code->

Fig. 34.

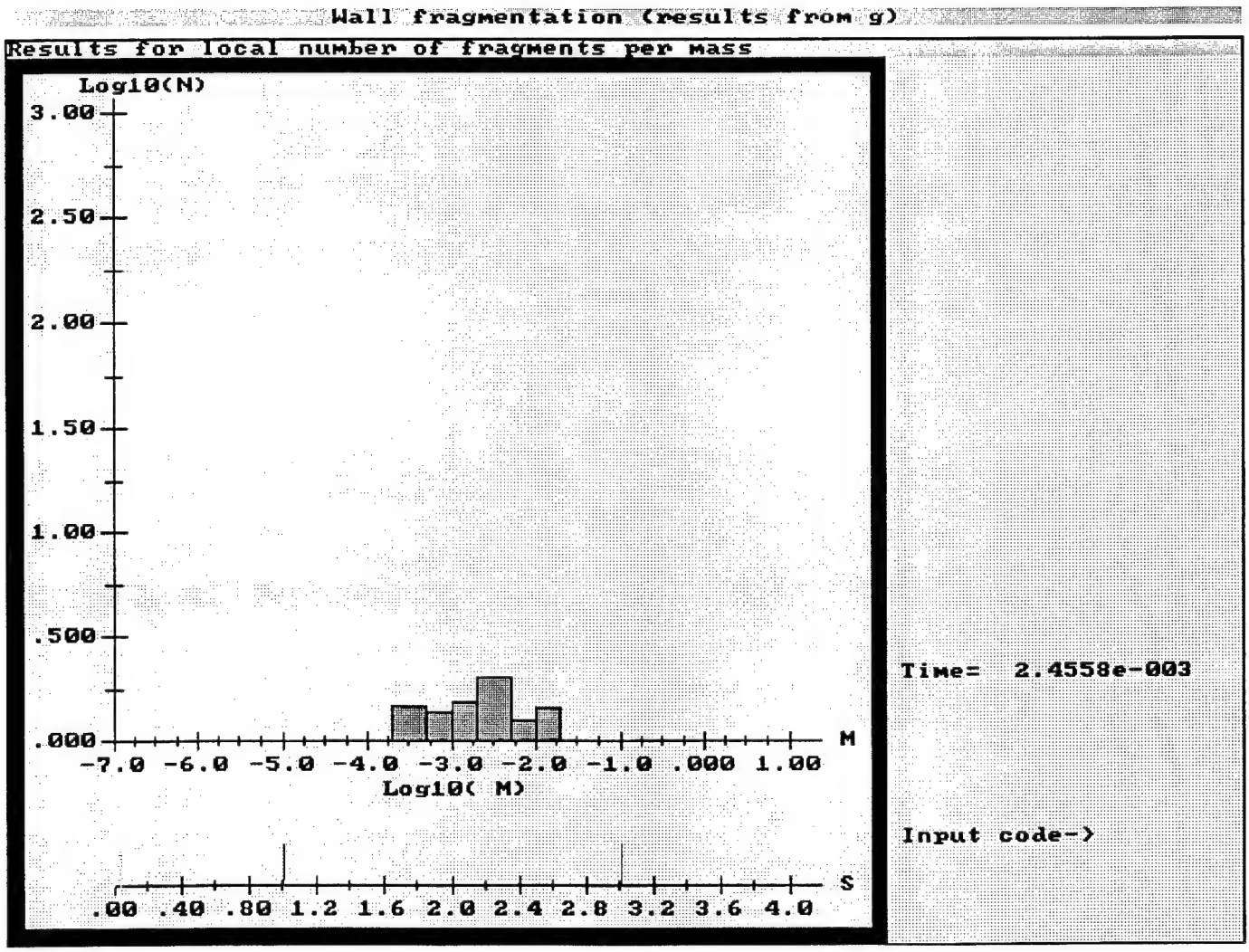
Wall fragmentation (results from g)
Results for local number of fragments per mass
Log10(N)
3.00
2.50
2.00
1.50
1.00
.500
.000
M
-7.0 -6.0 -5.0 -4.0 -3.0 -2.0 -1.0 .000 1.00
Log10( M)
S
.00 .40 .80 1.2 1.6 2.0 2.4 2.8 3.2 3.6 4.0
Time= 2.4558e-003
Input code->

Fig. 35a.

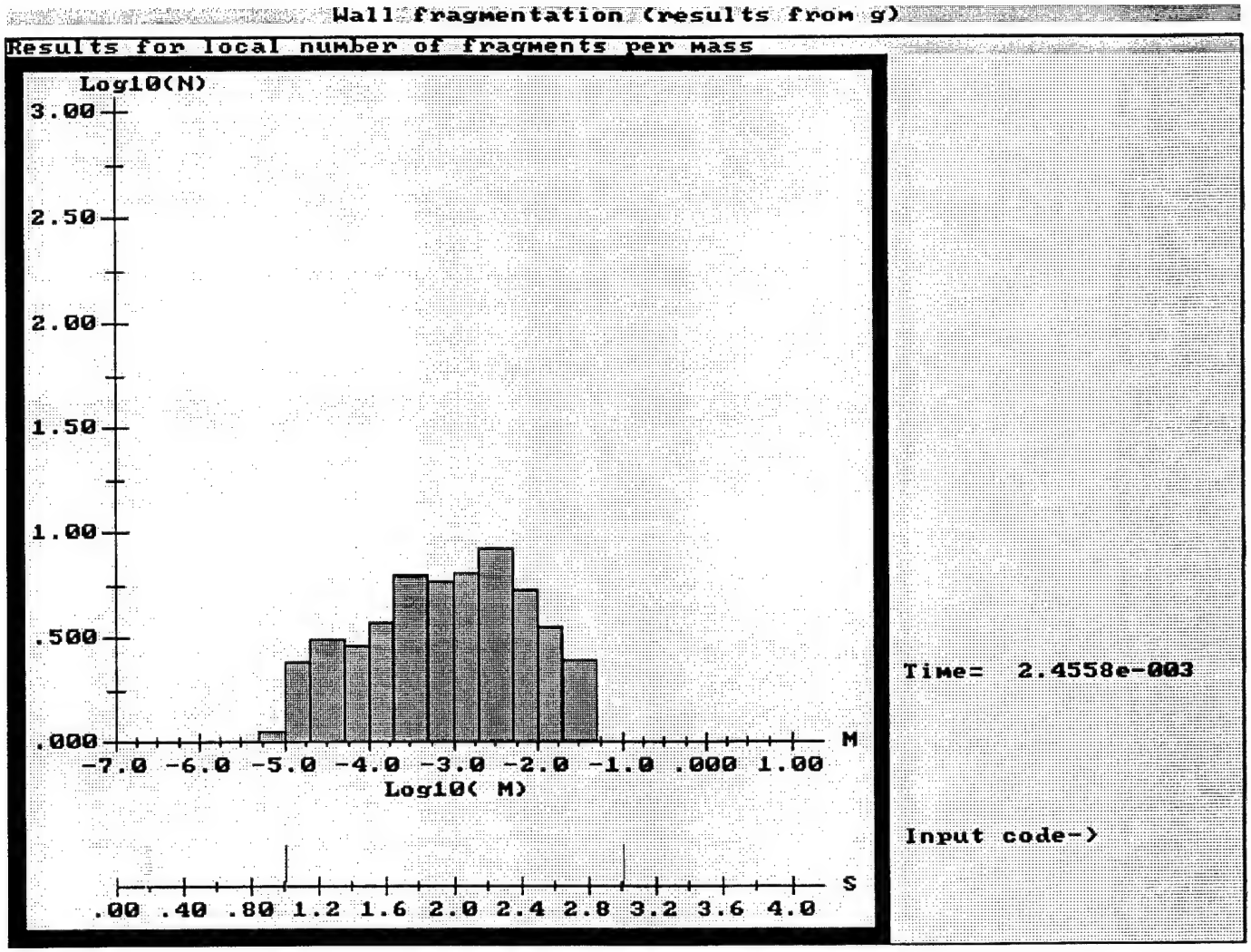
Wall fragmentation (results from g)
Results for local number of fragments per mass
Log10(N)
3.00
2.50
2.00
1.50
1.00
.500
.000
-7.0 -6.0 -5.0 -4.0 -3.0 -2.0 -1.0 .000 1.00
M
Log10( M)
.00 .40 .80 1.2 1.6 2.0 2.4 2.8 3.2 3.6 4.0
S
Time= 2.4558e-003
Input code->

Fig. 35b.

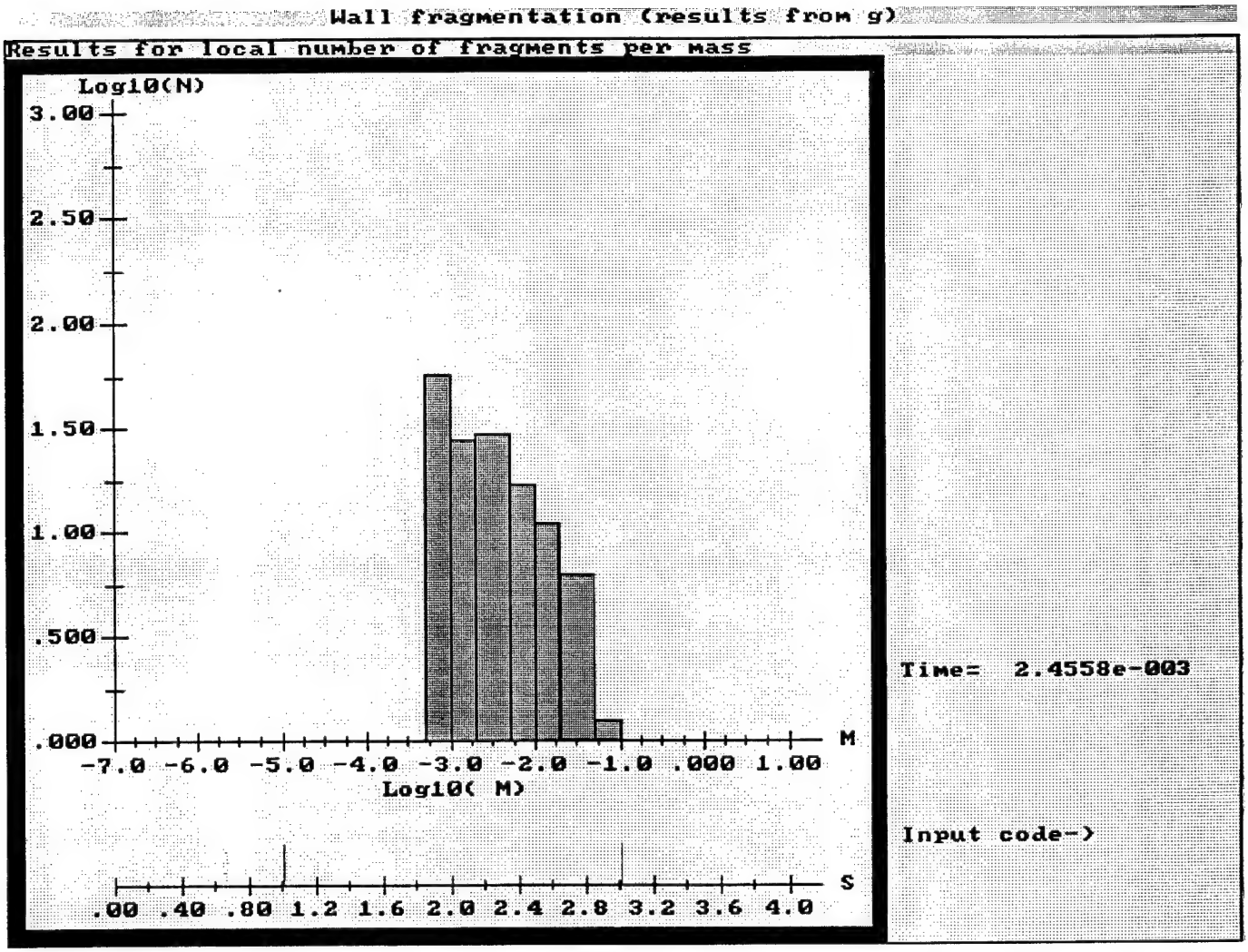
Wall fragmentation (results from g)
Results for local number of fragments per mass
Log10(N)
3.00
2.50
2.00
1.50
1.00
.500
.000
M
-7.0 -6.0 -5.0 -4.0 -3.0 -2.0 -1.0 .000 1.00
Log10( M)
S
.00 .40 .80 1.2 1.6 2.0 2.4 2.8 3.2 3.6 4.0
Time= 2.4558e-003
Input code->

Fig. 35c.

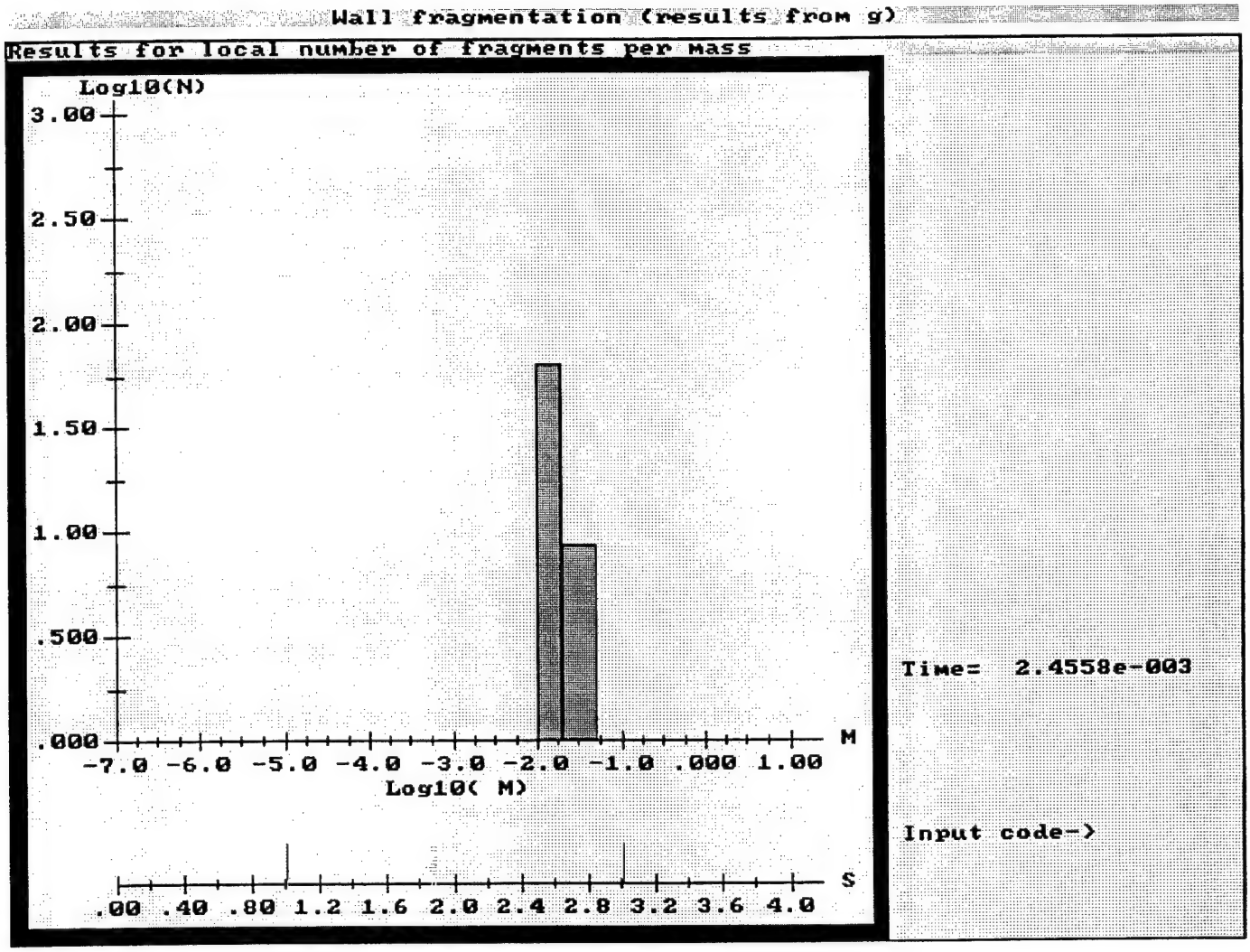
Wall fragmentation (results from g)
Results for local number of fragments per mass
Log10(N)
3.00
2.50
2.00
1.50
1.00
.500
.000
M
-7.0 -6.0 -5.0 -4.0 -3.0 -2.0 -1.0 .000 1.00
Log10( M)
S
.00 .40 .80 1.2 1.6 2.0 2.4 2.8 3.2 3.6 4.0
Time= 2.4558e-003
Input code->

Fig. 35 d.

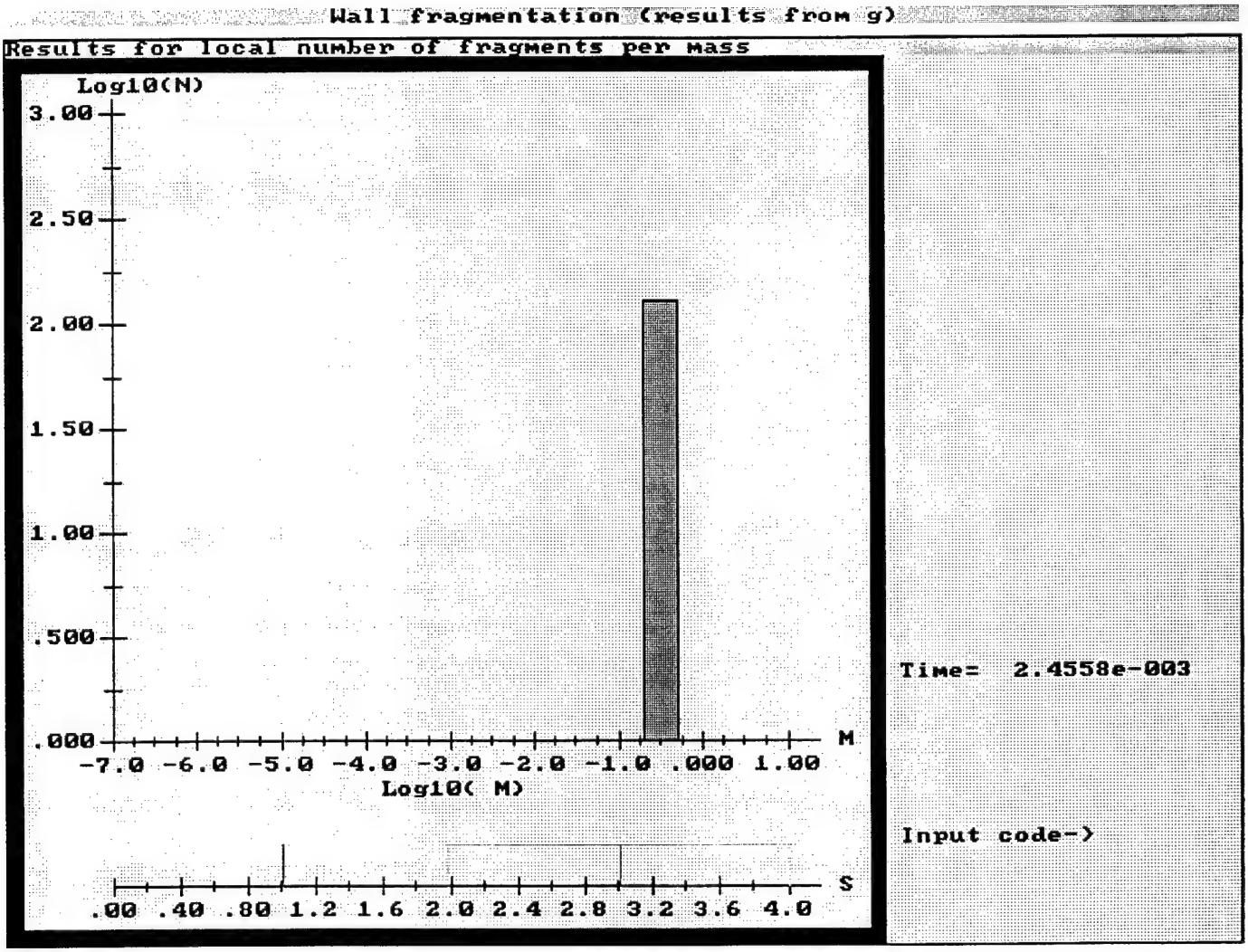
Wall fragmentation (results from g)
Results for local number of fragments per mass
Log10(N)
3.00
2.50
2.00
1.50
1.00
.500
.000
M
-7.0 -6.0 -5.0 -4.0 -3.0 -2.0 -1.0 .000 1.00
Log10( M)
S
.00 .40 .80 1.2 1.6 2.0 2.4 2.8 3.2 3.6 4.0
Time= 2.4558e-003
Input code->

Fig. 35e.

Hypergolic propellants combustion in the closed vessel.

The software package is splitted into 2 parts: calculation and results visualization. Both programs are written in C++ language. The calculation code in C++ is compatible with most C++ compilers; it uses only standard input-output functions and ANSI C type string and memory manipulation utilities. The visualization code is appliable to MSDOS only (versions 5.0 or higher). Codes are compiled by WATCOM C++ compiler (version 10.0). To run the programs, operative memory 4MB and Intel 486 processor are required; several megabytes of free space on a hard disk are also preferable.

The generic command file for calculation's module is named HYPR.EXE, to proceed calculations it must be run with parameters list:
HYPR [parameter1] ... [parameterN]
where the square brackets [] specify non-obligitory parameter and mustn't be typed in the command line. Each parameter has the following structure: <switch><specification>. Neither spaces nor braces are to be typed between the switch and specification of the parameter. Each switch consist of the hyphen and a letter, where <letter> is one of the symbols:
c,p,i,o,s,n,f,r,h,-,F,L,G ; specification can be empty or contain file name, some number or other information. The command list must contain at least one parameter (as a protective measure from instanteneous start). Also, any two switches in the command line must be different, otherwise the system will use the last switch with the same letter. Note that in MSDOS the command line must contain no more than 127 symbols.

The full list of the switches (with brief description) is:
-c specify Control data file,
-p specify initial Parameters file,
-i specify Input data file (to continue calculations),
-o specify Output data file,
-s specify output data file chain (Successuve output),
-f specify initial number of output File in the chain,
-F specify output file for Fragmentation results,
-L Long-term prediction of breakup,
-G force Gas phase calculation,
-r Restore initial parameters file from output data,
-n stop after initialization creating output data file (New data),
-- create control and parameters files with default values,
-h output a brief Help onto screen.
There is no required order of switches in the command line, but the first 2 symbols must be hyphen and one of the letters, listed above. At violation of these rules, program terminates with a message:
"Unknown parameter <parameter>".
Also if the command line is empty, program terminates with a message:
"To get a brief help, run hypr -h";

Some switches have priority above others, some are available only with other switches, some are antagonistic. This can be shown in a table:

| Switch | Ignores | Ignored by | Fails with | Fails without |
|---|---|---|---|---|
| -c | | -r,-n,--,-h | | |
| -p | | -i,-r,--,-h | | |

| | | | | |
|---|---|---|---|---|
| -o | | -s,--,-h,-r | | |
| -s | -o | --,-h,-r | -n | |
| -f | | if -s abscent | | |
| -F | | --,-h,-r,-n | | |
| -L | | -G,-r,-n,--,-h | | |
| -G | -L | -r,-n,--,-h | | |
| -r | -c,-s,-F,-L,-f,-n,-o | --,-h | | -i |
| -n | -c,-F,-L,-f | --,-h,-r | -i,-s | -o |
| -- | all except -h | -h | | |
| -h | all the others | | | |

Variations of the command list parameters provide all the functions of the calculative program. The functions can be divided into 2 groups: service functions and work functions. The first group has a priority above the second. The service functions can be listed in the order of their priority. We place here also the main switch providing the corresponding function.

Service functions group.

1. Output a brief help on the parameters list (-h).
2. Create files with default problem and control parameters (--);
3. Restore initial conditions from data file (-r);
4. Create data file at startup position (-n);

The work functions can be divided into 5 independent groups, in the each group we place them in the order of priority.

I. Control data specification group.

5. Specify file containing parameters to control calculations and output (-c);

II. Input specification group.

6. Continue calculations from a specified data file (-i);
7. Start calculations with specified initial conditions (-p);

III. Output specification group.

8. Make successive output into specified file chain, starting with specified file number (-s, -f);
9. Make output/backup into specified file (-o);

IV. Calculate fragmentation group.

10. Make system to calculate fragmentation and specify file to output results of fragmentation (-F);

V. Type of calculations specification group.

11. Make system to calculate gas dynamics process (-G);
12. Make system to calculate long-term breakup prediction (-L);

The detailed description of these functions is placed below.

Service functions group.

Functions of this group have the highest priority, it means that switches determining these functions being in the command line supress all the other functions and force execution of service functions.

(-h switch detailed description).

This switch has the highest priority: all the other parameters in the command line are ignored. The program outputs the following text onto screen:

```
Hypergolic propellants combustion calculation (axisymmetrical).
Usage: hypr [switches]
where the list of available switches:
-cFILENAME control parameters file name, default: none;
-pFILENAME problem parameters file name, default: none;
-iFILENAME input file name, default: none;
-oFILENAME output file name, default: none;
-sFILENAME successive output into FILENAME.???, default: none;
-fN successive output setup (N - file number), default: 0;
-rFILENAME restore problem parameters from input file;
-FFILENAME calculate wall fragmentation specifying output file;
-L long-term prediction only;
-G force the full process calculation;
-n create output at initial conditions;
-- create files with default problem parameters and control data;
-h this text output onto screen.
No required order of switches in the command line,
in case of 2 similar switches, system takes the last.
To get details, see manual.
```

2. Create files with default control and problem parameters (switch -- detailed description).

This function is supressed only by -h switch in the command line, and supresses all the other switches. It is used to create files containing default problem and control parameters. The files are named correspondingly PARAM.DAT and CTRL.DAT. After their creation, the files can be edited according to the rules placed below (see, for example, detailed description of -p switch application). It is suitable to rename such files after editing, because another usage of this function will lead to overwriting these files. To edit or to rename the obtained files one can use an external file editor (only in text mode) and any suitable operative system shell.
Specific cases:

A. When the file CTRL.DAT cannot be open in the write mode (existing file with the same name has Read-only attribute or some error is taking place), then the program will terminate with a message: "Cannot open control file CTRL.DAT for writing".
B. When the whole contens cannot be written into the file CTRL.DAT (no space on hard disk or some error), then the program will terminate with a message: "Cannot write into control file CTRL.DAT".
C. When the file PARAM.DAT cannot be open in the write mode (existing file with the same name has Read-only attribute or some error is taking place), then the program will terminate with a message: "Cannot open parameters file PARAM.DAT for writing".
D. When the whole contens cannot be written into the file PARAM.DAT (no space on hard disk or some error), then the program will terminate with a message: "Cannot write into parameters file PARAM.DAT".

Note that the system at first works with CTRL.DAT, then PARAM.DAT, so that if an error takes place while writing into PARAM.DAT, then CTRL.DAT will be already open, (over)written into and closed.

3. Restore initial conditions from data file

The problem parameters are saved in the output data files in binary format. This function serves to enscrypt them into a text file (with standard commentaries). To specify such destination text file the switch -rFILENAME is used. This function is ignored only if switches -h or -- are present in the command line. The source file is specified with -i switch (-iFILENAME), normally used to specify a file to continue calculations. In lack of this specification in the command line, the process will fail. Else the program reads a binary data file, specified by -i switch, writes the parameters into the file, specified by -r switch and terminates. All the other switches in the command line in this case are ignored.
Specific cases:

A. If a switch -i is not specified, program terminates with a message:
   "Switch -r must be used with -i switch".
B. If the file specified by -i switch cannot be open for reading (abscent, closed for reading or some error occurs), then the program will terminate with a message:
   "Cannot open input file <NAME>".
C. If the file specified by -i switch is somehow damadged so that the system cannot read the part of it, where the initial data is placed (near the begining of file), then the program will terminate with a message:
   "Cannot read from input file <NAME>".
D. If the file specified by -r cannot be open for writing or the program cannot write into it (existing file with the same name has Read-only attribute, no space on hard disk or some error), then the it will terminate with one of the messages:
   "Cannot open parameters file <NAME> for writing";
   "Cannot write into parameters file <NAME>".

4. Create data file at startup position (-n switch detailed description).

This is a specific function, helping to obtain binary data file for initial conditions. It is supressed by the other service functions, but supresses all the work (i.e. calculative) functions. With the switch -n in the command line, the program will: check the command line for abscence of input data file specification (switch -i), input initial conditions (default or specified in the command line with -pFILENAME parameter), make output of data into a binary file, specified by -oFILENAME parameter and finish. So the switch -n requires abscence of -i switch in the command line and presence of -o switch. But as far as the successive output (see switch -s for details) supresses -o switch, the switch -s also mustn't be in the command line together with -n. All the other switches (-c,-f,-F,-G, -L) are ignored.
Specific cases:

A. When -oFILENAME specification is abscent or switches -i,-s are present in the command line, then the program terminates with a message:
   "Switch -n must be used with -o and without -i or -s".
B. Other cases are related with situations, when the system falls into trouble with input-output. There can be possible messages:
   "Cannot open parameters file <NAME> for reading";
   "Cannot read from parameters file <NAME>";
   "Cannot open output file <NAME>";
   "Cannot write into output file <NAME>".

Working, or calculative, functions of the system.

These functions have less priority than the service functions listed above. The system will proceed them if the switches -h,--,-r and -n are abscent in the command line. We will not mention the service switches below regarding they are already abscent.

I. Control data specification group.

This group consist of only one item: specification of a text file containing parameters that control calculations and output. In case of lacking the specification, the system will use default parameters. Note that the text file containing default control parameters can be created by -- service switch in the command line (see above).

5. Specify file containing parameters to control calculations and output (-c switch detailed description).

The control parameters file is specified by -cFILENAME switch; the file containing these parameters has a text format and the following structure :

```
File containing program control information
You can insert your commentaries or rename it.
        1000            Timesteps before halt
        10              Timesteps before backup
        1               Timesteps before screen output
        0.3000000               Courant number
         1.0000         Artif viscos coeff for Vx equation
         1.0000         Artif viscos coeff for Vr equation
         0.0000         Artif viscos coeff for energy equation
         1.0000         Artif viscos coeff for Ka equation
         1.0000         Artif viscos coeff for Eps equation
         0.0000         Artif viscos coeff for oxidizer equation
         0.0000         Artif viscos coeff for fuel equation
         0.0000         Artif viscos coeff for products equation
        1               Display or not any gas phase res-s on screen
        1               Display or not: pressure
        1               Display or not: temperature
        0               Display or not: density
        0               Display or not: Vx
        0               Display or not: Vr
        0               Display or not: |V|
        0               Display or not: Ka
        0               Display or not: Epsilon
        0               Display or not: eddy viscosity
        0               Display or not: frequency
        0               Display or not: oxidizer concentration
        0               Display or not: fuel concentration
        0               Display or not: products concentration
         0.0000         Initial X position to display
         0.0000         Initial R position to display
         0.1000         Final X position to display
         0.0000         Final R position to display
        5               Number of points to monitor
        1               Display or not any wall load res-s on screen
        1               Display or not: effective radius
        1               Display or not: temperature
        1               Display or not: deformation
        1               Display or not: tangential stress
        1               Display or not: velocity
        1               Display or not: dissipation
        1               Display or not: elastic energy
```

```
10000          Timesteps before halt (long-term predict)
1000           Timesteps before backup (l-t prediction)
100            Timesteps before screen output (l-t pred)
5.00000e-005   Timestep magnitude (l-t prediction)
1              Display or not any wall fract res-s on screen
1              Display or not: total number of fragments

18595
```

User can change any commentaries in this file with the following regulations: first 2 lines are reserved for commentaries, any symbols are regarded as commentaries if they are placed between the number at the line begining and the end of the line, the last number (18595) near the end of the file is a signature and mustn't be changed, and an empty line before the signature is reserved. All the dimensionfull values in the file use SI system of units. Note that to switch off some output onto screen a zero value must be substituted at a corresponding position. The Courant number and the artificial viscosities must be changed with care, as far as the timestep magnitude for long-term prediction, because insufficient values can crush the calculations.
Specific cases:

A. If there are problems with file specified with -c switch (possible cases: file not exists, closed for reading, cannot be read to the end, hardware error), the program will terminate with one of the messages:
   "Cannot open control file <NAME> for reading".
   "Cannot read from control file <NAME>".

II. Input specification group.

This group consists of 2 items: specify file to continue calculations from, and specify file with initial parameters. The continuation of calculations has higher priority: switch specifying input file supresses parameters file specification. If no switches of input group are in the command line then the system will start calculations with default problem parameters.

6. Continue calculations from a specified data file (-i switch detailed description);

Calculations continue from a specified data file when the switch -iFILENAME is present in the command line. The format of the data file is binary, its length depends on grid sizes specified together with the problem parameters. As far as this binary file contains the problem parameters as a subset, the text file containing problem parameters is not needed to continue calculations. Thus specification -i in the command line supresses -p specification.
Specific cases:

A. In case of troubles with reading the specified file, the program will terminate with one of the messages:
   "Cannot open input file <NAME>".
   "Cannot read from input file <NAME>".
B. The data file is divided in two portions; at first part containing problem parameters is read, then the program allocates memory to store all the data required for calculations (its size depends on the data in the first part), then the rest of file is read into the part of allocated memory. In the case when memory allocation fails, the program will terminate with a message:
   "Cannot allocate memory".
C. If the wall dynamics is specified as a problem parameter, and the input file contains information that wall breakup already took

"Wall fractured",
and changes to calculate results of fragmentation if it is specified in the command line by -F switch (see below). Without this specification, the program terminates in this case.

7. Start calculations with specified initial conditions (-p switch detailed description).

Calculations will start from the begining, when the service switches and switch -i are abscent in the command line (so that switch -i has higher priority). Switch -pFILENAME specifies file containing problem parameters (including initial conditions) on the calculations startup. It is a text file, which name is arbitrary and the structure is:

File containing parameters (also initial)
You can insert your commentaries or rename it.

| | |
|---|---|
| 65 | Grid points along OX (must be 2^n+1) |
| 33 | Grid points along OR (must be 2^n+1) |
| 2.0000 | Vessel dimension along X |
| 1.0000 | Vessel dimension along R |
| 1.5000 | Fuel compartment length |
| 0.400 | Gap in the bulkhead radius |
| 5.00000e-002 | Molar weight of oxidizer |
| 5.00000e-002 | Molar weight of fuel |
| 5.00000e-002 | Molar weight of products |
| 1.00000e+000 | Stoicheometric coefficient for oxidizer |
| 1.00000e+000 | Stoicheometric coefficient for fuel |
| 2.00000e+000 | Stoicheometric coefficient for products |
| 4.15500e+002 | Heat capacity at V=const for oxidizer |
| 4.15500e+002 | Heat capacity at V=const for fuel |
| 4.15500e+002 | Heat capacity at V=const for products |
| 5.81700e+002 | Heat capacity at p=const for oxidizer |
| 5.81700e+002 | Heat capacity at p=const for fuel |
| 5.81700e+002 | Heat capacity at p=const for products |
| 3.00000e+005 | Initial pressure in fuel |
| 3.00000e+002 | Initial temperature in fuel |
| 8.00000e+005 | Initial pressure in oxid |
| 3.30000e+002 | Initial temperature in oxid |
| 1.00000e-005 | viscosity at norm cond in oxidizer |
| 1.00000e-005 | viscosity at norm cond in fuel |
| 1.00000e-005 | viscosity at norm cond in products |
| 9.00000e-001 | Prandtl number in oxidizer |
| 7.00000e-001 | Prandtl number in fuel |
| 7.20000e-001 | Prandtl number in products |
| 1.00000e+000 | Schmidt number in oxidizer |
| 1.00000e+000 | Schmidt number in fuel |
| 1.00000e+000 | Schmidt number in products |
| 5.20000e+006 | Reaction heat per fuel mass |
| 1 | Account wall stressing or not |
| 5.00000e-003 | Wall thickness |
| 2.70000e+003 | Wall density |
| 9.24300e+002 | Wall heat capacity |
| 1.00000e+002 | Wall thermoconductivity |
| 6.72000e-005 | Wall material volume extendibility |
| 2.70000e+010 | Shifting module |
| 3.20000e-001 | Poisson coefficient |
| 2.00000e-005 | Relaxation time |
| 2.90000e+008 | Elasticity limit |
| 6.80000e+008 | Maximal elasticity limit |
| 3.00000e+004 | Maximal dissipation energy per volume unit |
| 900. | Melting temperature |

```
6.50000e-010    S-G model constants: b
6.20000e-004    S-G model constants: h
1.00000e-001    S-G model constants: n
1.00000e+005    Breach creation energy per square unit
4.00000e-004    Effective square in distribution law
 0.5000         Power parameter in distribution law

18595
```

User can change any commentaries in this file with the following regulations: first 2 lines are reserved for commentaries, any symbols are regarded as commentaries if they are placed between the number at the line begining and the end of the line, the last number (18595) near the end of the file is a signature and mustn't be changed, and an empty line before the signature is reserved. All the dimensionful values in the file use SI system of units.
Specific cases:

A. In case of troubles with reading the specified file, the program will terminate with one of the messages:
   "Cannot open parameters file <NAME> for reading".
   "Cannot read from parameters file <NAME>".
B. After the parameters file is read, some of the parameters are checked in order to catch the most graveous faults. The following messages will appear before program's termination if some fault is caught:
   "Grid sizes must be 2^n+1, i.e. 17,33,65,129 etc";
   "Bad initial data" (many other faults).
C. After the file is read and parameters checked, then the program allocates memory to store all the data required for calculations (its size depends on specified grid sizes). In the case when memory allocation fails (usually it means that grid sizes are too large), the program will terminate with a message:
   "Cannot allocate memory".
D. If the wall dynamics calculation is specified as a problem parameter, then the program will stop calculating the process of combustion and wall if the breakup occurs, and change to calculate fragmentation results if it is specified in the command line by -F switch or terminate without -F specification. Anyhow, after breakup is reached, the program outputs onto screen:
   "Wall fractured".
   If, on the contrary, wall dynamics calculation is not specified, then all the parameters corresponding to the wall properties are ignored.

### III. Output specification group.

This group of functions consists of two items: single file output specification, and a chain of files specification. The last item has higher priority so that if both specifications are present in the command line, the system will supress single-file specification. Also note that in the case of abscence of output specifications, no output into binary files will take place (it doesn't relate to output of fragmentation's results, see below).

8. Make successive output into specified file chain, starting with specified file number (-s and -f switches detailed description).

The switch -sFILENAME is used to specify filename (without extension!) for output data files successive chain. This chain consists of files FILENAME.000, FILENAME.001, and so on. The initial number in the chain

chain is written after the calculations pass the number of timesteps, specified in control data file as "timesteps before backup". Note that if calculations begin, then NAME.000 will contain data for startup position, and if the user wants to continue to write into the chain, which last file was NAME.KLM, then he must use parameters -iNAME.KLM -sNAME -fKLM in the command line (KLM must consist of 3 digits only). The available file number is bounded with 900 from above. The switch -s always supresses switch -o (specify a single output file), even in service functions. The switch -f is ignored always when -s is abscent in the command line.
Specific cases:
A. If a problem will occur with writing into one of the files in the chain, then the program will terminate with one of the messages:
"Cannot open output file <NAME>".
"Cannot write into output file <NAME>".

9. Make output/backup into specified file (-o switch detailed description).

The switch -oFILENAME is used to specify a single output data file. The program proceeds output: after the startup, each time after specified in control data steps before backup, after the specified steps before halt (see control data structure above). This switch is always supressed by -s switch.
Specific cases:
A. If a problem will occur with writing into the specified file, then the program will terminate with one of the messages:
"Cannot open output file <NAME>".
"Cannot write into output file <NAME>".

IV. Calculate fragmentation group.

This group of functions consist of a single item, directing the program to calculate fragmentation if breakup occured in calculations. If no breakup occurs, this function is ignored.

10. Make system to calculate fragmentation and specify file to output results of fragmentation (switch -F detailed description).

Presence of switch -F in the command line (format: -FFILENAME) directs the program to calculate the fragmentation of the vessel's wall if wall breakup is calculated. This switch is forced to be ignored by any service switches in the command line, but there are two cases, when the functions specified by this switch are inachievable. First, if wall dynamics is not accounted (this is one of the problem parameters), and second, when the breakup of the wall doesn't take place. If the breakup takes place, the system calculates wall fragmentation and then puts the results into a specified binary file (its format differ from usual binary output file format).
Specific cases:
A. If a problem will occur with writing into the specified file, then the program will terminate with one of the messages:
"Cannot open output file <NAME>".
"Cannot write into output file <NAME>".
B. If wall dynamics is not accounted, the program will terminate with a message:
"Cannot calculate fragmentation: wall dynamics not accounted".

V. Type of calculations specification group.

2 types of calculations algorithm: full algorithm, including combustion calculation, together with the wall dynamics is one choice, the other is only wall dynamics, ignoring combustion and taking only average pressure and local temperature from it, constant in time. The second algorithm is rather weak but much more rapid than the first, it is named long-term prediction and is recommended to be used when the pressure in the vessel in calculations came to a plato but the wall breakup didn't take place. However, there is only one software restriction on using the second algorithm (see below). Forcing the first algorithm has a priority above long-term prediction.

11. Make system to calculate gas dynamics process (switch -G detailed description).

As a default, the first algorithm is always chosen. But there is one case when the program cannot start: if one wants to start with default control and problem parameters and no output into files (this can be used for debugging purposes). Such conditions require no parameters in the command line, but this is prohibited. To overcome the situation, the switch -G was involved, which only function is to play a role of a parameter in the command line. It is designed to supress the switch -L, which changes to long-term prediction algorithm.

12. Make system to calculate long-term breakup prediction (switch -L detailed description).

The switch is -L used to change to long-term prediction algorithm instead of combustion calculation. There is no restrictions on changing between the two algorithms twice or more times, but to obtain suitable results, one must use at first full algorithm, then long-term prediction. After this, new using the full algorithm is not recommended (but the software doesn't prohibit it). This switch is supressed by service switches and -G switch.
Specific cases:
A. When the wall dynamics is not accounted (parameter "account wall" set to zero), then if -L is specified, the program will terminate with a message:
"Cannot calculate long-term prediction: wall dynamics not accounted"

The results visualization part of the package.

The second part of the software package is used to represent the results of calculations on the monitor screen. It is appliable for MSDOS operational system only. The software requires VGA monitor.

Starting the program of visualization.

The generic command file for visualization's module is named VIPR.EXE, it must be run with parameters list:
VIPR [parameter1] ... [parameterN]
where the square brackets [] specify non-obligitory parameter and mustn't be typed in the command line, and each parameter has the following structure: <switch><specification>. Neither spaces nor braces are to be typed between the switch and specification of the parameter. Each switch consist of the hyphen and a letter, where <letter> is one of the symbols: i,s,f,v,F,h; <specification> can be empty or contain file name or some number. The command list must contain at least one switch (moreover, switch -i or -s must present in the command line). As like as for the calculation's module rules, any two switches must have different title letters, in case of two same switches in the command line the system will use the last. Note that in

The program returns a value into MSDOS environment, so that the environment variable ERRORLEVEL will obtain a certain value. If no errors occur, the ERRORLEVEL will be 0.

The full list of the switches for visualization program (with brief description) is:
-v specify Video parameters file,
-i specify Input data file,
-s specify input data Successive chain of files,
-f specify initial number of input File in the chain,
-F specify input file with fragmentation results,
-h output a brief help onto screen.
There is no required order of switches in the command line, but the first 2 symbols must be hyphen and one of the letters, listed above. At violation of these rules, program terminates with ERRORLEVEL 1 and a message:
"Unknown parameter <SWITCH>".
If the command line is empty, program terminates with a message:
"To get a brief help, run vipr -h"
and ERRORLEVEL 50.

The table of switches compatibility, analogical to the table in calculations module is:

| Switch | Ignores | Ignored by | Fails with | Fails without |
|---|---|---|---|---|
| -v | | -h | | |
| -i | | -s,-h | | |
| -s | -i | -h | | |
| -f | | all except -s | | |
| -F | | -h | | |
| -h | all the others | | | |

Variations of the command list parameters provide all the setup functions of the calculative program. The functions can be divided into 2 groups: service functions and work functions. The first group has a priority above the second. The service functions group consists of one item and has the highest priority. The full list of setup functions is:

Service functions group.

1. Output a brief help on the parameters list (-h).

The work functions can be divided into 3 independent groups, in the each group we place them in the order of priority.

I. Video setup file specification group.

2. Specify file with setup data for visualization (-v);

II. Input group.

3. Make successive picking up results from specified file chain, starting with specified file number (-s, -f);
4. Pick up results from a specified single data file (-i);

III. Input fargmentation group.

5. Pick up results of fragmentation from a specified file (-F);

The detailed description of these functions is placed below.

Service functions group.

This group consists of one item - output a brief help onto screen. It has the highest priority over all the other functions.

1. Output a brief help on the parameters list
   (-h switch detailed description).

This switch has the highest priority: all the other parameters in the command line are ignored. If there is the switch -h in the command line, then the program outputs the following text onto screen:

```
Hypergolic propellants combustion visualization (axisymmetrical).
Usage: vipr [switches]
where the list of available swithces:
-vFILENAME video parameters file name, default: none;
-iFILENAME input file name, default: none;
-sFILENAME successive input files chain filename
          (without extension), default: none;
-fN successive input setup (N - file number), default: 0;
-FFILENAME input file name with fragmentation's data, default: none;
-h this text output onto screen.
No required order of switches in the command line;
in case of 2 similar switches, system takes the last.
To get details, see manual.
```

After this the program terminates with ERRORLEVEL 50.

I. Video setup file specification group.

This groups consists of one item; this function is supressed only by service function (i.e. help).

2. Specify file with setup data for visualization
   (-v switch detailed description).

Parameters, where lower limit, upper limit and type of scale (normal, i.e. arithmetic progression, or logarithmic, i.e. geometric progression for intermediate levels) are set for each kind of output data, are placed in a text file, which can be specified by -vFILENAME switch in the command line. The file structure is:

```
File containing video parameters.
You can insert your commentaries or rename it.
        1.00000e+004    Lower limit for pressure
        5.00000e+006    Upper limit for pressure
        0               Normal(0),logarithmic(1) scale for pressure
        2.08333e+002    Lower limit for temperature
        4.32000e+003    Upper limit for temperature
        1               Normal(0),logarithmic(1) scale for temperature
        5.00000e-001    Lower limit for density
        5.00000e+000    Upper limit for density
        0               Normal(0),logarithmic(1) scale for density
        0.00000e+000    Lower limit for Vx
        5.00000e+002    Upper limit for Vx
        0               Normal(0),logarithmic(1) scale for Vx
        0.00000e+000    Lower limit for Vr
        5.00000e+002    Upper limit for Vr
        0               Normal(0),logarithmic(1) scale for Vr
        0.00000e+000    Lower limit for |V|
        5.00000e+002    Upper limit for |V|
```

```
1.00000e-002    Lower limit for Ka
2.50000e+004    Upper limit for Ka
0               Normal(0),logarithmic(1) scale for Ka
1.00000e-001    Lower limit for Epsilon
5.00000e+006    Upper limit for Epsilon
0               Normal(0),logarithmic(1) scale for Epsilon
1.00000e-006    Lower limit for eddy viscosity
1.00000e+003    Upper limit for eddy viscosity
1               Normal(0),logarithmic(1) scale for eddy viscos
1.00000e+000    Lower limit for frequency
1.00000e+003    Upper limit for frequency
1               Normal(0),logarithmic(1) scale for frequency
0.00000e+000    Lower limit for oxidizer concentration
1.00000e+000    Upper limit for oxidizer concentration
0               Normal(0),logarithmic(1) scale for oxid conc
0.00000e+000    Lower limit for fuel concentration
1.00000e+000    Upper limit for fuel concentration
0               Normal(0),logarithmic(1) scale for fuel conc
0.00000e+000    Lower limit for products concentration
1.00000e+000    Upper limit for products concentration
0               Normal(0),logarithmic(1) scale for prod conc
1.00000e-9      Lower limit for reaction intensity
1.00000e+000    Upper limit for reaction intensity
1               Normal(0),logarithmic(1) scale for react intens
0.00000e+000    Lower limit for effective radius
5.00000e-001    Upper limit for effective radius
0               Normal(0),logarithmic(1) scale for eff radius
1.00000e-003    Lower limit for temperature
1.00000e+001    Upper limit for temperature
0               Normal(0),logarithmic(1) scale for temperature
1.00000e-003    Lower limit for deformation
1.00000e-001    Upper limit for deformation
1               Normal(0),logarithmic(1) scale for deformation
1.00000e+000    Lower limit for tangential stress
1.00000e+009    Upper limit for tangential stress
0               Normal(0),logarithmic(1) scale for tangnt stres
0.00000e+000    Lower limit for velocity
5.00000e+002    Upper limit for velocity
0               Normal(0),logarithmic(1) scale for velocity
1.00000e+000    Lower limit for dissipation
5.00000e+004    Upper limit for dissipation
1               Normal(0),logarithmic(1) scale for dissipation
1.00000e+000    Lower limit for elastic energy
1.00000e+005    Upper limit for elastic energy
1               Normal(0),logarithmic(1) scale for elastic enrg
1.00000e+004    Lower limit for total number of fragments
1.00000e+007    Upper limit for total number of fragments
1               Normal(0),logarithmic(1) scale for tot nmb of f
3.00000e+002    Lower limit for NUMBER per mass (gross)
3.00000e+003    Upper limit for NUMBER per mass (gross)
1               Norm(0),log(1) scale for NUMBER per mass (gross
1.00000e+000    Lower limit for NUMBER per mass (gross)
1.00000e+004    Upper limit for NUMBER per mass (gross)
1               Norm(0),log(1) scale for NUMBER per mass (gross
0.00000e+000    Lower limit for VELOCITY per mass (gross)
5.00000e+002    Upper limit for VELOCITY per mass (gross)
0               Norm(0),log(1) scale for VEL per mass (gross)
1.00000e+000    Lower limit for NUMBER per square per sections
1.00000e+004    Upper limit for NUMBER per square per sections
1               Norm(0),log(1) scale for NUMB per sqr per sects
0.00000e+000    Lower limit for VELOCITY per sections
```

```
0               Normal(0),log (1) scale for VEL per sections
1.00000e+000    Lower limit for NUMBER per mass (local)
1.00000e+003    Upper limit for NUMBER per mass (local)
1               Norm(0),log (1) scale for NMB per mass (local)

18595
```

User can change any commentaries in this file with the following regulations: first 2 lines are reserved for commentaries, any symbols are regarded as commentaries if they are placed between the number at the line begining and the end of the line, the last number (18595) near the end of the file is a signature and mustn't be changed, and an empty line before the signature is reserved. All the dimensionfull values in the file use SI system of units. If -v switch is not specified, the default values will be used. User can change all of these values via program and rewrite this file (see below). With -vFILENAME specification, rewritten file will have the same name FILENAME, without it, file will be named VIDEO.DAT.
Specific cases:

A. If the filename is specified with -v switch but the file cannot be open (abscent or closed for reading), then the program will terminate with ERRORLEVEL 2 and a message:
   "Cannot open video data file <NAME> to read".
B. If the file is somehow damadged so that the signature cannot be correctly read to the end, then the program will terminate with ERRORLEVEL 3 and a message:
   "Cannot read from video parameters file <NAME>".
C. On rewriting file via program, if a trouble occur (no space on hard disk, file closed for writing or hardware error), the program will terminate with one of the messages:
   "Cannot open video data file <NAME> to write" (ERRORLEVEL 11),
   "Cannot write into video data file <NAME>" (ERRORLEVEL 12).

Note that changing limits via program must yeild some restrictions: one cannot change to logarithmic scale if the lower limit is zero, or one cannot change limits if after change the lower limit will exceed the upper. This is monitored by the system, and such cases lead to error messages without program termination.

## II. Input group.

This group consists of two items: input from a file chain and input from a single file. Both functions are supressed only by help service. One of functions of this group must present in the command line. Note that results of fragmentation are specified by another group of parameters.

3. Make successive input of results from specified file chain, starting with specified file number (-s, -f switches detailed description).

Parameter -sFILENAME (FILENAME without extension!) serves to specify a chain of files containing results; each file in the chain describes results for a single time moment. The initial file in the chain to be read will have the number 000 if -f switch is abscent, or number N (3-digital with leading zeros) if -fN is present in the command line. Note that N is bounded by 900 from above (see also "successive output" in the calculative module's description).
Specific cases:

A. If the specified first-to-read file in the chain cannot be open (closed for reading or abscent), then the program will terminate with ERRORLEVEL 5 and a message:

B. If the data file (first-to-read) cannot be correctly read to the end, then the program will terminate with ERRORLEVEL 6 and a message:
"Cannot read from input file <NAME>".
C. If neither -i, nor -s switch is specified, then the program will terminate with ERRORLEVEL 4 and a message:
"Input file name must be specified".
D. Switch -f without -s specification is ignored; if no number follows after -f switch, then it is also ignored, and the initial file to read will be FILENAME.000, where FILENAME is specified by -s switch.

4. Input results from a specified data file (-i switch detailed description).

Parameter -iFILENAME is used to specify a single binary file. This parameter in the command line is obligitory, unless switch -s is not specified. It has less priority than -s, so it is ignored when -s switch specifies a chain of input files in the command line. Also, some functions of the visualization function will be inachievable with -i specification (e.g., walk along the process, movie etc).
Specfic cases:
A. If the data file name is specified but the file cannot be open, then the program will terminate with ERRORLEVEL 5 and a message:
"Cannot open input file <NAME>".
B. If the specified file cannot be correctly read to the end, then the program will terminate with ERRORLEVEL 6 and a message:
"Cannot read from input file <NAME>".
C. If neither -i, nor -s switch is specified, then the program will terminate with ERRORLEVEL 4 and a message:
"Input file name must be specified".

III. Input fargmentation group.

This group consists of one item specifying input file with results of fragmentation (it is a binary file with format different from this in usual results files specified with -i or -s switshes). In lack of the fragmentation data specification some functions of the program are inachievable. Note also that there is no software restrictions regulating the connection between specified combustion/wall loading data and fragmentation data, so that the user must be sure that one data matches the other.

5. Input results of fragmentation from a specified file (-F switch detailed description).

Parameter -FFILENAME is used to specify a binary file containing results of fragmentation. This parameter has less priority than help service function. If it is abscent in the command line, functions of the visualization function concerning fragmentation results will be inachievable.
Specfic cases:
A. If the file name is specified but the file cannot be open, then the program will terminate with ERRORLEVEL 13 and a message:
"Cannot open fragmentations data file <NAME>".
B. If the specified file cannot be correctly read to the end, then the program will terminate with ERRORLEVEL 14 and a message:
Cannot read from fragmentations data file <NAME>".

Operating with the program of visualization.

from the specified input file (or first file in the chain) and data from video parameters text file (or use default parameters). Then if no errors occur, the system tries to register graphics font (which is placed in the file named 8FONT), allocate memory for variables and read the rest of the data file, allocate structures for contours drawing and enter graphics mode (VGA, 16 colors). If an error occurs at each of the stages, then the program will terminate with one of the messages:

"Cannot register graphics font" (ERRORLEVEL 8),
"Cannot allocate memory" (ERRORLEVEL 7),
"Cannot allocate contours drawing structure" (ERRORLEVEL 9),
"Cannot open graphics mode" (ERRORLEVEL 10).

After this a cycle of demonstration begins. There are 3 modes of demonstration: combustion mode, wall loading mode and fragmentation mode. The very first picture is always: combustion mode,pressure, drawn as color map, no velocity vectors and no grid scaling. The wall loading mode is achievable if wall was accounted in calculations (see problem parameters in the calculative program description). The fragmentation mode is achievable if wall loading is achievable and the fragmentation results file is specified in the command line.

There is an invitation to input code in the right lower part of the screen. Every time when this invitation is present, user can enter a numeric code (no more than 4 digits) from the keyboard. Keys distinct from digits are ignored, except <ENTER>, that completes the code input.

All the codes can be collected into the following groups:

1. Change kind of data to represent
   (codes 1,2,3,4,5,6,11,12,13,14,21,22,23,25) - combustion mode
   (codes 31,32,33,34,35,41,42,43,44) - wall loading mode
   (codes 51,52,53,54,55) - fragmentation mode
2. Switch on/off velocity vectors and scaling axes,
   switch between map and contours (combustion mode only)
   (codes 61,63,66);
3. Change limit values (all modes)
   (codes 100,101,102,103,110,111,112,113,120,121,122,123);
4. Switch between normal/logarithmic scales (all modes)
   (code 125);
5. Switch between modes
   (codes 131,132,133)
6. Save video parameters (all modes)
   (code 200);
7. Change files in the chain (combustion and wall loading modes)
   (codes 202,212,222,232);
8. Change current wall section (fragmentation mode)
   (codes 252,262,272,282)
9. Start movie (combustion and wall loading modes)
   (code 333);
10. Terminate (code 999).

The list of codes above is full. Any other code is ignored, and the code invitation will be repeated. If some code is input and the current mode do not match this code, then it is also ignored. Note that an empty code string followed by <ENTER> is regarded as zero and ignored.

The detailed description of code groups.

1. Change kind of data to represent.

Codes available in combustion mode have the following functions:
1 - show pressure (default),

3 - show density,
4 - show velocity module,
5 - show velocity axial component,
6 - show velocity radial component,
11 - show turbulent energy (K),
12 - show turbulent dissipation (Epsilon),
13 - show eddy viscosity,
14 - show turbulent frequency (i.e. epsilon divided by K),
21 - show oxidizer mass concentration,
22 - show fuel mass concentration,
23 - show products mass concentration,
25 - show reaction's intensity (special units).

Codes available in wall loading mode are designed to show results as diagrammes along horizontal axis; its coordinate begins at the bottom of the cylindrical vessel, follows radius, then goes up along lateral wall, then turns to the top of the cylinder along the radius. Sections (low, lateral, high) are separated on the diagrammes by blue vertical lines.
31 - show pressure near wall (default),
32 - show temperature near wall,
33 - show tangential stress,
34 - show temperature increase in the wall,
35 - show tangential deformation,
41 - show effective radius shifting,
42 - show wall velocity,
43 - show elastic energy per mass,
44 - show dissipative energy per mass.

Codes available in fragmentation mode are designed to show results along mass of fragments coordinate (always fixed logarithmic scale) or wall coordinate similar to this for wall loading mode.
51 - show gross number of fragments per mass (default),
52 - show gross velocity of fragments per mass,
53 - show distribution of fragments number per square along wall coordinate,
54 - show distribution of fragments velocity along wall coordinate,
55 - show number of fragments per mass for selected section.

2. Switch on/off velocity vectors and scaling axes, switch between map and contours

These codes are available only in combustion mode.
71 - switch on/off velocity vectors display. The screen vector's represented length is governed by levels of the velocity module (code 4 to change to velocity module, see above).
73 - switch on/off scaling axes. The unit length in each direction is 10 cm for big segment and 2 cm for little.
77 - switch between color map and contours representation.

3. Change level values.

This group of codes is available in all modes. For combustion mode codes of this group change upper and lower limit values. The intermediate levels change according to these two (taking into account the type of scale for current chart). For the other modes these codes change upper and lower limits for the vertical axis of the current diagramme. Note that this is related to "actual" limits with arbitrary values. Real limits displayed depend on "actual" so that for normal type of scale the displayed limits are equal to 10^n,

exceeds or equal to the "actual" upper limit, and lower limit is less or equal to the "actual" lower limit. For logarithmic scale, displayed limits are integer in terms of decimal logarithm of module (with the same rule of relation between displayed and "actual" limits.
100 - divide lower limit by 10,
101 - multiply lower limit by 10,
102 - divide upper limit by 10,
103 - multiply upper limit by 10,
110 - divide lower limit by 2,
111 - multiply lower limit by 2,
112 - divide upper limit by 2,
113 - multiply upper limit by 2,
120 - divide lower limit by 1.2,
121 - multiply lower limit by 1.2,
122 - divide upper limit by 1.2,
123 - multiply upper limit by 1.2.
Note that: 1) all the values of limits must be non-negative, 2) if some limit is equal to zero, it cannot be changed (such a change can be done directly in the file with video data).
Specific case: if a change will lead to a situation when the lower limi exceeds the upper, then the change is not proceeded, and a message will be typed: "Cannot change level".

4. Switch between normal/logarithmic scales.

This code is available in all the modes.
125 - switch between normal and logarithmic scales.
This function does not affect upper and lower limits. Note that switching to logarithmic scale is blocked by the program if one of the limits is zero. In this case a message is typed: "Cannot change scale".

5. Switch between modes.

This group of codes is formally available in all the modes, but with limitations: one cannot change to wall loading mode if wall dynamics was not accounted in calculations (this flag is placed in the input files), also one cannot change to fragmentation mode if file with results of fragmentations is not specified in the command line.
131 - change to combustion mode (default mode),
132 - change to wall loading mode,
133 - change to fragmentations mode.

6. Save video parameters.

Code 200 is used to write video parameters to a text file which file name is specified in the command line. If the last is not specified, then a file VIDEO.DAT is created. When writing fails, the program will terminate (see information of video parameters file specification in the command line above).

7. Change files in the chain.

Codes of this group are available in combustion and wall loading modes only when a successive chain of data files is specified in the command line (with -s switch). Changing between files leads to determining extension for new file in the chain, attempt to open it and reading. Possible problems that may occur, are solved in the following way. If there is an attempt to determine a file which number is less than zero, then the system changes to zeroth file. If the determined file cannot be open or read, then the system changes to zeroth file. If then the zeroth file cannot be open or read correctly, then the program

"Cannot open input file <NAME>.000" (ERRORLEVEL 5).
"Cannot read from input file <NAME>.000" (ERRORLEVEL 6).
202 - walk 5 files backward,
212 - walk to next file backward,
222 - walk to next file forward,
232 - walk 5 files forward.

8. Change current wall section.

This function is available only in fragmentations mode, and only if "number of fragments per mass for selected section" is currently displayed (see code 55). The position of current section is shown in magenta on the scale placed in the lower left part of the screen. If the user tries to walk beyond the margin section, then the walk continues from the opposit end of scale in the same direction (along the wall coordinate, its description see above).
252 - walk 5 sections backward (to the left),
262 - walk to next section backward,
272 - walk to next section forward,
282 - walk 5 sections forward.

9. Start movie.

This code 333 is available in combustion and wall loading modes if the chain of files is specified as an input parameter (switch -s in the command line). The movie is just automatic walking forward via the specified chain of files (manual walk description see above as "change files in the chain". All the problems, that may occur, are the same as in the manual walk. When the program reaches the end of the chain or breach in it, it begins from the zeroth file, so that the process is recycling. User can stop this pressing <ESC>. The state of movie demonstration is characterized by abscence of the input-code inquiring in the lower right part of the screen.
333 - start movie,
<ESC> - break movie.

10. Terminate.

Code 999 is used to terminate the program with ERRORLEVEL 0.

# CONCLUSIONS

Investigations of peculiarities of breakup caused by combustion of mixing hypergolic propellants after a destruction of the common bulkhead are carried out.

Mathematical modelling of unsteady turbulent mixing and combustion of hypergolic propellants in two-sectional cylindrical tank was performed. Diffusion flame and the flow itself manifested macroscopic pulsations: oxidant penetrated fuel tank and combustion was initiated in it; the increase of pressure caused a reverse flow of the reaction products and fuel that initiated combustion in the oxidant tank; the further pressure increase caused again flow of mixture through the opening from the oxidant into the fuel tank and initiated combustion in the last.

On increasing the diameter of the opening the combustion process turned to be more rapid and pressure and temperature increased to a higher values.

Numerical modelling showed large nonuniformities in wall loading and heating in diffusion combustion of hypergolic propellants.

These nonuniformities are essential during the time of combustion process and decrease gradually due to turbulent diffusive and viscous dissipation.

Mathematical model of breakup of a fuel tank under the influence of internal nonuniform loading caused by nonuniform energy release in combustion of hypergolic propellants is worked out.

Theoretical investigations show that nonuniform loading bring to a wider spectrum of mass distribution of fragments in a breakup event. Velocity distribution of fragments versus mass shows that mean velocity of a larger fragments is much lower than that of a smaller ones. The smallest fragments have nearly one and the same velocity.

Two different scenario of breakup are possible. If breakup criterion is satisfied within the time of pressure increase in combustion the process will follow the scenarium described above.

If the criterion is not satisfied the shell will be stabilized at a higher rate of uniform internal load. But high temperatures near the walls will cause gradual heating of the shell, lowering the elasticity limit, increasing plastic deformations, thus satisfying the breakup criterion. In this case breakup takes place much later after the internal combustion has been terminated. Velocity spectrum of the fragments distribution is much more narrow.

A software is constructed making it possible to simulate numerically breakup events of fuel tanks with account of peculiarities of energy release in diffusive combustion of mixing hypergolic propellants, and to determine mass and velocity distributions of fragments.

## REFERENCES


[1] "Inventory of Orbiting Hypergolic Rocket Stages" technical memorandum SN-3-81-55. technical planning office, NASA-JSC, March 1981.

[2] I.J.Webster, T.Y.Kawamura. Precluding Post-Launch Fragmentation of Delta Stages. Mc Donnel Douglas Space Systems Company Tech. Rept. 5.05.92.

[3] "Generation of Space Debris from Explosions of Spacecrafts' Fuel Tanks" by N.N.Smirnov et al. Technical Report No.2, Moscow State University, June 1994.

[4] "Investigation of Delta Second Stage On-Orbit Explosions" Report MDC-H0047, McDonnel Douglas Astronautics Company Huntington Beach, CA, April 1982.

[5] "Orbital Debris from Upper Stage Breakup" edited by J.P.Loftus, AIAA Proceedings of the conf. 1987.

[6] N.N.Smirnov et al. Investigation of peculiarities of the process of energy release involved in the mixing of hypergolic propellants in weightlessness. Approaches to mathematical modelling. Prelim. Rpt. on SPC 94-4107, 1994.

[7] N.N.Smirnov et al. Mathematical Modelling of the Process of Energy Release Involved in the Mixing of Gaseous Hypergolic Propellants in Weightlessness. The Rates of Wall Loadings and its Dependence on the Rates of Mixing. Second (Interim) Report on SPC 94-4107, 1995.

[8] O. Pironeau, B. Mohammadi. Analysis of the K-Epsilon Turbulence Model. Masson Editeur, Paris, 1994.

[9] R.W. MacCormack. Numerical Solution of the Interaction of a Shock Wave with a Laminar Boundary Layer. Proc. Second Int. Conf. Num. Methods Fluid Dyn., Lecture Notes in Physics, v.8, New York: Springer-Verlag, 1971, p.151 - 163.

[10] R.W. MacCormack. An Efficient Numerical Method for Solving the Time-Dependent Compressible Navier-Stokes Equations at High Reynolds Number. - NASA TM X -73, 129 (1976).

[11] D.A. Anderson, J.C. Tannehill, R.H. Pletcher. Computational Fluid Mechanics and Heat Transfer. Hemisphere Publishing Corporation, 1984.

[12] A.A.Samarsky. Basis of Numerical Methods. Moscow, Nauka, 1987 (in Russian).

[13] A.B.Kiselev, M.V.Yumashev. On Dynamic Failure Criterion for Viscoelastic Medium. // Vestnik Moscow University Bulletin, Mathematics, Mechanics, 1990, vol.45, No.4, pp.38-43.

[14] M.L.Wilkins. Modelling the Behaviour of Materials.// Struct. Impact and Crashworth: Proc. Int. Conf. V.2, L., N.-Y., 1984, pp.243-277.

[15] V.A.Chobotov, D.B.Spencer. Debris Evolution and Lifetime Following an Orbital Breakup. // Journal of Spacecraft and Rockets. Vol. 28, Number 6, 1991, pp.670-676.